

**Rational Selection of Cyanines as NIR-Sensitive  
Photoinitiating Systems up to 1000 nm Applied in  
Coating Sciences**

Dissertation

to obtain the academic degree of  
Doctor of Natural Sciences  
- Dr. rer. nat. -

**Qunying WANG**

born in Sichuan, China

Faculty of Chemistry  
University of Duisburg Essen

**2024**

The present work was carried out in the period from September 2019 to October 2022 under the supervision of Prof. Dr. Jochen S. Gutmann from the Faculty of Chemistry at University of Duisburg-Essen in cooperation with Niederrhein University of Applied Sciences in the working group of Prof. Dr. Bernd Strehmel from the Institute for Coatings and Surface Chemistry.

Date of Defence: 22.01.2024

Thesis Advisors:

**Prof. Dr. Jochen S. Gutmann**

University of Duisburg-Essen

**Prof. Dr. Bernd Strehmel**

Niederrhein University of Applied Sciences

**Prof. Dr. Cyrille Andre Boyer**

University of New South Wales

Chair:

**Prof. Dr. Bettina Siebers**

University of Duisburg-Essen

## Explanation

I hereby confirm that I am entitled the present work with the title

“RATIONAL SELECTION OF CYANINES AS NIR-SENSITIVE PHOTOINITIATING SYSTEMS UP TO 1000 NM APPLIED IN COATING SCIENCES”

independently written and have not used other than the sources and resources indicated, and this work submitted in this or similar form has never been done at any other university.

Qunying Wang



Duisburg-Essen Publications online



Offen im Denken



universitätsbibliothek

Diese Dissertation wird via DuEPublico, dem Dokumenten- und Publikationsserver der Universität Duisburg-Essen, zur Verfügung gestellt und liegt auch als Print-Version vor.

**DOI:** 10.17185/duepublico/81471  
**URN:** urn:nbn:de:hbz:465-20240202-104718-2

Alle Rechte vorbehalten.

---

## Foreword

It's time to wrap up my last period of time being an official student when I start with this page, during which I had so many very inspiring, exciting and challenging memories.

First and foremost, I would like to express my appreciation to my supervisor Prof. Dr. Bernd Strehmel for always being so patient, inspiring and helpful during my study and research. I appreciate a lot for the opportunity that Prof. Strehmel offered me to start my PhD in his group, where I could get much deeper into the research field of photochemistry and photopolymerization. It was a period of great experience coming to another country in Germany to study and work with him. His great and extensive knowledge, effort and support always help and motivate me to do better in both scientific research and daily life. His prospective insight, hard-working style, and enthusiasm of climbing the mountain of science always inspire and guide me with big encouragement. I would not be able to reach the breakthrough of my research during this thesis without his contribution. I would also like to thank him for the support to make my life in Germany easier.

Meanwhile, I would like to show my thanks to Prof. Dr. Jochen S. Gutmann, who also supervised me during my PhD study, his immense knowledge and guidance helped me a lot and also extended the frame of my knowledge. His encouragement and valuable professional suggestions contributed to finally improving this thesis.

I am really grateful to have the lovely colleagues in Prof. Strehmel's group for the nice working atmosphere and their warm-hearted friendship. Although I did not have the chance to spend much time with all of them, such as Dr. Dennis Oprych, Serbest Sheikmous, Dr. Christian Schmitz, Dr. Ceren Kütahya and Dr. Yulian Pang, I do appreciate the time together, support and suggestions from them. I would also like to thank my conference travel buddies Paul Hermes and Lukas Appelhoff, who are always nice to help me especially improving my German speaking. Besides, it is also big pleasure to work with friendly Nicolai Meckbach, Taner Poplata and Sascha Driesen.

I would also thank Prof. Dr. Veronika Strehmel for her valuable inspiring suggestions and nice cooperation. Her earnest manner to work and science also motivates me a lot. I would express my thanks to Prof. Dr. Jun Nie, who was supervisor during my master study and led me to this field and always wishes the best for both my life and academic career.

At last but not least, I would like to deeply thank all my families especially my parents for their encouragement. They're always strongly supportive to me and give their love, they did their best to set a good example for me. I also want to thank my fiancé Dr. Qing Li for his help, encouragement and support during the whole period of my PhD.



# Table of Contents

Explanation.....	I
Foreword.....	I
Table of Contents .....	II
Abbreviations.....	VI
List of Figures .....	VIII
List of Schemes .....	XII
List of Charts .....	XIV
List of Tables .....	XV
Abstract.....	XVI
Kurzfassung .....	XVIII
<b>1. Introduction and Motivation.....</b>	<b>1</b>
1.1 General Aspects .....	1
1.2 Motivation of the Thesis.....	6
<b>2. State of Art in the Field of NIR-Sensitized Photopolymerization.....</b>	<b>13</b>
2.1 Requirements for Light Sources Needed for Photopolymerization from UV to Near-Infrared Range.....	13
2.1.1 Mercury Lamps for Photopolymerization .....	15
2.1.2 LEDs for Photoinitiating Polymerization between 250-1100 nm.....	17
2.1.3 Lasers for Photopolymerization Based on the Excitation in NIR Range .....	19
2.1.4 Sunlight as An Alternative Green Source Makes Dream Reality .....	21
2.2 Key Points for Photopolymerization Systems in NIR.....	22
2.2.1 Fundamentals of Photochemical Process to Generate Initiating Species for Radical and Cationic Polymerization .....	22
2.2.2 Photoinduced Electron Transfer between the Initiators and Energetic Barriers	26
2.2.3 Heat as Additional Impact to Promote Systems with Dual Working Function....	30
2.3 Sensitizers in NIR Light-Mediated Photopolymerization.....	33
2.3.1 Structural Patterns of Absorbers and Sensitizers in NIR Range .....	33
2.3.2 Cyanines as Sensitizers in Photopolymerization.....	37
2.3.3 Selection of Cyanines on Demand Based on Their Structural Patterns .....	40
<b>3. Materials and Methods .....</b>	<b>43</b>
3.1 Chemicals for Photopolymerization .....	43

---

3.1.1 NIR Sensitizers Derived from Cyanines of Different Structural Pattern.....	43
3.1.2 Co-Initiators Combined with Sensitizers.....	44
3.1.3 Monomers for Free Radical and Cationic Polymerization .....	44
3.1.4 Materials to Quantify the Conjugate Acid .....	46
3.1.5 Water-Based Polyurethane Dispersions.....	46
3.1.6 Nanoparticle Comprising Sol-Gels .....	47
3.1.7 Solvents.....	49
3.2 Light Sources.....	49
3.2.1 NIR-LEDs .....	49
3.2.2 UV-LED at 395 nm.....	50
3.2.3 NIR Laser .....	51
3.3 Characterization Methods and Equipments.....	51
3.3.1 UV-Vis-NIR Spectroscopy .....	51
3.3.2 Cyclic Voltammetry.....	51
3.3.3 Fluorescence and Lifetime Measurement .....	51
3.3.4 Conductivity Measurement of Iodonium Salt in Monomers .....	53
3.3.5 Real Time- and Fourier Transfer Infrared (FTIR) Spectroscopy.....	53
3.3.6 Photo- and Differential Scanning Calorimeter (DSC).....	53
3.3.7 Thermal Camera.....	54
3.3.8 Mass Spectrometry Coupled with High-Performance Liquid Chromatography (HPLC).....	54
3.3.9 Nuclear Magnetic Resonance (NMR) Analysis.....	54
3.3.10 Rheometer Coupled with Heat Program.....	54
3.3.11 Dynamic Mechanical Analysis (DMA).....	55
<b>4. Experimental Section .....</b>	<b>56</b>
4.1 Structural Pattern of Cyanines Regulates the Efficiency of Non- and Radiative Processes upon Exposure of High-Power NIR-LEDs.....	56
4.1.1 Selection of Sensitizers Based on Structural Patterns and Physical Properties of the Cyanines.....	56
4.1.2 Bleaching Kinetics of Sensitizers with and without Iodonium Salts by Excitation with High-Power LEDs.....	59
4.1.3 Activity of the System Comprising Sensitizers and Iodonium Salt to Generate Conjugate Acid .....	59

---

4.2 Reactivity of Different Sensitizers and Iodonium Salt to Initiate Free Radical and Cationic Photopolymerization .....	60
4.2.1 Cyclic Voltammetry .....	60
4.2.2 Conductivity Measurement .....	60
4.2.3 Initiation upon Low-Power Exposure Determined by Photo-DSC .....	61
4.2.4 Kinetics of Photopolymerization Followed by Real-Time FTIR.....	61
4.3 Performance of the Initiating System Comprising Sensitizers and Iodonium Salt to Initiate Free Radical/Cationic Co-Polymerization .....	62
4.3.1 Viscosity Measurement .....	62
4.3.2 Final Conversion of the Monomers from Hybrid Polymerization Systems.....	62
4.3.3 Characterization for Mechanical Properties of Polymer Films Applied by DMA	63
4.4 Contribution of the Heat Generated in the System Comprising Sensitizers and Iodonium Salts upon Exposure.....	63
4.4.1 Thermal Stability of the Photoinitiators Comprising NIR Sensitizers and Iodonium Salt.....	63
4.4.2 Temperature Tracking of the Systems during Free Radical Polymerization .....	64
4.4.3 Thermally Initiated Polymerization.....	64
4.4.4 Comparison between Photopolymerization and Thermally Initiated Polymerization .....	65
4.4.5 Laser Radiation .....	65
4.5 Heptamethine Sensitizer-Comprising Systems Applied to Coatings upon High-Power NIR Exposure .....	66
4.5.1 Photocuring of Nanoparticle-Based Sol-Gels.....	66
4.5.2 Physical Drying of Water-Based Polyurethane Coating System .....	67
<b>5. Results and Discussion .....</b>	<b>68</b>
5.1 Relation between Structural Patterns of Cyanines and Their Performance to Generate Moieties for Initiation of Photopolymerization.....	68
5.1.1 Selection of Cyanines Based on Structural Patterns.....	68
5.1.2 Chemistry of the First Excited Singlet State .....	75
5.1.3 Performance on Generation of Radical and Conjugate Acid as Initiating Species Combined with Iodonium Salt.....	80
5.1.4 Heat Release Regulated by the Structural Patterns of Cyanines.....	88
5.2 Polymer Network Formation by Radical and Cationic Crosslinking Applying NIR-Radiation for Excitation.....	92

---

5.2.1 Activated Free Radical Photopolymerization .....	92
5.2.2 NIR-Sensitized Photoinitiated Cationic Photopolymerization .....	102
5.2.3 Enhanced Performance of Cationic Photopolymerization in Hybrid Systems .....	105
5.3 Heptamethine-Based Cyanine and Iodonium Salt as Initiators for Photocuring of Coatings Based on Sol-Gels Comprising Nanoparticles .....	109
5.3.1 Efficient Photocuring of the Coatings via NIR Exposure .....	109
5.3.2 Properties of the Coatings Made from Sol-Gels Comprising Nanoparticles by Photopolymerization Technique .....	111
5.4 Performance of Heptamethine Cyanine Applied to Aqueous Coatings for Physical Drying with NIR-Radiation Followed by Chemical Drying with UV Exposure .....	113
5.4.1 Physical Drying of Waterborne Polyurethane Dispersions .....	113
5.4.2 Chemical Crosslinking by UV Radiation of Physically Dried Films Applying NIR Exposure.....	116
<b>6. Conclusion &amp; Outlook .....</b>	<b>118</b>
<b>7. References.....</b>	<b>123</b>
<b>Acknowledgements .....</b>	<b>145</b>
<b>Curriculum Vitae .....</b>	<b>146</b>

## Abbreviations

---

UV	Ultraviolet
NIR	Near-Infrared
<b>Sens</b>	Sensitizers
<b>Sens*</b>	Sensitizers at excited state
HOMO	Highest Occupied Molecular Orbital
LOMO	Lowest Unoccupied Molecular Orbital
<b>PET</b>	Photoinduced Electron Transfer
LED	Light-Emitting Diodes
<b>ITX</b>	2-Isopropyl thioxanthane
<b>PI</b>	Photoinitiator
<b>IS</b>	Iodonium salt
<b>[NTf<sub>2</sub>]<sup>-</sup></b>	Bis(trifluoromethanesulfonyl)imide anion ( $[(CF_3SO_2)_2N]^-$ )
FRP	Free Radical Polymerization
CP	Cationic Polymerization
UV-Vis-NIR	Ultraviolet-Visible-Near Infrared
E'	Storage Modulus
E''	Loss Modulus
Tanδ	Ratio of Loss Modulus to Storage Modulus
DMA	Dynamic Mechanical Analysis
T <sub>g</sub>	Glass Transition Temperature
NMR	Nuclear Magnetic Resonance
HPLC	High Performance Liquid Chromatography
DSC	Differential Scanning Calorimeter
Photo-DSC	Photo Differential Scanning Calorimeter
FTIR	Fourier-Transform Infrared Spectroscopy
RT-FTIR	Real Time Fourier-Transform Infrared Spectroscopy
ATR	Attenuated Total Reflectance
λ <sub>max</sub>	Maximum Absorption Wavelength
ε <sub>max</sub>	Extinction Coefficient at Maximum Absorption Wavelength
λ <sub>f</sub>	Wavelength of Fluorescence Emission
Φ <sub>f</sub>	Quantum Yield of Fluorescence Emission

---

$\tau_f$	Lifetime of Fluorescence Emission
F	Fluorescence
$E_{ox}$	Oxidation Potential
$E_{red}$	Reduction Potential
$E_{00}$	Excitation energy
$\Lambda_m$	Molar Conductivity
<b>UDMA</b>	Urethane Dimethacrylate
<b>TMPTA</b>	Trimethylolpropanetriacrylate
<b>TPGDA</b>	Tripropylene Glycol Diacrylate
<b>OXT 03</b>	3,3'-(Oxybis(methylene))bis(3-ethyloxetane)
<b>OXT 09</b>	3-Ethyl-3-(Methacryloyloxy)Methyloxetane
<b>EP</b>	Epilox P 13-21
<b>Epikote 357</b>	Blend of Bisphenol F resin and Bisphenol A resin
RhB-L	Rhodamine B lactone
RhB-H	Rhodamine B
<b>HBVE</b>	4-Hydroxybutyl Vinyl Ether
<b>TEOS</b>	Tetraethyl Orthosilicate
<b>MEMO</b>	3-Methacryloxypropyltrimethoxysilane
<b>TMOS</b>	Tetramethyl Orthosilicate
<b>SG</b>	Sol-Gel
<b>PU</b>	Polyurethane
IPNs	Interpenetrating Polymer Networks
CV	Cyclic Voltammetry
<b>ISC</b>	Intersystem Crossing
<b>IC</b>	Internal Conversion
<b>IVR</b>	Intramolecular Vibrational Redistribution
<b>VC</b>	Vibrational Cooling
<b>VR</b>	Vibrational Relaxation
<b>S<sub>0</sub></b>	The Ground State
<b>S<sub>1</sub></b>	The Excited Singlet State
UCNPs	Up-Conversion Nanoparticles
$\nu$	Vibrational State
$\Delta G$	The Gibbs Free Energy

## List of Figures

Figure 1. Summary of the absorption for materials covering from UV to NIR range, modified from[151, 154].	14
Figure 2. Emission wavelength dependence of the scattering coefficient, modified from[97, 105].	15
Figure 3. Image of the alignment of mercury conveyor from Heraeus with integrated microwave lamp.	17
Figure 4. Emission of sunlight. The optical spectra were taken at 14:35 on 19th, April 2023 in the city of Krefeld in Germany using the spectrometer described below, while the image was obtained at 14:30 on 26th, February 2023 in the city of Turku in Finland.	21
Figure 5. Structural patterns of cyanines with 1-substitution of trimethylindolium, benzo[g]indolium, benzo[e]indolium and benzo[c,d]indolium salts lead to the symmetric patterns a/a', b/b', c/c' and d/d' based on the terminal substituent A, modified from[20].	37
Figure 6. Emission spectrum and profiles of the NIR-LEDs used in this thesis.	50
Figure 7. Emission spectrum and profiles of the UV-LEDs used.	50
Figure 8. Profiles of the samples during exposure and the polymer obtained.	65
Figure 9. Geometry of S5a showing a nearly planar pattern with a) front and b) side view, graphs c) and d) depict HOMO and LOMO, respectively, cited from[90].	70
Figure 10. Geometry of S7c showing a nearly planar pattern with a) front and b) side view, graphs c) and d) depict HOMO and LOMO, respectively, cited from[90].	70
Figure 11. Geometry of S7e showing a nearly planar pattern with a) front and b) side view, graphs c) and d) depict HOMO and LOMO, respectively, cited from[90].	70
Figure 12. Geometry of S7g showing a nearly planar pattern with a) front and b) side view, graphs c) and d) depict HOMO and LOMO, respectively, cited from[90].	71
Figure 13. Geometry of S9 showing a nearly planar pattern with a) front and b) side view, graphs c) and d) depict HOMO and LOMO, respectively, cited from[90].	71
Figure 14. Traces of fluorescence lifetime of the absorbers S3-S9 obtained after the excitation at 670 nm in MeOH applying time-correlated single photon counting to collect the data. The maximum fluorescence emission ( $\lambda_{fmax}$ ) from the samples show up at the following wavelengths: a): S3a ( $\lambda_{fmax}$ = 782 nm); b): S3b ( $\lambda_{fmax}$ = 843 nm); c): S7h ( $\lambda_{fmax}$ = 801 nm); d): S7e ( $\lambda_{fmax}$ = 835 nm); e): S7c ( $\lambda_{fmax}$ = 824 nm); f): S7g ( $\lambda_{fmax}$ = 869 nm); g): S9 ( $\lambda_{fmax}$ = 884 nm) and h): S7g ( $\lambda_{fmax}$ = 869 nm). Experimental details could be found in Section 3.3.3, (the red curve represents the instrumental response of a scatter comprising Ludox in water whose detection is close to 670 nm; blue: decay traces of the samples detected; black: calculated decay traces by iterative convolution between	

- the instrumental response and exponential curves), modified from[90].....79
- Figure 15. Profiles of optical density (OD) decrease from the NIR-absorbers ( $[Sens] = 5.0 \times 10^{-4} \text{ mol} \cdot \text{L}^{-1}$ ) in acetonitrile upon exposure in the presence of iodonium salt ( $[IS] = 3.0 \times 10^{-3} \text{ mol} \cdot \text{L}^{-1}$ ) applying the big-size of LED emitting at 860 nm with the intensity of  $1.0 \text{ W} \cdot \text{cm}^{-2}$ ; a) S3b, b) S5a, c) S7b, d) S7d and e) S7f, modified from[90]. .....83
- Figure 16. Profiles of optical density (OD) decrease from the NIR-absorbers ( $[Sens] = 5.0 \times 10^{-4} \text{ mol} \cdot \text{L}^{-1}$ ) in acetonitrile upon exposure in the presence of iodonium salt ( $[IS] = 3.0 \times 10^{-3} \text{ mol} \cdot \text{L}^{-1}$ ) applying the big-size of LED emitting at 820 nm for S7a, S7e and S7h and LED emitting at 860 nm for S7g and S9 with the intensity of  $1.0 \text{ W}/\text{cm}^2$  respectively; a) S7a, b) S7e, c) S7h, d) S7g and e) S9, modified from[90]. .....84
- Figure 17. The profiles showing the capability of the NIR-initiators to generate conjugate acid. a) The evaluated amount of conjugate acid formed in the system comprising Sens ( $2.0 \times 10^{-5} \text{ mol} \cdot \text{L}^{-1}$ ) and IS ( $1.2 \times 10^{-4} \text{ mol} \cdot \text{L}^{-1}$ ) after exposure for 15 mins applying the NIR-LEDs with the intensity of  $1.0 \text{ W}/\text{cm}^2$ , LED emitting at 820 nm was used for S3a, S7a, S7c, S7e, S7h and LED emitting at 860 nm was applied for S3b, S5a, S5b, S7b, S7g, S7f, S7g and S9, respectively. After the exposure, amount of Rhodamine B was added into the solutions ( $[Rhodamine \text{ B}] = 1.0 \times 10^{-4} \text{ mol} \cdot \text{L}^{-1}$ ; b) the values of the concentration ratio of conjugate acid formed to the original concentration of the Sens. ....86
- Figure 18. Temperature traces from the system of free radical photopolymerization in a) and b) UDMA comprising Sens ( $1.05 \times 10^{-3} \text{ mmol} \cdot \text{g}^{-1}$ ) and IS ( $1.56 \times 10^{-2} \text{ mmol} \cdot \text{g}^{-1}$ ). c) Comparison of the temperature in TPGDA/UDMA and different concentration of S3b in UDMA (0.05 wt% of S3b is approximately  $0.53 \times 10^{-3} \text{ mmol} \cdot \text{g}^{-1}$ ), modified from[91]. .....89
- Figure 19. Conversion-time profiles of UDMA based on thermally initiated polymerization at  $150^\circ\text{C}$  comprising Sens ( $1.05 \times 10^{-3} \text{ mmol} \cdot \text{g}^{-1}$ ) and IS ( $1.56 \times 10^{-2} \text{ mmol} \cdot \text{g}^{-1}$ ) with the comparison from Sens and IS with the same aforementioned concentration in neat UDMA respectively. ....90
- Figure 20. Profiles from rheology measurement based on a programmed heating up process. a) Curves of storage modulus, loss modulus as well as the temperature from the system in UDMA comprising IS (1.0 wt%) and S7d (S7d:IS = 1:6 (molar)) and; b) Profiles of storage modulus-temperature of the system of UDMA comprising Sens and IS following the aforementioned concentration, as a comparison, the data from neat UDMA and IS dissolved in UDMA was considered, respectively. ....92
- Figure 21. Profiles of conversion-time and polymerization rate ( $R_p$ ) obtained via photo-DSC of the system comprising Sens and IS (1 wt%,  $[Sens]:IS = 1:6$  (molar)) in the monomer of TPGDA exposed by NIR-LEDs emitting at 770 nm ( $I = 45 \text{ mW}/\text{cm}^2$ ) taken at different temperatures (Figure 21a; Sens = S7a) and the systems comprising different Sensitizers (Figure 21b) with either an open polymethine chain (S7a) exposed by 820 nm LED or a bridged polymethine chain (S7g and S9) exposed by 860 nm NIR-LED with an



- intensity of 1.0 W/cm<sup>2</sup> carried out at 40°C, cited from[90]......96
- Figure 22. Conversion-time profiles for free radical photopolymerization measured by RT-FTIR in a) UDMA and b) TPGDA comprising [Sens] = 1.05×10<sup>-3</sup> mmol·g<sup>-1</sup> and [IS] = 1.56×10<sup>-2</sup> mmol·g<sup>-1</sup> applying with NIR-LEDs with the intensity of 1 W/cm<sup>2</sup>. The data of photopolymerization from S7b, S7d, S7f was missing because of the small area of wavelengths overlap between the emission of available light sources and the absorption of the Sens. S7i was missing because of its water solubility which is not possible to dissolve into the organic monomers while S7j was investigated previously from[118]. This graph was modified from[91] .....97
- Figure 23. DMA profiles including storage modulus, loss modulus and tanδ curves of the polymer films obtained from free radical photopolymerization where UDMA as monomer applying with a) NIR-LED emitting at 860 nm comprising [S9] = 1.05×10<sup>-3</sup> mmol·g<sup>-1</sup> and [IS] = 1.56×10<sup>-2</sup> mmol·g<sup>-1</sup>, and b) UV-LED emitting at 395 nm comprising [ITX] = 5.25×10<sup>-3</sup> mmol·g<sup>-1</sup> and [IS] = 2.1×10<sup>-2</sup> mmol·g<sup>-1</sup>, respectively, cited from[91]......99
- Figure 24. Curves of tanδ-temperature measured by DMA characterization of the polymer samples obtained from free radical photo-polymerization in the monomer of UDMA comprising IS with the concentration of 1.0 wt% and Sens (where [Sens] : [IS] = 1:6 (molar ratio was used)). .....100
- Figure 25. DMA profiles of the polymer films of UDMA comprising S7c and IS in UDMA at area A (a)) and B (b)) shown in Figure 8, respectively. c) and d) showed the DMA curves of the samples obtained via thermally initiated polymerization of UDMA in the comparison of S7c (c)) and S7d (d)) ([Sens] : [IS] = 1:6 (molar ratio) and IS: 1.0 wt%)......101
- Figure 26. Optical absorption of the Sens in photopolymerization of UDMA in solution (before exposure) and in polymer films (after exposure), respectively. The concentration of the components in the experimental condition was the same as that in Figure 22, while the condition of the spectral collection was the same as that from Figure 15, cited and modified from[90]. .....102
- Figure 27. Conversion-time curves obtained from RT-FTIR for the investigations of cationic photo-polymerisation in the monomer of HBVE comprising Sens and IS. S9 was used as sensitizer in b). The experimental conditions were the same as that in the Figure 22, modified from[91]. .....103
- Figure 28. Conversion-time profiles for free radical photopolymerization measured by RT-FTIR in TMPTA comprising [Sens] = 1.05×10<sup>-3</sup> mmol·g<sup>-1</sup>, [IS] = 1.56×10<sup>-2</sup> mmol·g<sup>-1</sup> applying with NIR-LEDs with the intensity of 1.0 W/cm<sup>2</sup> (same experimental conditions for exposure as that in Figure 22), cited from[91]. .....106
- Figure 29. Profiles of DMA curves showing tanδ of the polymer films obtained by NIR-sensitized hybrid photopolymerization in the matrix of a) TMPTA and b) UDMA for free

radical polymerization combined with different monomers for cationic polymerization comprising S9 as sensitiser and IS acting as co-initiator. The exposure was applied by 860 nm LED with an intensity of 1.0 W/cm<sup>2</sup>. Cited and modified from[91]. ..... 108

Figure 30. Conversion-time profiles of the sol-gels obtained from RT-FTIR evaluated based on the monomer of Epilox P 13-21 comprising IS-PF6 (2.0 wt%) and a) ITX (0.5 wt%) for UV-initiated system exposed by LED device emitting at 395 nm and b) S7e-PF6 (0.5 wt%) for NIR system exposed by LED emitting at 820 nm, respectively. (The intensity of the LED devices were 1.0 W/cm<sup>2</sup>). ..... 110

Figure 31. Appearance of the coatings obtained (left side) and performance during the adhesion test (right side) from a) UV and b) NIR systems, respectively. The initiator combination of IS-PF6 with either ITX for UV system or S7e-PF6 for NIR was applied. The red frame in the graphs focused on the area where adhesion test was applied (The test was carried out following the instruction of ASTM D3359-22 Test Method B). ..... 112

Figure 32. DMA profiles from the cured coating films obtained from the monomer of Epilox P 13-21 (a) and d)) and the sol-gels (b) and e) from SG1, c) and f) from SG2) initiated by UV (a, b) and c)) and NIR (d, e) and f)) systems, respectively. The exposure was finished by either the LED device emitting at 395 nm for UV system or NIR-LED emitting at 820 nm with an intensity of 1.0 W/cm<sup>2</sup>. The data of SG3 was missing because the coatings from SG3 were too brittle to be applied for DMA characterization. .... 113

Figure 33. FTIR spectra of the PU coating precursor exposed in the ambient for 24h for drying and as a comparison the sample without any treatment. .... 114

Figure 34. Conversion-time profiles collected by real time FTIR spectroscopy of the PU coating precursors comprising the absorber S7i with different concentration upon exposure by the NIR-LED emitting at 860 nm with an intensity of 1.0 W/cm<sup>2</sup> for physical drying to get rid of the water. The data of neat PU and that without exposure were also included as a comparison, the evaluation of the conversion was based the decrease of the strong O-H bond at 3200 cm<sup>-1</sup> following the results from Figure 33. The thickness of the sample applied for the FTIR measurement was 100 μm. .... 115

Figure 35. Profiles of storage modulus and loss modulus-temperature of the PU films obtained from the PU precursors comprising different concentration of S7i following the previous physical drying collected by DMA characterization following the same method aforementioned. .... 116

Figure 36. DMA profiles of the PU films obtained from the PU precursor comprising 0.02% S7i with a) different time of NIR-LED exposure and b) following with a step of UV exposure for cross-linking, the intensity of the UV-LED emitting at 395 nm is 1.0 W/cm<sup>2</sup>. .... 117

---

## List of Schemes

Scheme 1. Emission spectra of high pressure mercury lamp, cited from[163].	16
Scheme 2. Emission spectra of the NIR light sources, cited from[9].	18
Scheme 3. Profiles (left) of high-power NIR-LED emitting at 805 nm and the temperature surrounding the working circumstance of it (right), cited from[118, 154].	19
Scheme 4. Line-shape focused laser with emission at 808 nm and 980 nm (left) with the respective intensity profile (right) visualized by up-converting phosphorescent material, cited from[154].	20
Scheme 5. Illustration of Law of photochemical equivalence, cited from[195].	23
Scheme 6. Activation energy for Norrish type I cleavage of basic aromatic ketones, modified from[194].	24
Scheme 7. Mechanism of generation of initiating species from type II initiators, modified from[196].	24
Scheme 8. Energetic relations of photoinduced electron transfer depicting internal activation barrier resulting in threshold systems under a) endothermal condition, b) thermoneutral condition and c) exothermal conditions, cited from[154].	28
Scheme 9. Chemical structures of the widely used electron acceptors iodonium salt A1 and triazines A2 as an example, cited from[20].	29
Scheme 10. Self-initiation of ethyl acrylate and n-butyl acrylate following the Flory and Mayo mechanism, cited and redrawn from[232].	32
Scheme 11. The chemical structures and absorption spectra of the perylene anhydride fused porphyrin compounds used as NIR sensitizers in solar cells, cited from[238].	34
Scheme 12. Structural pattern of phthalocyanines with possible substitutes, cited from[246].	34
Scheme 13. Energy level of respective transitions for excitation, energy transfer and emission of the up-conversion nanoparticle (UCNP) of NaYF <sub>4</sub> :Yb <sup>3+</sup> /Tm <sup>3+</sup> @NaYF <sub>4</sub> with high excitation intensity. cited from[148].	35
Scheme 14. General structural pattern of cyanines with potential substitutions. n <sub>1</sub> , n <sub>2</sub> = 0, 1, 2, etc.	36
Scheme 15. Photo cleavage of cyanine namely 33 comprising bridged chain in the meso-position at excited states reacting with cationic radical of iodonium salt resulting in the moieties of 33a-f, cited from[20].	39
Scheme 16. Photo-ATRP (Photo-induced Atom Transfer Radical Polymerization) mediated by dyes/sensitizers under the participation of UV, visible and NIR light, cited from[20].	40

---

Scheme 17. Workflow to develop technology for the design and fabrication new materials in a setup based on an intelligent Design-of Experiment (DoE) with the combination of chemistry, engineering and informatics generating artificial intelligence, cited from[20].	42
Scheme 18. Synthesis route for polyurethanes of general structure, which was used for practical training of students in the Department of Chemistry in Hochschule Niederrhein, cited from[277].	47
Scheme 19. Process of silanization with general structural pattern. X/X', Y/Y' vary based on the reaction degree of silanization, drawn based on[278].	47
Scheme 20. Illustration of the representative electronic ground state (S0) with its vibrational states $v = 0$ , $v = 2$ , and $v = n$ , as well as the first electronic excited state (S1) following with the respective vibrational states $v' = 0$ , $v' = 3$ , and $v' = n$ , and the vibronic transition where proceeded through the absorption of one-photon energy $h\nu$ . Graph was modified from[90, 267].	76
Scheme 21. Energetic representation of the relation between PET and internal barrier in the occasions where similar exothermal condition ( ) exists while internal barrier ( ) differs, modified from[154].	82
Scheme 22. a) Mechanism to evaluate the conjugate acid generated upon exposure on the sensitizers in presence of IS modified from[88]; b) an example from S9 (blue: absorption spectrum of S9 in acetonitrile, red: the spectrum of the solution of S9 and IS after 10 min exposure applying 860 nm emitting LED and added rhodamine B, experimental detail is disclosed in Section 4.1.2).	85
Scheme 23. Proposal of photoproducts according to the molecular mass of ions detected by LC-MS spectra by analysing the ions available from the solution in CH <sub>3</sub> CN upon exposure comprising S9 in the presence of IS by the LED at 860 nm, cited from[90].	87
Scheme 24. Structural pattern of the product formed by acid-catalyzed self-polyaddition of HBVE based on the ref[295], cited from[90].	104

---

## List of Charts

Chart 1: Structures of monomers used for photopolymerization in this thesis.....	46
Chart 2. Chemical structures of the NIR absorbers (sensitizers) used in this thesis. These cations comprise the following anions: S3a, S5b, S7d, S7e and S7f: BF <sub>4</sub> <sup>-</sup> ; S3b, S5a, S7g and S9: [PF <sub>3</sub> (C <sub>2</sub> F <sub>5</sub> ) <sub>3</sub> ] <sup>-</sup> ; S7a, S7b: PF <sub>6</sub> <sup>-</sup> ; S7c, S7h: p-CH <sub>3</sub> -Ph-SO <sub>3</sub> <sup>-</sup> ; S7i: [NH(C <sub>2</sub> H <sub>5</sub> ) <sub>3</sub> ] <sup>3+</sup> . S7j: Cyanine with zwitterion.....	58

---

## List of Tables

Table 1. Co-initiators used in this thesis.....	44
Table 2. Components and viscosity of the sol-gels used in this thesis. ....	48
Table 3. Photophysical data of the absorbers used in this thesis including absorption maximum $\lambda_{max}$ , extinction coefficient $\epsilon_{max}$ , fluorescence emission maximum $\lambda_{fmax}$ , fluorescence quantum yield $\Phi_f$ and decay time $\tau_f$ , and rate constant for fluorescence of the cyanines S3-S9. Electrochemical data discloses their oxidation $E_{ox}$ and redox potential $E_{red}$ . In addition, the values of solubility show the compatibility of the cyanines in the monomer of TPGDA and water for S7i, respectively. Furthermore, the information of commercial name and supplier of these absorbers is also included.....	73
Table 4. Summary of molecular mass of the ions detected from the exposed solution comprising S9 and IS at 860 nm with an intensity of 1.2 W/cm <sup>2</sup> for 10 min. Some of the ions appeared as doubly charged ions and/or NA <sup>+</sup> -adducts, modified from[90]. ....	88
Table 5. Data of the sensitizers showing the molecular weight, solubility and initiation temperature in the monomer of TPGDA. ....	94
Table 6. The final conversions and T <sub>g</sub> values obtained from the photopolymerization systems.....	99
Table 7. Values of final conversions of free radical photopolymerization (FRP) from TMPTA and hybrid polymerization from TMPTA and cationic polymerization (CP) from cationic monomers applied with initiators comprising S9 (0.5 wt%) and IS (1.5 wt%) upon the exposure of NIR-LED emitting at 860 nm with an intensity of 1.0 W/cm <sup>2</sup> and UDMA, respectively. Cited from[91].....	107
Table 8. Final conversions of the samples after exposure evaluated from FTIR spectra. .	111

---

## Abstract

A series of cyanines possessing varied terminal groups and substitutions were selected for the investigations into the relation between structural pattern of cyanines and their performance on initiation of free radical and/or cationic photopolymerization induced by near-infrared light, where cyanines served as photosensitizers and iodonium salts as co-initiators. The LEDs emitting between 750 nm-1000 nm exhibiting a high-power intensity of  $\geq 1.0 \text{ W/cm}^2$  were introduced for the excitation according to the absorption spectra of the absorbers. This technology of prototypes brings new impetus into the world of photochemistry under the photoinduced electron transfer (**PET**) reaction where these cyanines served as light sensitizers. The terminal patterns showed unexpectedly stronger impact than the substitutions at the main chain of the cyanines at specific positions regarding radiative deactivation by fluorescence emission and non-radiative deactivation upon exposure. A longer methine chain of the cyanine facilitates photobleaching in combination with iodonium salt. The open unbridged connecting methine chain shows higher reactivity regarding chemistry than bridged connecting chain. The terminal groups as presented by indolium, benzo[*e*]- and benzo[*g*]indolium resulted in photochemical reactions following a high efficiency to initiate photopolymerization, while benzo[*c,d*]-indolium-substitution of the terminal group favors the systems rather non-radiative deactivation facilitating to initiate thermally activated processes.

The initiator system consisting of cyanine and iodonium salt could efficiently initiate free radical photopolymerization in the monomer of **UDMA**, **TPGDA** and **TMPTA**. Surprisingly, the combination of this initiator system could also sufficiently initiate the polymerization of **4-hydroxybutyl vinyl ether**. Some cyanines based on heptamethine and nonamethine succeeded in the initiation of cationic photopolymerization using epoxides and oxetanes as monomers. In particular, a remarkably efficient initiation of cationic polymerization in hybrid photopolymerization systems based on radical and cationic photopolymerization took place, which was confirmed by the final conversions of the monomers obtained by FTIR measurement and the mechanical properties of the polymer films characterised by DMA analysis.

Furthermore, the heptamethine cyanine initiator system based on the selection, together with iodonium salt, also successfully initiated the sol-gel coatings comprising nanoparticles obtained by silanization. This led to the fact that the coated films showed a higher glass transition temperature compared to the system which were processed by UV irradiation.

---

In addition, the heat generated upon excitation from water soluble heptamethine cyanine carrying benzo[g]indolium as terminal group in coatings functioned as a novel tool for physical photonic drying, which appears much more energy efficient, can be considered as a replacement of oven-based technology. This opens a new window with highly environmentally friendly technology for the applications in coating industry. These findings also show promising potentials to design tailor-made materials/absorbers for ON/OFF process on demand.



## Kurzfassung

Eine Reihe von Cyaninen mit unterschiedlichen Endgruppen sowie Substitutionen wurde ausgewählt, um die Beziehung zwischen dem Strukturmuster von Cyaninen und ihrer Effektivität hinsichtlich der Initiierung von radikalischer und/oder kationischer Photopolymerisation, die durch Nahinfrarotlicht induziert wird, unter Verwendung von Cyaninen als Sensibilisatoren und Iodoniumsalzen als Coinitiatoren zu untersuchen. LEDs, die zwischen 750 nm–1000 nm mit einer hohen Intensität von  $\geq 1,0 \text{ W/cm}^2$  emittieren, wurden entsprechend der Absorptionsspektren zur Anregung der Absorber eingesetzt. Diese Prototypetechnologie brachte neue Impulse in die Welt der Photochemie im Zusammenhang mit dem photoinduzierten Elektronentransfer(PET), bei welchem die ausgewählten Cyanine als Sensibilisatoren dienten. Die Endgruppe zeigte einen unerwartet stärkeren Einfluss als die Substitution am Cyanin an bestimmten Positionen hinsichtlich der Deaktivierung mittels Fluoreszenz im Nahinfrarot und nichtstrahlender Desaktivierung bei Bestrahlung. Eine längere verbindende Methinkette des Cyanins erleichtert das Ausbleichen in Kombination mit Iodoniumsalz. Eine offene unverbrückte Methinkette zeigt eine höhere chemische Reaktivität als die überbrückte Methinkette. Die Endgruppen Indolium, Benzo[e]- und Benzo[g]indolium führen zu photochemischen Reaktionen mit hoher Effizienz zur Initiierung der Photopolymerisation, während die Benzo[c,d]indolium-Substitution der Endgruppe des Systems eher eine strahlungslose Deaktivierung favorisiert, welches zum Überwinden von thermisch aktivierten Prozessen erforderlich ist.

Die Kombination dieses Initiatorsystems konnte die radikalische Photopolymerisation im Monomer wie **UDMA**, **TPGDA** und **TMPTA** initiieren. Überraschenderweise konnte auch die Polymerisation von **4-hydroxybutyl vinyl ether** mit einem Initiatorsystem bestehend aus Cyanine und Iodoniumsalz ausreichend initiieren. Einige Cyanine auf Basis von Heptamethinen und Nonamethinen konnten erfolgreich, die kationische Photopolymerisation von Epoxiden und Oxetanen initiieren. Insbesondere erfolgte eine überraschend effiziente Initiierung der kationischen Polymerisation in den hybriden Photopolymerisationssystemen basierend auf einer radikalischen und kationischen Photopolymerisation, was durch die durch FTIR-Messung erhaltenen Endumsätze der Monomere und die durch DMA-Analyse charakterisierten mechanischen Eigenschaften der Polymerfilme bestätigt wurde.

Darüber hinaus initiierte das ausgewählte Heptamethin-Cyanin-Initiatorsystem zusammen mit Iodoniumsalz Sol-Gel-Beschichtungen auch erfolgreich, die Nanopartikel enthielten,

---

welche durch Silanisierung erhalten wurden. Das führte dazu, dass die beschichteten Filme eine höhere Glasübergangstemperatur  $T_g$  im Vergleich zu Systemen zeigten, die mittels UV-Bestrahlung prozessiert wurden.

Darüber hinaus fungierte die in Beschichtungen bei Anregung durch wasserlösliches Heptamethin mit Benzo[*g*]indolium-Substitution erzeugte Wärme als neuartiges physikalisches Trocknungswerkzeug, was als energieeffizienterer Ersatz in ofenbasierenden Trocknungstechnologien betrachtet werden kann. Damit öffnet sich ein neues Fenster hoch umweltfreundlicher Technologien für Anwendungen in der Lackindustrie. Diese Ergebnisse zeigen vielversprechende Potenziale, um maßgeschneiderte Materialien/Absorber zu entwerfen und für Prozesse bereitzustellen, die auf Anforderung EIN- bzw. AUS-schalten.

# 1. Introduction and Motivation

## 1.1 General Aspects

Natural macromolecular materials such as silk, wood and rubbers have been widely used in many aspects of applications for many years although the concept of polymers were later introduced by Staudinger in the early 1920s[1-3]. In the next 100 years, these materials started to dominate in this field and have played a very important role in natural sciences bringing the benefits based on their properties into different fields such as material sciences, chemistry, physics, biology and engineering as well as numerous technical applications[4-11]. Chemists have been putting their effort on the development and optimization of the synthetic conditions and procedures for macromolecular materials since these materials can be used in different circumstances due to their distinct chemical composition, physical and chemical properties, rheological behaviour and mechanical properties as well as their numerous possible architectural structures[12-17]. In the past decades, the development in this field has achieved of course big progress and success based on extensive research and exploration. During this time, photopolymerization was introduced as a new efficient technology to convert monomers into polymer materials[9, 18-21]. The first patent related to radical photopolymerization came up in 1948[22].

In the following decades, the technology of photopolymerization was introduced to synthesis respective polymer materials by using unsaturated electron deficient monomers where light-sensitive initiators generated radicals resulting in initiation of polymerization for polymers synthesis in the presence of light exposure[9, 19, 20, 23, 24]. This process represents an alternative synthetic strategy which is mostly operated at ambient conditions. Such circumstance brings the benefits of high efficiency in light-mediated technologies resulting in energy saving since the procedures are driven and controlled by light[8, 10, 25-27]. Thus, the course of the reaction can be easily controlled and stopped/terminated just by switching ON/OFF the light sources on demand[9, 28-30]. Furthermore, this technology also shows environmentally friendly aspects because it keeps the release of volatile organic compounds (VOCs) down to a negligible level during the polymerization process. This follows the worldwide goal to decrease the emission of VOCs as low as possible[31]. Photopolymerization, therefore, has been playing the most important role among the photo-mediated research in polymer sciences. Consequently, this process has been widely explored and applied in great quantities of fields such as the coating industry[10, 11, 32], dental repair and filling[33-36], holography[4, 37, 38], 2D[39, 40], 3D[7, 26, 30, 41-43] and 4D[44-47] printing including the development of the respective

inks[48-52], adhesives[53-56], photoresists[39, 40, 57, 58] and electronics[59] just to name a few examples. Recently, the combination of photonic physical drying and chemical crosslinking of aqueous dispersions in the presence of light sources was also introduced into the coating industry[8, 29, 60, 61]. As well-known, the introduction of light during photopolymerization also initiates the discussion about the utilization of heat generated in systems requesting light for processing[8-11, 20, 62, 63].

Photochemical reactions can be initiated and driven by an absorber that absorbs the excitation of light energy. The latter is generally classified based on the emitting wavelength into ultraviolet (UV) light, visible light and near infrared (NIR) light[64-67]. It also requires a certain output of energy by the light sources applied to excite the light sensitive materials to initiate photopolymerization process. The photochemical reactions start from the first excited singlet or triplet state of the initiator molecules. The latter can only convert this part of radiation released by the excitation source overlapping with its absorption spectrum. This part of radiation absorbed contributes to generate reactive species for the initiation of light-mediated polymerizations, which can be proceeded by radical[18, 19], cationic[68-72] and a mechanism requesting a base[73-76]. In the past 30 years, UV-induced photopolymerization systems have been dominated technologies in numerous branches due to its fast development[56, 77-79]. There are a series of well-operated equipments such as mercury lamps[80, 81] and LEDs[79, 80] fitting well with UV lights and those have been widely used in both industry and academic laboratories.

Meanwhile, there also exist the most well developed compounds available such as photo-initiators initiating directly photopolymerization by generating a reactive species such as free radicals, conjugate acid or base. This often requires to cleave a bond, which can proceed up to 400-500 nm depending on the respective bond dissociation energy[82-84]. In parallel, light sensitive systems based on the combination of sensitizers absorbing the light energy with initiators were introduced into the field[85-87]. Here, photoinduced electron transfer (**PET**) results in generation of initiating radicals and in case of an oxidative mechanism conjugate acid[6, 88, 89]. This works well up to 900 nm, which was developed partly in this thesis[90, 91]. This example demonstrates that the system can be divided into two systems Type I and Type II initiating systems[13].

However, UV-induced systems also demonstrate several shortcomings due to the utilization of those light sources emitting UV light. Firstly, the disadvantages of mercury lamps should not be ignored because of the issues to release ozone into the ambience in such systems, because it becomes more and more urgent for the society to protect the

environment[92]. Additional problem exists in their short life cycle of some thousand operational hours requesting a special handling of the mercury waste[93]. Moreover, a large amount of radiation generated by mercury lamp is not absorbed by the sensitizers or initiators resulting in energy wasting due to its broad emission spectra. These facts initiated in the EU commission to prohibit the use of mercury-comprising devices[94]. Fortunately, there have been existing several alternatives. LEDs exhibiting an emission spectrum with peak maximum in UV and blue range facilitate to enable this technology with higher efficiency to save energy and to reduce the aforementioned environmental issues[95, 96]. In addition, the higher effect of scattering coefficient of UV light disables deep penetration of the light exposure into the samples, thus, the UV-mediated system fails to form polymer materials with large curing thickness[97]. This can be improved by shifting the absorption wavelength of the absorbers/sensitizers into visible (Vis) or near infrared (NIR) range[11, 20, 98, 99]. Here, only Type II systems are disclosed. The energy absorbed in the NIR is not sufficient for direct bond cleavage. Absorbers can be seen as the compounds that absorbs energy between 300-1700 nm. Sensitizers connects to the functionality in a sensitizing mechanism proceeding in a similar wavelength region. Sometimes compounds absorbing over 400 nm were named as dyes[100]. This is supposed to relate specially to the visible range between 400-700 nm[100].

In the past decades, the development of a photopolymerization system excited by visible light (400-700 nm) has achieved significant progress due to its capability of deeper penetration with longer emission wavelength[58, 99, 101, 102]. These systems also exhibited sufficient sensitivity but their use often requested to operate under red light condition to prevent pre-exposure during sample preparation[103]. This can lead in daily handling to depression of the user with such systems. Here, NIR-sensitive systems have received increasing attention[104-106] because their tolerance to visible light in combination with special light sources releasing only a small fraction of NIR has brought such systems into the printing market in the late 1990s[39, 107, 108]. Furthermore, light-mediated photopolymerization facilitates processing of larger curing thickness because the scattering coefficient decreases with increasing wavelength[97, 105]. Nevertheless, this technology did not gain big success compared to other systems since the lower photon energy of NIR light (> 800 nm) as well as insufficient efficiency for photopolymerization sensitization limit its development in several practical applications[109, 110]. It started to grow up in the technologies in the graphic industry from the 1990s since it was introduced for digital imaging to pattern lithographic plates[39, 40, 57, 58]. Such system has received

increasing attention and significant development especially in the production of Computer to Plate (CtP) systems using lasers as excitation source[39, 40, 57, 58].

Recently, research about photopolymerization in the presence of cyanines as light absorbers/sensitizers applying high-power NIR-LEDs (> 750 nm) as light source for the excitation has brought new impetus into this field[102, 111-113]. These procedures can be achieved with a two components initiator system namely a Type II initiator where excitation of the sensitizers results in population of its first excited singlet state after absorption of NIR light. Thus, the excited absorbers are able to sensitize the co-initiators added to generate species such as radicals and conjugated acid for efficient initiation of both free radical and cationic photopolymerization reactions following the mechanism of **PET** process[19, 114, 115]. During this procedure, a large amount of heat needed to overcome an internal activation barrier can be also generated via non-radiative deactivation[90, 116-118]. It is a very efficient way to generate heat on demand[11, 90, 119]. Thus, the heat formed in these systems can be seen of great interest and has been widely used in some new applications such as drying of printing inks[48, 50], NIR laser welding[120], and thermally triggered chemical reactions[121-124].

Such NIR absorber-comprising systems also show huge potential to generate heat for the application of physical drying of coatings or waterborne dispersions under respective light exposure[60, 61]. Furthermore, those NIR-sensitizers combined with co-initiators especially diaryliodonium salts appear increasingly interesting to initiate the photocuring/solidification of the systems comprising inorganic components such as sol-gels[125, 126], which still remains undisclosed based on our best knowledge. Nevertheless, partial studies based on heptamethine cyanines were recently investigated regarding the initiation reactivity of both free radical and cationic photopolymerization in such systems applying high-power NIR-LEDs emitting at either 805 nm, 820 nm or 860 nm[27, 91, 118]. However, there still exists open questions related to their behaviour in activated **PET** process of these NIR-light sensitive compounds[20, 88, 90, 118]. There is no clear understanding and comprehensive disclosure regarding the relation between the structural patterns and their performance in both photochemical and photophysical point of view. Surprisingly, such systems exhibit completely different efficiency and reactivity although they share the similar photophysical properties demonstrating similar oxidation ( $E_{ox}$ ) and reduction ( $E_{red}$ ) potentials values[90]. Therefore, such NIR sensitised photopolymerization systems can be seen still in its infancy[11, 20].

In a matter of fact, the terminal group of cyanines varies typically among benzo[*e*]-, benzo[*g*]-, benzo[*c,d*]- and indolium and the length of polymethine chain connecting the terminal structures differs from tri- to sometimes nonamethine while the substitution at other positions on the molecular skeleton offers much more possibilities to change the structural pattern[90, 91]. Furthermore, there still exists a lack of optimal structural selection of the cyanines regarding both radiative deactivation and non-radiative deactivation. Some of them work well in an activated **PET** protocol while some others result in insufficient reactivity confirmed by kinetics measurement and evaluation[9, 14, 20, 115, 118, 127]. The NIR absorbing cyanines exhibit significantly distinguished efficiency for the participation of photochemical reactions and heat generation[90, 91]. The characterization of photophysical properties (fluorescence emission maximum  $\lambda_{f_{max}}$ , quantum yield  $\Phi_f$  and decay time  $\tau_f$ ) of those cyanines provides a deeper insight into the impact of the structural patterns[88, 90]. This also helps to target the compounds whether it mainly contributes to radiative deactivation and activated **PET** chemistry or non-radiative deactivation processes resulting in release of heat into the surrounding matrix[20]. This also addresses the challenge to design tailor-made cyanines from a synthetic point of view[128]. These synthetic works also lead to produce NIR-absorbing materials exhibiting acceptable shelf-life in practical photopolymer systems applied in industry[39, 40].

Previous studies reported the success of such systems for the initiation of cationic photopolymerization using oxiranes, and oxetanes as reactive monomers[27, 126, 129]. These investigations did not put the focus on the economically easier available anion  $[(CF_3SO_2)_2N]^-$  (**[NTf<sub>2</sub>]**<sup>-</sup>), which shows excellent solubility in numerous monomers[130]. A big advantage can be seen in the easier availability due to its use in battery systems and features of no issues to release **HF** under certain circumstances[131, 132]. In addition, these NIR absorber-comprising systems provide a novel strategy to generate heat while the redox potentials facilitate **PET** by the heat released by the absorbers. This only efficiently works in combination with high-power NIR-LEDs controlling ON/OFF by a click without a warm up of the systems as requested in oven driven process. It addresses the advantages of high efficiency and energy saving compared to conventional methods such as oven-based technologies[29, 133]. This heat released by the NIR absorbers can be seen as great potential for applications relating to efficient thermal triggers or drying on demand.

## 1.2 Motivation of the Thesis

Photoinduced polymerization processes have been leading as strategy widely used in plenty of fields in chemical industry[5, 7]. Many applications used in different fields would not exist without the use of photopolymerization. In recent decades, NIR-sensitized systems were already introduced into both scientific research and industrial applications in the graphic industry with the focus on CtP technology[39, 40]. However, there still lacks fundamental knowledge about NIR-sensitized polymerization. This thesis contributes to bring more light into this field[90, 91]. Furthermore, the longer wavelength of NIR light facilitates deeper penetration due to less scattering[97] into the samples resulting in the feasibility to prepare materials with larger curing thickness. This can be seen as a big benefit compared to UV-based systems because it also enables to embed UV and blue absorbing additives[102].

Photopolymerization as light-operating technique switches the process ON/OFF on demand which can be seen as a huge economic benefit in industrial manufacturing[102, 134]. Its optical aspects appear more friendly to the users[99]. Furthermore, the necessity to take energy consumption into consideration in industrial processes appears more and more urgent due to the current situation in the whole world. Therefore, it is essential to find alternatives which represent energy saving and environmentally friendly techniques on the one hand while sustainability additionally possesses a crucial role to replace traditional high energy consuming technologies and equipments such as ovens or environmentally issue causing mercury lamps[94].

Interestingly, NIR light-mediated photopolymerization still focuses on continues wave (*cw*) lasers demonstrating big progress of successful applications regarding development of digital imaging technologies such as CtP systems in the past years[40, 58]. Here, the exposure of a pixel exhibiting a size of  $20 \times 20 \mu\text{m}$  requests an exposure time in the  $\mu\text{s}$ -timeframe[40, 57]. This can be seen as a big effort but this technology possesses much more potential. Thus, the NIR-induced polymerization process was also successfully applied to the solidification of powder coatings which appears potential to replace huge energy consuming oven technology[8]. This is a big breakthrough to introduce energy saving technologies in high-energy consuming manufacturing processes.

This requires to deliver effective operating NIR-absorbers. Here, the NIR-induced photopolymerization comprising heptamethine-based cyanines as light absorbers has brought 'fresh blood' into this field[20, 60, 61, 118, 126]. These cyanines operate as sensitizers and their combination with diaryliodonium salts serving as initiators following a mechanism of



activated **PET**, which has brought application potential and room for new scientific discussions of **PET** after the Nobel Prize to R. Marcus in 1992[135]. Nevertheless, the fundamental knowledge of such systems has not been well understood and investigated compared to UV-induced systems. The large availability of distinct structural patterns of cyanine sensitizers distributes sometimes no clear understanding and disclosure regarding the relation between the structures of cyanines and their performances as well as the selection on demand[20, 90]. Although some reactivity studies of heptamethine-based cyanines serving as sensitizers focused to initiate photo-polymerization, results obtained demonstrate different efficiency from distinguished structures of cyanines[88, 105, 111, 118, 136]. There were no clear structural concepts regarding the design of cyanines for NIR-sensitized photopolymerization. This thesis brings more insight into the field of NIR-sensitized photopolymerization regarding the selection of the structures[27, 90, 91].

Furthermore, it is well known that the conversion of the excited state of cyanines into its respective ground state connects to an excessive release of heat into the environment caused by internal conversion[118, 137, 138]. This proceeds on demand by turning on this light source. It may be seen as beneficial thermal energy source for systems requesting both thermal triggering of chemical and physical reactions. The latter may relate to physical processes such as removal of solvent by evaporation[29]. This can be physical drying of dispersions[60, 61]. Nevertheless, the impact of the distinguished structural patterns of cyanine sensitizers on their efficiency of heat generation and initiation of photopolymerization has not been well understood[20, 90]. Additionally, the function of the heat formed in such systems combined with high-power NIR-LEDs may be also seen as efficient source for industrial applications such as physical drying of coating systems as replacement of conventional oven technology, which deserves more detailed exploration.

Furthermore, the iodonium salt coupling with the anion  $[\text{NTf}_2]^-$  exhibiting no issues to release **HF**[132] shows excellent solubility in different monomers. These features have enforced to explore and develop novel systems comprising components which shows more environmentally friendly and easier access by synthesis although it resulted in insufficient reactivity to initiate cationic photopolymerization in the previous report[91]. The  $[\text{NTf}_2]^-$  anion may also not fit into the PFAS issue introduced by the EU to prohibit the use of material exhibiting a  $\text{CF}_3\text{-C}$  pattern[139]. Here, fluorinated aluminates such as the  $[\text{Al}(\text{O}-t\text{-C}_4\text{F}_9)_4]^-$  anion would match in this definition. This anion was evaluated to exhibit the best performance in both radical and cationic NIR-sensitized photopolymerization[27]. Consequently, there exists a certain demand to develop alternatives for which the  $[\text{NTf}_2]^-$

anion addressed some challenges. This thesis showed feasible routes to incorporate this anion even in cationic polymerization although first studies failed.

Further motivation of this thesis focused to explore the relation between structural patterns of the cyanines and their photophysical properties as well as photochemical performance enabling activated **PET** for the initiation of photopolymerization. Therefore, this thesis investigates how the structural patterns of cyanines affect the efficiency to generate initiating moieties such as radicals and conjugate acid upon exposure in the NIR range between 750 nm and 1000 nm with respect to the optical absorption of the compounds to initiate free radical and cationic photopolymerization, respectively, where the cyanines operated as photosensitizers and iodonium salts functioned as co-initiator. Thus, the selection of these sensitizers enables sufficient overlap of wavelength from their absorption and the emission of the available LED sources in the NIR range to incorporate the functional monomers absorbing in both UV and visible range. The NIR-sensitized systems comprising heptamethine cyanines were already introduced into the industrial application such as lithographic printing plates following a radical photopolymerization process[39, 40, 57, 58]. Nevertheless, their use in coating applications can be still seen in its infancy. This thesis brings more insight regarding the selection of structural pattern of the cyanine and its contribution in the activated **PET** protocol[11, 20, 29, 66, 118, 127].

Thus, the aim of this thesis is to comprehensively disclose and understand the impact of the structure of cyanines functioning as sensitizers in combination with co-initiators. The cyanine sensitizers exhibited distinct terminal moieties, namely indolium, benzo[*e*]-, benzo[*g*]- and benzo[*c,d*]-indolium. A further structural feature is the *meso*-position carrying different substitutions such as barbiturate, chlorine, phenyl, diphenyl(amino), phenyl-(mercapto)triazole. They had a different impact on the activated **PET**[11, 20, 29, 66, 118, 127]. Moreover, a distinguished length of polymethine chain including tri-, penta-, hepta- and nonamethine between the terminal groups were introduced for the investigation. This bridge can be either open or connect by methylene groups to restrict rotations. In this thesis, the properties regarding fluorescence emission ( $\lambda_{\text{max}}^f$ ,  $\Phi_f$ ,  $\tau_f$ ) of the sensitizers were investigated to provide a deeper insight into the contribution of the radiative and non-radiative deactivation from a photophysical point of view, which could hopefully bring a more clear understanding into this field as well as the rational selection for initiators based on the structures of cyanines[90]. Moreover, electrochemical studies complement the pattern regarding the level of the HOMO and LOMO of the cyanines derived from the oxidation and reduction potential, respectively.

The efficiency of such combinations of photoreactive compounds to generate radicals and conjugate acid was also evaluated via exposure. Results obtained demonstrated an efficient initiating system for both free radical and cationic photopolymerization under exposure by NIR-LEDs. The photopolymerization reactivity and mechanical properties of the polymer films obtained by NIR irradiation were compared to that in UV-initiated systems[27, 66]. This comparison brought a clearer pattern into this field particularly to compare this new technique with traditional UV-curing. Nowadays, there has existed nearly no fundamental knowledge regarding the photochemistry in **PET** systems using the cyanines explored in this thesis. This work builds some bridges to reduce the uncertainties in this field.

Furthermore, the heat generated upon excitation from water soluble heptamethine based cyanine in coatings functioned as a novel tool for physical drying considered as a replacement of oven technologies[10, 29, 60, 61, 119]. This opens new doors in high-energy consuming technologies to establish environmentally friendly technologies for applications in coating industry. These findings show the potential to design on demand tailor-made materials/absorbers. There exist widespread ideas about the generation of heat in such NIR absorbing systems. The selection of structural patterns chosen helps to find some answers.

In addition, the introduction of functional nanoparticles into the neat systems resulting in sol-gels can be expected to improve the mechanical properties of the polymer materials[125, 140] obtained via photopolymerization on the one hand. Nanoparticles or other fillers can cause scattering of excitation light during exposure on the other hand[137]. Other inorganic materials can also exhibit an intrinsic absorption and would operate as internal filter materials. In this case, the NIR-sensitized system appears beneficial to decrease the scattering due to the less scattering coefficient at longer wavelength compared UV systems[97, 105, 111]. This thesis showed opportunities to enable NIR-sensitized radical and cationic photopolymerization in such sol-gel systems, which has not been disclosed yet.

The results aforementioned demonstrate parts of this thesis while most of those were already reported in the following publications and patents. Results were also represented at national and international conferences with peer review system.

Publications as First Author:

1. Q. Wang, S. Popov, V. Strehmel, J. S. Gutmann and B. Strehmel, "NIR-Sensitized Hybrid Radical and Cationic Photopolymerization of Several Cyanines in Combination with Diaryliodonium Bis(trifluoromethyl)sulfonyl imide", *Polym. Chem.*, **2023**, 14, 116-125. Selected with Front Cover from the editor based on the reviews.
2. Q. Wang, S. Popov, A. Feilen, V. Strehmel, and B. Strehmel, "Rational Selection of Cyanines to Generate Conjugate Acid and Free Radicals for Photopolymerization upon Exposure at 860nm", *Angew. Chem. Int. Ed.* **2021**, 60, 2–13; "Rationale Auswahl von Cyaninen zur Erzeugung von konjugierter Säure und freien Radikalen für die Photopolymerisation durch Belichtung bei 860 nm", *Angew. Chem.* **2021**, 51, 27059 – 27070. Selected as VIP Paper with Front Inside Cover from the editor based on the reviews.

Publications as Co-author:

1. Y. Pang, S. Fan, Q. Wang, D. Oprych, A. Feilen, K. Reiner, D. Keil, Y. L. Slominsky, S. Popov, Y. Zou, B. Strehmel, "NIR-Sensitized Activated Photoreaction between Cyanines and Oxime Esters: Free-Radical Photopolymerization", *Angew. Chem. Int. Ed.* **2020**, 59, 11440 – 11447; *Angew. Chem.* **2020**, 132, 11537 – 11544, Contributed with Polymer Characterization.

Patents:

1. L. Appelhoff, Q. Wang, B. Strehmel, Farblose Oberflächenbeschichtung, DE2021032211455000, Niederrhein University of Applied Sciences, DE, **2021**, Contributed with Coating Preparation.
2. V. Strehmel, B. Strehmel, M. Kepkow, M. Heinz, Q. Wang, J. Prieto, M. Prieto, Verfahren zur Beschichtung von harten Oberflächen mit Pigmentfilmen, EP23174116.6, Lignocolor GmbH, EP, **2023**, Contributed with formulation and photocuring of coating systems.

Conference Contributions as Oral Presentation:

1. Photopolymerization of Aqueous Dispersions and Solvent Free Coatings Comprising Nanoparticles with Photonic Technique of NIR radiation, Q. Wang, B. Strehmel, RadTech China 2023, Yixing, China, 18-21 July, 2023 (accepted).

2. Photophysical Properties and Photochemical Performance of Cyanines Enable Activated Photoinduced Electron Transfer to Initiate Photopolymerization between 700-1100 nm, Q. Wang, B. Strehmel, French, Swiss and German Conference on Photochemistry, Photophysics and Photosciences (CP2P'23), Mulhouse, France, 15-17 May, 2023.
3. Photocuring of Aqueous PU Dispersions and Solvent Free Systems Comprising Nanoparticles with a New Photonic Drying Technique Based on Radical and Cationic Polymerization, Q. Wang, S. Popov, B. Strehmel, European Coating Show (ECS 2023) Conference, Nürnberg, Germany, 27-28 March, 2023.
4. Pattern of Cyanines Regulates Initiation Efficiency of Radical and Cationic Photopolymerization with Iodonium Salt by Excitation between 750-900 nm, Q. Wang B. Strehmel, 7<sup>th</sup> European Symposium of Photopolymer Science (ESPS), Istanbul, Turkey, 19-22 September, 2022.
5. Pattern of Cyanine Controls Photopolymerization in NIR, Q. Wang, B. Strehmel, S. Popov, 28<sup>th</sup> PhotoIUPAC, Amsterdam, Netherlands, 17-22 July, 2022.
6. Structural Selection of Cyanines Combined with Diaryliodonium Salt to Generate Conjugate Acid and Free Radicals for Photopolymerization in NIR Range (860 nm), Q. Wang, B. Strehmel, Central European Conference on Photochemistry (CECP 2022), Bad Hofgastein, Austria, 13-17 February, 2022.
7. Rational Design Based on the Relation between Structural Pattern of Cyanines and Their Efficiency to Initiate Free Radical and Cationic Photopolymerization upon 860 nm, Q. Wang, B. Strehmel, 22<sup>nd</sup> RadTech China, Tianjin, China, 27-29 September, 2021
8. Photocuring of Nanoparticle-Based Coatings via Near-Infrared Sensitised Free Radical and Cationic Polymerization, European Coating Show (ECS 2021) Conference, Online, 13-14 September, 2021.

*Conference Contributions as Poster Presentation with Flash Talk:*

1. Photocuring of Nanoparticle Comprising Coatings Based on Heptamethine Cyanines with NIR Exposure between 800-1000 nm, Q. Wang, B. Strehmel, 84. Lacktagung, Würzburg, Germany, 14-16 September, 2022.
2. Structural Effects of Cyanines Combined with Diaryliodonium Salt to Initiate Free Radical and Cationic Photopolymerization between 750-1000 nm, Q. Wang, S. Popov, B. Strehmel, GDCh MAKRO 2022, Aachen, Germany, 12-14 September, 2022.

3. Relation between Structural Pattern of Cyanines and Their Efficiency to Initiate Free Radical and Cationic Photopolymerization, 6<sup>th</sup> virtual European Symposium of Photopolymer Science (vESPS), Online, 15-17 June, 2021.

Conference Contributions as Poster Presentation:

1. Photocuring of Nanoparticle Comprising Coatings Based on Heptamethine Cyanines with NIR Exposure between 800-1000 nm, Q. Wang, B. Strehmel, European Technical Coatings Congress (ETCC 2022), Krakow, Poland, 12-14 July, 2022.
2. Near-Infrared Sensitised Free Radical and Cationic Photopolymerization between Cyanines and Iodonium Salt and Potential Applications, Q. Wang, B. Strehmel, 23<sup>rd</sup> GDCh JCF-Frühjahrssymposium, Online, 29 March-1 April, 2021.

## 2. State of Art in the Field of NIR-Sensitized Photopolymerization

The technology of photopolymerization has obtained significant attentions and has been widely introduced into both academic research and practical processes in industry in the past decades based on its beneficial features[141-145]. It is distinctly noted that the essential aspects of light sources and photoinitiating systems could be very well incorporated for the applications[65, 115, 124]. The species for the initiation of photopolymerization are generated of the initiators via photochemical decomposition often following a Norrish I cleavage[82, 83] after absorbing energy upon light. Therefore, many efforts and improvements focused on the design and development of photoinitiator compounds exhibiting higher efficiency with large selections for distinct systems and applications. Meanwhile there are also novel light sources based on LEDs and semiconductor lasers with emission in the NIR opening more and more feasibilities such as multi-wavelength availability for excitation with higher and adjustable output intensity, portability for specific occasions and improved safety for the users and environment as demonstrated for up-conversion nanoparticles[146-148]. Furthermore, the investigations on photochemical processes and initiating mechanism also provide deeper insight into such systems. This chapter summaries the state of the art about the fundamentals of NIR-sensitized photopolymerization.

### 2.1 Requirements for Light Sources Needed for Photopolymerization from UV to Near-Infrared Range

As aforementioned noticed, the choice of the appropriate light sources are significantly vital for the application of photopolymerization. Thus, they are supposed to show sufficient overlap on the emission wavelength with the absorption wavelength of the initiator or sensitizer as well as to provide efficient energy to excite the initiator molecules and penetrate into the sample systems for the further trigger of photochemical reactions[65, 149, 150]. As depicted in **Figure 1**, the electromagnetic radiation regarding the light sources for irradiation locates in the wavelength from 100 nm to 1200 nm, although the term 'optical radiation' refers to 100 nm to 1 mm[151]. Conventionally, the electromagnetic radiation is classified based on the wavelength into ultraviolet (UV) light including UV-C (100-280 nm), UV-B (280-315 nm) and UV-A (315-400 nm), visible light (400-700 nm) and near infrared light (700-2000 nm)[151, 152]. The term 'visible light' refers to the perception of the light to the human eyes and how the eyes feels about it. Thus, the physical range of NIR typically starts at 700 nm while the human eyes still feel to see red light. This explains

why some references define the range of red light up to 780 nm. Therefore, literature often does not strongly distinguish between physical range and physiological feeling by the human eye[153]. Furthermore, the infrared light shares a broader wavelength range between 700 nm to 1 mm[151].

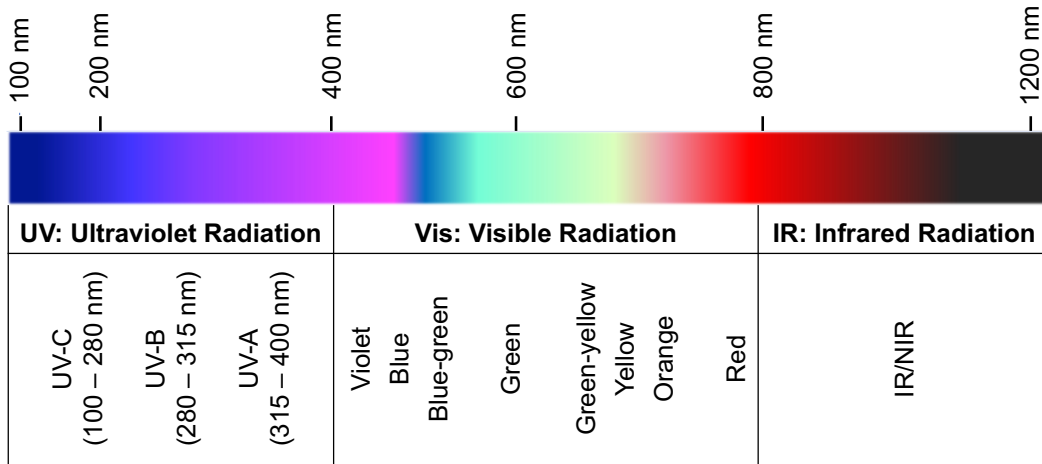


**Figure 1.** Summary of the absorption for materials covering from UV to NIR range, modified from[151, 154].

The light sources emitting UV, visible and NIR light are widely used for the photochemical systems such as photopolymerization, photocatalytic reactions and phototherapeutic applications in medicine[155-158]. According to the Equation (1) and **Figure 2**, the light of longer wavelength exhibits lower photonic energy and less scattering coefficient. Thus, the radiation energy could be more deeply penetrated into the samples when exposed by the light sources emitting longer wavelength.

$$E = \frac{h \cdot c}{\lambda} \quad (1)$$

Therefore, this outstanding feature of NIR light shows the potential to fabricate polymer materials with a larger photocuring thickness among the photopolymerization systems applying distinct light sources, followed by visible and UV light, respectively[97, 99, 105]. As a result, there are more and more research interests moving the focus onto the systems of longer wavelength considering both chemical and electronic aspects[99, 159, 160]. Particularly, the NIR-sensitized photopolymerization systems have obtained increasing attention in fundamental investigations such as design and development of novel respective initiator systems[104, 118, 136, 161] and practical applications such as in coating industry[29, 48, 101].



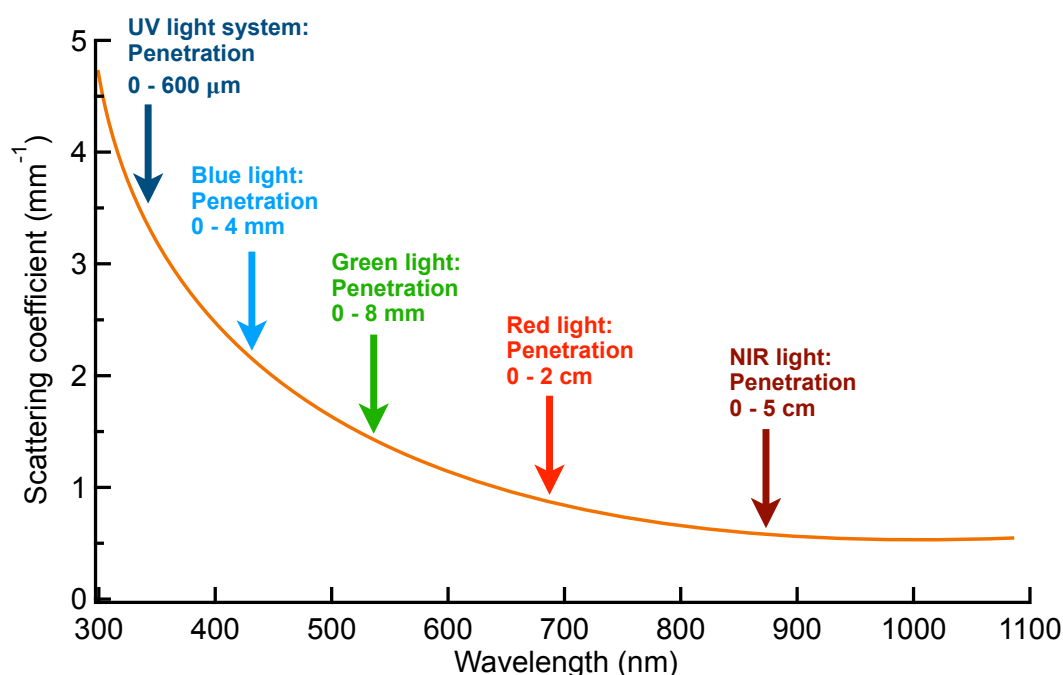
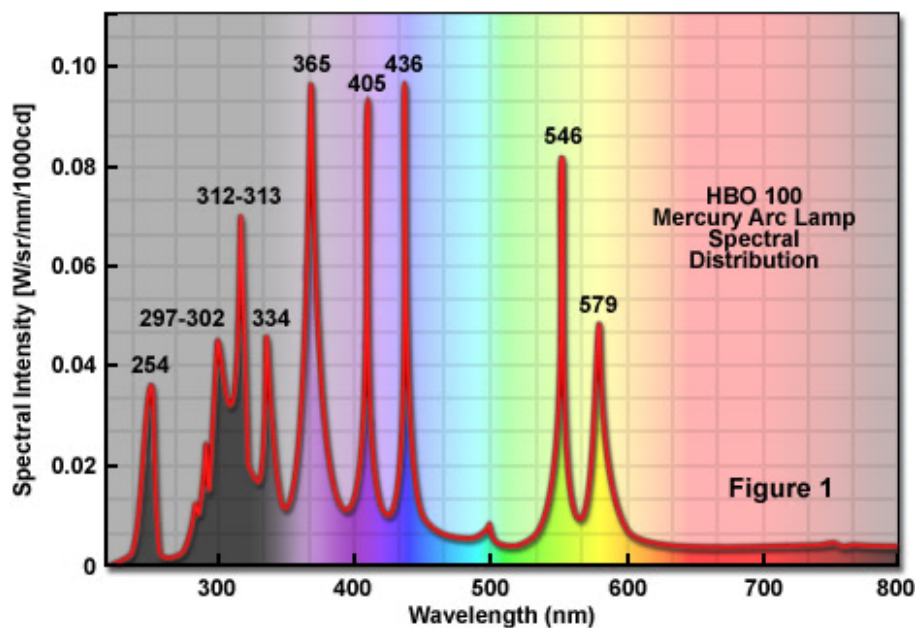


**Figure 2.** Emission wavelength dependence of the scattering coefficient, modified from [97, 105].

### 2.1.1 Mercury Lamps for Photopolymerization

The occurrence of mercury lamp has showed its great contribution for the development of photochemical sciences and technologies particularly photopolymerization [162]. Mercury lamps exhibit excellent brightness compared to conventional incandescent lamps. They can provide the intense illumination over selected wavelength throughout visible spectra region combined with appropriate filters [163]. As depicted in **Scheme 1**, the mercury lamps mostly cover a broad and strong spectral region in UV which appears at 254 nm in UV-C, 313 nm, 365 nm as well as availability at 300 nm and 334 nm, and additionally in visible light wavelength at 405 nm and 436 nm, which is essential for the photochemical and photopolymerization systems. Higher wavelengths available in the visible region did not play a major role in photopolymer systems. Nevertheless, mercury lamp has dominated in these fields for many applications as conventional light source for a long time with these significant features of multiple emission wavelength feasibility [164].



**Scheme 1.** Emission spectra of high pressure mercury lamp, cited from[163].

Mercury lamps are classified into high, medium and low pressure mercury lamps, respectively[164]. In particular, the medium-pressure mercury lamp presents the wavelength from 200 to 600 nm, which provides the feasibility of utilization in efficient systems comprising multi-components initiators or absorbers[81]. Therefore, they were widely used in industries and selected for the applications of photopolymerization to fabricate the photopolymer materials exhibiting a of thick layer[80], or optical fibre via photografting[165].

However, there are also some 'hard to neglect' disadvantages associated with mercury lamps despite their high efficiency and great contributions. For instance, the devices performed numerous loss of intensity up to more than 50% in a working period of approximately only 1000-2000 hours and significant limitation of spatial variation and temporal stability as shown in **Figure 3** below[163]. This addressed the necessity to design photosensitive systems tolerating these changes within the life cycle of a mercury lamp.



**Figure 3.** Image of the alignment of mercury conveyor from Heraeus with integrated microwave lamp.

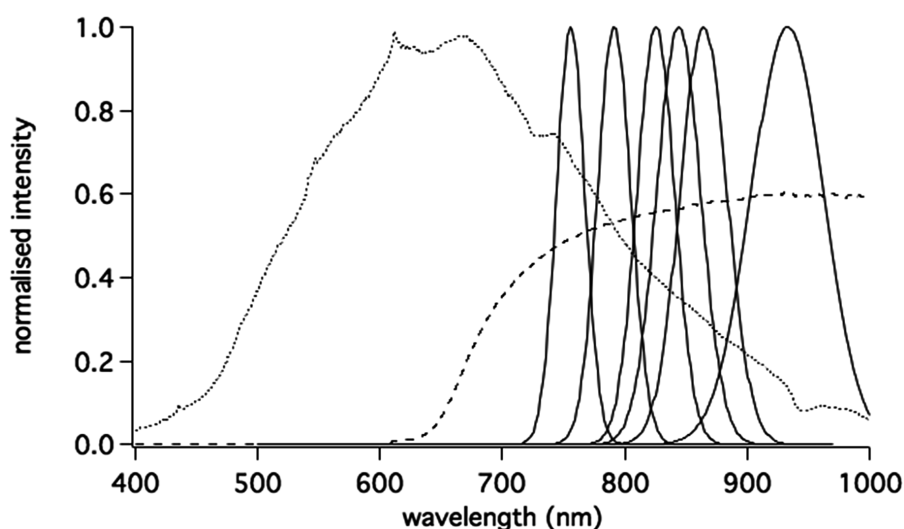
Furthermore, such equipments also bring huge concerns to the society regarding health of users and environmental issues particularly the release of hazardous substances such as ozone and the fact that they comprise mercury[92, 166]. In addition, the committees in the department of energy in the USA and the European commission have already published their decision to prohibit the utilization of mercury-comprising devices with the intention to protect the users' health and environment[92, 167]. Therefore, there exists urgent need to develop replacement of novel devices with the features of high working efficiency, easy operation procedures, low maintenance costs and of course easier feasibility to distinct working circumstances. Fortunately, we move into the period switching from mercury lamps to LEDs in recent years.

### **2.1.2 LEDs for Photoinitiating Polymerization between 250-1100 nm**

The development of light-emitting diodes (LEDs) can be seen as a big jump of progress to use such light sources in practical applications since their first production in 1960s. Such devices are nowadays available as ultraviolet (UV), visible and near-infrared (NIR) LEDs[168]. The remarkable advantage of LEDs is the capability to obtain the light sources with tailor-made emitting wavelength from deep UV to visible range based on distinct combination and doping of the crystal and electrical materials[169]. Their use requires efficient absorption of the light sensitive compounds used in the photochemical processes while the emission often appears in a limited fraction of the wavelength range. As a result, there exists a huge availability of respective efficient absorbers and light sensitive substances fitting in this range[66, 90, 170-172]. Therefore this feature of the LED devices

appears as an excellent alternative. Meanwhile, the significant higher average lifetime ( $\approx 50000$  hours) and output stability of the LEDs also show as significantly beneficial compared to mercury lamp[169].

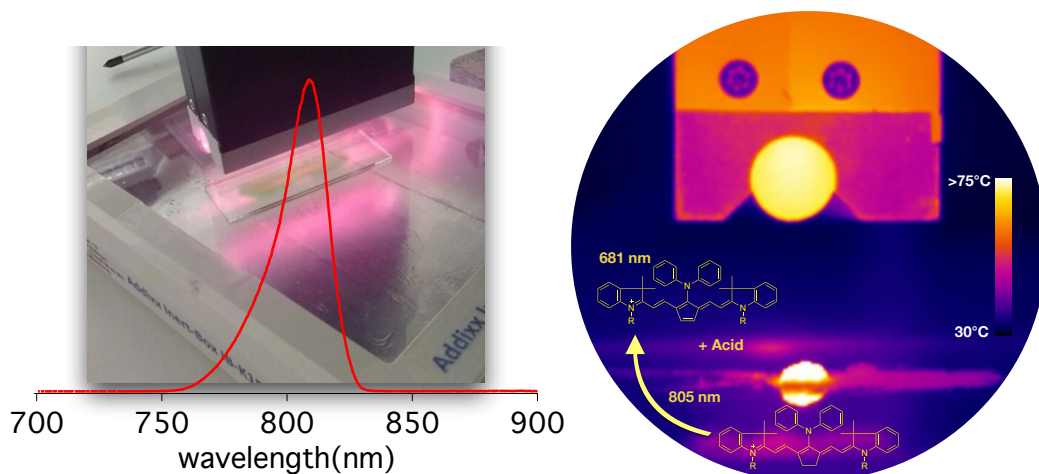
Particularly, the instant ON/OFF working mode without any necessary warming up process has brought LEDs into the industrial fields such as inkjet printing, adhesives, printed circuit boards (PCB) and photoresists[7, 40]. Recent investigations found that the radiation using UV-LED with high intensity enables the fabrication of photopolymer materials with deep curing depth via achieved deep penetration[79]. In general, the development of LEDs demands adjustable intensity and feasibility of flexibility for working with spatial variation. On the other hand, the capability of deeper penetration of visible light brings it into the applications such as dental curing and photodynamic therapy[147, 173]. Moreover, the design and development of novel NIR-LEDs have also received increasing interests and attention as shown in **Scheme 2**, although they are still not widely distributed compared to UV and visible LEDs. Therefore, it still appears a lack of development of efficient initiator systems which are suitable in NIR range.



**Scheme 2.** Emission spectra of the NIR light sources, cited from[9].

Recently, it obtained big success to develop high-power NIR-LEDs, which received a lot of attention[118]. Such devices exhibit the capability to operate at longer wavelength enabling deeper penetration of excitation light into the sample during exposure. An additional benefit can be seen in the much higher intensity that promotes to overcome internal activation barriers in **PET** protocols[127]. Furthermore, the photothermal dual working function of these systems enables more probability for applications in the future[174]. As shown in **Scheme 3**, the emission band of NIR-LEDs appears narrow, this indicates a system of higher efficiency of photonic energy absorption by the samples[20, 118]. The

lower scattering coefficient from longer wavelength shows better compatibility with other components such as fillers and additives[97]. In addition, the utilization of NIR light in combination with specific absorbers and sensitizers exhibits great potential for phototherapeutic applications and photopolymerization combined with respective co-initiators[147, 155, 175, 176].

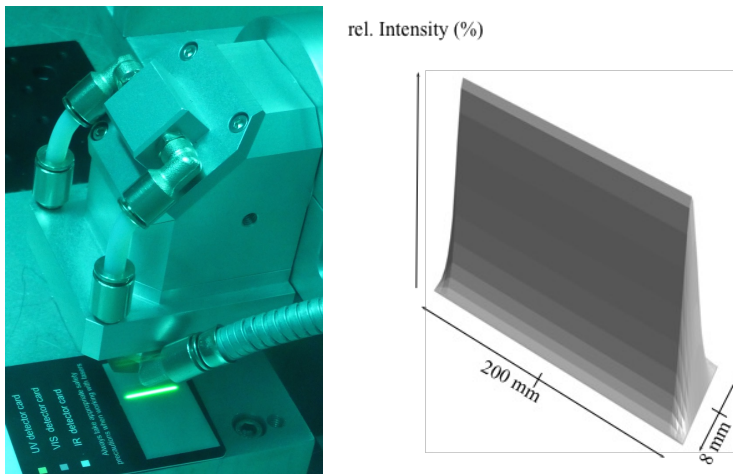


**Scheme 3.** Profiles (left) of high-power NIR-LED emitting at 805 nm and the temperature surrounding the working circumstance of it (right), cited from[118, 154].

### 2.1.3 Lasers for Photopolymerization Based on the Excitation in NIR Range

Lasers have received as a type of light source increased interest in technical applications. These devices presenting the distinct features of a radiation source of spatial coherence of emitted light are typically available with continuous-wave (*cw*) mode while application of pulsed lasers is rather rare in technological applications requesting a high throughput. Here, lasers with line-shaped focus have obtained attention after their first introduction for laser drying of offset printing inks in the graphic industry[177]. The biggest challenge to create such devices was to convert gaussian intensity distribution of a laser spot into a line with almost similar intensity as shown in **Scheme 4**. This line can have width of several dozens of centimeters[178]. These devices emit light through a process of optical amplification based on the stimulated emission of electromagnetic radiation. It facilitates the light to directly expose to a focused spot or spatially modulated line[178]. Thus, lasers were introduced to the applications of laser cutting, lithography and pattern the transparent conducting oxide (TCO)[179]. This enables a strong output radiation intensity on the working spots, which also requires a necessary security protection for the users during the operation. As a result, the lasers are expected to be applied into 2.5D surface shaping, thin film patterning, hole drilling and engraving[179] as well as welding and marking[57, 120], photocuring and physical drying of coating systems as a replacement of conventional oven

technology[10, 29]. Nowadays, these lasers with line-shaped focus preferentially emit in the NIR depending on the specific design between 930-1050 nm. In contrast to LEDs or mercury lamps, the emission monochromatically proceeds at one wavelength.



**Scheme 4.** Line-shape focused laser with emission at 808 nm and 980 nm (left) with the respective intensity profile (right) visualized by up-converting phosphorescent material, cited from[154].

Therefore, the emitted wavelength and of lasers can be adjusted or modified via doping and a combination of specific crystal materials resulting in different output energy and wavelength[177, 180]. On the other hand, pulsed-mode lasers provide significant higher output in the pulses generated in a distinct interval. This would certainly bring benefits particularly to applications where high energy delivery for excitation is needed. This also requests specific alignment in daily handling which can often be operated by well trained personal. Therefore, they show limited application in some production although they are able to bring higher output of energy[180]. On the other hand, *cw*-lasers appear with the advantages to make the exposure and energy distribution more uniform as a competitive alternative[124, 181, 182]. They also facilitate easier handling connected with less maintenance costs. As aforementioned, the line-shape focused lasers (see **Scheme 4**) show up with a narrow emission band as it was literally described. This technology possesses the probability to adjust emission wavelength by keeping a uniform distribution of the photonic energy on the exposure target. Therefore, it is already introduced into many practical applications such as physical drying and photocuring of coatings, lithograph as well as laser-mediated polymerization in the presence of up-conversion nanoparticles (UCNPs) in the near-infrared range[10, 89, 124, 148, 182]. Particularly, the UCNPs have received attention for exposure of objects with large thickness up to 13 cm[181] or for 3D printing of functional materials[183].



The development of novel light sources greatly contributed to the field of photochemistry and photopolymerization for both academic research and practical applications. Particularly, the occurrence of recent high-power NIR LEDs inspires the population to explore more into this field.

#### 2.1.4 Sunlight as An Alternative Green Source Makes Dream Reality

Sunlight can be seen as an eternal and clean source of energy in human life on our planet, which makes all life to exist on earth. Its importance has been sometimes underestimated because the fast industrialization focused more on the development of technologies based on fossil sources. It has been mainly collected for heating purpose and to generate electricity for human's daily life[184, 185]. As shown in **Figure 4**, sunlight also exhibits huge potential from the point view of photochemistry, since its emission band appears from UV to NIR located between 300 nm to 1000 nm. There are already many investigations harvesting sunlight as the source for photocatalyst[186, 187].

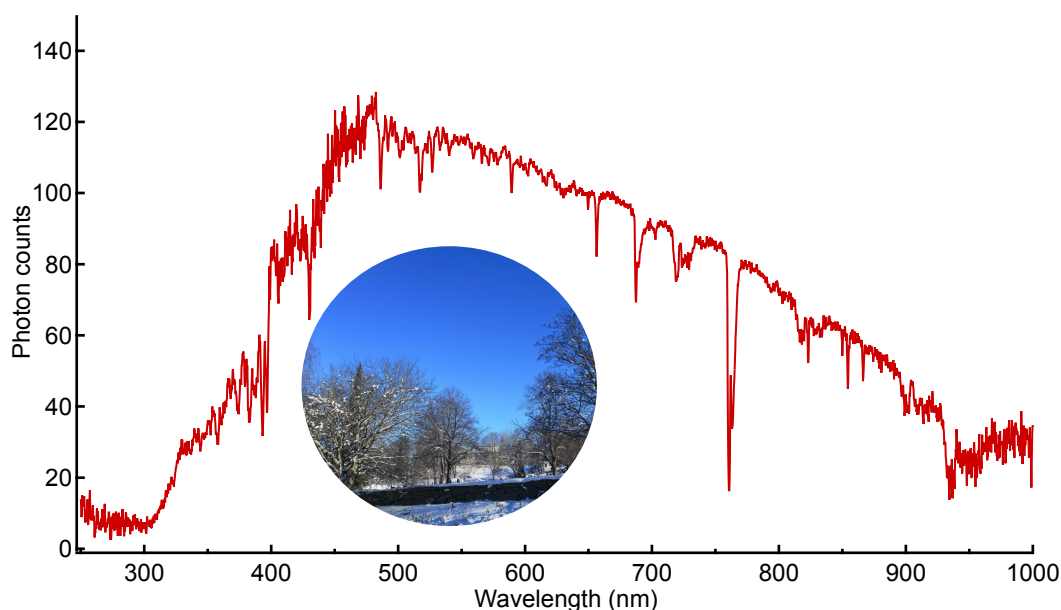


**Figure 4.** Emission of sunlight. The optical spectra were taken at 14:35 on 19th, April 2023 in the city of Krefeld in Germany using the spectrometer described below, while the image was obtained at 14:30 on 26th, February 2023 in the city of Turku in Finland.

However, applications using sunlight still face the challenges of the availability and stability of the sunlight shining. On the one hand, these challenges would cause low efficiency and perhaps non-repeatable results in the photochemical processes. On the other hand, the exceptional advantages of sunlight still inspire the population to develop environmental friendly and mild light-mediated systems. Recent studies reported the success of RAFT photopolymerization using methyl methacrylate (MMA) as reactive monomer initiated by sunlight[156, 188]. This application showed a big progress to design photochemical

particularly photopolymerization utilising sunlight as the natural and clean light source. Moreover, sunlight may be still seen as an alternative for the applications or programs 'do it yourself' due to its feature of safety to the operators. Here, first attempts demonstrated the use of an iron oxide catalyst covered with demethylated lignin to initiate photopolymerization while its proper work as photocatalyst to clean waste water with the photoreactive material using sunlight as source[189]. Of course, sunlight is not available in 24/7 based production processes but appears huge potential as the first step.

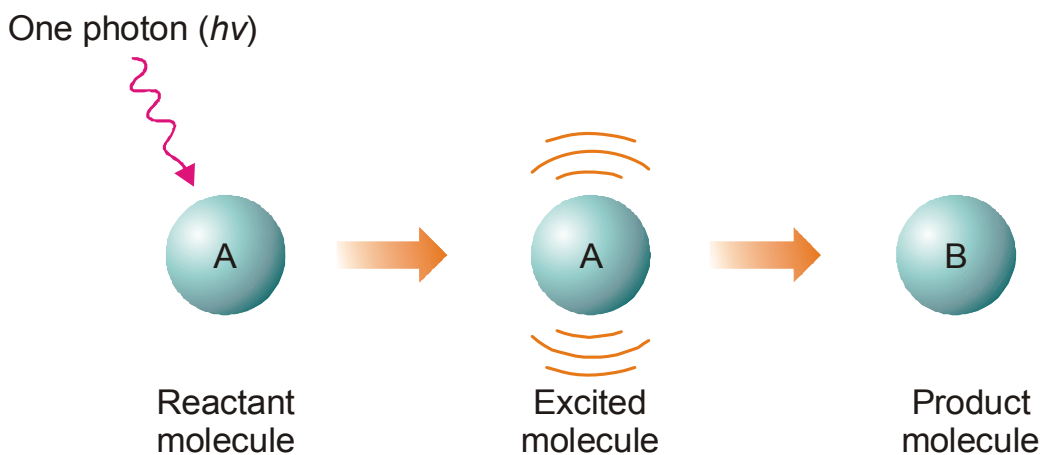
## **2.2 Key Points for Photopolymerization Systems in NIR**

Near-infrared (NIR) light-mediated photopolymerization systems have attracted numerous interests and attention since it was brought into the graphic industry in the early 1990s[25, 109, 190, 191]. As aforementioned, NIR light provides significant benefits such as lower scattering coefficient at the respective wavelength compared to UV light[97]. This helps to enable the feasibility for applications and systems with deeper light penetration into the samples and materials. Nowadays, NIR-sensitized systems require deeper understanding and further investigations to explore more details. Nevertheless, it can be still seen in its infancy although this technology has been introduced to the 24/7 production lines in graphic industry[101, 104, 130]. Recently, it received increasing attraction with the focus to develop NIR-sensitized photopolymerization for further holographic patterning[58, 192]. This subchapter describes the state of art regarding the key points for photopolymerization systems used in NIR between 700-1100 nm.

### **2.2.1 Fundamentals of Photochemical Process to Generate Initiating Species for Radical and Cationic Polymerization**

Photochemical reactions and processes are generally governed by two basic laws named as Grothus-Draper Law and Stark-Einstein Law of Photochemical Equivalence[83, 193]. The Grothus-Draper Law qualitatively demonstrates that only partial light is absorbed by the components and is capable for the effective production of reactions while the remaining light is transmitted and chemically inefficient[193]. The latter Law states that each reacting molecule absorbs one photon of radiation promoting the photoreaction and forming the products as illustrated in **Scheme 5**[194].





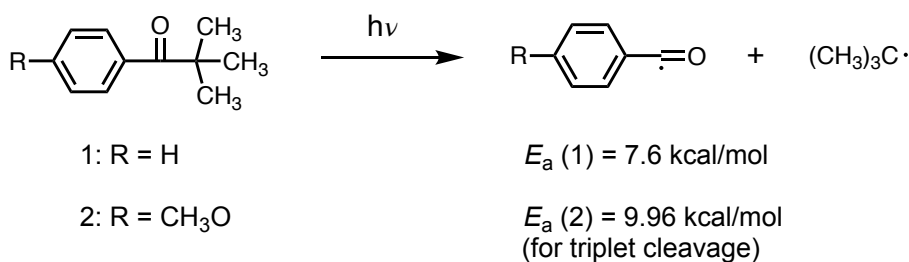
**Scheme 5.** Illustration of Law of photochemical equivalence, cited from [195].

As well-known, except light sources aforementioned, the initiating species needed to initiate photopolymerization such as radicals, cations, radical cations, acids and/or bases generated by the photoinitiators (**PIs**) represent as extremely crucial elements in the photochemical reactions and processes [196, 197]. Moreover, the **PIs** are mainly grouped as type I and type II systems based on the proceeding photochemical reactions [18]. Formation of initiating species can be promoted via following pathways [196, 198, 199]:

- Bond cleavage after photon absorption followed by either homolytic or heterolytic cleavage (**Scheme 6** as an example), which assigns to Type I initiators [18, 81];
- Photoinduced electron transfer (**PET**) between sensitizers and co-initiators enables the group if Type II initiators follow the rules based on the electrochemical potentials, excitation energy and internal activation barrier [20, 118];
- Initiation of a chemical reaction need to start with thermal energy while heating of the surroundings is promoted by a process where a proceeded photochemical reaction is accompanied with huge release of heat caused by internal conversion (**IC**) between the excited state and ground state.

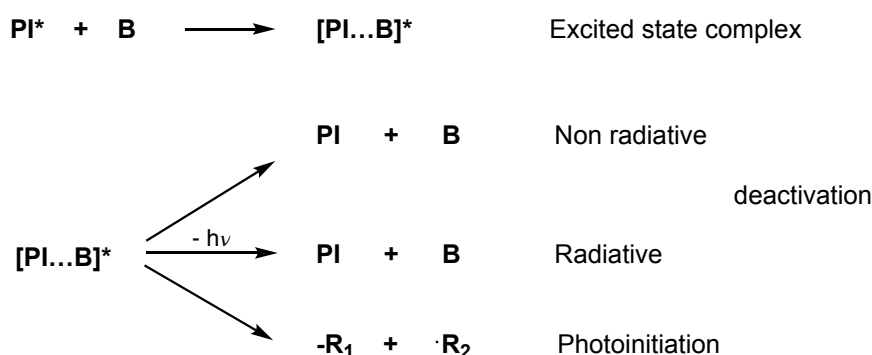
Photoinitiators assigned to a process with homolytic bond cleavage have been extensively used as efficient compounds for the initiation of free radical photopolymerization, photocuring and crosslinking for over 50 years especially applied in industrial applications using UV and visible light sources for excitation [76, 200]. Moreover, the Norrish I cleavage has been one of the best understood photochemical reactions [194]. The type I initiators represent a lower value of bond dissociation energy than the excitation energy of the reactive excited state, which connects therefore to an improved thermal stability [196]. The initiators are promoted into their first singlet excited state after light absorption followed by triplet state formation by fast intersystem crossing (**ISC**) from which lifetime is typically

larger than that of the excited singlet state. Reactions occurring from the excited state promote the generation of initiating species, which is sometimes accompanied by consecutive reactions in the dark[196].



**Scheme 6.** Activation energy for Norrish type I cleavage of basic aromatic ketones, modified from[194].

The selection and utilization of photoinitiators is of great importance with regard to the efficiency and applications. The **PIs** convert the light energy absorbed from the light irradiation into chemical energy resulting active intermediates such as radicals and cations for the subsequent initiation of both free radical and cationic photopolymerization of reactive monomers and oligomers[196]. For instance, free radical polymerization can be directly initiated by radicals formed via direct bond cleavage of a precursor[81]. The type I initiator proceeds a unimolecular reaction referring to a direct bond fragmentation of photoinitiators controlled by the dissociation energy. Furthermore, type II initiators undergo a bimolecular reaction, where other molecules refer to the co-initiators participate in the process to generate reactive initiating moieties (see **Scheme 7**).



**B = Co-initiator**



**Scheme 7.** Mechanism of generation of initiating species from type II initiators, modified from[196].

The type I initiators typically function as single component undergoing the cleavage photoreaction dominantly from the triplet state resulting in reactive intermediates for the

initiation of photopolymerization[201]. These initiator systems can be sometimes replaced by a sensitizer which gives access to higher excitation up to the NIR. Those systems, combined with co-initiators, react in the excited state resulting subsequently in generation of initiating species by **PET**, which is short-living radical[19]. These reactions can occur from the first excited state  $S_1$  or triplet state  $T_1$  formed by intersystem crossing[202, 203]. However, the intermediated triplet state can undergo the following processes[196]:

- Reaction with oxygen resulting in generation of singlet oxygen;
- Production of complex with the co-initiator followed by photolysis;
- Quenching by the monomer/oligomer via energy or electron transfer resulting in no any chain extension;
- Radiative or non radiative deactivation resulting in light emission or heat release to the matrix;

Among them, the presence of oxygen always serves as inhibitor resulting in the quenching and reaction/combination with the reactive moieties such as radicals[157, 204]. Therefore, except the factor of light sources, the efficiency of the **PIs** in the photopolymerization systems generally depends on the reactivity of excited state and formation of initiating radicals. Nowadays, there are already numerous effective methods which could be applied for the measurement, evaluation and monitor of reactivity and kinetics regarding (*in situ*-)photopolymerization[205]. Primarily, the efficiency of the photoinitiating system is exclusively dominated by the overlap of optical spectra from the light emission and the absorption of the **PIs**, furthermore, the reactivity of the photopolymerization is related to[196, 206]:

- Extinction coefficient ( $\epsilon$ ) of the photoinitiators at the respective wavelength range of the light sources;
- Concentration of the **PIs** in the systems;
- The presence of pigments and fillers operating sometimes as inner filter;
- The presence of the oxygen;
- The initiating efficiency of the formed radicals referring to the type of **PI**.

Thus, the presence of oxygen initiates the problem of unreacted monomers resulting in sticky surface of the photopolymer materials obtained via photopolymerization as well as the disability of depth curing since UV and visible light-mediated systems are still dominating the industrial market[207]. To overcome these problems, there are studies and

investigations putting their focus to design more efficient and adaptable initiators for extended applications, especially the development of type II initiators[208, 209]. Furthermore, the type II initiators exhibit the advantages of broad feasibility regarding structural patterns and absorption wavelength, since as aforementioned, the light absorption of the initiator systems can be achieved through either the initiator/sensitizers or the co-initiators or both molecules[198]. In addition, the photochemical reactions can be proceeded by electron transfer reactions[19], which enables higher excitation wavelengths that are beyond the dissociation energy of a single bond of the photoinitiator.

### 2.2.2 Photoinduced Electron Transfer between the Initiators and Energetic Barriers

The photosensitized formation of reactive intermediate species for initiation of polymerization such as radicals and conjugate acid follows the process of photoinduced electron transfer (**PET**) between the light absorber and respective co-initiators also by excitation with NIR light[20, 88]. Because the generation of radicals by homolytic bond cleavage here does not occur due to lower absorbed light energy compared to the C-C bond cleavage. This needs 349.8 kJ, which directs to 569 nm, while NIR ranges from 700-1100 nm[210, 211]. Therefore, **PET** has been dominantly involved to generate these short-living moieties for photopolymerization in the case of NIR sensitive systems[19]. Surprisingly, recently released strong emitting LEDs facilitate **PET** reactions in the NIR while low intensity sources do not follow this[118]. This surprises because other Type II systems run well by UV excitation[212]. These experimental results support the opinion that an internal activation barrier exists in the system which indicates a certain energy threshold[20, 118, 213].

The principle of **PET** was developed based on the Marcus theory which was proposed in the 1950s as a model[135, 214]. While the experimental approval was brought out with the introduction of modern NMR techniques, where exposure in the NMR machine resulted in generation of a radical pair and the Chemically Induced Dynamic Nuclear Polarization (CIDNP) technique imaged the appearance of either a singlet or triplet radical pair by an enhanced absorption or emission in the NMR spectrum[215, 216], this phenomenon in the spectrum is described by the Kaptein rules[217].

**PET** as fundamental theory describes the contribution to an internal activation barrier by taking the thermodynamic properties into consideration, for instance, the oxidation potential  $E_{ox}$ , the reduction potential  $E_{red}$ , the excitation energy  $E_{00}$  and the reorganisation energy  $\lambda$ . The coulomb term  $E_{coul}$  is included in Equation (2) referring to the ionic species formed while it demonstrates less impact in organic medias. Equation (3)[135] depicts the

influence of temperature (T) and the free enthalpy of electron transfer ( $\Delta G_{et}$ ) on the rate constant of electron transfer  $k_{et}$ . The reorganisation energy  $\lambda$  shows additional effect to  $k_{et}$  where  $\lambda$  refers to the contribution by an inner sphere  $\lambda_i$  and outer sphere term  $\lambda_o$ , respectively ( $\lambda = \lambda_o + \lambda_i$ )[213, 218, 219].

$$\Delta G_{et} = F \cdot (E_{ox} - E_{red}) - E_{00} - E_{coul} \quad (2)$$

$$k_{et} = \nu_N \cdot \kappa \times e^{-\frac{\Delta G^\ddagger}{RT}} = \nu_N \cdot \kappa \times e^{-\frac{(\Delta G_{et} + \lambda)^2 / 4\lambda}{RT}} \quad (3)$$

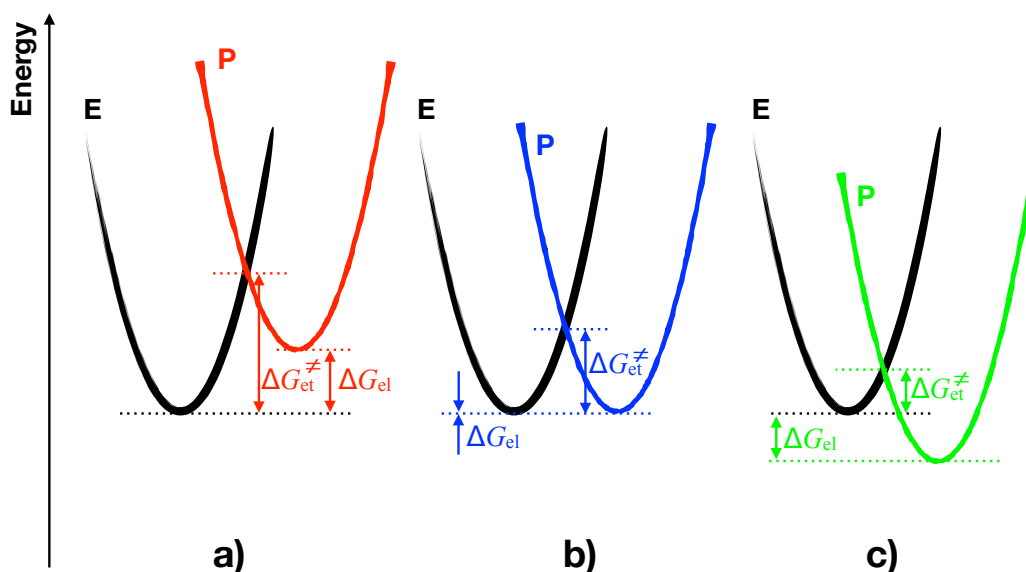
$$\lambda_o = N_A e^2 \left( \frac{1}{2r_A} + \frac{1}{2r_B} - \frac{1}{d} \right) \left( \frac{1}{n_D^2} - \frac{1}{\epsilon_s} \right) \quad (4)$$

$$\lambda_i = \sum_i \left( \frac{f_i^R \cdot f_i^P}{f_i^R + f_i^P} \right) \Delta q_i \quad (5)$$

As shown in Equation (4), the outer sphere reorganisation energy  $\lambda_o$  in the electron transfer is related to the radii size of the reaction materials  $r_A$  and  $r_B$ , the distance between these substances  $d$ , refractive index  $n_D$  as well as dielectric constant  $\epsilon_s$ . Furthermore, the inner reorganisation energy  $\lambda_i$  is affected by the geometric changes which refers to the changes of the bond property. For instance, the typical chemical bond of carbon-carbon double bond (C=C) possesses the distance of 1.4 Å while it changes to around 1.5 Å as a single bond (-C-C+) after the process of electron transfer[135, 220]. Equation (5) describes that the force constants of the reactants  $f_i^R$  (index R) and products  $f_i^P$  (index P) contribute to the inner reorganisation energy  $\lambda_i$ , respectively. The term  $\Delta q_i$  represents the changes of geometry coordinates proceeding during **PET** reactions. Thus, the parameter  $\lambda_i$  needs additional attention when describing the operational function of the internal activation enthalpy  $\Delta G_{et}^\ddagger$ .

**Scheme 8** discloses the scenario showing the reactant materials crossing the potential energy curves where sensitizers acting as electron donor while the electron acceptor often relates to either electron-deficient compounds such as onium salts or triazines, see **Scheme 9** for the structures[11, 118]. **Scheme 8** shows that additional energy is necessary to be introduced to overcome this internal activation barrier also in the case where  $\Delta G_{et} < 0$ . Here, the situation where the systems demonstrate extremely large  $\Delta G_{et}$  is not taken into consideration since it also proceeds to large intrinsic free activation enthalpy  $\Delta G_{et}^\ddagger$ [20]. **Scheme 8b** relates to the condition where  $\Delta G_{et}^\ddagger \approx 0$ . This would facilitate excitation under conditions using a low intensity light source[90]. Non-radiative

deactivation relates to formation of heat that contributes to overcome the internal activation barrier shown in **Scheme 8c** as discussed in detail *vide infra* in **Section 2.2.3**.

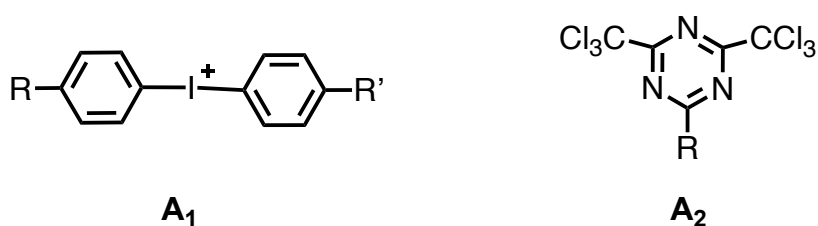


**Scheme 8.** Energetic relations of photoinduced electron transfer depicting internal activation barrier resulting in threshold systems under a) endothermal condition, b) thermoneutral condition and c) exothermal conditions, cited from[154].

As aforementioned, the **PET** reaction connects to geometry changes as disclosed by  $\Delta q_i$ . In case that the expected changes are not as large,  $\Delta G_{et}^{\ddagger}$  would decrease since  $\Delta q_i$  shows a smaller value. However, there still lacks reliable experimental tools available providing the access to explore such occurring process[88]. The time resolved spectroscopy has been well developed for which the Nobel Prize in chemistry was awarded to A. Zewail in 1999[221]. This gives nowadays time resolutions down into the femtosecond absorption time frame[222]. Other techniques, such as time correlated single photon counting providing information about the reactivity to release radiation where the development of red sensitive photomultipliers gives access to record emission kinetics also in the NIR until 900 nm with time-dependent emission ports[90]. Nevertheless, many modern systems failed to disclose to image the geometry change related to  $\Delta q_i$  on an appropriate time scale although first attempts were made with step-scan FTIR[223].

Many NIR sensitive systems exhibit an internal activation barrier although  $\Delta G_{et} < 0$  regardless using a positively charge iodonium compound **A<sub>1</sub>** ( $E_{red} = -0.64$  V[88]) or material exhibiting no charge such as the triazine **A<sub>2</sub>** ( $E_{red} = -0.64$  V[88]) as shown in **Scheme 9**. Both **A<sub>1</sub>** and **A<sub>2</sub>** depict similar reduction potential resulting in similar  $\Delta G_{et}$ . Thus, the positive charge of the iodonium salt might not be the reason because two molecules together exhibiting the same charge sign may repulse each other. The combination of LEDs with high power output intensity helps to overcome this internal activation barriers

facilitating remarkable reactivity to the photopolymerization initiation[118]. Here, the internal conversion (**IC**) from the lowest vibrational mode of the excited state into a higher vibrational mode of the ground state leads to a formation of very hot state, which stabilizes by transfer of its excessive vibrational energy by collision with matrix molecules resulting in a huge increase of temperature[90, 118]. This heat released consequently helps to overcome internal activation barriers. The higher intensity of the light exposure relates to higher temperature of the surrounding. Heptamethine-based cyanines comprising a barbiturate group in the *meso*-position exhibit the only group of NIR-sensitive material with low internal activation barrier[161], with which low output intensity light sources successfully worked to start **PET** protocol applying 805 nm for excitation[127].



**Scheme 9.** Chemical structures of the widely used electron acceptors iodonium salt **A<sub>1</sub>** and triazines **A<sub>2</sub>** as an example, cited from[20].

These systems worked well according to an oxidative mechanism comprising cyanines at the excited state as sensitizers regardless the existence of high or low internal activation energy[118]. The sensitizer at the excited state **Sens<sup>\*</sup>** transfers an electron to the acceptor (**A**) resulting in the radical pair of **Sens<sup>+·</sup>** and **A<sup>-·</sup>** as depicted in Equation (6). This can be proceeded by the sensitizers comprising the general cyanine structural pattern shown *vide infra* in **Scheme 14** from the first excited singlet state **S<sub>1</sub>**. Systems operating from the triplet state have not been disclosed for such patterns yet[20, 118].



Consequently, the radical pair formed in the solvent cage appears as singlet pair. As a result, the electron back transfer can also occur based on the thermodynamic point of view with high efficiency, which is significantly higher than leaving the solvent case by diffusion. However, the rate of electron back transfer diminishes due to the unimolecular cleavage of **A<sup>-·</sup>** into initiating radicals **R<sub>i</sub><sup>·</sup>**, which makes the system irreversible, see Equation (7). In

addition, Equation (8) also depicts the release of conjugate acid and formation of respective products by the formed cation radical **Sens<sup>•+</sup>** via stabilizing itself. Thus, it explains that the conjugate acid originates from the sensitizer instead of the acceptor although they are often called as initiator. This claims that the structures of sensitizers appearing low with nucleophilicity might achieve effective initiation of cationic photopolymerization, which was reported for the NIR-sensitized systems few years ago[224].

Thus, the combination of embedded cyanines in a coating and newly developed high output intensity NIR-LEDs results in high temperature in these materials which is inside the matrix. This working mode appeared much more efficient to generate energy by a light source on demand by turning a switch ON/OFF compared to external heat transfer into the sample. Herein, the heat generated in such systems can be seen as an internal furnace proceeding on the surface of the molecules being directly surrounded by the matrix materials[90]. These very hot molecules transfer the heat into the surroundings by collision with the matrix molecules resulting in a change of the Boltzmann-distribution and therefore acceleration of the reaction in **Scheme 8**. Nevertheless, the mechanism of heat release can be seen still poor disclosed in literature. This interpretation appears as a very rough model based on available data[90, 118, 127].

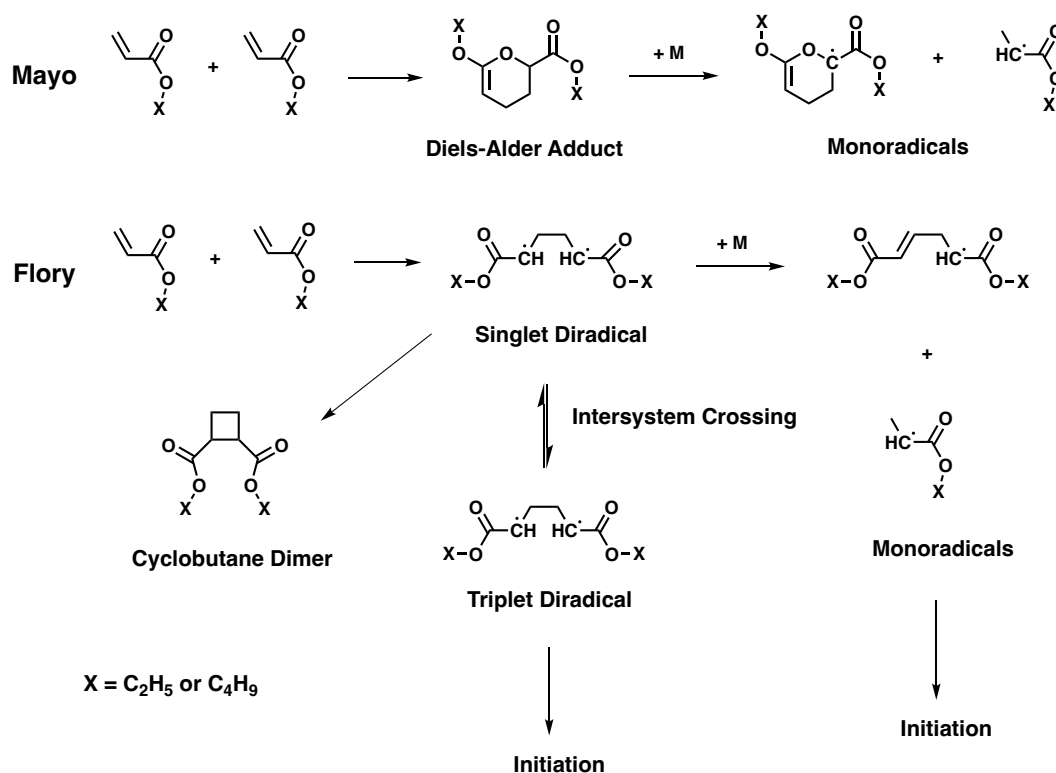
### **2.2.3 Heat as Additional Impact to Promote Systems with Dual Working Function**

Heat has been a tool of media exhibiting of great importance applied into a huge number of applications relating to both human's daily life and industrial market[190, 225, 226]. As an important energy source, heat can be broadly generated by the conversion from other sources based on conventional pathways such as electrical, chemical energy resulting in arise of temperature of the objects[116, 227, 228]. Among those, the conventional oven technology using electricity has been dominantly applied to heat up the matrix in many fields, while it still exhibits drawbacks under the consideration of energy saving since it always needs time for warming up to the thermal condition on request while can not provide constant heat output power in the respective surrounding during ON/OFF processes[229]. Therefore, there are increasing investigation and exploration of methods or technologies regarding both formation and utilization of the energy source of heat relating to a chemical process. Operation with oven driven technologies also requires time to warm up the devices until constant temperature. This relates therefore to huge energy consumption which may be reduced by technologies generating heat on demand, for instance, laser drying introduced into coating science[29].



Interestingly, the combination of a light source with a material that generates heat upon excitation has received increasing interest for thermal induced polymerization[117, 174, 199, 230]. It has become attractive in the field of medical and pharmaceuticals for treatments of photothermal therapy[228] or process of gene delivery[231]. These technologies are always developed by incorporation with other assisting mediators such as nanoparticles or other nanomaterials[155, 175]. This newly born technique has been focused to develop novel and efficient method for medical therapy targeted to kill cancer cells or tissues requesting accurate controlled heating and localization[175]. Therefore, this method based on a sufficient conversion process of Light-to-Heat exhibits huge potential for the practical applications. Moreover, the investigations on the kinetics of photocuring of dental composites also demonstrate that the heat released from surroundings with higher temperature promoted the photopolymerization process resulting in full final conversion of the monomers/oligomers and shorter time requested to reach the given level of conversion under the exposure of near infrared light[115, 190].

Furthermore, studies on the dual-cure polymerization following a photochemical and thermal mechanism using acrylates as reactive monomers has addressed the importance of heat during the photopolymerization systems by applying a low exposure intensity of light source[199]. The addition of photoinitiators greatly contributed to the solidification despite the self-initiation of the acrylates (see **Scheme 10**) compared to the neat thermal samples resulting in fully polymerized materials obtained with large depth[199]. This example depicts that acrylates itself can undergo side reactions in bulk which relates to either stepwise polymerization in the Diels-Alder protocol or formation of diradicals resulting in existence of initiating radicals.



**Scheme 10.** Self-initiation of ethyl acrylate and n-butyl acrylate following the Flory and Mayo mechanism, cited and redrawn from[232].

Moreover, the heat formed plays an important role with the heat and thermal diffusion in the frontal polymerization systems[62], therefore, such systems always exhibit the capability to fabricate photopolymer materials with sufficient curing depth in numerous fields varying from photolithography, dental materials, micro fluidic devices to coating applications[12, 77, 199, 233]. Here, it also contributes sometimes to the thermal decomposition of initiating components such as iodonium salts in combination with a sensitizer[88].

In addition, recent investigations on the role and effect of the heat released in the NIR-sensitized photopolymerization systems in the presence of respective absorbers have obtained increasing attention[117, 118, 137]. The heat released by the internal conversion of the excited dye molecules after absorbing energy from the light radiation by applying NIR-LEDs with high-power of output intensity acts as the main thermal source to overcome the internal activation barrier, which contributes to facilitate **PET** reactions enabling the initiation of photopolymerization in the combination with co-initiators[19, 20, 90, 117, 127]. Herein, the heat formed in such systems appears of great potential can be considered as 'internal source' for physical drying and chemical crosslinking of solvent-comprising or often waterborne coating systems[60, 61]. While there still remains lack of deep understanding and applications with some open questions relating to the effects of the heat generated during the internal conversion process.

## 2.3 Sensitizers in NIR Light-Mediated Photopolymerization

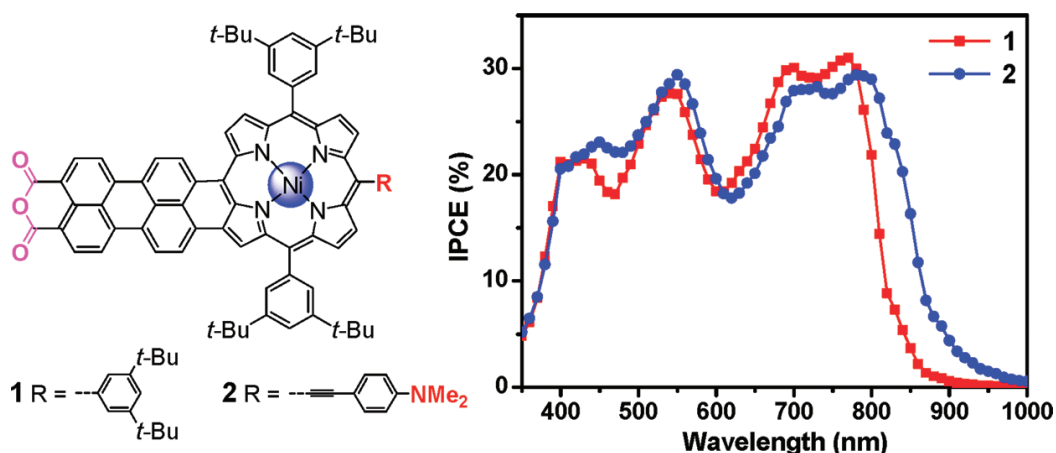
In recent decades, photopolymerization in NIR range has attracted great attention and interests thanks to its beneficial features and advantages of NIR light[101, 105, 130]. The capability of deep penetration of NIR light into the materials because of its lower scattering coefficient at higher wavelength[97, 105] in practical systems facilitates the applications for such as 3D or 4D printing[41, 234], photoswitching materials[235], photocuring of multicomponent composites and coatings[137, 236]. In particular, the development of novel NIR-LED devices enabling high-power output intensity has brought new impetus into this field[118]. NIR-sensitized polymerization was born in the graphic industry in the late 1990s[39] while the first commercialised printing plate came to the market in 2000[40, 108]. Moreover, there are several distinct types of compounds which function as respective sensitizers and absorbers[90, 91], this will be discussed more in details in the following subsections.

### 2.3.1 Structural Patterns of Absorbers and Sensitizers in NIR Range

The utilization of NIR light possessing its remarkable features of friendliness to users and broad working wavelength has obtained recognition in numerous different fields for both practical applications and academic research[27, 111, 113, 237]. Respectively, the design and development of those compounds acting as sensitizers or absorbers in this range have simultaneously achieved big progress including perylenes[238], rylenes[239], phthalocyanines[172], protein-based compounds[240], nanoparticles and other organic dyes such as cyanines[90, 237, 241], just name a few examples.

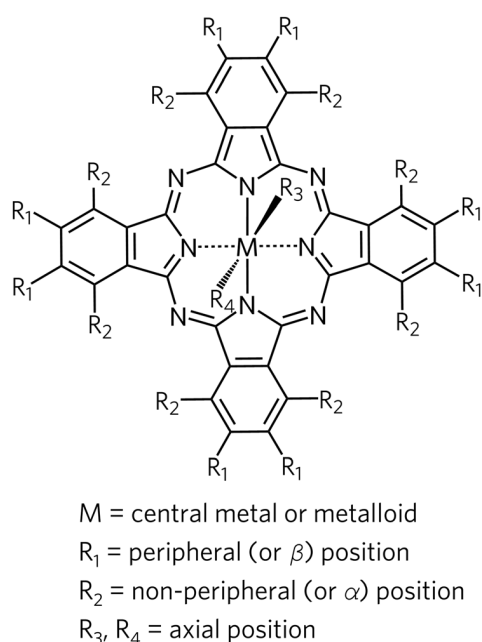
Solar cells as a promising source based on the cleanest and renewable energy have been getting extremely focused attention in the over few decades[172]. These systems can also comprise light-sensitive materials in photoredox cycles as shown in **Scheme 11**[238]. Furthermore, the development of organic solar cells, in which functional dyes/sensitizers absorbing in NIR range has become an ideal alternatives due to its sufficient efficiency and cost-effectiveness compared to conventional silicon-based objects. Therefore, porphyrin[238] stands out for this application due to their flexibility to tune the optical band allowing the absorption towards wavelength of lower energy[172]. Furthermore, the porphyrin derivatives were also widely studied for medical applications such as phototherapy guided by fluorescence imaging[123] and embedded into nanomedicines for cancer treatment[242] based on their optical absorption in NIR region. In addition, there are numbers of studies on the NIR light absorbing compounds for biological and/or

medical using such as fluorescent probes for protein-labelling[243] and proteins-capped gold nanoclusters for photodynamic therapy[244].



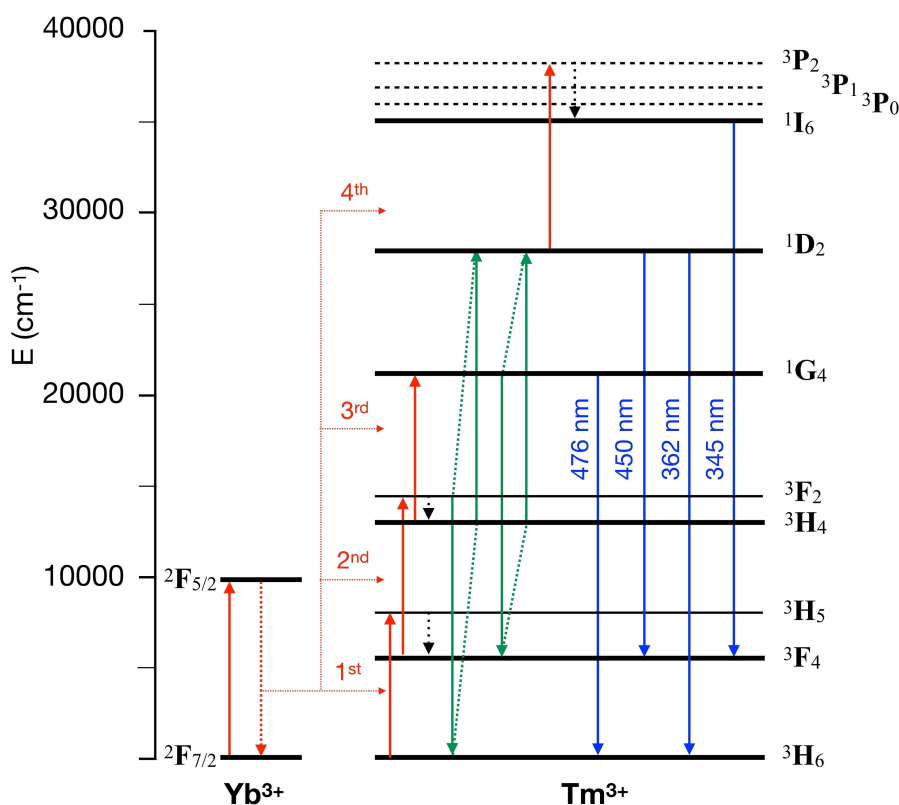
**Scheme 11.** The chemical structures and absorption spectra of the perylene anhydride fused porphyrin compounds used as NIR sensitizers in solar cells, cited from[238].

Phthalocyanines as of great importance class of colorant, have been synthesised and modified into derivatives of numerous structures[245] (general structural pattern demonstrated in **Scheme 12**), which can be used as NIR sensitizers in systems including electrocatalysis[246], or inkjet printing and materials to generate charge in electron photography such as for laser printers[247]. The absorption of those materials can be extended from visible to NIR range up to 1000nm. Thus, they are introduced into different fields covering biological applications such as photodynamic therapy, optical data storage and so on bringing their diverse properties[247].



**Scheme 12.** Structural pattern of phthalocyanines with possible substitutes, cited from[246].

Interestingly, up-conversion nanoparticles (UCNPs) present interesting materials where light absorption in the NIR range has attracted more and more attention resulting in excellent light stability demonstrating a large hypsochromic shift of the radiation released in the upconversion process particularly using lasers as excitation sources[248, 249]. Those materials can efficiently emit ultraviolet/visible light with a narrow wavelength band gap for following light-mediated reactions (illustrated in **Scheme 13**) such as initiation of photopolymerization by excitation of embedded UV-initiators[65, 147]. This typically proceeds with lasers at 980 nm[147, 241] converting the absorbed light into blue and UV-light[89]. Recently, this UV-light was additionally introduced into photo-ATRP reaction protocols to excite directly the copper complex[102]. Surprisingly, the addition of UV-sensitizers enabled metal-free photo-ATRP[250].

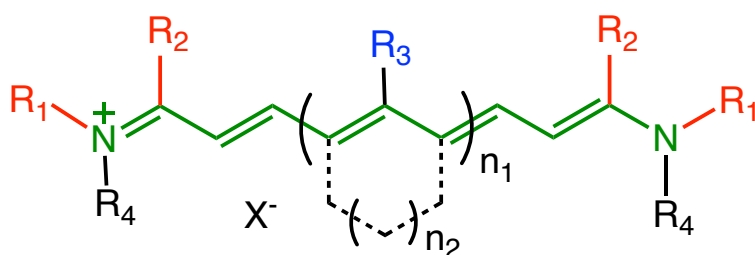


**Scheme 13.** Energy level of respective transitions for excitation, energy transfer and emission of the up-conversion nanoparticle (UCNP) of NaYF<sub>4</sub>:Yb<sup>3+</sup>/Tm<sup>3+</sup>@NaYF<sub>4</sub> with high excitation intensity. cited from[148].

Thus, photophysics of such interesting materials are investigated in order to understand the mechanism[148, 241]. Many reports disclosed that UCNPs showed sufficient reactivity to generate reactive moieties for the initiation of both free radical and cationic photopolymerization with the assistance of co-initiators[89, 241] enabling chemical solidification of coating layers[251, 252]. Furthermore, UCNPs also surprisingly facilitate significantly deep photocuring of the systems using difunctional bisphenol A epoxy acrylate

oligomer, which still holds the record with 13 cm[181]. In addition, UCNPs also show up in the application of biolabelling after specific and suitable chemical modification on the surface[253]. However, there still remain challenges regarding the applications particularly the lack of rare earth metal compounds and the limit of available scale-up considering the synthesis of UCNPs in a size of kilograms or even several grams[147, 254]. The latter can be still seen as a dream.

In addition, cyanines, well-known as a subgroup of classified polymethine dyes comprising two terminal heterocyclic rings, each of which contains a nitrogen atom linking with the polymethine chain[255], have led to a diverse structure variations based on the structural pattern illustrated in **Scheme 14**. Thus, there arise numerous investigations based on those materials as absorbers and sensitizers exhibiting a broad variation of the absorption wavelength in NIR range from 700 to 1300 nm just with the change of the terminal indolium moiety by benzo[*c,d*]indolium on the one hand and extend the methine chain length from three to nine methine group[90]. These materials access the applications in broad fields[160, 256], pharmacology and medical treatment[257, 258].



**Scheme 14.** General structural pattern of cyanines with potential substitutions.  $n_1, n_2 = 0, 1, 2$ , etc.

In general, the optical absorption of the cyanines may appear a bathochromic shift of approximately 100 nm with extension of an additional methine group[255]. Furthermore, the terminal patterns and distinct substitutions may also cause an impact on the physical properties, and optical absorption wavelength of cyanines. This helps to tailor on demand the absorption ranging from visible to NIR range[259]. Thus, the cyanine dyes with tri-, penta-, and heptamethine structures were widely studied and applied in diverse areas of science[161, 256, 260], engineering[127, 261] and biological applications[159] according to their respective excellent absorption properties[262]. Interestingly, in recent reports, heptamethine cyanines were also introduced into industrial technology such as solar cells due to their significant efficiency of Light-to-Electricity transfer[170]. Moreover, those materials could play an important role in the photopolymerization systems as sensitizers and initiators facilitating to generate a huge amount of heat to overcome the internal

activation barrier and initiate both free radical and cationic polymerization which would be discussed more in details in the following subsections *vide infra*[90, 118].

### 2.3.2 Cyanines as Sensitizers in Photopolymerization

Cyanine dyes have been applied in different fields since its birth over 100 years ago[255, 260, 263]. Those materials are widely introduced to the systems of photolithography, 3D printing, physical drying of coatings comprising water as dispersing solvent and photochemical crosslinking of coatings[160, 234]. Moreover, they have obtained great attention in recent decades in the procedures of polymer synthesis for the initiation of photopolymerization due to their outstanding photophysical and photochemical properties including high extinction coefficient and broad absorption variability in NIR range since this light is recognised as an economic, safe and friendly in the respective light sources devices[136]. Respectively, there exist a large group of well-established chain builders and scaffolds for the synthesis of cyanines. **Figure 5** shows the examples of typical terminal patterns. Furthermore, the substitutions at the *meso*-position of the molecules and on the terminal moieties also open the possibility to change the counterion affecting the compatibility with the matrix.

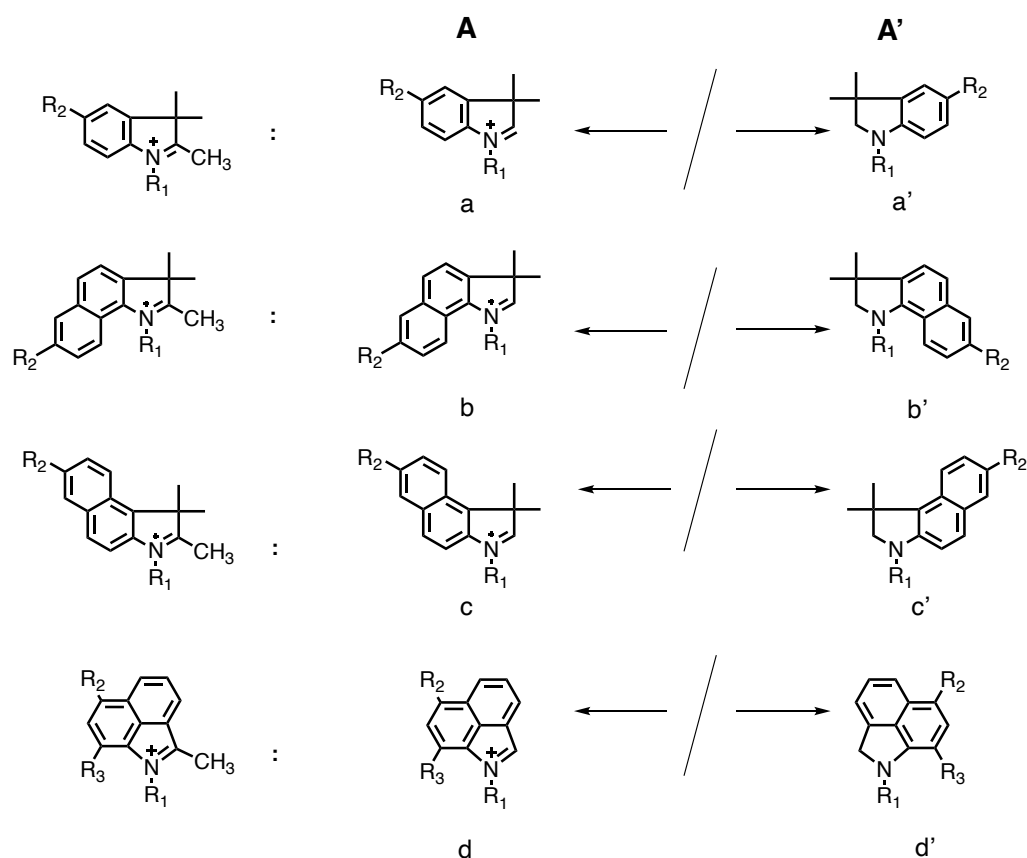


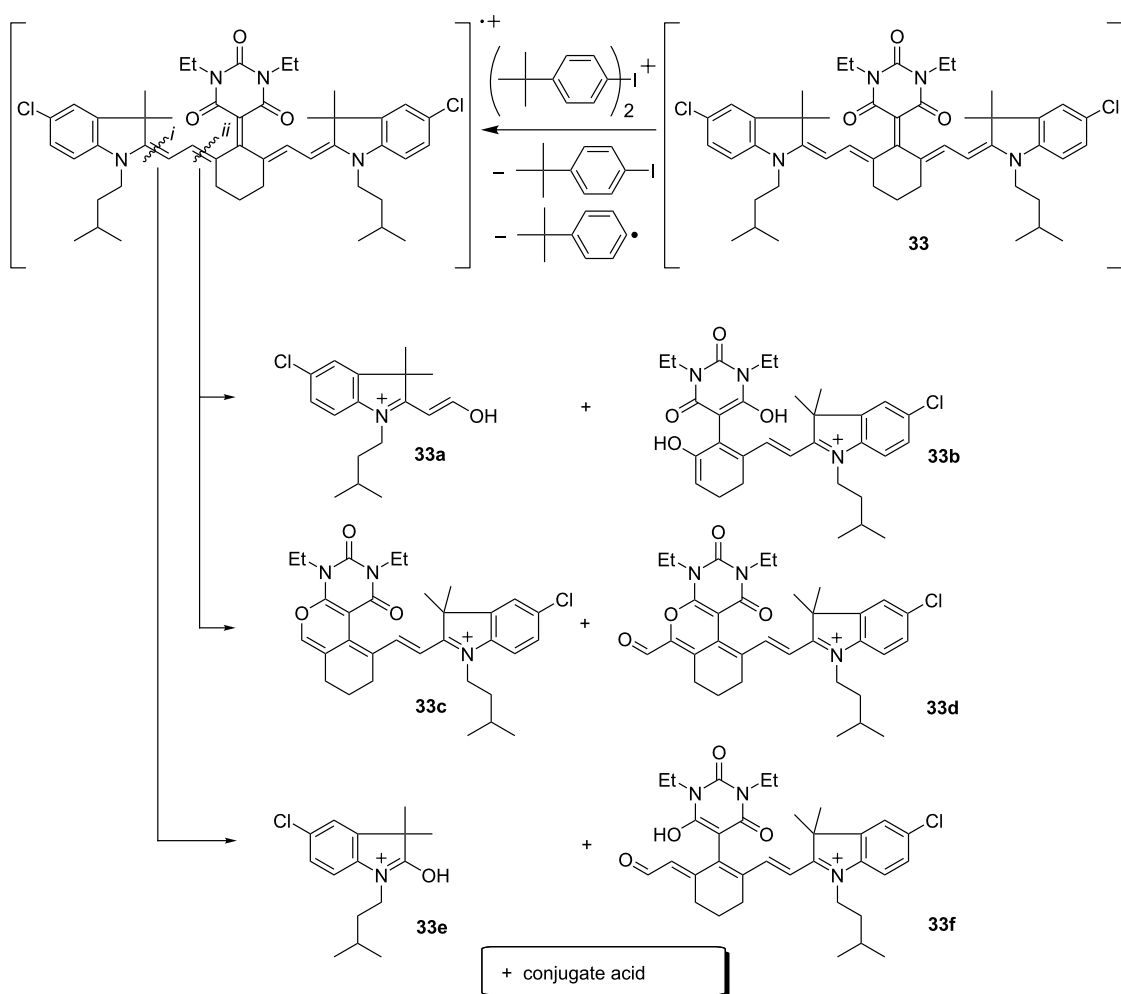
**Figure 5.** Structural patterns of cyanines with 1-substitution of trimethylindolium, benzo[g]indolium, benzo[e]indolium and benzo[c,d]indolium salts lead to the symmetric patterns a/a', b/b', c/c' and d/d' based on the terminal substituent **A**, modified from[20].

The great effort devoted to synthesis leads to cyanines therefore with different structural patterns and substitutes exhibiting distinct optical and electrochemical properties[20, 90, 264]. These aspects facilitate their performance acting as absorbers and sensitizers in the point view of photochemistry[20]. Upon the exposure by high-intensity NIR-LEDs, the excitation based on one-photon absorption results in formation of the  $S_1$  in a higher vibrational level followed by a fast process of relaxation in the lowest vibrational level at the  $S_1$ , from where several competitive pathways of deactivation may occur[20, 265, 266]. These relate to photochemical reactions such as aforementioned **PET** which indicates to generate reactive intermediates such as radicals and conjugate acid for the initiation of free radical and cationic photopolymerization, respectively[115, 136] (**Scheme 15** shows the mechanism as an example). Photophysical events simultaneously occur in the excited state including sometimes radiative deactivation resulting in observed emission of fluorescence. While non-radiative deactivation mostly contributes in cyanines absorbing in the NIR with an efficiency of greater than 75% depending on substitutions[20]. Here, several competitive processes resulting in generation of huge amount of heat from internal intramolecular vibrational relaxation (**VR**) and internal conversion (**IC**) were considered to contribute to heat generation[90]. Nevertheless, the most likely event contribution to heat release are caused by **IC** from the lowest vibrational level of the  $S_1$  to a higher vibrational mode of the  $S_0$ . Therefore, the extremely hot state can only stabilize by collision with matrix molecules namely vibrational cooling (**VC**)[20, 90, 267]. Other mechanism as the *vide supra* discussed **VR** would lead to burn the molecules due to the excessive energy of the residence of heat within the lifetime of the higher vibronic state which remains in the picosecond range[20]. Thus, non-radiative deactivation could likely be achieved through the coupling of vibrations between the aforementioned vibrational states of the participating ground and excited states[267]. In addition, **ISC** resulting in the respective triplet in cyanines has not been reported yet based on our best knowledge.

As discussed in **Section 2.2.2**, internal activation barrier exists between the cationic absorbers and the electron acceptors which is an iodonium salt in this study while the heat released in such systems promotes to overcome the internal barrier and facilitates **PET**[11, 20, 118]. Generally, the heat generated is mainly considered from the contribution of vibrational cooling by the collision with matrix molecules[11, 20, 90, 268]. Therefore, the NIR-sensitized photopolymerization systems comprising cyanines and iodonium salts as initiators exhibit benefits compared to UV irradiation, since the heat generated in those systems enables the **PET** reactions with deep penetration and promotes to distribute into the whole systems resulting in homogeneous polymer networks. The cyanines also



showed sufficient reactivity combined with iodonium salts to generate conjugate acid for the initiation of cationic photopolymerization upon the exposure with the high-intensity NIR-LEDs and further initiation of hybrid polymerization resulting in interpenetrating polymer networks (IPNs) exhibiting excellent mechanical properties[27]. Here, phase separation was not observed while the use of UV-initiation systems resulted in phase separation in the polymer networks[27].

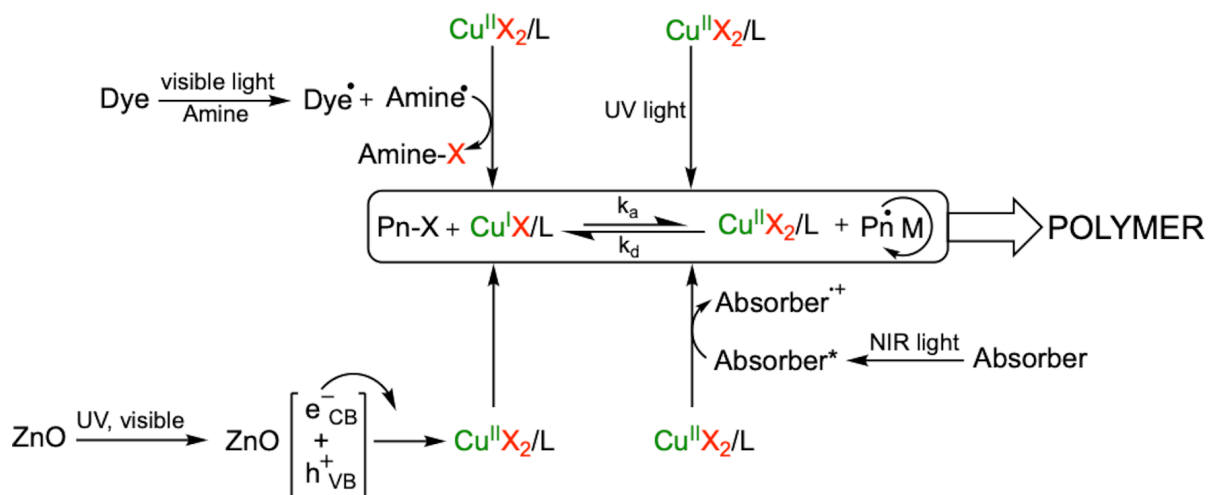


**Scheme 15.** Photo cleavage of cyanine namely **33** comprising bridged chain in the *meso*-position at excited states reacting with cationic radical of iodonium salt resulting in the moieties of **33a-f**, cited from[20].

Compatibility with the matrix and surroundings can be big challenges in the practice, the cyanines with distinct counterions such as  $[\text{PF}_3(\text{C}_2\text{F}_5)_3]^-$ ,  $[\text{PF}_6]^-$ ,  $[(\text{CF}_3\text{SO}_2)_2\text{N}]^-$  (**[NTf<sub>2</sub>]**<sup>-</sup>), *p*- $\text{CH}_3\text{-Ph-SO}_3^-$  and  $\text{BF}_4^-$  showed remarkable solubility in different reactive monomers for both free radical and cationic polymerization, for instance, multifunctional acrylates, epoxides and oxetanes and coating systems[60, 91, 126]. Particularly, a combination of the **[NTf<sub>2</sub>]**<sup>-</sup> anion with respective cation of sensitizer or iodonium salt resulted in sometimes significant increase of solubility. Here, it reached a 1:1 compatibility depending on the iodonium cation[130]. The  $[\text{PF}_3(\text{C}_2\text{F}_5)_3]^-$  was introduced by Merck while their patent

protected the use of this anion for almost all uses where it operated as counterion[269]. The previously assumed super-performance was ruled out by the  $[\text{NTf}_2]^-$  anion in 2015[130] and later by the  $[\text{Al}(\text{OC}_4\text{H}_9)_4]^-$  anion[66].

In addition, there exists few examples to apply NIR-sensitized controlled polymerization for tailor-made polymer synthesis via a process of reversible addition-fragmentation chain transfer (RAFT)[15, 104]. Here, NIR also worked successfully to prepare self-healing hydrogels[113]. Furthermore, as shown in **Scheme 16**, a recent study reported the success of NIR sensitizer-mediated photoinduced atom transfer radical polymerization (photo-ATRP) resulting in tailor-made block polymer, where  $\text{Cu}^{\text{II}}/\text{Ligand}$  complex at a ppm scale and a heptamethine cyanine served as photocatalytic system following a process of **PET** reaction mechanism[102]. This strategy significantly reduces the amount of heavy metal in the polymerization systems into a very low level and therefore facilitates to develop systems with low concentration of metal catalyst by continuous regenerating  $\text{Cu}(\text{I})$  using  $\text{Cu}(\text{II})$  as starting materials[161, 224]. Therefore, these features of the cyanine compounds depict great interest and huge potential for the applications of photopolymerization and polymer materials synthesis[270, 271]. These controlled polymerization were mostly pursued in solution while the application to make network materials can be still seen in its infancy although a recent report showed the first breathtaking achievement[272].



**Scheme 16.** Photo-ATRP (Photo-induced Atom Transfer Radical Polymerization) mediated by dyes/sensitizers under the participation of UV, visible and NIR light, cited from[20].

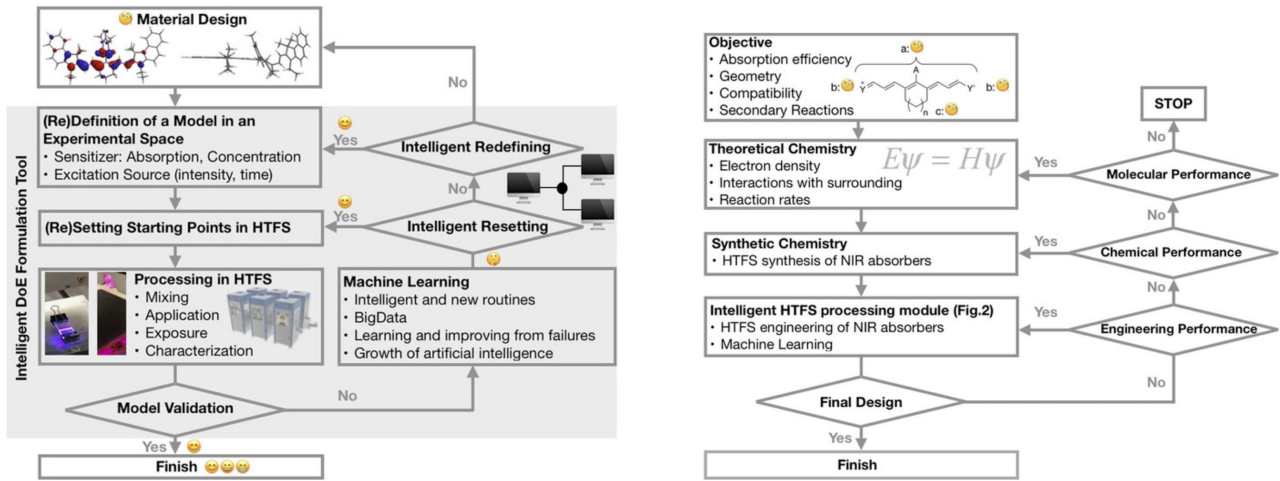
### 2.3.3 Selection of Cyanines on Demand Based on Their Structural Patterns

The chemists have made huge efforts to the synthesis of those cyanine dyes and sensitizers for the applications such as coating and printing ink systems[50, 273]. The huge variation of the structural patterns regarding the terminal moiety, polymethine

connecting chain and its substituents as well as counterions result in a large scale of existence of those materials[274, 275]. The positive charge of cyanines distributes over the entire conjugated pattern although the structures demonstrate only one valence scheme. And it appears easier feasibility to the bridged connecting moiety than the open middle chain with flexibility due to the availability at the point view of synthetic chemistry[276]. This works according to a library where huge variations would be possible while only a few would end up with a useful application. Here, first ideas about the combination between machine learning, synthesis and applications were introduced[11].

The different structures or structural patterns relate to distinct properties and performance of those materials. For instance, the sensitizers depict different efficiency regarding heat generation and reactivity for **PET** in the light-mediated systems. On the one hand, the cyanine dyes facilitate to generate heat upon exposure by just an ON/OFF click. Thus, these materials can be seen as 'internal furnace' exhibiting benefits for physical drying to get rid of water as solvent for coatings compared to conventional ovens which needs time and consume a huge amount of energy to heat up to required temperature[14]. On the other hand, the sensitizers carrying different structural patterns lead to distinct efficiency for **PET** process and significantly different efficiency and lifetime of fluorescence although they share the similar value of  $E_{ox}$  and  $E_{red}$  at the point view of photophysics. As an example, the absorber comprising barbiturate group on the methine chain shows negligible internal barrier (net charge of the molecule equals zero) between the iodonium salts while those carrying other substitutions with net charge of the molecule equals one exhibit high internal barrier[118, 161]. Furthermore, the effort made to improve the solubility and compatibility in/with the matrix result in cyanines with more options of structural patterns, substituents and counterions[20, 130].

Therefore, the matter of fact is that there exist still a lack of deeper understanding and clear strategy for the selection of those compounds on demand relating their structures, performance in specific applications[111, 160, 256, 261]. As demonstrated in **Scheme 17**, the intelligent design-of experiment systems in a so-called Chemistry 4.0 circle may play an important role in the future for the selection and optimization, while this process still requires sufficient reliable data and results from experimental aspects. Moreover, one is also supposed to take sustainability and energy saving into consideration which would bring such systems to Chemistry 5.0 as the implementation of sustainable chemistry.



**Scheme 17.** Workflow to develop technology for the design and fabrication new materials in a setup based on an intelligent Design-of Experiment (DoE) with the combination of chemistry, engineering and informatics generating artificial intelligence, cited from[20].

### 3. Materials and Methods

This chapter describes the materials and light sources applied in the experiments of this thesis. All the reagents except some of the reactive monomers were used without any further purification as obtained from the suppliers. The monomers **TPGDA**, **TMPTA**, **HBVE**, oxetanes (**OXT03** and **OXT09**) were run through the basic  $\text{Al}_2\text{O}_3$  columns to remove the inhibitors before applied to polymerization.

#### 3.1 Chemicals for Photopolymerization

##### 3.1.1 NIR Sensitizers Derived from Cyanines of Different Structural Pattern

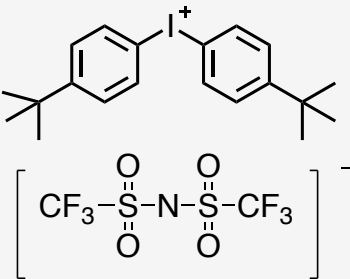
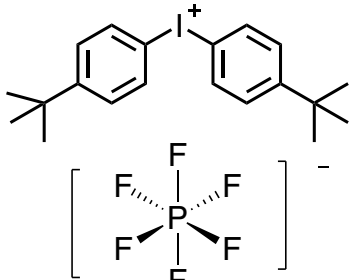
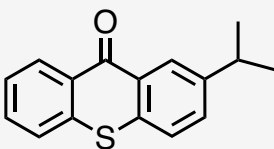
In this thesis, a series of cyanines comprising variable structural pattern were selected to investigate the relation between the structure of the cyanines functioned as NIR range photoabsorbers and/or sensitizers particularly to optimize the regarding performance combined with iodonium salts. The structure of cyanines could vary from different aspects based on the symmetrical structural pattern as shown in **Scheme 14** *vide supra*, which includes changes of the terminal groups ( $R_1$ ,  $R_2$ ), length of connecting chain ( $n_1$ ), substitutions at the *meso*-position ( $R_3$ ,  $n_2$ ) as well as on the terminal groups ( $R_4$ ). The length of connecting chain in the middle changes the distribution of  $\pi$ -electron on the conjugate cyanine molecule. Therefore, based on the structural pattern in **Scheme 14**, cyanines derived from tri-, penta-, hepta- and nonamethine structure carrying specific substitutions on the connecting chains were chosen. They also possess different terminal groups derived from either benzo[*e*], benzo[*g*] or benzo[*c,d*]-Indolium and carry different substitutions on the terminal groups. Moreover, cyanines with either an unbridged/open connecting chain or bridged connecting chain substituted with different indolium groups such as five or six-membered ring as well as other  $\pi$ -electron donating or accepting groups. In addition, the respective counter anions of the cyanines also differ in sizes.

The previous work from our group disclosed that the heptamethine based cyanines could actively contribute during a **PET** process by reducing iodonium cation based on their redox properties [115, 118]. As a comparison, 2-isopropylthioxanthone (**ITX**) was used for the samples exposed with ultraviolet (UV) radiation. These NIR-sensitizers were obtained either from FEW Chemical GmbH in Germany or Spectrum Info Ltd in Ukraine. More details such as physical properties could be found in **Table 3** while the distinct structures of these sensitizers is depicted in **Chart 2**.

### 3.1.2 Co-Initiators Combined with Sensitizers

Based on the previous important findings, co-initiators operating as electron acceptors represent necessary prerequisites to initiate the generation of reactive species such as conjugate acid which is related to cationic photopolymerization and/or radicals to initiate free radical polymerization, respectively. This proceeds according to reactions in the Equation (6-8) disclosed in **Section 2.2.1**. Therefore, in this thesis, an iodonium salt (**IS**) coupling with the anion **[NTf<sub>2</sub>]<sup>-</sup>** was selected and combined with NIR-sensitizers to operate in the most of the experiments. The structures of the co-initiators **IS** and **IS-PF<sub>6</sub>** used could be found in **Table 1**. **IS** comprises the **[NTf<sub>2</sub>]<sup>-</sup>** anion bringing advantages compared to the **[PF<sub>6</sub>]<sup>-</sup>** anion, which would release **HF** under some circumstances[132].

**Table 1.** Co-initiators used in this thesis.

Commercial name*	Structure	Name in text
S2430		<b>IS</b>
Bis(4-tert-butylphenyl)iodohexafluorophosphate		<b>IS-PF<sub>6</sub></b>
Isopropylthioxanthone		<b>ITX</b>

\*: commercial names are from the suppliers.

### 3.1.3 Monomers for Free Radical and Cationic Polymerization

There are several kinds of typical monomers commonly applied in photopolymerization systems including (meth)acrylates relating to free radical polymerisation protocol while oxiranes (epoxides), oxetanes and vinyl ethers following a cationic polymerization process. In this work, three different (meth)acrylates comprising the -C=C- bond functional groups exhibiting different features were used to explore the efficiency of the NIR initiating system

to initiate free radical photopolymerization. Here, the difunctional acrylates represent tripropylene glycol diacrylate (**TPGDA**, viscosity of 15 mPa·s) and di-2-methacryloxyethyl 2,2,4-trimethylhexamethylenedicarbamate (**UDMA**, viscosity of 7493 mPa·s). In addition, a trifunctional acrylate trimethylolpropane triacrylate (**TMPTA**, viscosity of 41 mPa·s) functioned to generate highly crosslinked polymer networks. These monomers were all purchased from Sigma-Aldrich. **TPGDA** and **TMPTA** went through basic Al<sub>2</sub>O<sub>3</sub> (from Carl Roth GmbH) columns to remove the inhibitors prior to use while **UDMA** was used without any purification due to the high viscosity.

On the other hand, cationic photopolymerization was also explored based on the cationic monomers oxiranes, oxetanes and vinyl ethers. That is oxiranes such as bisphenol A diglycidyl ether, an oligomer (commercially named as **Epikote 357**, here available from Hexion) showing a viscosity of 636 mPa·s and butanediol diglycidyl ether (**Epilox P 13-21**) received from FEW Chemicals showing a viscosity of 16 mPa·s. The oxetanes were gratefully obtained from Gurun Technology in China namely 3,3'-(oxybis(methylene))bis(3-ethyloxetane) (**OXT03**, viscosity of 11 mPa·s) and 3-Ethyl-3-(methacryloyloxy)-methyloxetane (**OXT09**, viscosity of 4 mPa·s), respectively. Furthermore, 4-hydroxybutyl vinyl ether (**HBVE**) (purchased from Sigma-Aldrich) exhibiting a very low viscosity of 5 mPa·s was also taken for cationic photopolymerization experiments. Among the cationic monomers, **OXT03**, **OXT09** and **HBVE** ran through basic Al<sub>2</sub>O<sub>3</sub> while **Epilox P 13-21** and **Epikote 357** were used as received. The viscosity of all the monomers above was obtained in the lab at 25 °. The structures of these monomers could be found in **Chart 1**.

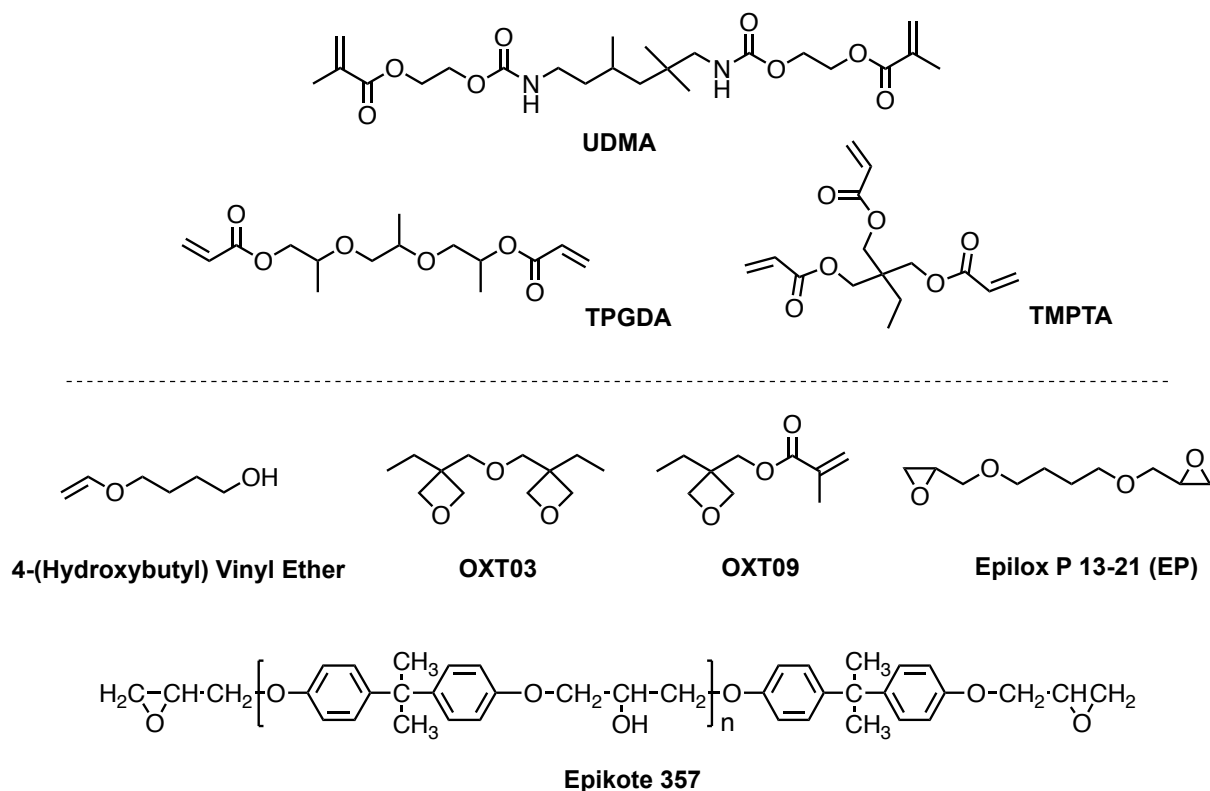


**Chart 1:** Structures of monomers used for photopolymerization in this thesis.

### 3.1.4 Materials to Quantify the Conjugate Acid

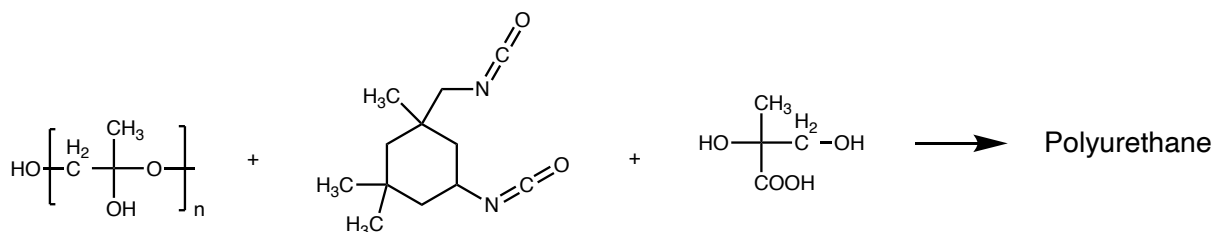
As shown from the mechanism of traditional cationic polymerization, conjugate acid presents as a necessary mediated agent to initiate the polymerization. Herein, the ability of the initiator systems to generate conjugate acid was evaluated following an optical assessment. In this process, colourless Rhodamine B lactone (**RhB-L**) was used as reagent to react with the conjugate acid, which was generated during the **PET** protocol by light exposure resulting in a red coloured Rhodamine B (**RhB-H**) showing an absorption maximum at 550 nm[88].

### 3.1.5 Water-Based Polyurethane Dispersions

Water-based polyurethane binder available as an aqueous dispersion was introduced to study the performance and efficiency of the NIR absorbers on photonic drying of coatings combined with the irradiation using high-power NIR-LEDs. Because based on the investigations of the cyanine materials, some candidates among these NIR absorbers showed big potential to generate heat which could be prospective for physical drying of coatings. Herein, polyurethane aqueous dispersions (waterborne polyurethane dispersions comprising UV-sensitive initiators as standard and without photoinitiator, respectively) gratefully received from Rhein-Chemotechnik GmbH (Breitscheid in Germany) were used as coating systems. The experiments were pursued on the surface of construction bricks.



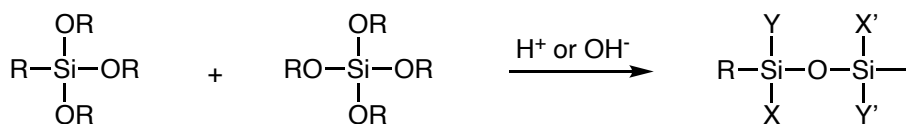
The specific structure and component of these polyurethane solutions were not disclosed due to the commercial confidential reasons. To provide more information, as an example, **Scheme 18** depicts the general procedure to synthesis polyurethanes based on the documents for the practical training of students in Hochschule Niederrhein.



**Scheme 18.** Synthesis route for polyurethanes of general structure, which was used for practical training of students in the Department of Chemistry in Hochschule Niederrhein, cited from[277].

### 3.1.6 Nanoparticle Comprising Sol-Gels

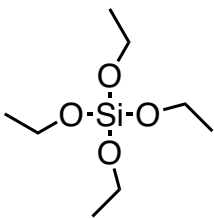
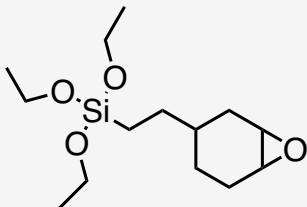
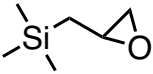
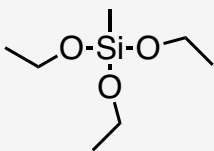
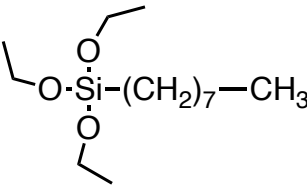
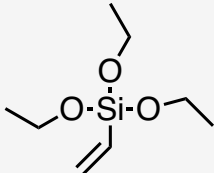
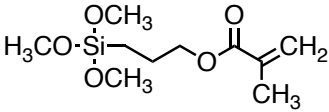
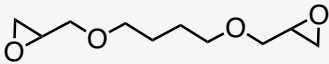
In addition, we have the intention to bring this novel initiating system together with high-power light sources into practical application fields, therefore, the initiator system comprising NIR sensitizer and iodonium salt was taken to study the efficiency to initiate a sort of sol-gel coatings comprising nanoparticles generated based on the silanization of silanes possessing different functional groups. **Scheme 19** depicts the general procedure of silanization to generate silica-based nanoparticles from silanes.



**Scheme 19.** Process of silanization with general structural pattern. X/X', Y/Y' vary based on the reaction degree of silanization, drawn based on[278].

The functional groups (-R) could be transferred onto the silica nanoparticles after the silanization process. Thus, the prepared coatings could still carry the respective functional groups. In this section, three different kinds of sol-gels (**SG1**, **SG2** and **SG3**) comprising different functional nanoparticles based on silanes carrying different groups were used as coating precursor. **Table 2** lists the components in the sol-gels.

**Table 2.** Components and viscosity of the sol-gels used in this thesis.

Silanes	Chemical Structure	SG1 (wt%)	SG2 (wt%)	SG3 (wt%)
Filck S10 (Flour)	*	0.15	-	-
Tetraethoxysilane (TEOS)		22	37	-
Epoxy-cyclohexy-TEOS		20	20	20
Glymo-tetramethoxysilane (TMOS)		4.85	5	15
Methyl-TEOS		50	35	22
Octyl-TEOS		3	3	3
Vinyl-TEOS		-	-	20
3-Methacryloxypropyl-trimethoxysilane (MEMO)		-	-	20
Epilox p 13-21 (EP)		70	70	70
Viscosity (mPa·s)	16 <sup>[a]</sup>	200	290	80.4

\*: structure not found from open access sources as obtained from FEW Chemicals GmbH. <sup>[a]</sup>: Viscosity of the monomer **EP** self-measured in the lab.

### 3.1.7 Solvents

The high purity solvent methanol (MeOH) was used to prepare the samples when measuring fluorescence while deuterated acetone was needed for the measurement of Nuclear Magnetic Resonance (NMR) spectroscopy. Furthermore, spectroscopic grade acetonitrile (ACN) was used for the experiments of photobleaching and UV-Vis-NIR Spectroscopy. Further details could be found in [90].

## 3.2 Light Sources

There were several different types of light sources used in this thesis. The information of intensity of the LEDs used was provided by a fibre optic spectrometer (USB4000 from Ocean Optics) combined with the software Oceanview while the output power of the laser was determined by using the power intensity meter (model 407A from Spectral-Physics Corp.).

### 3.2.1 NIR-LEDs

#### *High-Power NIR-LEDs*

A high-power NIR-LED prototype emitting at 820 nm exhibiting a size of 8 cm × 13 cm × 3 cm (left picture in **Figure 6**) was gratefully obtained from Phoseon Ltd.. It originally reached the intensity of 2.5 W/cm<sup>2</sup>. Nevertheless, the output power mostly applied here was 1.0 W/cm<sup>2</sup> covering a directly exposed area of an approximative rectangle of 14 cm<sup>2</sup> with the corresponding distance.

Due to the difference of the maximum absorption of the NIR sensitizers, an alternative high-power NIR-LED emitting at 860 nm equipped with two alignments of LEDs of 13.5 cm × 4 cm was received from EASYTEC GmbH (**Figure 6**). As an experimental comparison, the output power intensity of 1.0 W/cm<sup>2</sup> was also reached by adjusting the distance between samples and light sources. In addition, the direct exposed area was available with 36 cm<sup>2</sup> (12 cm × 3 cm). Furthermore, a portable LED (in **Figure 6**) emitting at 860 nm purchased from EASYTEC GmbH with the exposure density of 1.0 W/cm<sup>2</sup> was taken to carry out the investigations of kinetics of photopolymerization by real time FTIR spectroscopy.

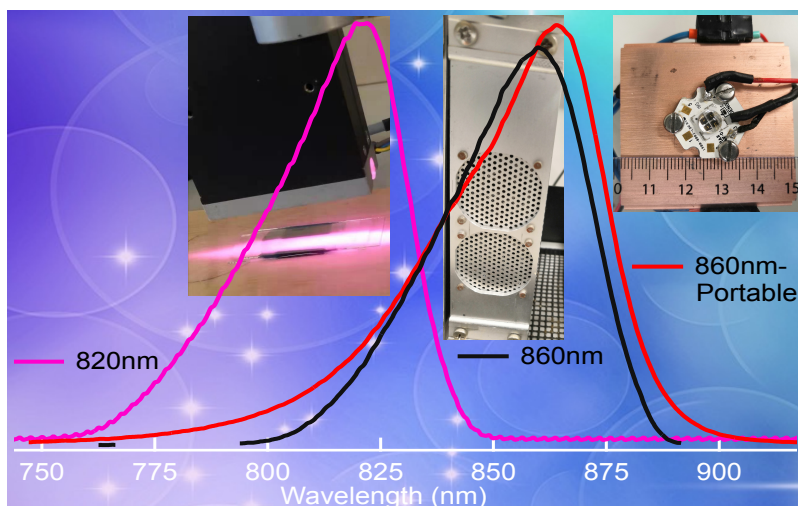


**Figure 6.** Emission spectrum and profiles of the NIR-LEDs used in this thesis.

### NIR-LED with low intensity

A NIR-LED emitting at 770 nm available from Roithner Lasertechnik GmbH was used to study the system comprising **S7a** and **IS** in **TPGDA** for the photo-DSC setup. The output intensity of this NIR-LED in the experiment was measured with 45 mW/cm<sup>2</sup>.

### **3.2.2 UV-LED at 395 nm**

As shown in **Figure 7**, a UV-LED prototype emitting at 395 (right picture) nm exhibiting the similar size to the aforementioned high-power NIR-LED at 860 nm, was used for irradiation of UV active systems, The intensity of this device could be also adjusted to 1.0 W/cm<sup>2</sup> for the exposure to initiate photopolymerization. In addition, a portable UV-LED device (left picture) emitting at 395 nm was also taken due to the feature of portability for real-time FTIR measurement.

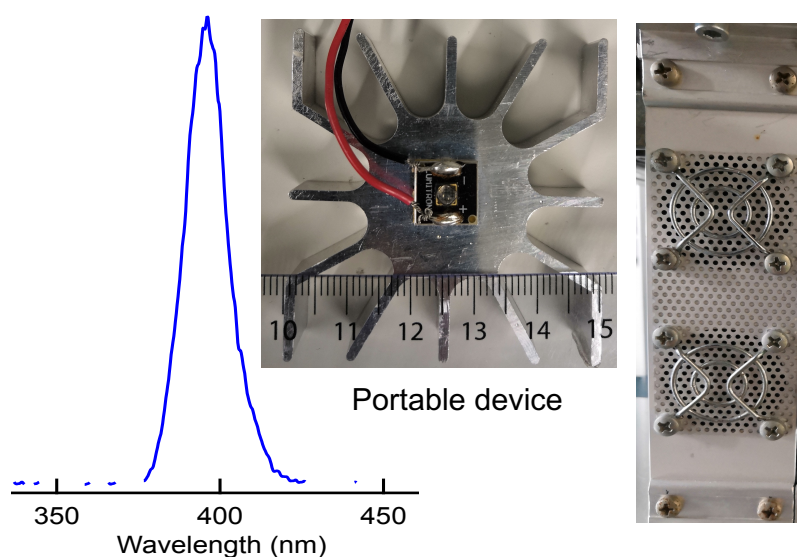


**Figure 7.** Emission spectrum and profiles of the UV-LEDs used.

### 3.2.3 NIR Laser

A diode laser emitting at 974 nm coupled with an adjustable fibre (CNI-980-25 W-5-FC-A1-TTL1- MM400SMA from Changchun New Industries Optoelectronics Technology Co., Ltd.) was used as an irradiation source to investigate the polymerization reactivity of the **UDMA** system comprising **S7b**. The operation of this experiment was done under the instruction and help by Paul Hermes[254]. The output power of this laser could be adjusted and controlled on a tabletop laser driver. The exposure with this laser was operated in an ON/OFF mode for 10 s ON and OFF for 5 s to avoid unnecessary warming due to the high power intensity ( $I = 125 \text{ W/cm}^2$ ).

## 3.3 Characterization Methods and Equipments

The measurements and characterizations were operated using the following devices and equipments, respectively. All the subsequent data analysis and evaluation as well as graphs were carried out on the software Igor Pro 8 version 8.04 from WaveMetrics.

### 3.3.1 UV-Vis-NIR Spectroscopy

The UV-Vis-NIR spectra were performed on an Evolution 200 from Thermo SCIENTIFIC using high precision cell cuvettes of  $1 \times 1 \text{ cm}$  from HellmaAnalytics. Some of the measurements were also carried out on UV-3600 i Plus from SHIMADZU because of the limitation of detection the NIR on the aforementioned device. The data points of the measurements were collected every second.

### 3.3.2 Cyclic Voltammetry

In this work, the oxidation and reduction potentials of the NIR sensitizers were determined by following a previous protocol by using the cyclic voltammetry (followed with a Versastat4-400 from AMETEK functioned as potentiostat) in which the solution ( $0.1 \text{ mol} \cdot \text{L}^{-1}$ ) of tetrabutylammonium hexafluorophosphate from Sigma Aldrich in acetonitrile functioned as a supporting electrolyte and ferrocene served as an external standard in acetonitrile. All the data points were collected at a scanning rate of  $0.015 \text{ V/s}$  by using platinum disc as a working electrode and Ag/AgCl as reference electrode[88, 118].

### 3.3.3 Fluorescence and Lifetime Measurement

Fluorescence quantum yields of **S3b**, **S5a**, **S7g**, and **S9** were taken by a FS 920 from Edinburgh Instruments by use of a reference carried out with Sulforhodamine 101 applying correction mode for both excitation and emission using  $1 \text{ cm}$  cuvette at  $22^\circ\text{C}$ . More details can be found elsewhere[90]. GMBU (Jena) took these measurements on request as

service to provide data for this contribution that resided mainly outside of the spectral response ( $> 900$  nm) of the lifetime spectrometer used in this thesis from PicoQuant.

Some other data obtained were carried out by a regular fluorescence set up (FluoTime 300 from PicoQuant GmbH) with diode laser excitation at 677 nm (LDH-P-C-670) until 900 nm for recording fluorescence emission  $\lambda_{\text{max}}^f$  to take decay time  $\tau_f$  and quantum yield  $\Phi_f$ . Time correlated single photon counting was the technique to take the emission decay[279]. This instrument from PicoQuant provides the opportunity to measure decay between 25 ps and several milliseconds. The instrument was equipped with high resolution emission double monochromator operated in subtractive mode (2 x 300 mm focal length, UV/VIS/IR grating pair 1st stage: 600 l / mm blaze 1250 nm and 1200 l / mm blaze 500 nm, dispersion: 4.5 nm / mm, UV / Vis grid pair 2nd stage: 1200 l / mm blaze 500 nm 1200 l / mm blaze 500 nm (-), 2.7 nm / mm (-), PMA-C 192-M Cooled photomultiplier) for the emission side. Excitation was proceeded by using a computer controlled diode laser driver for picosecond pulses (196 kHz and 80 MHz, external trigger input). The system can be also operated in a *cw*-mode to record spectra in additive mode (monochromator: blaze 500 nm (+), dispersion: 1,4 (+)). EasyTau software and laser control software controlled the system. This also facilitated to calculate decay time by the software by iterative convolution. An appropriate scatter (Ludox in water) was taken to record the instrumental response function of the system. Time resolution of the instrument is  $> 25$  ps. For preparation, the sample was dissolved in methanol (spectroscopic grade) to get the absorption of extinction of  $< 0.1$  at 677 nm. The EasyTau Software also operated to calculate the decay time by iterative convolution between the instrumental response and the sample.

Absolute fluorescence quantum yields were measured with an integrating sphere provided by PicoQuant for the FluoTime 300 spectrometer. First the respective counts available by the laser were measured using a blank cuvette comprising spectroscopic grade solvent. Then the sample was exchanged with a cuvette comprising the same solvent and the absorber exhibiting an absorption between 0.05-0.1 at 677 nm. This treatment resulted in the absorption of the absorber taken for measurement needed to determine fluorescence quantum calculated with the EasyTau software that also controlled the instrument, reported in[90].

### 3.3.4 Conductivity Measurement of Iodonium Salt in Monomers

Conductivity of the mixture of Iodonium salts (ISs) in monomers was determined with 856 Conductivity Module combined with 900 Touch Control panel from Metrohm. A 5-ring measuring cell with cell constant of  $c = 0.7 \text{ cm}^{-1}$  with Pt 1000 was equipped on this device.

### 3.3.5 Real Time- and Fourier Transfer Infrared (FTIR) Spectroscopy

In this work, the final conversions of the respective monomers after photopolymerization were determined by Fourier Transfer Infrared (FTIR) spectroscopy carried out on the device Vertex 70 (Alpha-P) from Bruker by using Attenuated Total Reflection (ATR) mode operated for setting and data collection on the software OPUS (Version 6.5 from Bruker). A small amount of solid samples were applied on the sample stage pressed by an arm lever, for the measurements, 25 scans from  $400\text{-}4000 \text{ cm}^{-1}$  were applied to acquire satisfying spectra.

In addition, real-time FTIR spectra provide the necessary kinetic information relating to the whole process of photopolymerization. For this procedure, the reactive liquid solutions were first applied on the sample plate. Then the FTIR spectra (data points) for the subsequent analysis were collected continuously every 0.2 s for free radical polymerization system while 0.733 s was set up for cationic polymerization during irradiation in ATR mode[91].

### 3.3.6 Photo- and Differential Scanning Calorimeter (DSC)

In order to explore the effect of the heat in the monomers comprising NIR absorbers, a differential scanning calorimeter (DSC Q2000 from TA Instruments) was used to determine thermal initiation temperature  $T_i$  of the system comprising NIR sensitizers and iodonium salt in the monomers.  $T_i$  represents the temperature where significant generation of heat for polymerization occurs during continuous heating[88, 118, 280]. These measurements were carried out through a heating procedure from room temperature up to  $200^\circ\text{C}$  following a ramping rate of  $10 \text{ }^\circ\text{C}/\text{min}$  with sample amount of approximately 5 mg. Subsequently  $T_i$  was determined at the onset point from the exothermal peak on heat flow curves. It is a parameter disclosing the thermal stability of a radical polymerization system without treatment of light[88].

Moreover, a regular photo-DSC procedure on the same device was carried out to investigate the efficiency of the NIR initiating system to initiate photopolymerization, which offers the possibility to run the experiments approving the necessity of additional heat needed to activate photopolymerization under isothermal condition at different

temperatures. The aforementioned NIR-LEDs were taken as the irradiation source. The NIR light for irradiation was collected by a lens and projected into a two-arm y-fibre connected to the sample chamber of DSC device. Here, the intensity of the output light through the fibre arms was adjusted to be identified for the sample and reference pan, respectively. In addition, a shutter placed between the light source and the lens controlled by a programmed Arduino Uno board was introduced to synchronise the light source and experiment[130].

### 3.3.7 Thermal Camera

The temperature of samples and surroundings during the irradiation of NIR light was recorded by using a NIR sensitive camera purchased from Testo SE & Co. KGaA (Version TEST 0563 0885 V7). The live process was carried out with the software IRSoft from Testo[118].

### 3.3.8 Mass Spectrometry Coupled with High-Performance Liquid Chromatography (HPLC)

The products of the sensitizers from photoreaction were analysed by carrying out mass spectrometry coupled with HPLC via a QTOF-LCMS system (G6530B) from Agilent where Dual AJS ESI was used as the ion source operated in positive mode[118]. A column Hypersil C4 (125 x 4mm) from Thermofischer Scientific was used with acetonitrile/water (80:20) as dilution solvent, which was changed to 95:5 after 20 minutes.

### 3.3.9 Nuclear Magnetic Resonance (NMR) Analysis

A Fourier 300 from Bruker served as source to record the  $^1\text{H}$ -NMR spectra to explore the reaction of **HBVE**. The system comprising sensitizer **S9** ( $0.005 \text{ mmol}\cdot\text{g}^{-1}$ ) and **IS** ( $0.03 \text{ mmol}\cdot\text{g}^{-1}$ ) in **HBVE** was exposed in a round glass dish (height: 1 cm, diameter: 3 cm) for 10 min applying an 860 nm LED-array (power:  $1.0 \text{ W}/\text{cm}^2$ , exposed area:  $3 \text{ cm} \times 12 \text{ cm}$ ) for excitation. This was done under continuous nitrogen purging. Then, 20 mg of the product obtained was dissolved in 1 mL deuterated acetone for NMR measurement. The subsequent data acquisition and analysis was finished on the software Topspin 4.1.0 (Bruker).

### 3.3.10 Rheometer Coupled with Heat Program

In photopolymerization systems, quantitative knowledge about the viscosity of the reactive monomers is very important. Therefore, a modular compact rheometer (Version MCR 102 from Anton Paar GmbH) was taken to collect the viscosity of the monomers used in this



work using a PP25 parallel plate with a shear rate of  $50 \text{ s}^{-1}$  at the temperature of  $25^\circ\text{C}$ . Data points were obtained every second. Moreover, the crosslinking of **UDMA** comprising NIR sensitizers was also investigated while coupling with a programmed heating up process using the heating device from Julabo GmbH (Version F 26).

### 3.3.11 Dynamic Mechanical Analysis (DMA)

In order to investigate the mechanical viscoelasticity of the materials obtained from photopolymerization, a dynamic mechanical analysis (DMA) device (version DMA Q800 from TA Instruments) equipped with a linear tension clamp was used to measure mechanical properties of the polymer films. The measurements ran at the condition of a constant frequency of 1 Hz, an amplitude of 10 mm as well as a preload of 0.01 N varying from  $-50^\circ\text{C}$  to  $200^\circ\text{C}$  with a ramping rate of  $3^\circ\text{C}/\text{min}$  where a sinusoidal force (stress) was applied to the samples and resulting in strain. With this oscillating loading, the mechanical properties measured could be reflected by the value of the storage modulus  $E'$  and loss modulus  $E''$ . Due to the large segments of the polymer, there is a phase lag or mechanical damping during the movement of polymer chains which is known as  $\tan\delta$  ( $\tan\delta = E''/E'$ ) [281]. This can be also seen as a critical factor to describe the mechanical property. Therefore, as a comparison, the values of the glass transition  $T_g$  determined by the onset of storage modulus  $E'$ , the peak maximum of loss modulus  $E''$  and the peak maximum of  $\tan\delta$  were displayed.

## 4. Experimental Section

This chapter describes the experimental information disclosed in this thesis. Further details could be also found in the publications[90, 91].

### 4.1 Structural Pattern of Cyanines Regulates the Efficiency of Non- and Radiative Processes upon Exposure of High-Power NIR-LEDs

This section discloses the experimental details applied to investigate the effects from the structural pattern of the cyanines functioned as NIR absorbers and photosensitizers (often abbreviated as **Sens** in the text) combined with iodonium salt to potentially initiate free radical and cationic photopolymerization.

#### 4.1.1 Selection of Sensitizers Based on Structural Patterns and Physical Properties of the Cyanines

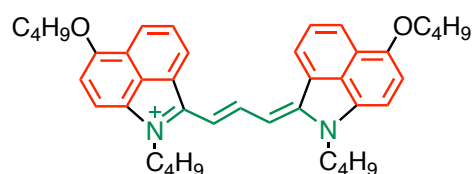
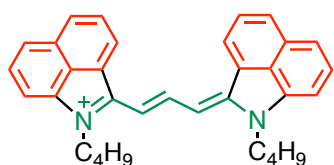
As shown in **Chart 2**, a series of polymethine compounds represented by the class of cyanines comprise different length of connecting methine  $(-\text{CH}=\text{)}_n$ - chains, variable substitutions at the *meso*-position and typically different terminal groups. Every specific substitutional aspect of the variation based on the structural pattern of cyanines brings respective features to these sensitizing compounds including absorption performance, redox behavior and photophysical properties such as fluorescence quantum yield and decay time.

**Chart 2** summarizes the structures selected in this thesis while properties are shown in **Table 3** in **Section 5.1** *vide infra*. These aforementioned properties can be affected by the substitution pattern. Comparison between **S3a/S3b** and **S5a/S5b** shows additional replacement of a butoxy group symmetrically located on the terminal position, respectively. **S7a** and **S7c** represent an additional structural feature. The both structures relate to the connecting chain between the symmetrical terminal parts, that is an unbridged open chain in the case of **S7a** while bridged chain exists in **S7c**. This has a huge impact on the chemical property in NIR-sensitized radical polymerization. An internal activation barrier must be overcome in the case of **S7c** while that appeared less in the unbridged **S7a**. Different terminal groups address a further comparison between **S7a** and **S7b**. Here, one can find that **S7a** carries an indolium group while benzo[*c,d*]indolium group remains in **S7b**. Similar changes also appear to the pair of **S7c** and **S7e** as well as **S7d** and **S7f**, respectively. Another comparison focusses on the material comprising the same terminal groups (indolium on **S7c** and **S7e**, benzo[*c,d*]indolium for **S7d** and **S7f**) but the substitution changes in the *meso*-position on the bridged chain between **S7c** and **S7e**, as well as **S7d**

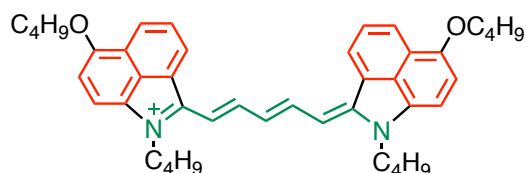
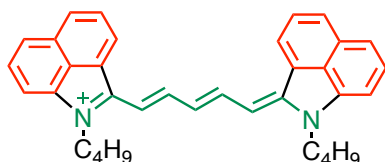
and **S7f**, respectively. Furthermore, **S7e**, **S7f** and **S7g** share completely the same connecting chain in the middle but differ regarding the terminal position; that is indolium in the case of **S7e**, benzo[*c,d*]indolium for **S7f** and benzo[*g*]indolium in the case of **S7g**. There is also little difference besides sharing the same terminal group between **S7c** and **S7h** that is **S7c** possesses a substitution in the middle chain comprising a five-numbered ring while **S7h** exhibits a six-numbered ring there. For the comparison between **S7i** and **S7j**, both carry the same ring substitution in the middle chain while difference comes up on the terminal group of benzo[*e*]indolium. One should keep in mind that the sulfonic acid group on the terminal position and butanesulfonic acid group at the position of nitrogen in the case of **S7i** facilitate this absorber good solubility in water. Moreover, **S9** possesses the longest connecting chain in the middle among these compounds while it shares the same six-numbered ring as **S7h** at the *meso*-position. One more word needs to be delivered here, that is the connecting methine chain between both terminal parts. It increases and becomes longer and longer following the larger number in the examples from **3** to **9**.

Methine  
Groups

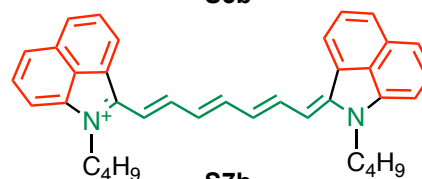
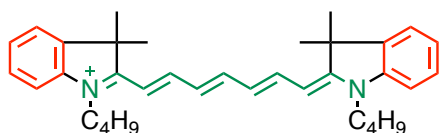
III



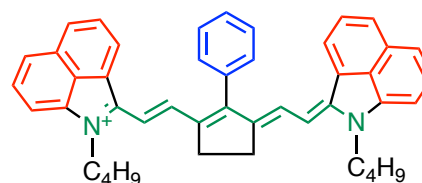
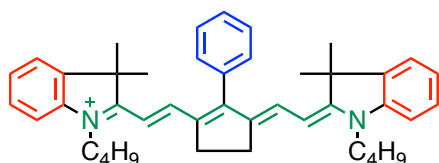
V



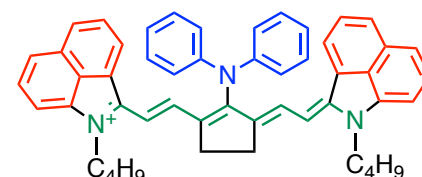
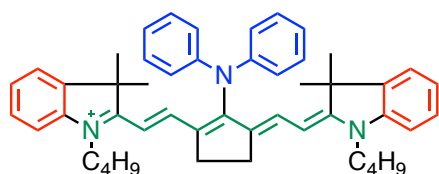
VII



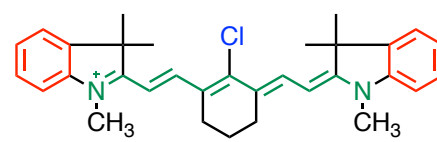
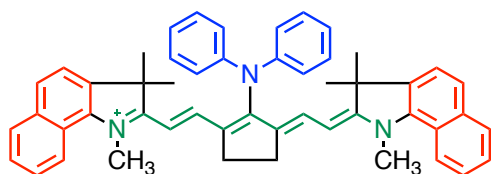
VII



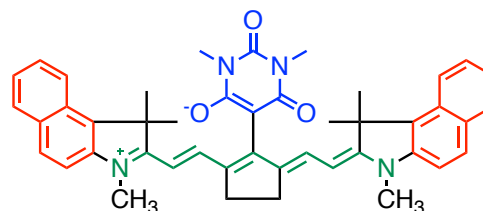
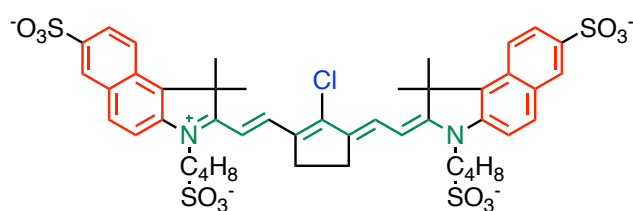
VII



VII



VII



IX

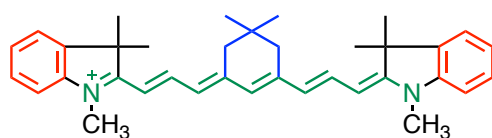


**Chart 2.** Chemical structures of the NIR absorbers (sensitizers) used in this thesis. These cations comprise the following anions: **S3a**, **S5b**, **S7d**, **S7e** and **S7f**:  $\text{BF}_4^-$ ; **S3b**, **S5a**, **S7g** and **S9**:  $[\text{PF}_3(\text{C}_2\text{F}_5)_3]^-$ ; **S7a**, **S7b**:  $\text{PF}_6^-$ ; **S7c**, **S7h**:  $p\text{-CH}_3\text{-Ph-SO}_3^-$ ; **S7i**:  $[\text{NH}(\text{C}_2\text{H}_5)_3]^3+$ . **S7j**: Cyanine with zwitterion.

#### 4.1.2 Bleaching Kinetics of Sensitizers with and without Iodonium Salts by Excitation with High-Power LEDs

Exploration of the influence of the structural patterns of the NIR absorbers to generate radicals appears essentially to understand efficiency for initiation of free radical photopolymerization. Here, photobleaching behaviour of the NIR sensitizers **S3-S9** combined with **IS** was studied by collecting and comparing the UV-Vis-NIR spectra of the samples before irradiation and after certain irradiation cycles. The samples comprising **Sens** ( $5.0 \times 10^{-6} \text{ mol}\cdot\text{L}^{-1}$ ) and **IS** ( $3.0 \times 10^{-5} \text{ mol}\cdot\text{L}^{-1}$ ) were prepared as solutions where acetonitrile served as solvent. The spectra of the original solutions were firstly collected using  $1 \times 1 \text{ cm}$  quartz cuvettes by UV-Vis-NIR spectrometer Evolution 200 from Thermo SCIENTIFIC. Then the solutions were exposed in different time interval, that is 2s, 5s, 15s, 30s, 1min, 2min, 5min, 10min, 15min and 30min to investigate changes in the spectra appearing as decrease at the exposure wavelength or build up of new absorptions with either hypsochromic or bathochromic shift with respect to the exposure wavelength.

The aforementioned high-power NIR-LEDs (intensity of  $1.0 \text{ W}/\text{cm}^2$  at emission maximum) emitting at 820nm or 860nm were taken as the light sources for the photobleaching exposure. One should keep in mind that the emission of LEDs is not tunable. Therefore, excitation at different range of the absorption spectra results in distinct penetration length taking similar conditions of the **Sens**. More details could be found in reference[90]. Systems comprising **S3a**, **S7a**, **S7c**, **S7e**, **S7h** and **S7j** as **Sens** were exposed by LED emitting at 820nm while **S3b**, **S5a**, **S5b**, **S7b**, **S7d**, **S7f**, **S7g**, **S7i** and **S9** were exposed with the 860 nm emitting LED in the bleaching experiment while the output intensity of the LEDs was kept at the same value. In addition, bleaching of **S7i** was carried out in aqueous surrounding combined with dispersed TPO-L followed the same aforementioned strategy.

#### 4.1.3 Activity of the System Comprising Sensitizers and Iodonium Salt to Generate Conjugate Acid

Conjugate acid generated during exposure of a solution comprising **Sens** and **IS** was quantified following a previous protocol[88]. Experimental details were also disclosed in previous reports[90]. The spectral changes caused by the protonation of Rhodamine B lactone serving as optrode were recorded by the aforementioned UV-Vis-NIR device. The protonation of colorless Rhodamine B lactone leads to the magenta coloured product of Rhodamine B exhibiting a spectral absorption maximum located at 550nm in the solvent acetonitrile. For sample preparation, **Sens** ( $2.0 \times 10^{-5} \text{ mol}\cdot\text{L}^{-1}$ ) and **IS** ( $1.2 \times 10^{-4} \text{ mol}\cdot\text{L}^{-1}$ ) were dissolved in a volumetric flask of 10 mL in acetonitrile and exposed in a cuvette ( $1 \times$

1 cm) applying NIR-LEDs of either 820 nm or 860 nm for 15 mins using the respective sensitizers while the iodonium salt was the same. Afterwards, the UV-Vis-NIR spectra of the neat solvent were taken as the background to be subtracted. The concentration of conjugate acid generated during exposure was evaluated based on the spectra of the solutions aforementioned following with addition of Rhodamine B lactone ( $1.0 \times 10^{-4} \text{ mol} \cdot \text{L}^{-1}$ ). The quantified conjugate acid formed approves the formation of acidic species for the initiation of cationic photopolymerization. Nevertheless, the amount of determined acid may not be comparable to the acid generated in actual photopolymerization experiment because both experiments were operated in different surroundings. While the reactivity tendency and potentials from **Sens** based on different patterns is comparable from this method[90].

## 4.2 Reactivity of Different Sensitizers and Iodonium Salt to Initiate Free Radical and Cationic Photopolymerization

This section describes the experimental conditions applied in the thesis. It also discloses the details related to the measurements.

### 4.2.1 Cyclic Voltammetry

The oxidation  $E_{\text{ox}}$  and reduction  $E_{\text{red}}$  potentials of the NIR sensitizers were measured through a previously reported procedure[101, 118]. Firstly, a solution of tetrabutylammonium hexafluorophosphate ( $0.1 \text{ mol} \cdot \text{L}^{-1}$ ) purchased from Sigma Aldrich, was prepared by dissolving in acetonitrile serving as electrolyte. Then the samples ( $1.0 \times 10^{-3} \text{ mol} \cdot \text{L}^{-1}$ ) were measured following a similar method applied on Versastat4-400 from AMETEK served as potentiostat while the data of ferrocene was taken as an external reference[88]. The data were recorded at a scanning rate of  $0.015 \text{ V} \cdot \text{s}^{-1}$  by using platinum disc as a working electrode and Ag/AgCl served as a reference electrode.

### 4.2.2 Conductivity Measurement

Conductivity depicting the movement of ions in the solutions and transfer of electrons and charges relates somehow to the reactivity of the cationic photopolymerization systems since initiation and ring opening proceeds by well solvated acidic cation. Therefore, the conductivity data of the cationic systems were measured by using a 5-ring conductivity measuring cell where the constant  $c = 0.7 \text{ cm}^{-1}$  with Pt 1000 equipped 856 Conductivity Module. The solutions dissolved with **IS** ( $3.8 \times 10^{-2} \text{ mmol} \cdot \text{g}^{-1}$ ) in the cationic monomers including **HBVE**, **OXT03**, **OXT09**, **Epilox P 13-21** and **Epikote 357** were measured at room temperature, respectively.

### 4.2.3 Initiation upon Low-Power Exposure Determined by Photo-DSC

A regular photo-DSC setup[101, 130] was applied to record the heat flux generated by polymerization of the monomer. It was carried out under isothermal conditions. Therefore, heat generated would not be directly available to activate chemical reactions but rather be compensated by the isothermal procedure of the equipment. Nevertheless, it offers the possibility to study the response of the system at different temperatures under isothermal conditions. The heat available from the ambient environment at different temperatures provides additional energy coming from outside to overcome partially internal activation barriers of the system to initiate the polymerization at a temperature above a certain threshold[90]. From the previous findings, below of this threshold, nearly no polymerization or very inefficient initiation shall proceed[88, 118].

The NIR light applied for irradiation was collected by a lens and projected into a two-arm fibre (Y-fibre) connected to the sample chamber of the DSC device. Here, the intensity of the output power through the fibre was controlled by a USB 4000 spectrometer aforementioned operating as radiometer. In addition, a shutter was introduced to synchronize the light source and measurement placed between the light source and the lens[88]. In order to investigate the reactivity of sensitizers, **S7a** ( $0.001 \text{ mmol}\cdot\text{g}^{-1}$ ) was firstly together with **IS** ( $0.015 \text{ mmol}\cdot\text{g}^{-1}$ ) dissolved in **TPGDA** followed by exposure for photo-DSC procedure at different temperatures ( $25^\circ\text{C}$ ,  $40^\circ\text{C}$  and  $60^\circ\text{C}$ ). This measurement was carried out under continuous purge of nitrogen with the NIR-LED emitting at  $770\text{nm}$  as light source matching very well with the maximum absorption of **S7a** with an output intensity of  $45 \text{ mW}/\text{cm}^2$ .

### 4.2.4 Kinetics of Photopolymerization Followed by Real-Time FTIR

Kinetics of photopolymerization in the ambient surroundings were followed by applying a real time fourier transfer infrared (RT-FTIR) procedure in an attenuated total reflection (ATR) mode where data points were collected every  $0.2 \text{ s}$ [91] in a time frame of  $600\text{s}$  for free radical polymerization systems. Regarding this procedure, **Sens** ( $0.001 \text{ mmol}\cdot\text{g}^{-1}$ ) together with the **IS** ( $0.015 \text{ mmol}\cdot\text{g}^{-1}$ ) were dissolved in the monomers followed with treatment in an ultrasonic bath for  $15 \text{ mins}$ . Photopolymerization occurred upon the irradiation of either  $820 \text{ nm}$  or the portable  $860 \text{ nm}$  LED aforementioned for the respective **Sens** with a power intensity of  $1.0 \text{ W}/\text{cm}^2$ . Moreover, the thickness of the samples during these measurements on the sample stage was controlled by a spacer to maintain a thickness of approximately  $30 \mu\text{m}$  covered with a microslide to get rid of the atmosphere

air. The wavenumber of  $\text{-C=C-}$  peak at around  $810\text{ cm}^{-1}$  was used to record spectral changes since they connect to conversion while vibration peak of  $\text{C=O}$  at around  $1725\text{ cm}^{-1}$  served as reference to compensate background changes to calculate the reaction degree of the photopolymerization of monomers **UDMA**, **TPGDA** and **TMPTA**.

In addition, for the cationic polymerization protocol, **Sens** ( $0.005\text{ mmol}\cdot\text{g}^{-1}$ ) and **IS** ( $0.03\text{ mmol}\cdot\text{g}^{-1}$ ) were dissolved in the monomers followed with the similar treatment as previous aforementioned but data collection in a time interval of  $0.733\text{ s}$  finished after  $900\text{ s}$ . The wavenumber for kinetics evaluation differs as disclosed and discussed in previous reference[91]. Here, the vibration of epoxy group between  $933 - 880\text{ cm}^{-1}$  and reference vibration band between  $1276 - 1191\text{ cm}^{-1}$  served to determine conversion of the epoxides **Epilox P 13-21** and **Epikote 357**. **HBVE** requested to take the  $\text{-C=C-}$  double bond between  $1682 - 1564\text{ cm}^{-1}$  while the peak at  $757 - 733\text{ cm}^{-1}$  operated as reference. Furthermore, the vibration between  $851 - 806\text{ cm}^{-1}$  was used for oxetanes (**OXT03** and **OXT09**) while the peak between  $1276 - 1191\text{ cm}^{-1}$  served as reference for evaluation of conversion. They respond to the data disclosed in refs[27, 88, 118].

### 4.3 Performance of the Initiating System Comprising Sensitizers and Iodonium Salt to Initiate Free Radical/Cationic Co-Polymerization

This section discloses the experiments carried out to investigate the efficiency of the aforementioned initiator systems to initiate free radical/cationic hybrid photopolymerization. More experimental details could be also found in[91].

#### 4.3.1 Viscosity Measurement

In order to find out the effects from viscosity of the monomers, the viscosity measurement was applied to neat monomers and mixtures, which composed polymerizable materials following one mechanism and monomers following at least two distinct mechanism. The latter relates to hybrid photopolymerization. For this experiment, the Modular Compact Rheometer (MCR 102 from Anton Paar GmbH) equipped with a PP25 parallel plate was used with a shear rate of  $50\text{ s}^{-1}$  at an isothermal condition of  $25^\circ\text{C}$  (controlled by a heating device F 26 from Julabo GmbH). Furthermore, data were collected every  $1\text{ s}$  while value of viscosity was determined by the average from 120 data points.

#### 4.3.2 Final Conversion of the Monomers from Hybrid Polymerization Systems

Instead of following the kinetics of hybrid polymerization by using real time FTIR, regular single FTIR spectra at ATR mode were taken to evaluate the polymerization degree by calculating the final conversion of the materials obtained. The solutions comprising **Sens**



and **IS** in monomers were dipped onto a glass plate with a spacer of around 60  $\mu\text{m}$  and covered with another glass plate and exposed by the high-power NIR-LEDs aforementioned for 12mins. And then polymer films obtained were removed from the glass plates and placed onto the FTIR sample stage for measurement. The samples went through for 25 scans and then the final conversions were calculated comparing the integration area with unreacted neat monomers by following the same method as real time FTIR. In addition, the average of 3 values from different sample areas was obtained as the final conversion of the measurement.

#### 4.3.3 Characterization for Mechanical Properties of Polymer Films Applied by DMA

Dynamic mechanical analysis (DMA, Q800 from TA Instruments) was applied for mechanical characterization of the film materials obtained by exposure. The experimental details are available in[91]. The materials were firstly prepared as surface flattened films with a width of 5 mm (determined by a specific knife from the measuring kit) and approximate thickness of 60  $\mu\text{m}$ . The sample chamber of the device must be cooled down to the starting point (around  $-50^{\circ}\text{C}$ ) by liquid nitrogen. Measurement was running with a linear tension clamp at the condition of a constant frequency of 1 Hz, an amplitude of 10 mm as well as a preload of 0.01 N varying from  $-50^{\circ}\text{C}$  to  $200^{\circ}\text{C}$  with a ramping rate of  $3^{\circ}\text{C}/\text{min}$ . A sinusoidal force (stress) was applied to the samples and resulted in strain. Afterwards, the mechanical properties of the materials measured could be determined based on the curves of storage modulus  $E'$  and loss modulus  $E''$ .

### 4.4 Contribution of the Heat Generated in the System Comprising Sensitizers and Iodonium Salts upon Exposure

This section describes the experiments designed to study the effects of the heat generated on demand of the NIR sensitizers.

#### 4.4.1 Thermal Stability of the Photoinitiators Comprising NIR Sensitizers and Iodonium Salt

The previous studies indicated that the introduction of NIR sensitizers significantly decreased the thermal stability of such an initiator system, while the influence and relation from the structural pattern of sensitizers has not been clearly understood and disclosed yet[88, 130]. Herein, the systems comprising **IS** ( $0.015\text{ mmol}\cdot\text{g}^{-1}$ ) and **Sens** ( $0.001\text{ mmol}\cdot\text{g}^{-1}$ ) carrying varied structures were investigated in **TPGDA** by following a regular differential scanning calorimetry (DSC Q2000) set up. The measurement was running by ramping from  $25^{\circ}\text{C}$  to  $220^{\circ}\text{C}$  with a heating rate of  $10^{\circ}\text{C}/\text{min}$ . As a result, the thermal

stability of the system was determined as  $T_i$  by the onset-point on the exothermal curve, where polymerization of the monomer starts to occur[282].

#### 4.4.2 Temperature Tracking of the Systems during Free Radical Polymerization

According to the previous findings[58, 118], heat generated from the system comprising NIR absorbers can not be ignored for several reasons. The heat formed could be reflected as continuous temperature in the surroundings. Thus, the NIR-sensitive thermal camera available from Testo (TEST 0563 0885 V7) was used to record the temperature of the free radical polymerization systems comprising **Sens** ( $0.001 \text{ mmol}\cdot\text{g}^{-1}$ ), **IS** ( $0.015 \text{ mmol}\cdot\text{g}^{-1}$ ) in **UDMA** exposed by LEDs emitting at either 820nm or 860nm with an intensity of  $1.0 \text{ W}/\text{cm}^2$  [91]. As a comparison, temperature of the sample comprising **S3b** ( $0.001 \text{ mmol}\cdot\text{g}^{-1}$ ) and **IS** ( $0.015 \text{ mmol}\cdot\text{g}^{-1}$ ) in **TPGDA** and the system comprising **S3b** ( $0.5\times 10^{-3} \text{ mmol}\cdot\text{g}^{-1}$ ) and **IS** ( $0.015 \text{ mmol}\cdot\text{g}^{-1}$ ) in **UDMA** was also collected, respectively.

#### 4.4.3 Thermally Initiated Polymerization

In order to study the heat contribution to the polymerization of monomers, a procedure of thermally initiated polymerization was carried out by placing the samples comprising respective **S7c** ( $0.001 \text{ mmol}\cdot\text{g}^{-1}$ ), **S7d** and **S9** in **UDMA** dissolved with **IS** ( $0.015 \text{ mmol}\cdot\text{g}^{-1}$ ) in the oven at  $150^\circ\text{C}$ . The samples were prepared according to the same method aforementioned for free radical polymerization exposure. After a certain time, the samples were taken to evaluate the conversion of  $-\text{C}=\text{C}-$  measured by FTIR in ATR mode. As a comparison, the samples of neat **UDMA** and **UDMA** comprising **IS** were also carried out for the comparison. In this experiment, **S7c** and **S7d** share exactly the same structure except the terminal groups, that is indolium of **S7c** and benzo[*c,d*]indolium for **S7d**.

In addition, the effects from the heat based on the structural pattern of the absorbers were further disclosed by using the rheometer coupled with an external heating device. **Sens** (**S7a**, **S7c**, **S7d** and **S9**:  $0.001 \text{ mmol}\cdot\text{g}^{-1}$ ) together with **IS** ( $0.015 \text{ mmol}\cdot\text{g}^{-1}$ ) were dissolved in **UDMA**. Again, as a comparison, the samples of neat **UDMA** and **UDMA** with **IS** were also taken for the measurement. The device was equipped with a PP25 parallel plate and connected to a heating program aforementioned. During the measurement, the samples were heated up with a programmed procedure from  $40^\circ\text{C}$  to  $120^\circ\text{C}$ . The temperature started with an isothermal condition for 20 min at  $40^\circ\text{C}$  and increased at a rate of  $1^\circ\text{C}/\text{min}$  to  $60^\circ\text{C}$ . There, it was isothermally kept for 20 min followed by similar ramping procedure until  $120^\circ\text{C}$ . The samples were cooled down to  $25^\circ\text{C}$  and heated up again to  $120^\circ\text{C}$  at a rate of  $1^\circ\text{C}/\text{min}$ , respectively. The value of storage modulus of the samples was collected

every 30s with an oscillating rate of  $2\text{ s}^{-1}$ , which relates to the change of viscosity of the systems and reflects the polymerization of the monomer.

#### 4.4.4 Comparison between Photopolymerization and Thermally Initiated Polymerization

As aforementioned and previously disclosed, the heat generated during the radiation in the systems comprising NIR absorbers and iodonium salts plays an important role in initiation of free radical polymerization. Therefore, these experiments were designed to study the difference between thermally initiated polymerization and photopolymerization. As described in 3.2.1, the direct exposed areas from the NIR-LEDs were limited due to the limited size of the light sources. Herein, the mechanical properties of the polymer materials obtained from thermally initiated polymerization disclosed in 4.4.3, inside (Part A) and outside (Part B) of directly exposed area from photopolymerization shown in **Figure 8** were analysed by DMA measurement. The samples were based on the same formulation comprising **S7c** ( $0.001\text{ mmol}\cdot\text{g}^{-1}$ ) and **IS** ( $0.015\text{ mmol}\cdot\text{g}^{-1}$ ) dissolved in **UDMA**. The polymer obtained from thermally initiated polymerization comprising **S7d** and **IS** in **UDMA** with the same concentrations was also taken to investigate the effects from different structures.

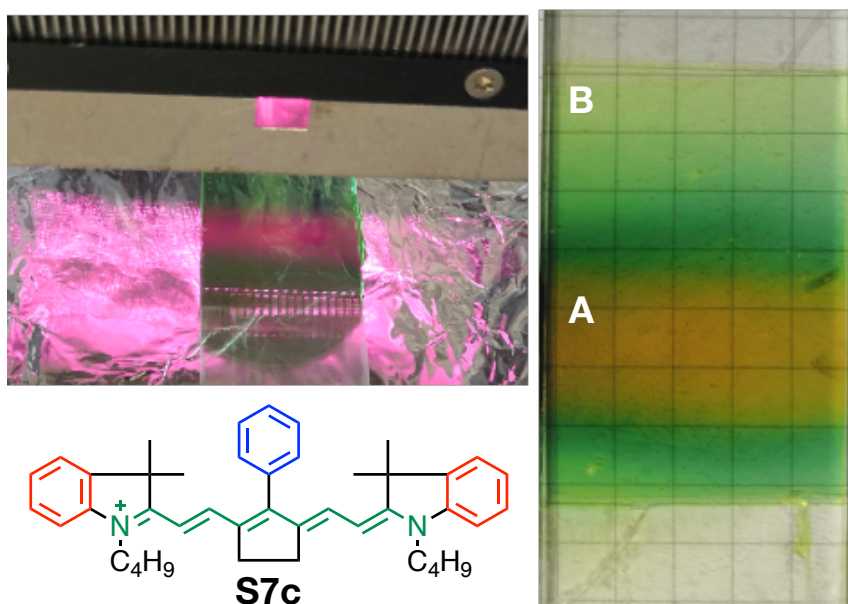


**Figure 8.** Profiles of the samples during exposure and the polymer obtained.

#### 4.4.5 Laser Radiation

In order to better overlap the wavelengths of absorption maximum of **S7d** ( $1027\text{ nm}$ ) with the emitting wavelength of light source, the laser emitting at  $974\text{ nm}$  was used for the exposure of **S7d**. The sample comprising **S7d** ( $0.001\text{ mmol}\cdot\text{g}^{-1}$ ) and **IS** ( $0.015\text{ mmol}\cdot\text{g}^{-1}$ ) in

**UDMA** was exposed by the laser with an output power of 125 W/cm<sup>2</sup> to initiate the polymerization. The radiation was carried out to be on for 10 s and off for 5 s due to the high intensity and safety consideration.

## 4.5 Heptamethine Sensitizer-Comprising Systems Applied to Coatings upon High-Power NIR Exposure

This section discloses the experiments designed to investigate the initiator systems comprising **Sens** and **IS-PF<sub>6</sub>** applied to initiate the photocuring of nanoparticle-comprised coatings based on sol-gels generated from functional silanes. According to the previous reports[27, 118, 161], the absorbers carrying heptamethine connecting chain and indolium terminal group showed significantly high efficiency for initiation of photopolymerization and for photobleaching kinetics upon exposure[90, 91]. Herein, heptamethine based cyanines were taken to practical coating systems, that is **S7e** was selected to apply for photocuring of coatings comprising silica nanoparticles combined with **IS-PF<sub>6</sub>** irradiated with NIR light and **S7i** was selected for physical drying of polyurethane coatings followed with a crosslinking process based on UV irradiation where UV-initiators operated.

### 4.5.1 Photocuring of Nanoparticle-Based Sol-Gels

#### Photocuring Kinetics of Sol-Gel Coatings

Based on the previous findings, the consistence of anions from NIR absorbers and **ISs** promoted the efficiency of the initiator system[130]. Therefore, **S7e** carrying heptamethine connecting bridged chain and indolium terminal group coupling with the anion of **PF<sub>6</sub><sup>-</sup>** was taken for the photocuring of the sol-gel precursors combined with iodonium salt coupling with anion of **PF<sub>6</sub><sup>-</sup>** (**IS-PF<sub>6</sub>**). The initiator system comprising **S7e** and **IS-PF<sub>6</sub>** was firstly dissolved in the sol-gels with a concentration of **S7e** (0.5 wt%) and **IS-PF<sub>6</sub>** (2.0 wt%), respectively. Then the solutions were transferred onto a glass plate followed by exposure under nitrogen atmosphere for 12mins with NIR-LED emitting at 820 nm ( $I = 1.0 \text{ W/cm}^2$ ). The thickness of 60  $\mu\text{m}$  was controlled by a bar coater. As a comparison, photocuring of the sol-gels by UV light (395 nm,  $I = 1.0 \text{ W/cm}^2$ ) was applied by the initiator system of **ITX** (0.5 wt%) and **IS-PF<sub>6</sub>** (2.0 wt%) irradiated for 120s.

#### Mechanical Properties of Coating Films Obtained

The coating films obtained from both NIR and UV exposure were removed from the matrix to evaluate the mechanical properties by using DMA analysis. The measurement was

carried out by following the same procedure aforementioned to characterize the mechanical properties of the polymer films.

#### 4.5.2 Physical Drying of Water-Based Polyurethane Coating System

##### Physical Drying of the Coatings via NIR Exposure

Previous studies showed that the heat generated from NIR absorbers also deeply impacts the chemistry. Therefore, the heat released during the exposure was additionally expected to dry coatings with the goal to replace conventional ovens. This would bring big benefits because ovens exhibit as less efficient to maintain a high temperature in a long time period. Furthermore, it consumes much more energy. On the other hand, water-based coating systems have obtained more and more interests due to the reason of using a green process solvent, which is water. Herein, **S7i** comprising benzo[*e*]indolium as terminal group and a  $\lambda_{\max}$  at 844 nm exhibiting water solubility of 40.5 g/L was selected as NIR light absorber for the physical drying. First step considered dissolution in the aqueous dispersion at different concentrations of 0.02, 0.05, 0.1 and 0.2 wt%. Exposure was carried out by the 860 nm LED. The kinetics of the drying was followed by real time FTIR spectra taking the peak of water between 3000 - 3500  $\text{cm}^{-1}$  for the evaluation comparing with the samples of neat oligomer dispersion dried with and without exposure. The experiment applied with real time FTIR was carried out following the same procedure aforementioned with a thickness of 60  $\mu\text{m}$  by using the portable 860 nm LED from EASYTEC emitting with an intensity of  $I = 1.0 \text{ W/cm}^2$ . For practical potential applications, the solutions dissolved with **S7i** was applied on construction bricks with a thickness of 100  $\mu\text{m}$  and followed by exposure with stationary big 860 nm LED from EASYTEC with an intensity of 1.1  $\text{W/cm}^2$ .

##### Mechanical Properties of Coating Films Obtained

In order to evaluate the potentials of this physical drying system before transfer to practical applications proceeds in industry, the mechanical properties of the coatings obtained by this drying method based on NIR exposure and consecutive crosslinking by UV irradiation were characterised by DMA. Due to the difficulty to remove the coatings from the bricks, the same procedure was applied to prepare coating films on the matrix of glass plate. Thus, the coating was removed from the matrix for the DMA measurement by following the same method aforementioned.

## 5. Results and Discussion

This thesis discloses the relation between the basic structural pattern of the cyanine dyes absorbing in NIR range and their reactivity to generate moieties to initiate both free radical and cationic photopolymerization combined with diaryliodonium salts. Their efficiency to generate heat, which appears as essential for the photopolymerization, could be taken for some further applications such as physical drying of coatings. The following subsections discuss the results and findings more in details based on the properties for potential applications of the selected cyanines. The main results and findings discussed in this chapter were disclosed in the published materials[60, 90, 91].

### 5.1 Relation between Structural Patterns of Cyanines and Their Performance to Generate Moieties for Initiation of Photopolymerization

This subchapter discusses the results regarding the performance of the sensitizers with respect to their photophysical and photochemical properties based on different structural patterns. Furthermore, the potential of these sensitizers combined with diaryliodonium salt to initiate photopolymerization also discusses the ability to generate radicals and conjugated acid based on the structural features of the sensitizer. In addition, the effect of the heat generated from these sensitizers based on the specific structural patterns was further investigated.

#### 5.1.1 Selection of Cyanines Based on Structural Patterns

Previous research disclosed the different cyanines regarding their optical absorption properties, which deeply affects the initiation reactivity for photopolymerization and their related applications combined with newly developed LED prototypes exhibiting high intensity[90, 118]. These cyanines mainly absorb in the NIR range that is located in the wavelength  $\geq 700$  nm. Their absorption spectra mostly overlap well with the emission spectra of the NIR-LEDs maximum emitting at either 820 nm or 860 nm. One should keep in mind that, cyanines belong to one of the subgroups of polymethines. Two fundamental essential features define cyanines according to the general definition, that is an odd number of  $\pi$ -centres ( $2n+3$ ,  $n \geq 0$ ) and an even number of  $\pi$ -electrons ( $2n+4$ ), where  $n$  equals to the number of the units of vinylene groups  $-\text{CH}=\text{CH}-$  (H could be replaced by other alkyl group R but vinylene group always shows up). The second feature is that  $(2n+1)$   $\text{sp}^2$ - hybridized carbon atoms on a conjugated chain directly connect a terminal group[255, 263, 265].

**Chart 2** *vide supra* depicts a series of cyanines possessing distinct structural patterns. They comprise specific numbers of  $\pi$ -electrons with comparable but distinct substitutions together with their respective terminal groups. Most of them are generally paired with a counterion. This variation leads to different optical properties and significant chemical reactivity combined with the **IS** as can be seen in **Table 3**. **S3-S9** are connected by three (**S3**), five (**S5**), seven (**S7**) and nine (**S9**) methine groups (=CH-) in the middle of the molecular chain. They were selected as NIR absorbers and/or sensitizers to investigate the efficiency for initiation of both free radical and cationic photopolymerization where **IS** served as co-initiator.

An extension of polymethine chain connecting different types of terminal indolium groups results in a red shift of the absorption maximum. As shown in **Table 3**, two additional methine chains or one vinylene group (-CH=CH-) more results in an expected bathochromic shift of about 100 nm by keeping the terminal moiety consistent [258, 265, 283]. This can be seen from the comparison of **S3a** and **S5a** as well as **S3b** and **S5b**, respectively. The substitution with an alkoxy (butoxy in the cases discussed) group at the 4-position with respect to the nitrogen of the indolium in **S3a** and **S5a** results in **S3b** and **S5b**, respectively. This shows 60 nm red shift of the absorption maximum in both cases. Furthermore, absorption of the unbridged chain of the cyanines exhibits about 100 nm bathochromic shift with an extension of one vinylene group when the terminal pattern stays with benzo[*c,d*]indolium in the case of **S3a**, **S5a** and **S7b**. In addition, **S9** assigns to a nonamethine exhibiting 100 nm bathochromic shift in comparison with heptamethine **S7a**.

A replacement of terminal indolium pattern by a benzo[*c,d*]indolium exhibits bathochromic absorption shift with around 230 nm in the case of the unbridged connection as concluded from an example between **S7a** and **S7b**. The shift of 200 nm difference can be also seen in the comparison between **S3a** and 1-ethyl-2-[3-(1-ethyl-3,3-dimethyl-1,3-dihydroindol-2-ylidene)propenyl]-3,3-di-methyl-3*H*-indolium iodide (CAS: 14696-39-0,  $\lambda_{\max}$  (MeOH) = 546 nm [274]). Furthermore, comparison between **S3b** and **S5b** comprising a terminal group as benzo[*c,d*]indolium substituted with alkoxy moiety, which improved solubility of the absorbers in monomers, showed similar behavior. This also occurs when **S5a** was compared with 1,3,3-Trimethyl-2-[5-(1,3,3-trimethyl-1,3-dihydroindol-2-ylidene)penta-1,3-dienyl]-3*H*-indolium tetrafluoroborate (CAS 38575-74-5,  $\lambda_{\max}$  (MeOH) = 638 nm [274]).

These variations of structural patterns facilitate a certain molecular engineering to tailor the absorption properties. Here, variation of both nature of terminal group and length of

connecting methine chain resulted in an absorption shift of several hundred 100 nm and made it therefore easier to optimize the overlap between the absorption of the cyanines with the emission of the LEDs. These changes also influence both geometry and electron density as shown by the patterns calculated by density functional theory in **Figures 9-13**.

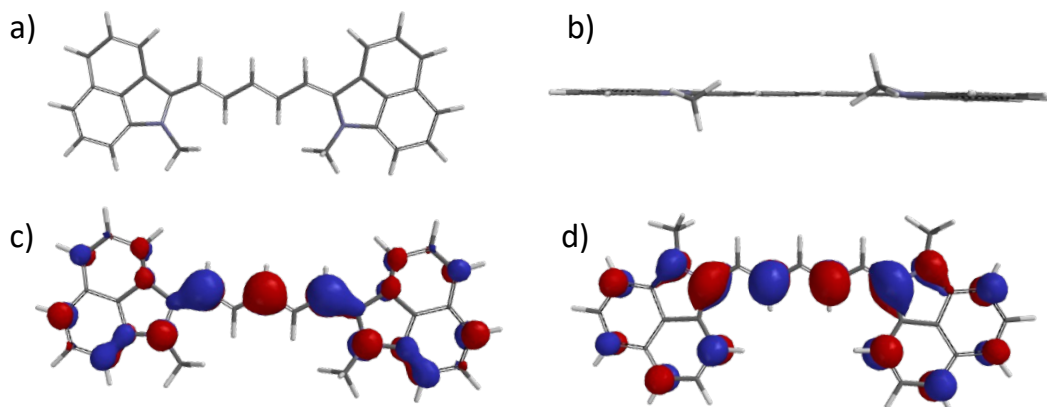


**Figure 9.** Geometry of **S5a** showing a nearly planar pattern with a) front and b) side view, graphs c) and d) depict HOMO and LOMO, respectively, cited from[90].

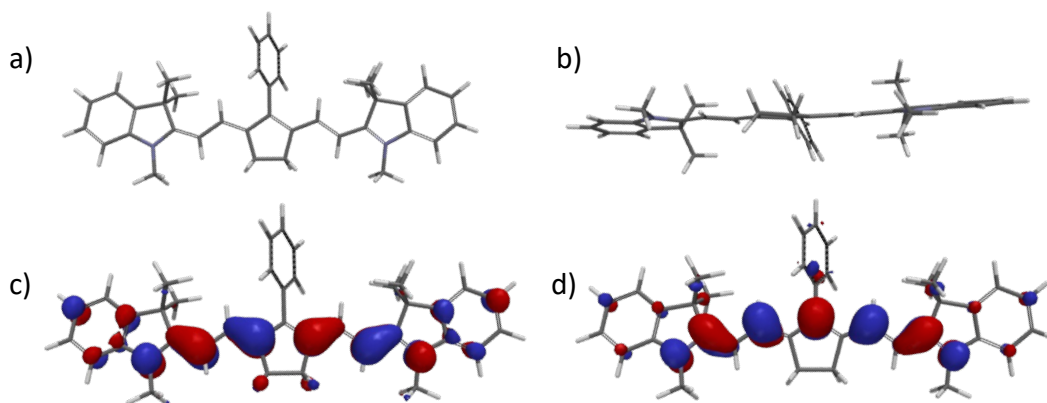


**Figure 10.** Geometry of **S7c** showing a nearly planar pattern with a) front and b) side view, graphs c) and d) depict HOMO and LOMO, respectively, cited from[90].

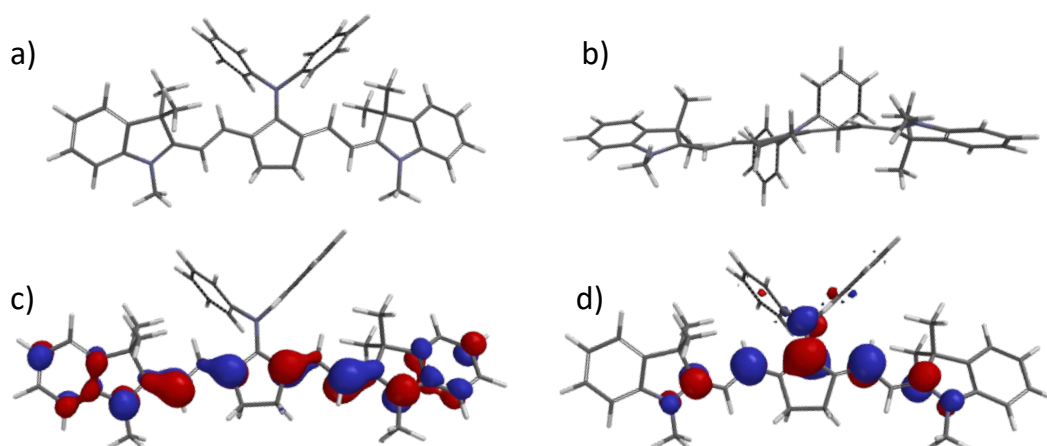


**Figure 11.** Geometry of **S7e** showing a nearly planar pattern with a) front and b) side view, graphs c) and d) depict HOMO and LOMO, respectively, cited from[90].



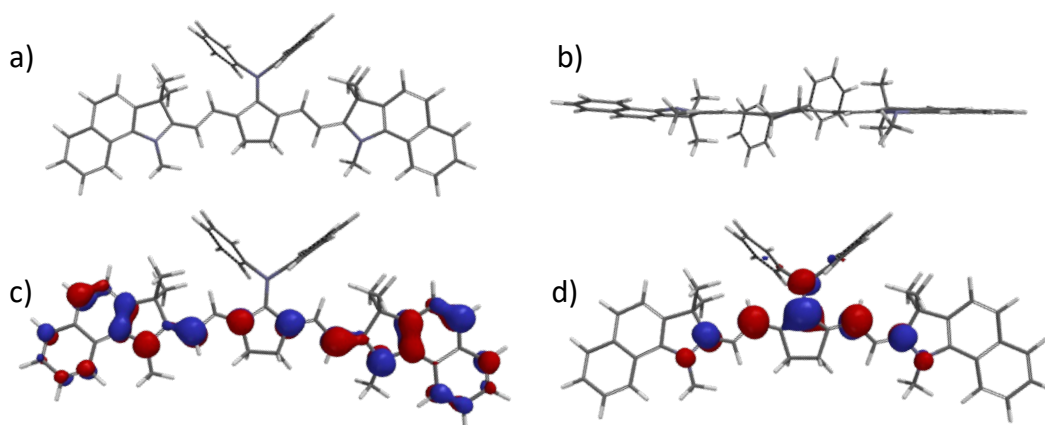


**Figure 12.** Geometry of **S7g** showing a nearly planar pattern with a) front and b) side view, graphs c) and d) depict HOMO and LOMO, respectively, cited from[90].

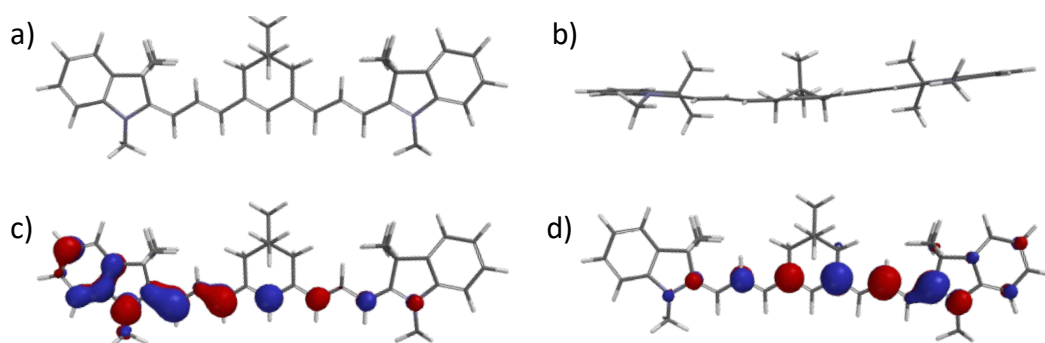


**Figure 13.** Geometry of **S9** showing a nearly planar pattern with a) front and b) side view, graphs c) and d) depict HOMO and LOMO, respectively, cited from[90].

Change from the length of the connecting methine chain more deeply influenced the absorption maximum as substituted with a specific group in the *meso*-position. Furthermore, distributing all  $\pi$ -electrons to one flat extended unsaturated moiety shows strong impact on absorption shift as well. This can be seen by comparison between **S7c** with **S7d** showing 240 nm shift. Here, the terminal group changes from Indolium to benzo[*c,d*]indolium. Similarly, **S7e** and **S7f** exhibit an absorption shift of 200 nm. Furthermore, the sensitizers **S7e**, **S7g** and **S7f** demonstrate a continuous significant bathochromic absorption maximum shift from 794, 835 and 998 nm by changes of the terminal moieties from indolium to benzo[*g*]- and benzo[*c,d*]indolium, respectively, supporting these general findings. Nevertheless, variation of the substitution at the *meso*-position with a bridged structure slightly distorts the planarity of the conjugated chain in the case of **S7c** bringing a 40 nm redshift in the comparison of unbridged **S7a** which shows an almost planar geometry as obtained by quantum chemical calculations comprising the indolium moiety as terminal group while a hypsochromic shift of about 50 nm proceeds when the terminal group changes to benzo[*c,d*]indolium in the case of **S7d** and **S7b**. Moreover, considering sensitizers comprising the same number of  $\pi$ -electrons in the

cyanine moiety but a distinct substituent at the *meso*-position, there is no remarkable difference regarding the absorption as concluded by the data of **S7c**, **S7e** and **S7h**. In addition, a further structural feature shall be mentioned. Cyanines comprising bridged connecting aliphatic chain in the *meso*-position with either five-membered ring or a six-membered ring result in a nearly flat or more strongly distorted geometry as concluded by comparing the respective patterns in **Chart 2**[90]. These geometric distortions were so strong in the case of compound **S9** with six-numbered ring shown in **Figure 13**. Here, only a slight distortion of the planarity occurs in the five-numbered ring compound shown in **Figure 11 (S7e)** and **Figure 12 (S7g)** exhibits the planar geometry[90]. The big features between these observations can be seen that **S9** comprises a nonamethine chain which brings obviously planarity back. These geometric changes can deeply affect the compatibility in multifunctional monomers used in coating systems. Here, completely flat molecules possess a stronger tendency of aggregation resulting in a loss of the absorption of a single absorber molecule and decrease of solubility in the matrix. The utilization of the organic salts proceeds thin films requesting a much higher solubility compared to literature reports[88] where often a highly diluted solution was investigated. This can be seen a big challenge to improve the solubility in the monomers used in this thesis which also exhibits a practical impact.

Furthermore, there exists a much smaller difference of the absorption changes comparing different substitutions in the *meso*-position considering the same terminal group which can be shown from the comparison form **S7d** and **S7f** of benzo[*c,d*]indolium, and indolium between **S7c**, **S7e** with **S7h** as well as benzo[*e*]indolium in the case of **S7i** and **S7j**, respectively. These different structural patterns of cyanines should lead to a different electron density. Nevertheless, the patterns of the HOMO and LUMO in **Figures 9-13** indicate the typical changes of the phase of the orbitals in the methine chain and terminal groups while changes from the substituents in the *meso*-position did not exhibit the expected impact although the electronic nature changes from an electron withdrawing phenyl group for **S7c** in **Figure 10** to an electron donating group such as N(Ph)<sub>2</sub> for **S7e** in **Figure 11**. There is nearly no electron density on both compounds observable for the substituent placed in the *meso*-position[265, 284]. Presumably, the methine chain in the *meso*-position possesses an orbital coefficient of around zero in **Figure 10** and **11** explaining why nearly no electron density would be transferred to the respective substituents.

In addition, **S7j** is an example of inner salt of a cyanine without additional counterion, and a further compound substituted with a sulfonate group shown in **S7i** facilitates sufficient solubility of itself in water, and therefore also in aqueous dispersions. It showed significantly different efficiency to bleach and generate heat under exposure of the high-power NIR-LEDs[90]. Such absorbers possess big potential particularly to dry aqueous dispersions[60]. They may also have a big impact to replace oven techniques by photonic systems where heat generation proceeds on demand. Moreover, **S7i** possesses an excellent water solubility of about 40 g/L, which can be seen as significantly beneficial for practical applications.

**Table 3.** Photophysical data of the absorbers used in this thesis including absorption maximum  $\lambda_{max}$ , extinction coefficient  $\epsilon_{max}$ , fluorescence emission maximum  $\lambda_{max}^f$ , fluorescence quantum yield  $\Phi_f$  and decay time  $\tau_f$ , and rate constant for fluorescence of the cyanines S3-S9. Electrochemical data discloses their oxidation  $E_{ox}$  and redox potential  $E_{red}$ . In addition, the values of solubility show the compatibility of the cyanines in the monomer of TPGDA and water for S7i, respectively. Furthermore, the information of commercial name and supplier of these absorbers is also included.

Entry	$\lambda_{max}$ (nm) <sup>[a]</sup>	$\epsilon_{max}$ (M <sup>-1</sup> ×cm <sup>-1</sup> ) <sup>[a]</sup>	$E_{ox}$ (V) <sup>[a]</sup>	$E_{red}$ (V) <sup>[a]</sup>	$\lambda_{max}^f$ (nm) <sup>[c]</sup>	$\Phi_f$ (%) <sup>[b]</sup>	$k_f$ (10 <sup>9</sup> s <sup>-1</sup> )	$\tau_f$ (ps) <sup>[b]</sup>	Solubility <sup>[c]</sup>	Name <sup>[d]</sup>	Supplier
<b>S3a</b>	758	0.59×10 <sup>5</sup>	0.99	-0.36	782	0.31	0.016	49	0.03	S0773	FEW
<b>S3b</b>	817	1.55×10 <sup>5</sup>	0.78	-0.51	843	0.11	0.011	99	6.2	S08731	[h]
<b>S5a</b>	859	1.83×10 <sup>5</sup>	0.80	-0.32	879	0.08	[e]	<25 <sup>[e]</sup>	1.76	S09426	[h]
<b>S5b</b>	919	2.42×10 <sup>5</sup>	0.57	-0.48	[e]	[e]	[e]	[e]	0.15	S2437	FEW
<b>S7a</b>	747	1.70×10 <sup>5</sup>	0.56	-0.63	774	26	0.23	1154	9.2	S2137	FEW
<b>S7b</b>	976	1.78×10 <sup>5</sup>	0.61	-0.30	1010	[e]	[e]	[e]	0.075	S2058	FEW
<b>S7c</b>	786	2.74×10 <sup>5</sup>	0.58	-0.56	824	19	0.19	1008	2.76	S2026	FEW
<b>S7d</b>	1027	2.48×10 <sup>5</sup>	0.60	-0.27	[e]	[e]	[e]	[e]	0.11	S0813	FEW
<b>S7e</b>	794	2.29×10 <sup>5</sup>	0.57	-0.60	835	6.6	0.071	934	10.28	S2025	FEW
<b>S7f</b>	998	1.43×10 <sup>5</sup>	0.58	-0.26	[e]	[e]	[e]	[e]	0.74	S2007	FEW
<b>S7g</b>	835	1.89×10 <sup>5</sup>	0.54	-0.61	869	0.76	0.034	213	14.1	S10761	[h]
<b>S7h</b>	775	2.02×10 <sup>5</sup>	0.64	-0.52	801	15	0.34	446	0.40	S0253	FEW
<b>S7i</b>	844 <sup>[f]</sup>	2.67×10 <sup>5</sup>	0.6	-0.48	860	<0.1	<0.007	152	40.5 <sup>[f]</sup>	S2493	FEW
<b>S7j</b>	811 <sup>[g]</sup>	3.17×10 <sup>5</sup> <sup>[g]</sup>	0.42 <sup>[g]</sup>	-0.87 <sup>[g]</sup>	834 <sup>[g]</sup>	13 <sup>[g]</sup>	0.46	281	0.6 <sup>[g]</sup>	S0325	FEW
<b>S9</b>	857	1.80×10 <sup>5</sup>	0.46	-0.33	884	1.49	0.052	285	12.2	S09442	[h]

a: In ACN. b: In MeOH. c: Solubility (g/L) in the matrix of monomer TPGDA measured based on UV-Vis-NIR spectra using ACN as solvent. d: Commercial name available. e: Not able to be determined because of the detection limitation of the device. f: In H<sub>2</sub>O, cited from[277]. g: [88]. h: The company named as Spectrum Info

Ltd. in Kiev, Ukraine.  $\epsilon_{\max}$ : Extinction coefficient was calculated following Beer-Lambert's law based on the collected UV-Vis-NIR spectra of the solutions with different concentrations.

Electrochemical properties confirmed discussions about structural effects of the conjugated patterns[90]. There is a visible decrease of the oxidation potential ( $E_{\text{ox}}$ ) by increase of an additional methine chain as proved by comparing **S3a** and **S5a** as well as **S3b** and **S5b**. This can be further concluded that the extension of polymethine chain from **S3** to **S5** to **S7** until **S9** results in a rough tendency of decrease on the oxidation potential values. In addition, the introduction of an electron-donating substituent on the terminal benzo[*c,d*]indolium expectedly leads to an easier oxidation as shown from **S3b** and **S5b**, respectively. Surprisingly, **S5b** and **S7s** exhibit similar oxidation potential between 0.64 and 0.54 which reflects similar ability to oxidize although they possess distinct numbers of  $\pi$ -electrons and substituent patterns. Besides, **S9** shows slightly easier oxidation capability with the value of  $E_{\text{ox}} = 0.46$  V. Therefore, it could be concluded that it does not have a strong impact whether the connecting conjugated chain was open as in **S5b**, **S7a** and **S7b** or bridged in the case of **S7c**, **S7d**, **S7e**, **S7f**, **S7g**, **S7h** and **S7i**. The bridged chain comprise either an amino, a chlorine or phenyl substituent at the *meso*-position. Furthermore, the inner salt **S7j** comprising barbiturate shows similar reactivity as **S9** with a value of 0.42 V[90].

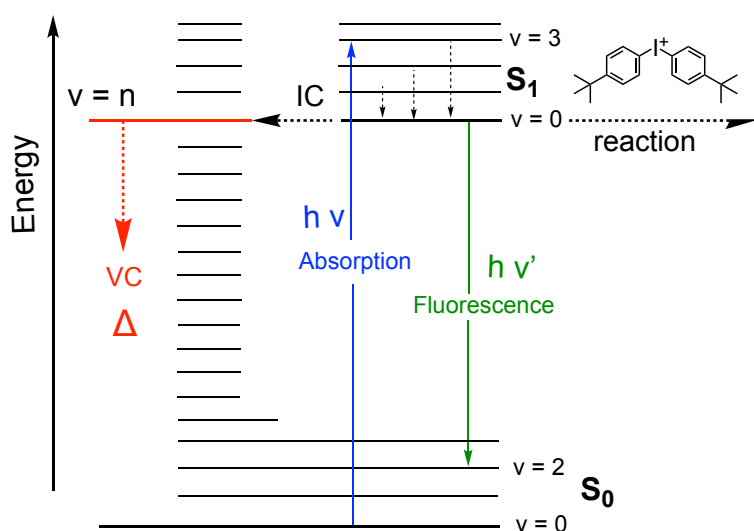
However, the situation changes comparing the reduction potentials ( $E_{\text{red}}$ ) of the materials. Most of the absorbers here show a reduction potential value with approximately -0.6 V considering **S7a**, **S7c**, **S7e**, **S7g**, **S7h**, **S7i** and **S7j** (see in **Table 3**). On the other hand, the compounds carrying benzo[*c,d*]indolium as terminal moiety exhibit higher  $E_{\text{red}}$  value of about -0.3 V in the case of **S3a**, **S5a**, **S7b**, **S7d** and **S7f**, which leads to more efficient reduction capability compared to those aforementioned. Interestingly, **S9** also shows similar reduction efficiency as shown by the respective potential of -0.33 V. Furthermore, the absorbers of benzo[*c,d*]indolium with alkoxy substituent exhibit less efficient reduction capability in the case of **S3b** and **S5b** compared with the compounds of **S3a** and **S5a**, respectively. Nevertheless, this system discloses a process to generate conjugate acid and initiating radicals following an oxidative mechanism. In this process,  $E_{\text{ox}}$  and  $E_{\text{red}}$  of the initiator and excitation energy ( $E_{00}$ ) from the sensitizers were considered to determine the free reaction enthalpy ( $\Delta G_{\text{el}}$ ) based on the viewpoint of thermodynamics. Therefore, the  $\Delta G_{\text{el}}$  could be calculated by Equation (2) in **Section 2.2.2**[213]. Here, the cation of **IS** served as oxidizing reactant exhibiting a  $E_{\text{red}}$  of -0.69 V[88]. This generally indicates that **PET** may occur based on a thermodynamic point of view[14]. Nevertheless, solvent

effects, internal activation barrier[218] and internal reaction coordinates[90, 118, 127, 218] are not discussed in detail in this thesis to avoid too much speculative discussions. **Scheme 8** explains well the scenario. Movement of the potential curve of the products also shifts the internal activation energy up or down, respectively. Until today, there have not been well-developed reliable tool disclosing such scenario. Nowadays available quantum chemical program often fail to disclose such big sensitizer molecules as shown by **S3-S9**. Nevertheless, the experimental results obtained illustrate huge difference between  $\Delta G_{el}$ , which was slightly negative in many cases regarding to the chemical reactivity[88, 90, 118]. This often requires to operate such systems with high intensity radiation sources emitting in the NIR. Such devices were first introduced in 2019, which has brought big progress in the field of free radical and cationic photopolymerization[118]. A deeper understanding of the proceeding processes occurring in the excited state provides answers in this matter.

### 5.1.2 Chemistry of the First Excited Singlet State

**Scheme 20** shows processes occurring from the  $S_0$  (ground state) to the  $S_1$  (excited state) with its vibrational states as well as the vibronic transition[285] where one-photon (**OP**) absorption proceeds with the energy  $h\nu$ . To deeply understand the  $S_1$  of the NIR-absorbers, stationary and time-resolved fluorescence emission of excited state was characterised. Here, non-radiative processes mainly contribute to the performance of excited state in the case of **S3a**, **S3b**, **S5a**, which depicts both low quantum yield and short decay time of fluorescence emission from the excited singlet state (**Table 3**). Data of **S5b**, **S7b**, **S7d** and **S7f** are not available at the moment due to the detection limitation (spectral response ends above 910 nm) of the available device used. Furthermore, the decay time of **S5a** was lower than the time resolution of the single photon equipment used for the investigation of the excited state, that is  $> 25$  ps. Extension of conjugated pattern decreases the excitation energy resulting in an increase of internal conversion (**IC**, see in **Scheme 20**) as experimentally shown by the bathochromic shift of absorption of the respective compounds. Thus, the longer wavelength and therefore lower energy difference between the  $S_0$  and the  $S_1$ , the larger probability that a vibration with higher energy of the  $S_0$  may couple with the lowest vibration of the  $S_1$  favouring **IC** between both states. Such non-radiative events can lead to temperature increase in an adiabatic system, which also facilitates the process to overcome internal activation barriers in **PET** existing in similar systems[90, 115]. Therefore, those non-radiative deactivation proceed more efficiently in the case of compounds possessing a benzo[*c,d*]indolium terminal pattern shown by **S3** and

**S5** indicated by both low fluorescence quantum yield  $\Phi_f$  and fluorescence decay time  $\tau_f$  as shown by the Equation (9) *infra vide*. The constants  $k_f$ ,  $k_{nr}$  and  $k_{PET}$  relate to the rate constant of fluorescence, non-radiative deactivation and rate constant of **PET**, respectively. Competition of fluorescence and non-radiative deactivation proceeding by **IC** controls the values of both  $\Phi_f$  and  $\tau_f$ , while the concentration of a reactant [Q] which is often called as quencher Q, is negligible. This follows by comparison of **S7s** (**S7a**, **S7c**, **S7e**, **S7g**, **S7h**, **S7i** and **S7j**) and **S9** carrying either a benzo[*e*]indolium or benzo[*g*]indolium exhibiting higher values of  $\Phi_f$  and  $\tau_f$  and of course higher reactivity combined with **IS** as determined by the bleaching experiments and the amount of conjugate acid generated as well as the respect to the original absorber concentration, this will be discussed more in detail in the following subchapter. **Scheme 20** shows the individual occurring photophysical processes. Furthermore, extension of the conjugated system from **S3a** to **S5a** and **S5a** to **S7b** by inserting an additional  $-\text{CH}=\text{CH}-$  group leads to the expected decrease of the energy gap between the **S<sub>0</sub>** and the **S<sub>1</sub>**. As a result, there comes a higher probability of coupling between vibrations of the **S<sub>0</sub>** with the lowest vibration of the **S<sub>1</sub>** favouring the internal **IC**. In these cases, only total-symmetric vibrations couple with the symmetry-allowed electronic transition[286].



**Scheme 20.** Illustration of the representative electronic ground state (**S<sub>0</sub>**) with its vibrational states  $v = 0$ ,  $v = 2$ , and  $v = n$ , as well as the first electronic excited state (**S<sub>1</sub>**) following with the respective vibrational states  $v' = 0$ ,  $v' = 3$ , and  $v' = n$ , and the vibronic transition where proceeded through the absorption of one-photon energy  $h\nu$ . Graph was modified from[90, 267].

Until today, heat formation by the excited states has not been well understood. There exist several possibilities. It has been accepted that the relaxation from higher vibrational levels of the **S<sub>1</sub>** to the lowest vibrational level of the same state results in release of energy as

heat. This contribution is not as high as that observed during laser drying using heptamethine based NIR absorbers[29]. The excessive vibrational energy from the excited molecules is distributed by a process of vibrational relaxation (**VR**) to the isoenergetic asymmetric and symmetric states which is related to intramolecular vibrational redistribution (**IVR**)[267]. Thus, the heat to the overall amount of heat which is released into the surroundings can be still seen as minor contribution, although **VR** within **S<sub>1</sub>** leads to a release of thermal energy. In addition, **IC** is considered to mainly contribute releasing heat into the surroundings[90]. According to the prerequisites aforementioned, the vibration at energetically lower level of the **S<sub>1</sub>** ( $v' = 0$ ) couples with a higher vibration of the **S<sub>0</sub>** ( $v = n$ ), resulting in formation of an extremely hot molecule. From here, the excessive energy is redistributed through vibrational cooling (**VC**) by transfer of this excessive energy by collision to surrounding matrix molecules. Otherwise the extremely hot molecules would burn. It would rule out models disclosing stepwise relaxation down into lower vibrational levels. A vibrational level typically possesses a lifetime in the picosecond time-frame. Therefore, the excessive energy would remain too long in higher excited states explaining the aforementioned idea of "burning" of the molecule. Some recent studies disclosed several examples in which the temperature can reach significantly higher than 100°C explaining the melting of powder coating followed by chemical curing > 150°C[8, 61, 118].

**Scheme 20** depicts the occurring processes based on a simple point of view, while one should keep in mind that the practical scenario appears much more complicated[267]. In fact, the evolution of heat in systems showing large amount of contribution to **IC** has not received very well-understood. Experimental data supporting this contribution exhibits a temperature increase upon exposure by NIR-LED emitting at 860 nm by using **UDMA** as a matrix (shown in **Figure 18**). In general, the temperature evolution observed during the exposure indicates the overall increase in the system which is influenced by the heat capacity of the samples. As a comparison, this temperature can reach much higher value than that observed in the systems where burning of CD-R and DVD-R occurred, and cyanines also serve as an important role[88, 118].

Equation (9) describes the relation between quantum yield  $\Phi_f$ ,  $\tau_f$ ,  $k_f$ ,  $k_{nr}$  and reaction with a reactant Q in an activated **PET** ( $k_{PET}$ ). The latter can be neglected because  $[Q] = 0$ . Therefore,  $\Phi_f$  and  $\tau_f$  decrease when the contribution amount of non-radiative deactivation gets higher. Furthermore, the probability to get involved in **PET** also decreases. In general, **IC** proceeds based on unimolecular kinetics. This unimolecular process facilitates faster deactivation of the **S<sub>1</sub>** instead of a bimolecular reaction as represented by  $k_{PET} \times [Q]$ [20].

Diffusion controls typically the latter by the viscosity of the surrounding matrix. The investigation of photoproducts proposed the mechanism in a deeper insight, which will be discussed in next section.

$$\Phi_f = \frac{k_f}{k_f + k_{nr} + k_{PET} \times [Q]} = k_f \times \tau_f \quad (9)$$

**Figure 14** shows the fluorescence decay traces of several cyanines as an example with absorption in the NIR. Data obtained provide information for the efficiency of radiative deactivation proceeded by fluorescence emission. As can be seen, substitution with alkoxy groups on the terminal benzo[*c,d*]indolium improves the contribution to radiative deactivation as concluded by comparing **S3a** and **S3b**. Furthermore, the decays of **S7a**, **S7c** and **S7e** exhibit approximately 20 times higher in comparison with **S3a**. It appears 10 times larger compared to **S3b**. This agrees with the findings that benzo[*c,d*]indolium favours non-radiative deactivation. Vibrational coupling can be also considered as an enhancement based on the theoretical point of view[266]. One can see therefore that longer polymethine chain facilitates radiative deactivation in the system shown in **S7** (except **S7d** and **S7f** with benzo[*c,d*]indolium) and **S9** while as a comparison, the terminal group of large stiff conjugated patterns in the case of **S3**, **S7d** and **S7f** directs the system towards non-radiative deactivation (see in **Table 3**).

A view on the data of **S7s** shows the intricacy but comes clear that the benzo[*c,d*]indolium responsibly connects to non-radiative deactivation. No big difference was observed between **S7a**, **S7c** and **S7e** when they share the same terminal structural pattern of indolium. Although **S7a** builds up with an open polymethine chain. **S7a** ( $\tau_f = 1154$  ps) exhibits similar but a bit longer decay as well as higher value of  $\Phi_f$  than that of **S7c** ( $\tau_f = 1008$  ps), which possesses a bridge with five-ring substitution in the middle of polymethine chain and a phenyl group in the *meso*-position. This might be seen as a slight difference but the data do not appear so different. **S7e** shows slightly decreased decay and  $\Phi_f$  comprising N(Ph)<sub>2</sub> in the *meso*-position comparing to **S7c** carrying phenyl group as electron-withdrawing substituent (see in **Table 3**).



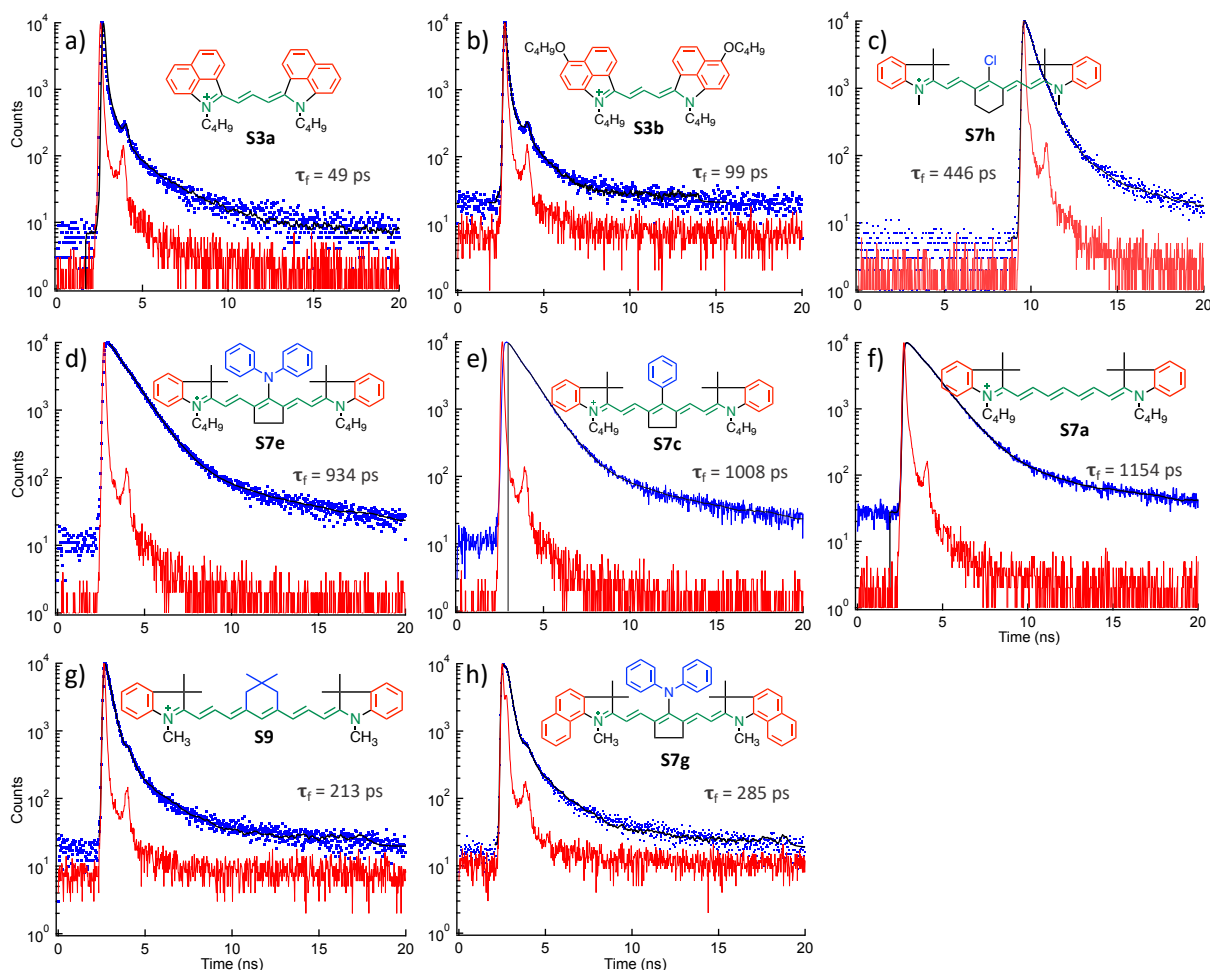
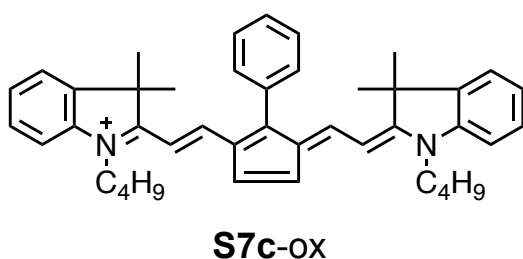


**Figure 14.** Traces of fluorescence lifetime of the absorbers **S3-S9** obtained after the excitation at 670 nm in MeOH applying time-correlated single photon counting to collect the data. The maximum fluorescence emission ( $\lambda_{f_{max}}$ ) from the samples show up at the following wavelengths: a): **S3a** ( $\lambda_{f_{max}} = 782$  nm); b): **S3b** ( $\lambda_{f_{max}} = 843$  nm); c): **S7h** ( $\lambda_{f_{max}} = 801$  nm); d): **S7e** ( $\lambda_{f_{max}} = 835$  nm); e): **S7c** ( $\lambda_{f_{max}} = 824$  nm); f): **S7g** ( $\lambda_{f_{max}} = 869$  nm); g): **S9** ( $\lambda_{f_{max}} = 884$  nm) and h): **S7g** ( $\lambda_{f_{max}} = 869$  nm). Experimental details could be found in **Section 3.3.3**, (the red curve represents the instrumental response of a scatter comprising Ludox in water whose detection is close to 670 nm; blue: decay traces of the samples detected; black: calculated decay traces by iterative convolution between the instrumental response and exponential curves), modified from[90].

Furthermore, replacement of six-ring with three methylene group by a moiety comprising two methylene bridges and an electron withdrawing moiety such as chlorine in the *meso*-position as shown in **S7h** significantly contributes to non-radiative deactivation compared to **S7c** when they comprise the same indolium terminal pattern. In addition, **S7g** exhibits both lower  $\Phi_f$  and  $\tau_f$  than **S7e** when they carry the same connecting bridge and substitution in the *meso*-position. This indicates that both benzo[*g*]indolium and N(Ph)<sub>2</sub> group significantly affect the fluorescence dynamics. Moreover, the cyanine **S9** possesses a nonamethine chain to connect the terminal indolium. The fluorescence decay was shorter comparing to **S7c** and **S7e**. The bathochromic shift on absorption of **S9** compared

to **S7e** decreases the energy gap between the  $S_1$  and  $S_0$ , which leads to an increase of non-radiative deactivation such as **IC**. However, the efficiency of these sensitizers to initiate radical and cationic polymerization was still sufficient. As a summary, fluorescence data collected roughly describe relation between structural features of these cyanines and emission dynamics as previously discussed. Nevertheless, the availability of preliminary can be seen as rare although some resources give a brief summary[90, 91]. There would be more research necessary in the field of photophysics of cyanines absorbing in the NIR to reduce the nowadays existing knowledge gap.

Interestingly, the oxidized photoproduct of **S7c** (**S7c-ox**) after **PET** showed similar fluorescence lifetime, which also turned to be sufficiently reactive with **IS**[90, 118]. It comprises an additional double bond and therefore would not fit in the classification of cyanines. This may explain the hypsochromic shifted absorption with respect to the cyanine substrate[118, 287].



### 5.1.3 Performance on Generation of Radical and Conjugate Acid as Initiating Species Combined with Iodonium Salt

The NIR sensitizers **S3-S9** comprise distinct structural features regarding to:

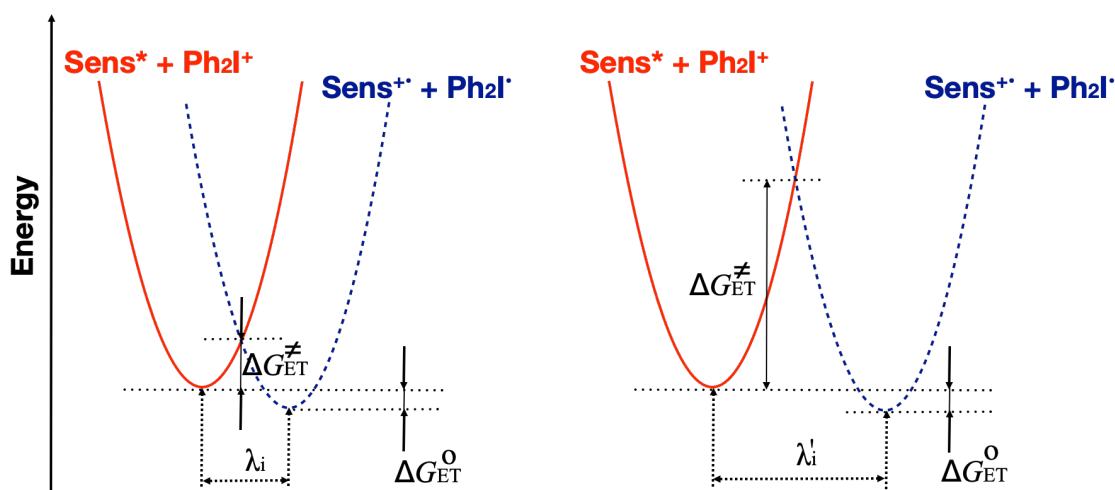
- Different numbers of methine groups connecting both terminal patterns (trimethine for **S3**, pentamethine for **S5**, heptamethine for **S7** and nonamethine for **S9**);
- Open connecting methine chain (**S3**, **S5**, **S7a** and **S7b**) or bridged chain (**S7c-S7j** and **S9**);
- Absorption changes summarised by the comparison of terminal pattern from benzo[*c,d*]indolium (**S3**, **S5**, **S7b**, **S7d** and **S7f**), indolium (**S7a**, **S7c**, **S7e**, **S7h** and **S9**), benzo[*g*]indolium (**S7g**) and benzo[*e*]indolium (**S7i** and **S7j**) derivatives;
- Substitution of the terminal benzo[*c,d*]indolium (**S3b** and **S5b**) or without additional substituents (**S3a** and **S5a**), as well as substituent on benzo[*e*]indolium (**S7i**);
- Replacement of substituents in the *meso*-position of the connecting bridge with either five-ring moiety (**S7c-S7g**, **S7i** and **S7j**) or six-ring moiety (**S7h** and **S9**);

- Substituted on the bridges by variation of groups in the *meso*-position with either phenyl (**S7e** and **S7d**), N(Ph)<sub>2</sub> (**S7e-S7g**), chlorine (**S7h** and **S7i**), barbiturate (**S7j**) or hydrogen (**S9**);
- Variable alkyl groups at the nitrogen atom on terminal indolium group by either butyl (**S3-S7f**), methyl (**S7g, S7h, S7j** and **S9**) or butanesulfonate (**S7i**);

The structural changes affect optical absorption and therefore excitation energy, redox potentials as well as the geometrical properties of the compounds as aforementioned. In general, the system comprising cyanine as sensitizer and iodonium salts as co-initiator mostly appears under slightly exothermal conditions where  $\Delta G_{\text{PET}} < 0$ [213, 288]. Equation (3) and (10) depicts the relation between the efficiency of electron transfer and the free activation enthalpy  $\Delta G^\ddagger$  in **PET** process based on the famous Marcus theory[135] in an almost exothermal reaction protocol (**Scheme 21**). Nevertheless, there exist different scenarios related to the activation enthalpy  $\Delta G^\ddagger$  as shown by their different potential curves (temperature change is not included)[118, 218]. This is a very simplified pattern because it only considers potential energy curves of a small molecule.

$$k_{et} = k_0 \times \exp\left(-\frac{\Delta G^\ddagger}{RT}\right) \quad (10)$$

Consideration of  $\Delta G_{\text{el}}$  by taking the oxidation potential of the cyanine sensitizers and reduction potential value of **IS** ( $E_{\text{red}} = -0.69$  V[58]) appears together with the respective excitation energy (**Table 3**) slightly negative based on Equation (2) *vide supra*. Thus, the sensitizers **S3-S9** are supposed to show similar performance due to the similarity of  $\Delta G_{\text{el}}$  from a thermodynamic point of view. As can be seen in **Scheme 21**, the geometric changes relating to internal coordinates of the sensitizers as defined by Equation (5) affect the potential curves resulting in obviously different value of  $\Delta G^\ddagger$  although the systems shows similar free enthalpy  $\Delta G_{\text{et}}$  of **PET**. Thus, geometric changes may have a deep impact on the shift of the reaction coordinate. Here, the activation enthalpy changes while the free enthalpy does not change. Therefore, the systems comprising cyanine and iodonium salt bring big impetus to understand **PET** more in detail because the cyanines differently contribute to the heat released. In the **PET** process, internal barrier significantly affects the reactivity while the heat released facilitates to overcome the internal reaction barrier. This works well with the high intensity radiation sources[118].



**Scheme 21.** Energetic representation of the relation between **PET** and internal barrier in the occasions where similar exothermal condition ( $\Delta G_{ET}^0$ ) exists while internal barrier ( $\Delta G_{ET}^\ddagger$ ) differs, modified from [154].

The results regarding photobleaching and conjugate acid generation using the sensitizers **S3-S9** combined with iodonium salt **IS** as co-initiator demonstrate the chemical reactivity of the systems. These data provide a deeper insight to understand the differences based on a chemical point of view (**Figure 15-17**). **Figure 15** exhibits the changes of the absorption spectra of the cyanines possessing benzo[*c,d*]indolium as terminal group (**S3b**, **S5a**, **S7b**, **S7d** and **S7f**) upon exposure in  $\text{CH}_3\text{CN}$  by NIR-LED emitting at 860 nm with an intensity of  $1.0 \text{ W/cm}^2$  in the presence of **IS**. Only a slight absorption decrease of the sensitizers was detected, these sensitizers always carry benzo[*c,d*]indolium terminal pattern appeared regardless the numbers of methine groups in the connecting chain (comparison between **S3b**, **S5a** and **S7b**), or substituents positioned in the *meso*-position of cyanines possessing bridged chain such as a phenyl group (see **S7d**) or  $\text{N}(\text{Ph})_2$  moiety (**S7f**). There was no significant change between the samples under exposure of different time (10 mins for **S3b**, **S5a** and 30 mins for **S7b**, **S7d** and **S7f**). So it can be concluded that the reactivity as indicated by bleaching of compounds comprising a benzo[*c,d*]indolium pattern proceeds with very low efficiency. Here, non-radiative deactivation instead of photochemical reaction, which is related to **PET** process, can be seen as the major deactivation process of the  $\text{S}_1$ . One should keep in mind that although the experimental condition of the sensitizers was adjusted to the same radiation intensity from each other, the emission of the LEDs is not tunable, thus, different penetration length or amount of energy absorbed could appear when the excitation was reached to the edges or maximum or different overlapped efficiency in the absorption of the absorbers.

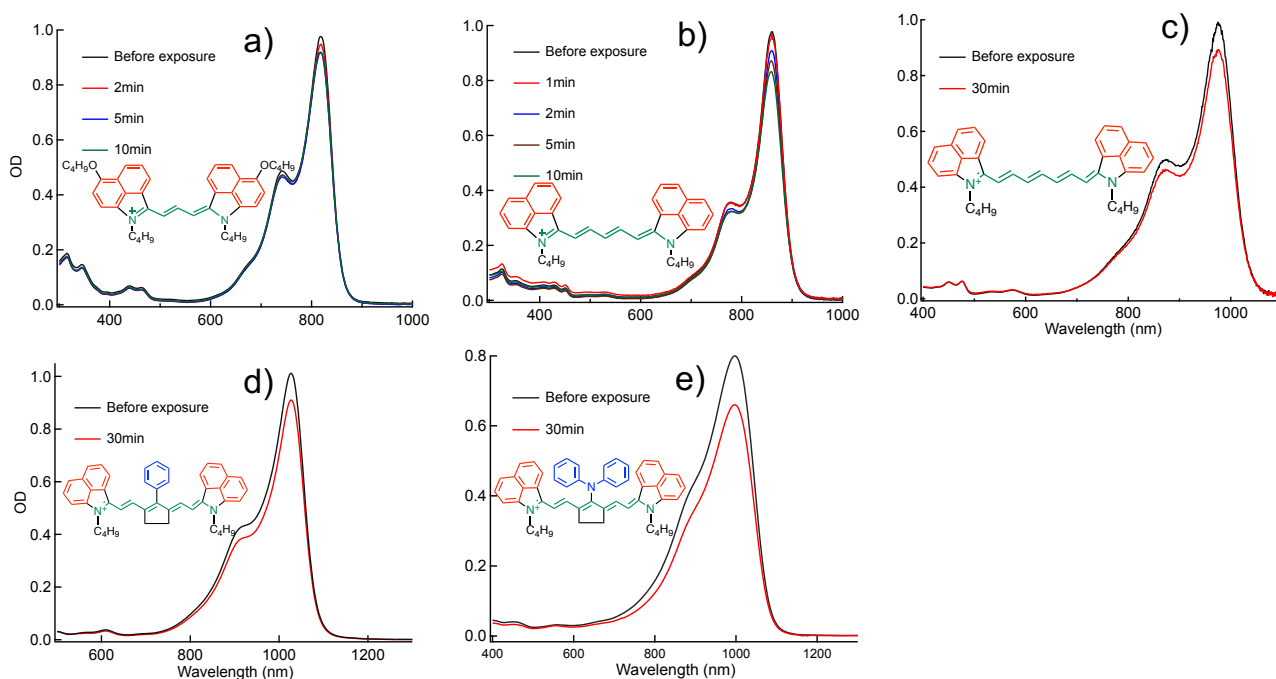


**Figure 15.** Profiles of optical density (OD) decrease from the NIR-absorbers ( $[Sens] = 5.0 \times 10^{-4} \text{ mol} \cdot \text{L}^{-1}$ ) in acetonitrile upon exposure in the presence of iodonium salt ( $[IS] = 3.0 \times 10^{-3} \text{ mol} \cdot \text{L}^{-1}$ ) applying the big-size of LED emitting at 860 nm with the intensity of  $1.0 \text{ W} \cdot \text{cm}^{-2}$ ; a) **S3b**, b) **S5a**, c) **S7b**, d) **S7d** and e) **S7f**, modified from [90].

Interestingly, the situation significantly differs in **Figure 16**. This relates to the indolium derivatives with either an open heptamethine connecting chain (**S7a** in **Figure 16a**), or bridged chain substituted by  $\text{N}(\text{Ph})_2$  in the *meso*-position (**S7e** and **S7g** in **Figure 16b** and **d**, respectively) and bridged chain with substitution of six-ring and chlorine in the centre of the cyanine (**S7h** in **Figure 16c**). This also holds for **S9** shown by **Figure 16e**, that is an indolium derivative with nonamethine pattern substituted by a six-ring in the center. In addition, the benzo[*g*]indolium derivative of **S7g** in **Figure 16d** also showed very efficient photobleaching, that is completely bleached after 5 minutes exposure and approximately 99% absorption decrease after 120 s in the presence of **IS** resulting in a significant hypsochromically shifted peak down to 600 nm. This relates to the oxidized moiety showing a fulvene structure as that similarly reported in the case of **S7c-ox** (see the structure *vide supra*) [118].

It is therefore not anymore a cyanine following the 100 nm rule by extension of an additional  $-\text{CH}=\text{CH}-$  moiety [263]. In addition, **S7e** (**Figure 16b**) and **S9** (**Figure 16e**) also exhibit new hypsochromically shifted absorption bands that relate to a similar oxidation product compared to **S7e** in the case of **S7g** (560 nm) and other conjugated molecules formed by oxidation which do not anymore assign to cyanines in the case of **S9** (450 nm).

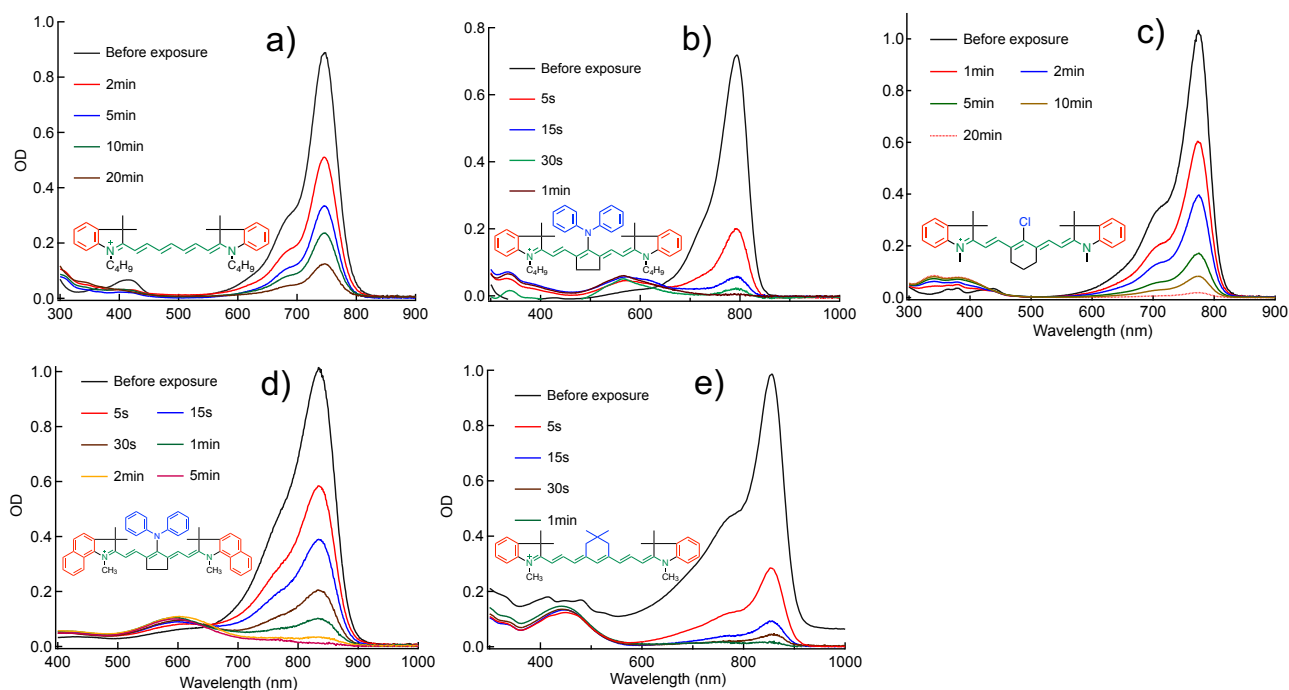
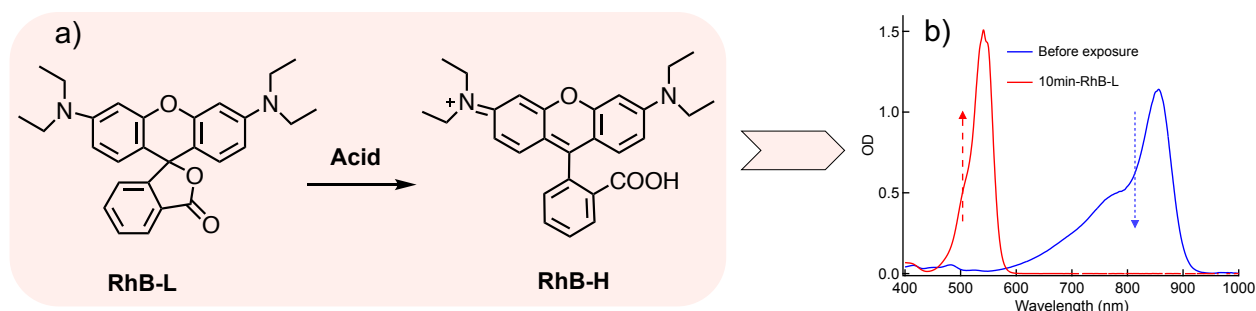


**Figure 16.** Profiles of optical density (OD) decrease from the NIR-absorbers ( $[\text{Sens}] = 5.0 \times 10^{-4} \text{ molL}^{-1}$ ) in acetonitrile upon exposure in the presence of iodonium salt ( $[\text{IS}] = 3.0 \times 10^{-3} \text{ molL}^{-1}$ ) applying the big-size of LED emitting at 820 nm for **S7a**, **S7e** and **S7h** and LED emitting at 860 nm for **S7g** and **S9** with the intensity of  $1.0 \text{ W/cm}^2$  respectively; a) **S7a**, b) **S7e**, c) **S7h**, d) **S7g** and e) **S9**, modified from[90].

These different bleaching efficiencies also enable different capability of the systems to generate conjugate acid  $\text{a}_{\text{H}^+}$ . Colorless rhodamine B lactone (RhB-L) can quantitatively probe the amount on acid formed by formation of coloured rhodamine B (RhB) as illustrated in **Scheme 22**[88]. Furthermore, the data of both  $[\text{a}_{\text{H}^+}]$  and  $[\text{a}_{\text{H}^+}]/[\text{Sens}]$  obtained and shown in **Figure 17** demonstrate the reactivity of the sensitizers to generate conjugate acid using **IS** as electron acceptor. The ratio  $[\text{a}_{\text{H}^+}]/[\text{Sens}]$  displays the amount of acid formed by one sensitizer molecule. It is clear also from Equations (11)-(14), that the acid originates from the sensitizer in case of an oxidative mechanism. Particularly Equation (12) contributes to acid formation. Again, both data exhibit higher efficiency and reactivity of the derivatives of benzo[*g*]indolium pattern with longer polymethine chain while the compound with stiff benzo[*c,d*]indolium group demonstrated much less reactivity regardless of the numbers of  $\pi$ -electrons (**S3**, **S5**, **S7b**, **S7d** and **S7f**). **S7i** was not included since its water solubility and **S7j** was already previously reported[118, 161]. **S7a-S7c**, **S7e** and **S7g-S9** exhibited higher reactivity which keeps the consistence regarding the photobleaching efficiency combined with **IS**. Particularly, **S7g** and **S9** indicate the most promising features served as sensitizers for NIR-induced photopolymerization in combination with more sophisticated high-power NIR-LED devices emitting at 860 nm.





**Scheme 22.** a) Mechanism to evaluate the conjugate acid generated upon exposure on the sensitizers in presence of **IS** modified from [88]; b) an example from **S9** (blue: absorption spectrum of **S9** in acetonitrile, red: the spectrum of the solution of **S9** and **IS** after 10 min exposure applying 860 nm emitting LED and added rhodamine B, experimental detail is disclosed in **Section 4.1.2**).

Equation (11) describes that the generation of oxidized **Sens**<sup>+\cdot</sup> through a process of **PET** between photoexcited sensitizer (**Sens**<sup>\*</sup>) and the cation of **IS**. The cation radical **Sens**<sup>+\cdot</sup> formed stabilises by release of conjugate acid (**a**<sub>H<sup>+</sup></sub>) and the photoproducts comprising either nitrogen (**Pr**(N)) or no nitrogen (**Pr**(O)) shown in Equation (12). Furthermore, the photoproducts which comprise nitrogen can additionally consume oxidized **Sens**<sup>+\cdot</sup> resulting in back to formation of **Sens** as illustrated in Equation (13). In addition, the amount of conjugate acid available to protonate colourless Rhodamine B lactone would be lower according to Equation (14) because **Pr**(N) can consume acid formed. This would not be available to initiate cationic polymerization. It also explains why the amount of acid measured in the systems appears often less than expected. Consequently, the ratio [**a**<sub>H<sup>+</sup></sub>]/[**Sens**] is less than 1.0 in such a case.

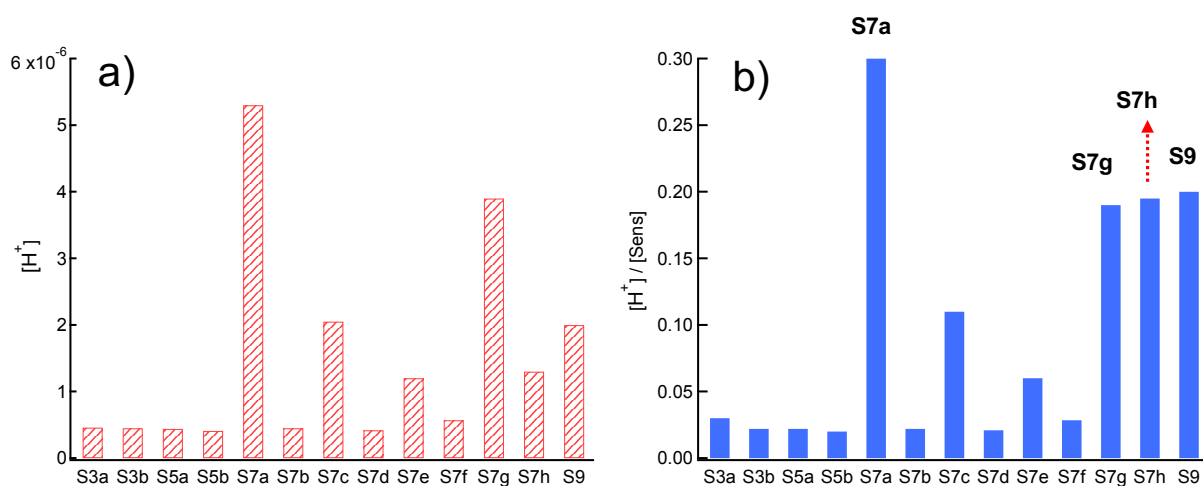


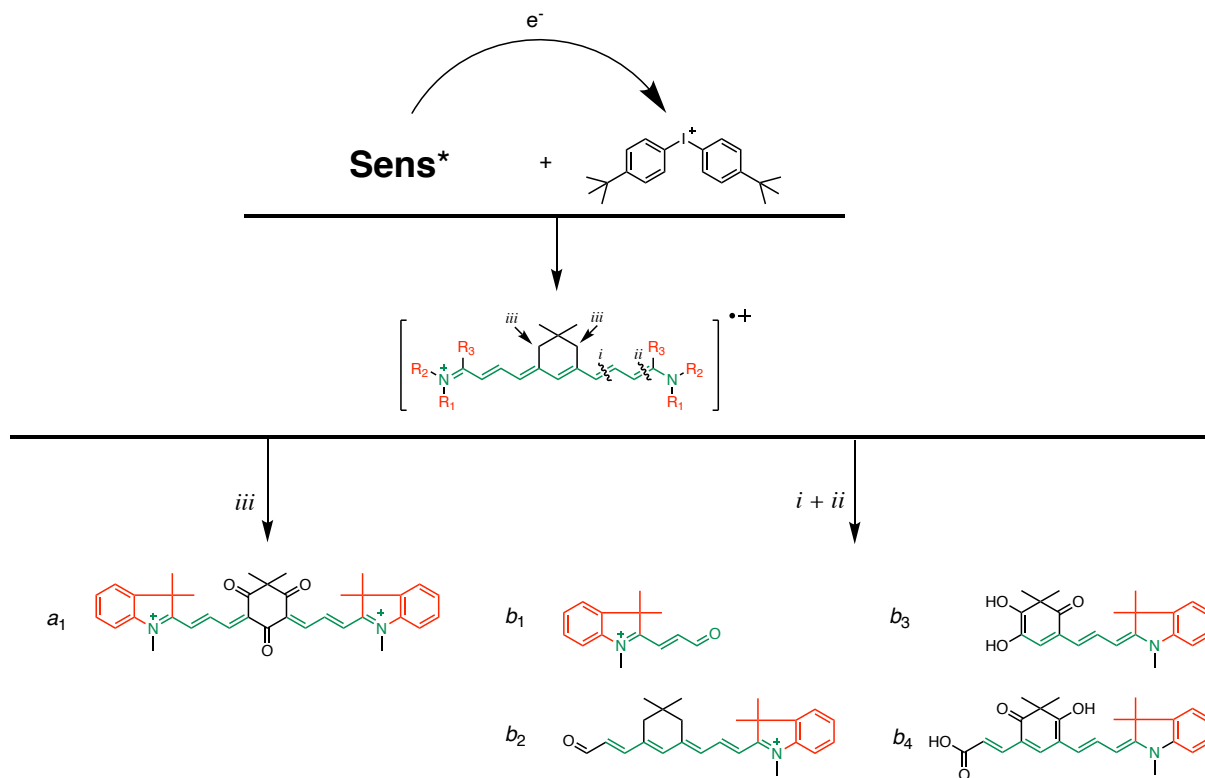
**Figure 17.** The profiles showing the capability of the NIR-initiators to generate conjugate acid. a) The evaluated amount of conjugate acid formed in the system comprising **Sens** ( $2.0 \times 10^{-5}$  molL $^{-1}$ ) and **IS** ( $1.2 \times 10^{-4}$  molL $^{-1}$ ) after exposure for 15 mins applying the NIR-LEDs with the intensity of 1.0 W/cm $^2$ , LED emitting at 820 nm was used for **S3a**, **S7a**, **S7c**, **S7e**, **S7h** and LED emitting at 860 nm was applied for **S3b**, **S5a**, **S5b**, **S7b**, **S7g**, **S7f**, **S7g** and **S9**, respectively. After the exposure, amount of Rhodamine B was added into the solutions ( $[Rhodamine\ B] = 1.0 \times 10^{-4}$  molL $^{-1}$ ); b) the values of the concentration ratio of conjugate acid formed to the original concentration of the **Sens**.

Data obtained through mass spectrometric analysis carried out by a LC-MS protocol helps to propose possible pathways for the formation of possible structures of the photoproducts Pr(N) and Pr(O) as shown in **Scheme 23**. This proposal bases on the molecular ions listed in **Table 4** that were detected in the mass spectrometer in the case of **S9** after exposure in the presence of **IS** following the strategy reported in the supporting of Ref[118]. Previous investigations of photoproducts disclosed originating from **S7c** and **S7e** followed similar treatment[118]. Therefore, **S7g** may expectedly follow the similar mechanism of **S7e** upon exposure.

The photoreaction related to PET process between **Sens** $^*$  and **IS** leads to oxidation of **Sens** as indicated by formation of **Sens** $^{+ \cdot}$ . The latter stabilizes by either oxidation at position *iii* or chemical bond cleavage at the position *i* and *ii* following the generation of nucleophilic moieties as discussed in **Scheme 23**. Compounds comprising an open methine chain such as **S3**, **S5**, **S7a** and **S7b** are not included here since the ions observed indicated the molecular mass related to the cleavage from the adjacent bond with respect to the indolium patterns, details could be also found from[90]. Particularly, **S9** exhibited oxidation reactivity at its *iii*-position through the yellowish photoproducts, **Figure 16e**, which do not anymore assigns to a cyanine[263]. Such unexpected phenomena may potentially facilitate the design of the photoswitching systems such as photo-controlled materials or devices. Because these materials bleach at the excitation wavelength which



exhibits an open window while the increase of hypsochromic absorption results in closure of an optical window.



**Scheme 23.** Proposal of photoproducts according to the molecular mass of ions detected by LC-MS spectra by analysing the ions available from the solution in  $\text{CH}_3\text{CN}$  upon exposure comprising **S9** in the presence of **IS** by the LED at 860 nm, cited from[90].

The dominant pathway of cleavage was expected to occur at either position *i* or *ii* since there was no indication showing the behaviour of the products based on oxidation at the position *iii* from the heptamethine derivatives with similar trimethylene structure in the center[115]. **Scheme 23** summarises the photoproducts based on the molecular ions observed in the MS spectra (listed in **Table 4**) in the case of **S9**.

**Table 4.** Summary of molecular mass of the ions detected from the exposed solution comprising **S9** and **IS** at 860 nm with an intensity of 1.2 W/cm<sup>2</sup> for 10 min. Some of the ions appeared as doubly charged ions and/or NA<sup>+</sup>-adducts, modified from[90].

t/min	m/z
2.35	214.0860
12.01	214.0860
12.82	279.1547
13.37	352.2404
13.47	284.3265
14.26	427.2403
15.44	338.3364
15.64	803.5300
16.07	566.3827
16.66	561.4208
16.96	537.4220
17.61	565.4525
19.21	663.4424
21.07	896.7540
21.49	872.7559
22.26	848.7519
23.98	876.7864
24.49	130.1569

The proposal of the products mixture may explain why the absorption spectra in **Figure 16e** did not show an isosbestic point which is typically observed in the photochemical process from A\* directly to B[289]. In addition, the structure of moieties b<sub>2-4</sub> also indicates the absorption of hypsochromic shift since those patterns do not any more belong to the classification of cyanines.

#### 5.1.4 Heat Release Regulated by the Structural Patterns of Cyanines

The NIR sensitizers showed distinct efficiency of photobleaching and exhibited significantly different fluorescence emission ( $\Phi_f$  and  $\tau_f$ ) as previously discussed due to the variation of structural patterns. The **IC** from the **S<sub>1</sub>** to the **S<sub>0</sub>** of the absorbers results in heat release into the surrounding matrix which can be considered as the main source to heat up the materials. **Figure 18** demonstrates the results observed in the system where **UDMA** as matrix. **Figure 18** a) and b) showed the temperature measured in the samples of **UDMA** comprising **IS** and different sensitizers upon NIR exposure by the LEDs emitting at either 820 nm or 860 nm.

Here the sample comprising **S3b** showed the highest final value of the temperature at 80°C followed by **S5**. The highest temperature point of the sample comprising **S3a** ends up at 45°C due to its insufficient solubility in the monomer. **S7a** and **S7c** reach at first the maximum temperature up to 42°C and 50°C, respectively, and end finally at 40°C. The

temperature of the systems comprising **S7g** and **S9** increases up to 70°C and drops down to 55°C at the end. The performance regarding heat contribution of **S7e** and **S7j** was previously reported[118]. Data of **S7b**, **S7d** and **S7f** is missing due to the excitation limitation of the LED devices. In contrast to **S3** and **S5**, where the temperature in the systems continuously increase until the end, the samples of **S7a**, **S7c**, **S7g** and **S9** demonstrate a significant drop after passing the maximum point. Here, sufficient photobleaching occurred with these compounds possessing either an indolium or benzo[g]indolium terminal pattern which confirms the results discussed in previous subsection. Thus, bleaching during exposure reduces the number of molecules contributing to non-radiative deactivation explaining the temperature decrease observed in these pictures.

Nevertheless, absorbers comprising a benzo[*c,d*]indolium terminal group exhibited insufficient efficiency to generate radicals related to photobleaching and conjugate acid which is necessary to initiate cationic photopolymerization. Thus, these sensitizers showed big potential as heat generators to facilitate chemical reactions or to promote physical process such as physical drying[14, 60, 61]. Furthermore, significant temperature increase was observed in the systems comprising **S3b** of the same concentration in both **UDMA** and in **TPGDA** as previously discussed that **S3** showed good efficiency to generate heat upon exposure. In addition, the temperature reaches higher point as expected with larger concentration in the matrix of **UDMA** due to the higher amount of photon absorption.

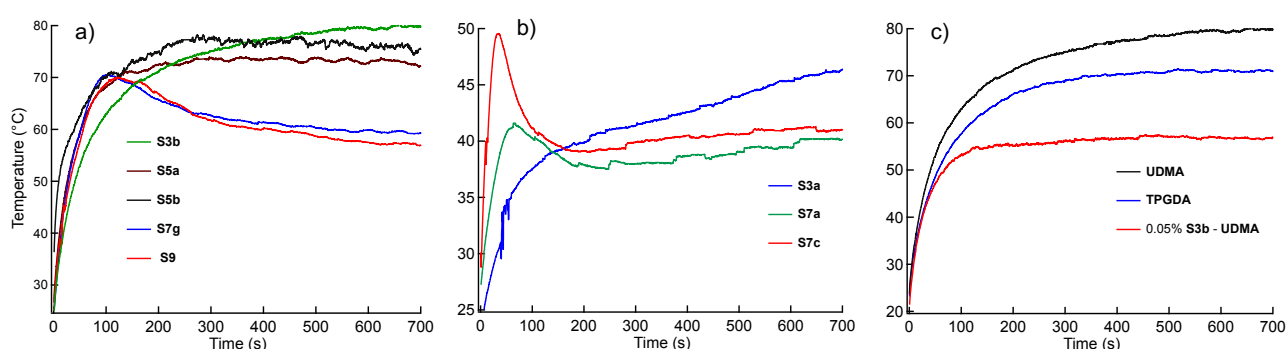


**Figure 18.** Temperature traces from the system of free radical photopolymerization in a) and b) **UDMA** comprising **Sens** ( $1.05 \times 10^{-3} \text{ mmol} \cdot \text{g}^{-1}$ ) and **IS** ( $1.56 \times 10^{-2} \text{ mmol} \cdot \text{g}^{-1}$ ). c) Comparison of the temperature in **TPGDA/UDMA** and different concentration of **S3b** in **UDMA** (0.05 wt% of **S3b** is approximately  $0.53 \times 10^{-3} \text{ mmol} \cdot \text{g}^{-1}$ ), modified from[91].

The introduction of NIR absorbers and their capability to generate and diffuse heat enables to promote thermally initiated free radical polymerization and polymer formation as shown in **Figure 19** by using **UDMA** as matrix. The heat generated also contributes to thermal initiated polymerization. Such monomers also possess an intrinsic temperature where

polymerization starts. Addition of NIR-sensitizer components such as cyanines and/or iodonium salts decreases this initiation temperature. Such an observation does not appear as unusual as previously shown in multi-functional acrylic esters[88, 290]. The conversion of monomer **UDMA** grew up obviously much faster in systems in a combination of **IS** and **Sens** regardless of the terminal patterns (indolium of **S7c** and **S9**, benzo[*c,d*]indolium of **S7d**) or the difference of substitution in centre of the sensitizer, or the length of connecting chain (heptamethine of **S7c** and **S7d**, nonamethine of **S9**). This can be seen as a certain thermal instability which decreases in the following order:

**(UDMA + IS + Sens) > (UDMA + IS) > (UDMA + Sens) > UDMA.**

Nevertheless, the neat monomers exhibit a much higher thermal stability compared to the systems comprising Iodonium salts and/or NIR absorbers as shown in **Figure 19**.

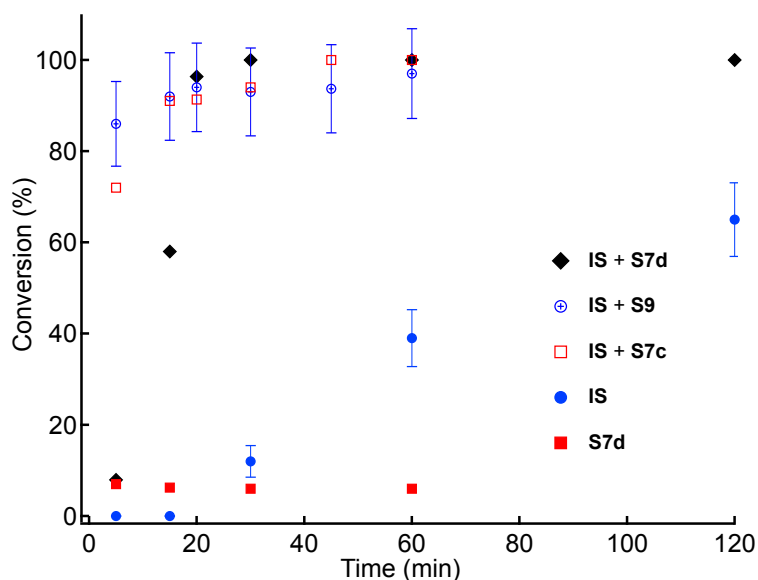


**Figure 19.** Conversion-time profiles of **UDMA** based on thermally initiated polymerization at 150°C comprising **Sens** ( $1.05 \times 10^{-3} \text{ mmol} \cdot \text{g}^{-1}$ ) and **IS** ( $1.56 \times 10^{-2} \text{ mmol} \cdot \text{g}^{-1}$ ) with the comparison from **Sens** and **IS** with the same aforementioned concentration in neat **UDMA** respectively.

In general, the generation of radicals from **IS** that is needed to initiate free radical polymerization of acrylate monomers resulted in by thermally induced cleavage explaining the acceptable final conversion of 60% without sensitizer[91]. Furthermore, the inflection point on the conversion curves appears much earlier in the case of **S7c** and **S9** than that in **S7d**. Here, cleavage occurred which promotes to generate radicals by a thermal reaction between **Sens** and **IS**. Thus, the synergistic effect from heat-induced cleavage and heat absorption/transfer in the systems comprising **S7c** and **S9** may explain why the final conversion of the sample comprising **S7d** responds later to the heat introduced into the system but still ends up with a sufficient value of 100%. This example demonstrates

that heat in general plays a vital role also in a system that follows radical polymerization using a monomer as matrix. According to the current experimental data, no detailed decision can be made whether the heat released by the sensitizer caused by light absorption or the heat externally introduced dominantly affects thermally initiated polymerization processes.

**Figure 20** confirms the thermal contribution of the introduced **Sens** in the systems to obtain crosslinked polymer using **IS** as co-initiator as concluded by recording the viscosity as response during the thermal treatment. This experiment also discloses the efficiency in such systems regarding the generation of initiating species by thermal reaction between **Sens** and **IS** in the case of **S7a**, **S7c** and **S9**. Thus, the inflection point where the real part and the imaginary part of the viscosity correspond to the storage and loss modulus, respectively, records the gel point ( $t_{gel}$ ) disclosing the time for first network formation[291]. This is a typical methodology to determine the storage and loss modulus of the system indicating detectable crosslinking occurrence during polymerization.

Here, **S9** exhibits very good efficiency to promote crosslinking by showing the earliest  $t_{gel}$ . This complements the results from DSC where  $T_i$  was determined. On the other hand, **S7d** exhibits also high efficiency to absorb and transfer heat showing with a gel point at around 87°C. In addition, the samples of neat **UDMA** and **UDMA** with **IS** showing no comparable storage modulus change in the comparison to those systems comprising **Sens**. This also indicates the function of the presence of sensitizers.

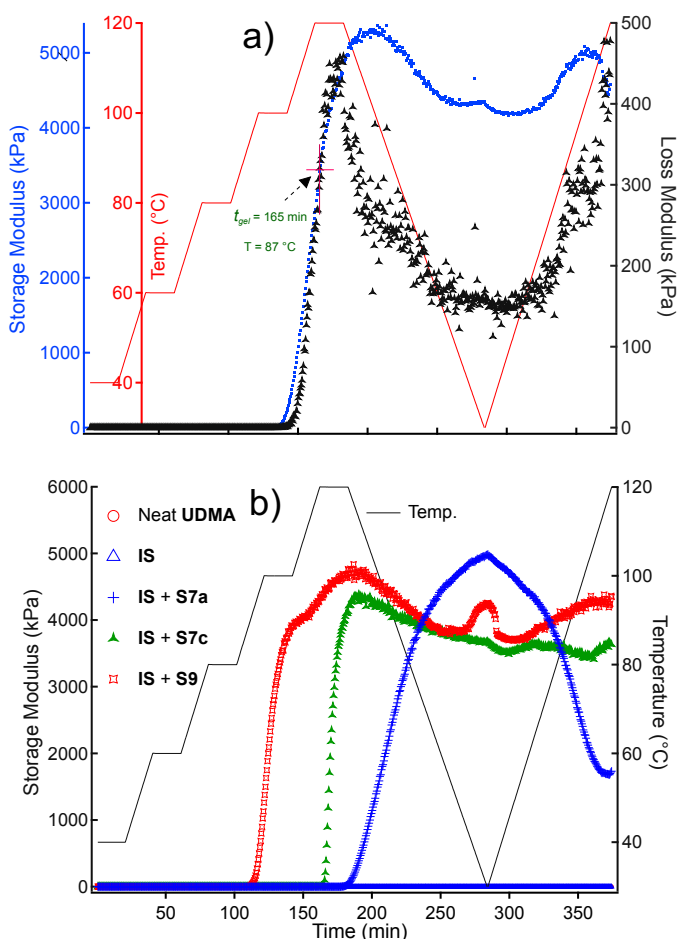


**Figure 20.** Profiles from rheology measurement based on a programmed heating up process. a) Curves of storage modulus, loss modulus as well as the temperature from the system in **UDMA** comprising **IS** (1.0 wt%) and **S7d** (**S7d:IS** = 1:6 (molar)) and; b) Profiles of storage modulus-temperature of the system of **UDMA** comprising **Sens** and **IS** following the aforementioned concentration, as a comparison, the data from neat **UDMA** and **IS** dissolved in **UDMA** was considered, respectively.

## 5.2 Polymer Network Formation by Radical and Cationic Crosslinking Applying NIR-Radiation for Excitation

### 5.2.1 Activated Free Radical Photopolymerization

Previous studies disclosed the significance to introduce heat needed to overcome an internal activation barrier promoting **PET** in systems where cyanines serve as sensitizers comprising diaryliodonium salts upon NIR exposure above 800 nm[118]. Sensitizers showing a large contribution of non-radiative deactivation can optimally proceed this process under adiabatic condition. The quantum yield for this process should be larger than 80% as concluded from fluorescence quantum yield, **Table 3**. Here, sensitizers comprising barbiturate group in the *meso*-position and a bridged connecting chain also respond to minor light intensity to succeed in initiation of free radical photopolymerization by using **TPGDA** as monomer[91]. Thus, there are no successful examples reported by using cyanine sensitizers comprising an open methine chain between the two indolium

terminal groups for excitation above 750 nm to generate aryl radicals and conjugate acid in the presence of **IS** as co-initiator[88, 118].

There still remains open questions how structural patterns of cyanine-based sensitizers affect the internal barrier of **PET**. This relates to the structural pattern of the terminal groups and length of methine chain as well as its sensitizing efficiency in **PET** by NIR excitation with high or low intensity. Previous research reported successful examples of cationic photopolymerization but investigation did not go so much in detail regarding the structure of cyanines. Therefore, the comparison between **S3-S9** may make it more clear whether an open chain in **S3**, **S5**, **S7a** and **S7b** or those with substituted bridge affect the sensitization efficiency. In addition, the variation of the terminal moiety may also affect the sensitization efficiency as depicted in the comparison between the patterns of benzo[*c,d*]indolium in the case of **S3**, **S5**, **S7b**, **S7d** and **S7f**, indolium of **S7a**, **S7c**, **S7e**, **S7h** and **S9**, and benzo[*g*]indolium of **S7g** as well as benzo[*e*]indolium of **S7j**[90]. Particularly, these structures may also bring effects to the size of internal activation barrier of **PET**. According to the results regarding reactivity, those from **S9** and **S7**, except **S7b**, **S7d** and **S7f**, would move into higher reactive systems while the rest would not follow, **S7i** is not included due to its water solubility. **Table 5** compiles the solubility of the cyanines investigated. There does not exist a clear relation of the molecular pattern regarding compatibility and thermal stability in combination with **IS** as determined by the temperature where radical polymerization significantly begins. Here, only systems carrying benzo[*c,d*]indolium moiety showed high thermal stability, which is still below its melting point of **IS**,  $T_m=153^\circ\text{C}$ [130].

**Table 5.** Data of the sensitizers showing the molecular weight, solubility and initiation temperature in the monomer of **TPGDA**.

Entry	Mn (g/mol) <sup>[a]</sup>	Solubility (g/L) <sup>[b]</sup>	T <sub>i</sub> (°C) <sup>[c]</sup>
<b>S3a</b>	544.4	0.03	117.6
<b>S3b</b>	1046.9	6.2	148.0
<b>S5a</b>	928.7	1.8	168.1
<b>S5b</b>	714.7	0.2	140.8
<b>S7a</b>	638.7	9.2	113.7
<b>S7b</b>	654.7	0.08	107.2
<b>S7c</b>	766.4	2.8	116.2
<b>S7d</b>	698.7	0.1	94.8
<b>S7e</b>	773.8	10.3	84.6
<b>S7f</b>	789.8	0.7	105
<b>S7g</b>	1147.9	14.1	113.5
<b>S7h</b>	655.3	0.4	82.6
<b>S7i</b>	1277.2	34 <sup>[d]</sup>	[e]
<b>S7j</b>	730.9	1.2 <sup>[f]</sup>	77.1 <sup>[f]</sup>
<b>S9</b>	948.8	12.2	100.0

<sup>a</sup>: data is from the provider; <sup>b</sup>: determined in untreated **TPGDA** according to the method reported[118]; <sup>c</sup>: determined in the system comprising **IS** in **TPGDA** by DSC setup according to the method reported[88], [**IS**] = 1.0 wt%, [**Sens**] : [**IS**] = 1:6 (molar), <sup>d</sup>: determined in H<sub>2</sub>O; e: not carried out due to its solubility; f: cited from[90].

As recently reported, iodonium salts comprising weak coordinating anions showed significantly large solubility in the acrylate monomers[130]. One question arriving from practice always addresses the loading with initiator components. This should be as low as possible. Thus, the molecular size would be one point of the selection by keeping the benefits of compatibility in the matrix. The [**NTf<sub>2</sub>**]<sup>-</sup> anion would be favourite because it exhibits only a half of the molecular weight compared to [**Al(O-t-C<sub>4</sub>F<sub>9</sub>)<sub>4</sub>**]<sup>-</sup>. The latter showed good performance to initiate both free radical and cationic photopolymerization due to its excellent compatibility in the matrix[27, 127]. However, the big size of it can be an undesirable feature considered for the practical applications aforementioned. Thus, **IS** could be taken as alternative with the benefit of excellent solubility and the feature not to release **HF**, which certainly relates to the [**PF<sub>6</sub>**]<sup>-</sup> anion[132]. These NIR sensitizers exhibit sufficient solubility (see in **Table 5**) using **TPGDA** as matrix determined by the previously disclosed method[88].



Preliminary results demonstrate the possibility of **S7c** and **S7g** to overcome an internal activation barrier in the systems combined with **IS** applying a high-power NIR-LED excitation[90, 118]. It also indicated that a dimethylene bridge as in **S7c** and **S7e** favours cationic photopolymerization while those comprising trimethylene bridge failed[27, 88, 118]. Surprisingly, **S7a** showed a remarkable reactivity in free radical photopolymerization by using NIR-LED with low exposure intensity of 45 mW/cm<sup>2</sup> as obtained through photo-DSC depicted in **Figure 21a**. This sensitizer behaves similarly in the case of high-power LED ( $I = 350$  mW/cm<sup>2</sup>) as shown in **Figure 21b**. On the other hand, the cationic sensitizers **S7g** and **S9** did not show acceptable reactivity for polymerization in the photo-DSC experiment while they did when using FTIR to follow monomer consumption. Only **S7e** exhibited slight response when the experimental temperature increased. Therefore, **S7a** can be seen as an interesting and promising candidate in the systems combined with low exposure intensity NIR-LEDs compared to those **S7b-S7h** since its lower intrinsic activation barrier as confirmed by the higher reactivity.

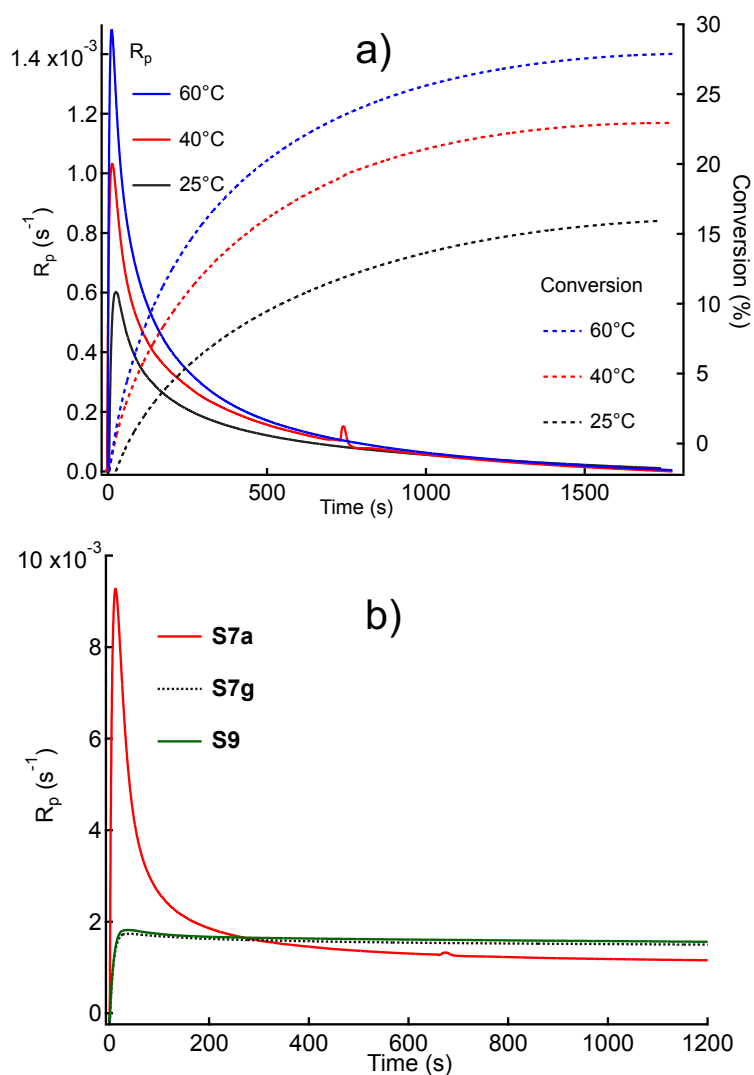


**Figure 21.** Profiles of conversion-time and polymerization rate ( $R_p$ ) obtained via photo-DSC of the system comprising **Sens** and **IS** (1 wt%, [**Sens**]:**IS** = 1:6 (molar)) in the monomer of **TPGDA** exposed by NIR-LEDs emitting at 770 nm ( $I = 45 \text{ mW/cm}^2$ ) taken at different temperatures (**Figure 21a**; **Sens** = **S7a**) and the systems comprising different Sensitizers (**Figure 21b**) with either an open polymethine chain (**S7a**) exposed by 820 nm LED or a bridged polymethine chain (**S7g** and **S9**) exposed by 860 nm NIR-LED with an intensity of  $1.0 \text{ W/cm}^2$  carried out at  $40^\circ\text{C}$ , cited from[90].

The photo-DSC setup proceeds an isothermal experimental condition. Thus, the heat released by the sensitizers and the polymerization would immediately be compensated by the instrument in the chamber via immediate cooling. Thus, this fraction of energy would be taken by the instrument and not the molecule to overcome the internal activation barrier. Therefore, this mechanism differs from that in real-time FTIR setup (see in **Figure 22**), where the heat formed remains in the systems resulting in a situation that reside between an adiabatic and isothermal condition in the time frame of the reaction. This always favors NIR-sensitized radical photopolymerization where both photon and heat are necessary to proceed **PET** based on an activated scheme[11, 19, 20]. Therefore, these results may open a new window for the applications where devices operating with minor intensity are desired for application.

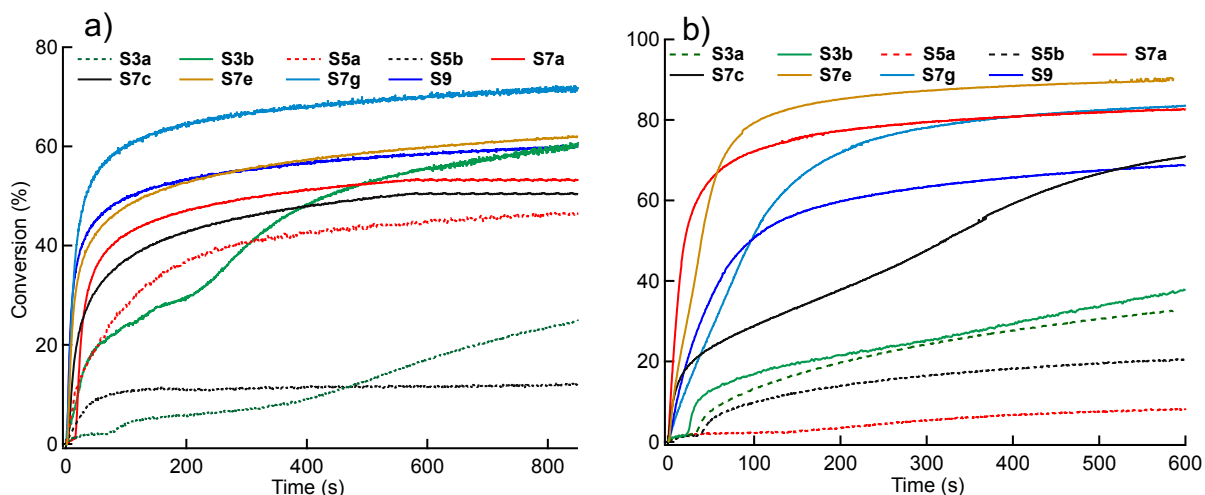


**Figure 22.** Conversion-time profiles for free radical photopolymerization measured by RT-FTIR in a) **UDMA** and b) **TPGDA** comprising  $[\text{Sens}] = 1.05 \times 10^{-3} \text{ mmol} \cdot \text{g}^{-1}$  and  $[\text{IS}] = 1.56 \times 10^{-2} \text{ mmol} \cdot \text{g}^{-1}$  applying with NIR-LEDs with the intensity of  $1 \text{ W/cm}^2$ . The data of photopolymerization from **S7b**, **S7d**, **S7f** was missing because of the small area of wavelengths overlap between the emission of available light sources and the absorption of the **Sens**. **S7i** was missing because of its water solubility which is not possible to dissolve into the organic monomers while **S7j** was investigated previously from [118]. This graph was modified from [91].

The combination of the sensitizers depicted in **Chart 2** with **IS** exhibited distinguished reactivity of free radical photopolymerization in either **UDMA** or **TPGDA** due to the specific structural patterns resulting in the scenario of **Figure 22**. As a comparison, the UV-sensitized system was included where **ITX** served as a sensitizer and the **IS** remained the same functioned as co-initiator as that in NIR systems [91]. The examples comprising either nonamethine or heptamethine showed comparable reactivity compared to UV excitation systems. As a result, **S7g** possessing a benzo[*g*]indolium terminal group exhibited the highest reactivity of polymerization (higher value of  $R_p$ ) and final C=C conversion in **UDMA**, **Figure 22a**, followed by the nonamethine **S9**. **S7e** also showed comparable reactivity, it bears the same substitution as **S7g** while the terminal pattern was the same as in the case of **S9**. Furthermore, the samples of **S7a** and **S7c** performed slightly less reactive but still exhibited a better than reactivity than **S3** and **S5**. Surprisingly, the sample of **S3b** ended up with sufficient final conversion although it showed lower polymerization reactivity as concluded from the conversion-time profiles. Comparatively, **S3** and **S5** showed the lowest reactivity. Both comprise the benzo[*c,d*]indolium terminal group which facilitate more strongly the non-radiative deactivation process [90, 91]. Change of the monomer as matrix with lower viscosity such as **TPGDA** leads to the results in **Figure 22b**. Similarly, the examples comprising **S7e**, **S7a** and **S7g** depicted the highest reactivity at the point of view of both  $R_p$  and final conversion, followed by **S9** and **S7c**. In addition, the higher viscosity of **UDMA** brings lower mobility of the molecules which results in higher reactivity in the case of **S3** and **S5**. The different overlap between the absorbers

absorption and the LED emission may also cause the differences observed because only the light absorbed can operate in a light-mediated reaction. In general, the non-radiative process decreases the efficiency of the excited state resulting in a lower lifetime of the excited state. As a consequence, less **Sens\*** would be available to participate in the electron transfer reaction between **IS**, this also explains the different reactivity of these sensitizers in a specific matrix.

Besides the initiation efficiency of photopolymerization, mechanical properties of the polymer films prepared by NIR excitation also brings importance of research. Here, dynamic mechanical analysis (DMA) was carried out as characterization protocol by applying sinusoidal force with ramping from -50°C to 200°C. The glass transition temperature  $T_g$  of polymer materials would typically pass through in this range. There exists sometimes a phase lag between the storage and loss modulus exhibiting contribution of elastic and plastic components to the mechanical behaviour. This is determined by the complex modulus  $E^*$  and phase shift  $\omega$ . Furthermore, the ratio of loss modulus  $E''$  to the storage modulus  $E'$  of the materials results in  $\tan\delta$ , Equation (15)[281, 292].

$$\tan\delta = \frac{E''}{E'} = \frac{\sin\delta}{\cos\delta} \quad (15)$$

$E'$  can be simply considered as a feature of solid nature of the materials while  $E''$  leads to the characteristics of a liquid appearing material[293]. An ideal elastic material is supposed to exhibit a phase lag  $\delta$  of zero since all the energy applied onto the substance could fully recover after the force released. On the other hand, an ideal viscous material shows a  $\delta$  of 90°. Therefore,  $\tan\delta$  values narrow to zero in case of an ideal elastic material while it approaches infinity in the case of an ideal liquid appearing as viscous material in which age deformation energy dissipates as heat in the surroundings.

**Figure 23** depicts the curves of  $E'$ ,  $E''$  and  $\tan\delta$  of the films obtained in the monomer of **UDMA** comprising **IS** and **S9** exposed by NIR radiation (**Figure 23a**) and **ITX** of UV radiation (**Figure 23b**), respectively. The original storage modulus of the polymer film of **S9** exhibited a value of approximately 5000 MPa and the peak of  $\tan\delta$ , which is often determined as glass transition temperature  $T_g$ , appears at around 90°C with a value of 0.4. In parallel, the film of the UV system exhibited an original storage modulus of 2000 MPa and comparable value of  $\tan\delta$  while  $T_g$  appears at 65°C. Furthermore, the measurement

was terminated at around 70°C because the polymer film was broken before the experiment was finished. This result indicates that the use of sensitizers in NIR-initiated systems leads to an improvement regarding the materials mechanical performance. It agrees with the data from other monomer systems[91].

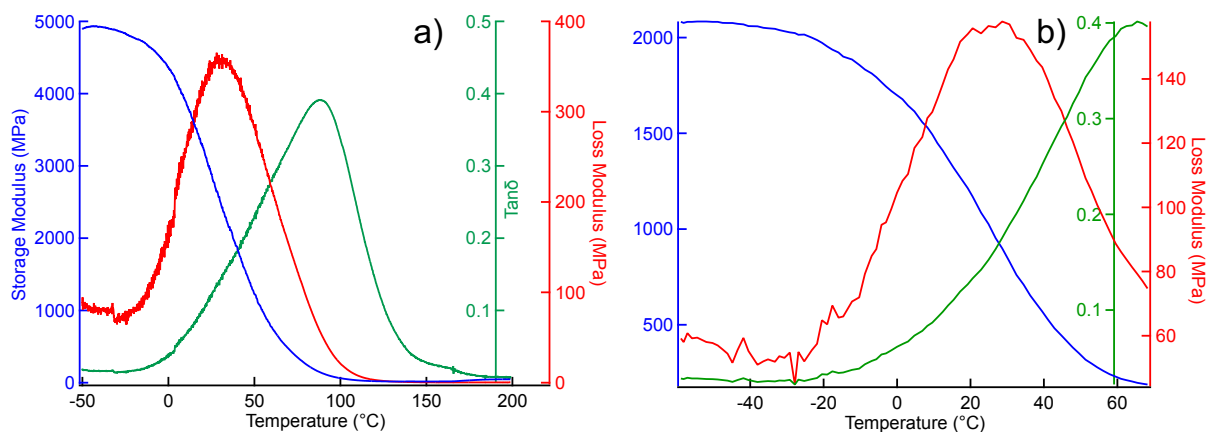


**Figure 23.** DMA profiles including storage modulus, loss modulus and  $\tan\delta$  curves of the polymer films obtained from free radical photopolymerization where **UDMA** as monomer applying with a) NIR-LED emitting at 860 nm comprising  $[S9] = 1.05 \times 10^{-3} \text{ mmol} \cdot \text{g}^{-1}$  and  $[IS] = 1.56 \times 10^{-2} \text{ mmol} \cdot \text{g}^{-1}$ , and b) UV-LED emitting at 395 nm comprising  $[ITX] = 5.25 \times 10^{-3} \text{ mmol} \cdot \text{g}^{-1}$  and  $[IS] = 2.1 \times 10^{-2} \text{ mmol} \cdot \text{g}^{-1}$ , respectively, cited from[91].

In addition, **Figure 24** exhibits similar amplitudes of the films comprising distinct sensitizers while the  $T_g$  varies as compared to the final conversions as summarized in **Table 6**. Except the insufficient value of **S3a**, the final conversions ranges around 60% in the case of **S7a** to about 81% shown in **S7e**.  $T_g$  also changes between 81°C as shown for **S5a** and 137°C in the case of **S5b** while it was 130°C for **S7e**. These data demonstrate that a higher reactivity or higher conversion does not always result in higher  $T_g$  in the polymer materials. **Table 6** also shows that the final conversions of the polymer films do not always match to the results obtained from real-time FTIR shown in **Figure 22**.

**Table 6.** The final conversions and  $T_g$  values obtained from the photopolymerization systems.

Sens	S3a	S3b	S5a	S5b	S7a	S7c	S7e	S7g	S7h	S9
$x_{\infty}$ (%) <sup>a</sup>	28	72	67	75	62	64	81	76	77	70
$T_g^*$ (°C)	-	95	81	4, 137	88	86	130	113	94	89

<sup>a</sup>: The final conversions of C=C from **UDMA** detected via FTIR in ATR mode after the exposure. \*:  $T_g$  of the polymer films obtained via free radical photopolymerization was determined according to the temperature at the peak of the  $\tan\delta$  curve measured via DMA characterization. -: No polymer film that could be used for proper DMA analysis was obtained.

This difference between the measurement could be explained by the difference between the light exposure pursued. Real-time FTIR measurement was carried out with a portable

small LED device while polymerization characterized on the ATR device. Exposure of the film materials was proceeded in a condition with a different heat capacity and heat conductivity. Both procedures operated with a similar excitation intensity of  $1.0 \text{ W/cm}^2$  explaining the differences observed. Thus, heat generated by the sensitizer differently remains in the system. Furthermore, the sample of **S5b** exhibits 2 peaks of  $T_g$  in the  $\tan\delta$  curve although the system showed insufficient reactivity for photopolymerization recored by RT-FTIR measurement (**Figure 22a**). One also needs to keep in mind that the heat released by the sensitizers plays a different role in the contribution of chemical crosslinking, which leads to a distinguished  $T_g$ . Therefore, the radicals needed to initiate polymerization are not only generated from a photonic process. It can be also originated by the heat released from the sensitizers. Data in **Table 5** show that a certain response exists in such systems upon heat as indicated by the temperature  $T_i$ . Particularly, the combination of sensitizer and **IS** significantly decreased the initiating temperature for the monomers used[91]. Nevertheless, the light-mediated process works with higher efficiency as a thermal-initiated process.

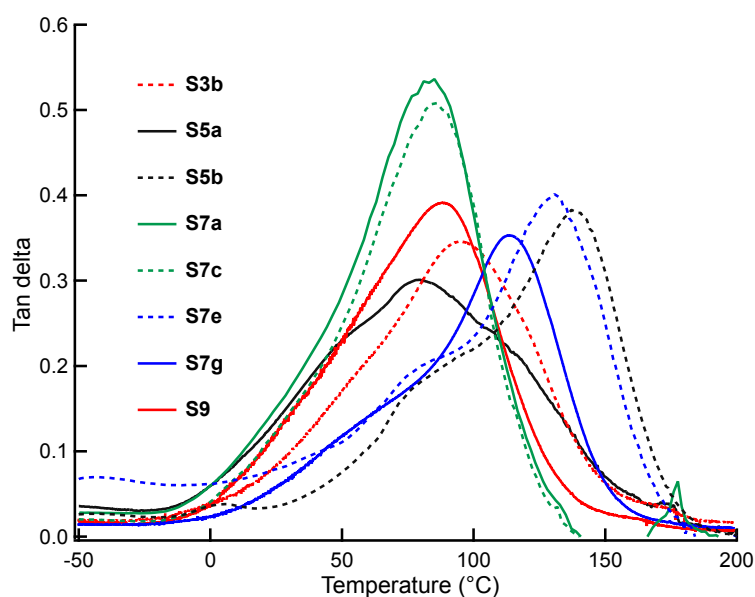


**Figure 24.** Curves of  $\tan\delta$ -temperature measured by DMA characterization of the polymer samples obtained from free radical photo-polymerization in the monomer of **UDMA** comprising **IS** with the concentration of 1.0 wt% and **Sens** (where  $[\text{Sens}] : [\text{IS}] = 1:6$  (molar ratio was used)).

**Figure 25** further describes the mechanical response of the systems operating with NIR sensitizers. It depicts the data for  $E'$ ,  $E''$  and  $\tan\delta$  of the polymer films obtained through photoinduced polymerization but from different areas of the sample exposed using the monomer of **UDMA** comprising **IS** and **S7c** as photoinitiating system. The sample shown in **Figure 25a** was directly exposed while that of **Figure 25b** was collected at the edge of

the sample. Both exhibited similar mechanical properties and similar  $T_g$  as characterised by DMA. The films obtained through thermally initiated polymerization from either **S7c** (Figure 25c) or **S7d** (Figure 25d) using **UDMA** as matrix showed obviously two peaks on the curve of loss modulus and  $\tan\delta$ . This can be a hint of phase separation proceeding in the material during crosslinking, which is not unusual[27].

These examples showed again that systems comprising NIR sensitizers take bivalent functions where both photonic and thermal processes contribute to generation of initiating radicals for free radical polymerization. Furthermore, the heat transfer in the systems also helps to increase the the mobility and diffusion of radicals formed. This facilitates to obtain homogenous polymer materials, which can be seen as a big benefit. These features and benefits may promote such systems into the focus in future research in coating sciences.

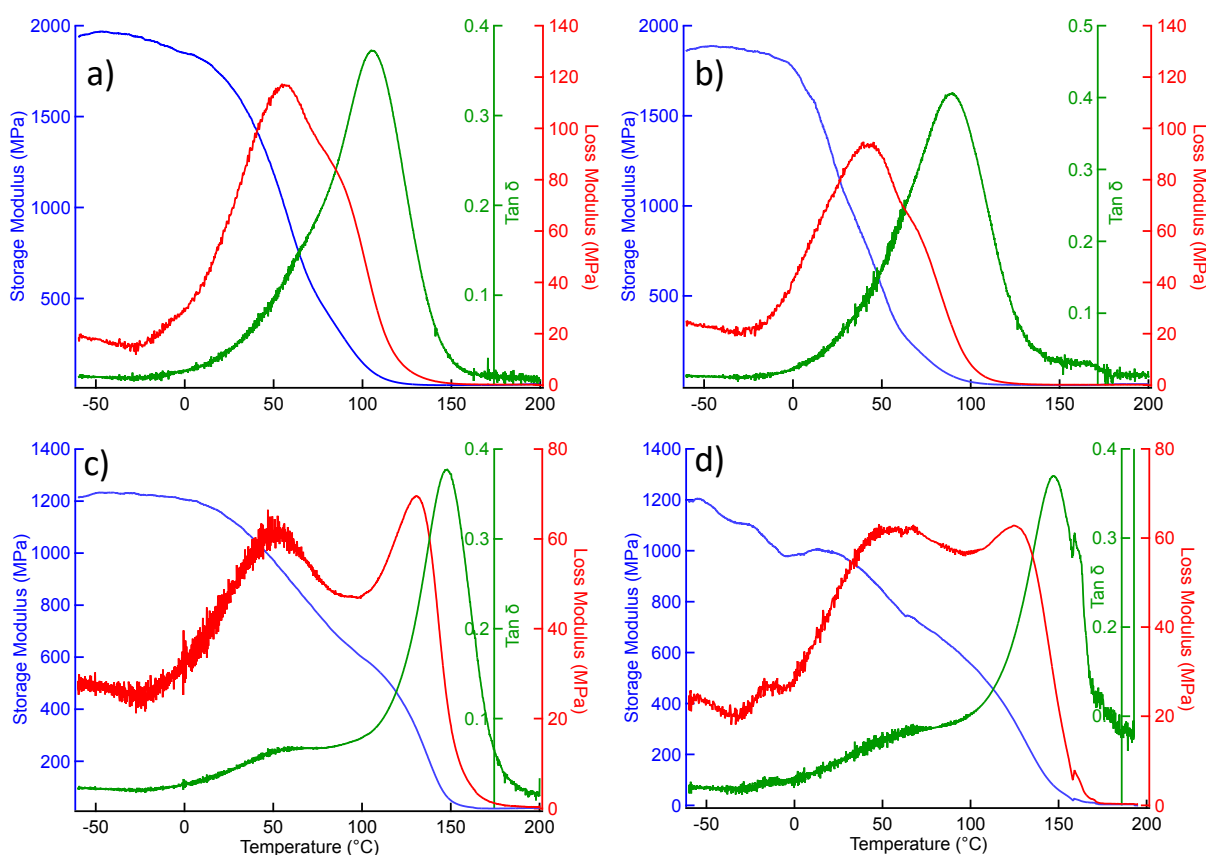


**Figure 25.** DMA profiles of the polymer films of **UDMA** comprising **S7c** and **IS** in **UDMA** at area **A** (a) and **B** (b) shown in **Figure 8**, respectively. c) and d) showed the DMA curves of the samples obtained via thermally initiated polymerization of **UDMA** in the comparison of **S7c** (c) and **S7d** (d) ( $[\text{Sens}] : [\text{IS}] = 1:6$  (molar ratio) and **IS**: 1.0 wt%).

**Figure 26** confirms the photobleaching of **S7a**, **S7g** and **S9** after photopolymerization in the matrix of **UDMA** using **IS** as co-initiator. There appear new peaks with bathochromic shift while no complete bleaching occurred in the case of either **S3b** or **S5a** after exposure. Moreover, **S7a** showed efficient but no complete bleaching in the exposure time frame with

new hypsochromic shifted band with respect originating absorption of **Sens**. An additional rising new peak was observed at around 400 nm. The lower mobility in the matrix could be explained by the high viscous matrix because unimolecular reactions rather prefer to proceed than bimolecular reactions under such conditions. Furthermore, a new broad shoulder peak showed up between 600-750 nm and a new peak generated at around 450 nm appeared in the case of **S7g** and **S9**, respectively. The proposed chemical structures of the photoproducts derived based on the specific oxidation products, which was previously disclosed[90, 118].

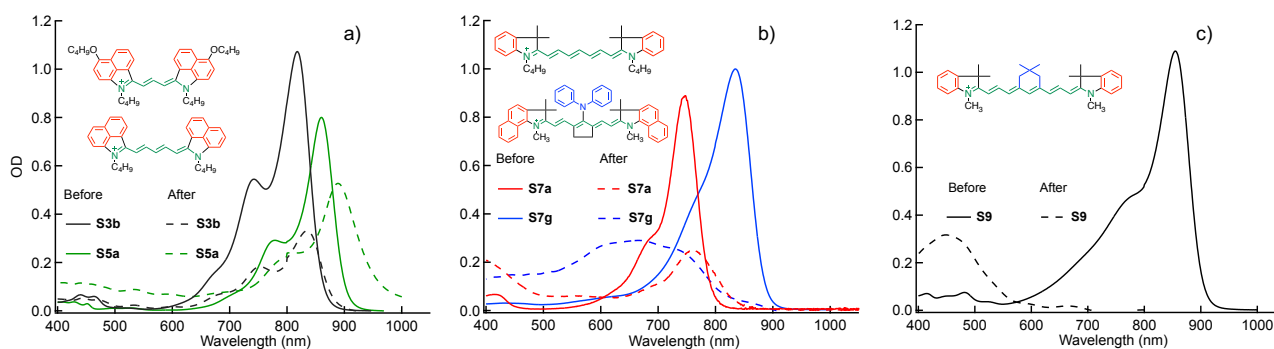


**Figure 26.** Optical absorption of the **Sens** in photopolymerization of **UDMA** in solution (before exposure) and in polymer films (after exposure), respectively. The concentration of the components in the experimental condition was the same as that in **Figure 22**, while the condition of the spectral collection was the same as that from **Figure 15**, cited and modified from[90].

### 5.2.2 NIR-Sensitized Photoinitiated Cationic Photopolymerization

**Figure 17** shows substantial formation of conjugate acid generated by the initiating systems that is typically needed for the initiation of cationic photopolymerization. Nevertheless, **S7c**, **S7g** and **S9** exhibited similar reactivity while **S7a** generated the largest amount followed by **S7c** and **S7e**. **Figure 27a** exhibits the difference of the reactivity to initiate cationic photopolymerization. Here, **HBVE** ends up with a significantly high conversion of nearly 100%. Previously reported results demonstrated high reactivity of polymerization initiated by the initiating systems comprising sensitizers combined with an iodonium salt coupling by aluminates ( $[\text{Al}(\text{O}-t\text{-C}_4\text{F}_9)_4]^-$ )[27, 130]. Here, **S7c** exhibited the highest reactivity of cationic polymerization initiation, followed by the similar results in the case of **S7g** and **S9**. Surprisingly, the reactivity reduces in the case of **S7a** although it has the highest amount of conjugate acid generated. Here, bond cleavage of the polymethine chain inhibits cationic photopolymerization by the formation of the nucleophilic products on the one hand. On the other hand, oxidation of position *iii* illustrated in **Scheme 23** *vide supra* explains the higher reactivity in the case of **S7c**, **S7g** and **S9** since it impedes the formation of nucleophilic moieties. While **S7a** still appears more reactive compared to **S3**



and **S5**, the introduction of the sensitizers possessing benzo[*c,d*]indolium brings no significant benefit in this application since these compounds mostly lead to non-radiative deactivation instead of facilitating the **PET** reaction between the **Sens\*** and **IS**. It gives the clue that the combination of longer methine chain as well as indolium and benzo[*g*]indolium terminal patterns as shown either in **S7c**, **S7g** or **S9** facilitates the polymerization of **HBVE** better by a NIR-sensitized acidic catalyzed process with higher efficiency. This process obviously follows rather a stepwise growth mechanism than chain reaction based on polyaddition[294]. However, the results also show disadvantages; that is the typically poor reactivity in cationic photopolymerization in systems with iodonium salts comprising **[NTf<sub>2</sub>]**- as anion using epoxides and oxidants as monomers[88, 130], **Figure 27b**.

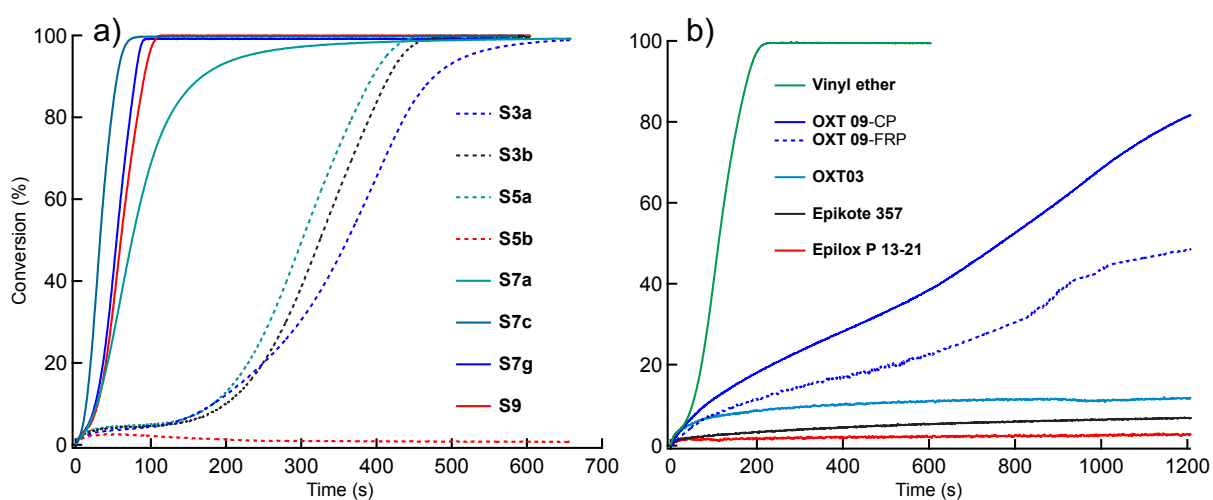
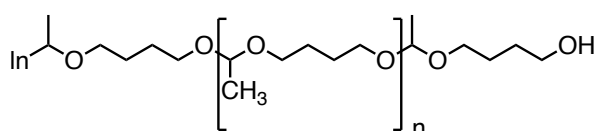


**Figure 27.** Conversion-time curves obtained from RT-FTIR for the investigations of cationic photopolymerisation in the monomer of **HBVE** comprising **Sens** and **IS**. **S9** was used as sensitizer in b). The experimental conditions were the same as that in the **Figure 22**, modified from[91].

**Figure 27b** exhibits the kinetics of cationic photopolymerization sensitised by **S9** and **IS** in the distinct cationic monomers. **S9** was additionally selected for further investigations because of its high reactivity of photobleaching and large tendency to generate a high amount on conjugate acid. In addition, the absorption spectra of **S9** showing a maximum at 854 nm overlaps very well with the emission spectrum of the NIR-LED prototype at 860 nm. These monomers used possess different viscosity, that is 5, 4, 11, 636, and 16 mPa·s for **HBVE**, **OXT 09**, **OXT 03**, **Epikote 357** and **Epilox P 13-31**, respectively, whose structures are depicted in **Chart 1**. It shows acceptable kinetics in the system using **OXT 09** as monomer, which proceeds both free radical with efficient final conversion of 80% and cationic polymerization protocol for the oxetane group with final conversion of 50%. While cationic photopolymerization was observed with much lower reactivity of less than

10% of final conversion in the case of **OXT 03**, **Epikote 357** and **Epilox P 13-21**, these monomers only polymerize based on a cationic mechanism. These results confirmed the conclusion that the  $[\text{NTf}_2]^-$  anion of **IS** does not proceed so efficiently in the initiation of neat cationic photopolymerization. Nevertheless, it can be seen as an acceptable comprise.

The isolated polymer of **HBVE** indicated a molecular weight ( $M_n$ ) of 1053 g/mol. This situation with relatively low polymerization degree of about 64% with  $M_w = 26500$  g/mol was also observed in previous studies where materials of high molecular weight were proceeded by two competitive pathways, that is conventional cationic photopolymerization and a polyaddition protocol promoted by the ring closure of hydroxybutyl ether[294]. Thus, a self-polyaddition reaction of **HBVE** can explain the competition of the reaction in an acidic environment since this conjugate acid-initiated polymer formation was observed with a reactive rate comprising  $[\text{NTf}_2]^-$ . Onium salts coupling with this anion exhibited insufficient reactivity in the systems where polymer formation follows a mechanism of carbocation serving as intermediate rather than to proceed by traditional cationic photopolymerization while oxiranes functioned as typical monomers[27]. Thus, the slightly higher nucleophilicity of  $[\text{NTf}_2]^-$  here somehow failed to accomplish a reactive system in cationic photopolymerization because of the higher nucleophilicity impeding efficient chain growth based on a cationic polymerization protocol. Therefore, the self-polyaddition results in polymer as shown in **Scheme 24**.



**Scheme 24.** Structural pattern of the product formed by acid-catalyzed self-polyaddition of **HBVE** based on the ref[295], cited from[90].

Apparently, it can tolerate involved moieties with higher nucleophilicity. Furthermore, the  $\alpha$ -hydrogen of the ether carbon exhibits a lower C-H bond dissociation energy, from where the electrophilic radical formed for initiation can easily abstract a hydrogen resulting in a nucleophilic radical. This intermediate can transfer an electron to the **IS** resulting in release of further conjugate acid[118]. This proceeds as a consecutive chain reaction in the dark and explains the high reactivity of **HBVE** in cationic polymerization[294, 295]. Such electron transfer reactions are not unusual and almost reported for photoinitiating systems where onium salts were used as co-initiators. This agrees to the results aforementioned

regarding the generation of a high amount of conjugate acid in the reaction between the **Sens\*** and **IS**. These features of **HBVE** additionally show the potential to develop efficient systems for manufacture interpenetrating polymer networks where these materials serve as plasticizer in the combination with free radical polymerization of multifunctional (meth)acrylic esters. Nevertheless, cationic polymerization typically proceeds more slowly compared to free radical polymerization[27].

### 5.2.3 Enhanced Performance of Cationic Photopolymerization in Hybrid Systems

**Figure 28** depicts the kinetics of NIR-sensitized free radical photopolymerization obtained by real-time FTIR choosing **TMPTA** as monomer. **S7g** shows the highest conversion which ends at 45%. **S9** accomplished with around 40% followed by **S7e** with a final conversion of 30%. The remaining sensitizers exhibited a final conversion between 7% and 20%[91]. Regarding the different features available from monomers used for radical polymerization as previously discussed, **TMPTA** possesses tri-functional groups appearing therefore usable as crosslinkable monomer comprising no special backbone such as those favouring hydrogen bonding in **UDMA** or flexible chain as can be seen in **TPGDA**, which would affect the properties of the polymer materials. Final conversion of **TMPTA** shown in **Figure 28** did not reach the values of that in the monomers with two functional groups (**TPGDA** and **UDMA**) as shown in **Figure 22**. Molecular segments in this matrix exhibited limited mobility during crosslinking due to the highly concentrated three functional groups that are available to participate in the crosslinking process. Nevertheless, formation of polymer networks starts earlier with larger number of functionality leading to a decrease of segment mobility resulting in therefore relatively low final conversion.

As mentioned in previous section, **HBVE** and **OXT 09** enable efficient self addition and cationic photopolymerization. Here, polymerization of the double bond enables polymer materials comprising cationic oxetane group on the polymer chain in the case of **OXT 09** as a hybrid monomer. Hybrid indicates in this case that two distinct polymerization mechanisms in the system can occur. The structure of **OXT 09** can therefore covalently connect two networks formed by two different mechanisms resulting in formation of one crosslinked material. Such structural feature may exhibit more beneficial than those bearing only cationic polymerization protocol such as **OXT 03**. Combination of suitable monomers from both free radical and cationic polymerization may proceed formation of semi-interpenetrating polymer networks in the case of the monomers aforementioned such as cationic polymerizable **HBVE**, **OXT 03**, **Epilox P 13-21**, and **Epikote 357** and (meth)acrylic **TPGDA**, **UDMA** and **TMPTA**. There appears often phase separation

observed as reported in UV-initiated systems[27] while NIR-sensitized photopolymerization did not show this problem in the case of  $[\text{Al}(\text{O}-t\text{-C}_4\text{F}_9)_4]^-$  anion[27]. Presumably, the heat generated by the sensitizers avoids phase separation in the NIR-based systems.

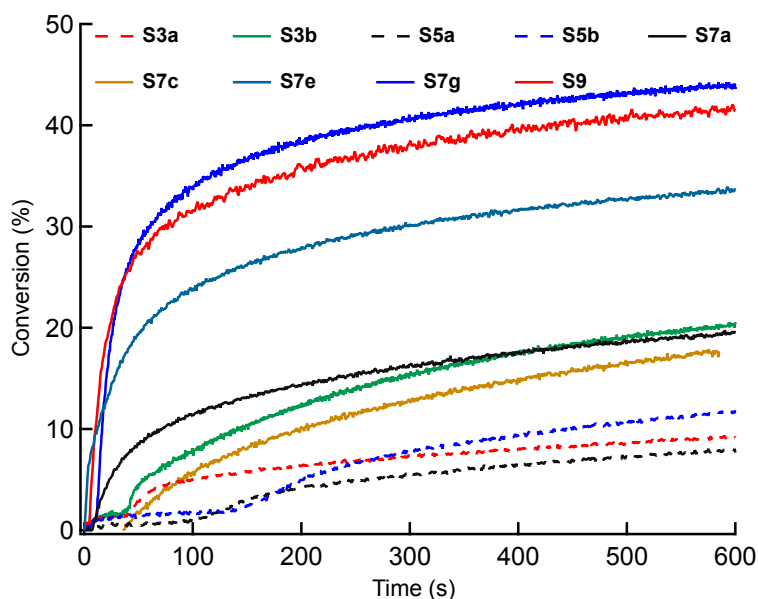


**Figure 28.** Conversion-time profiles for free radical photopolymerization measured by RT-FTIR in **TMPTA** comprising  $[\text{Sens}] = 1.05 \times 10^{-3} \text{ mmol} \cdot \text{g}^{-1}$ ,  $[\text{IS}] = 1.56 \times 10^{-2} \text{ mmol} \cdot \text{g}^{-1}$  applying with NIR-LEDs with the intensity of  $1.0 \text{ W/cm}^2$  (same experimental conditions for exposure as that in **Figure 22**), cited from[91].

Recent reports assumed that the reactivity of iodonium salts correlates with conductivity in the matrix of acrylic esters, that is the higher the conductivity is, the better the dissociation the salts resulting in higher reactivity with the excited state of the sensitizers[27, 126]. Data obtained in the monomers following cationic polymerization did not agree with these results (molar conductivity ( $\Lambda_m$ ) of the solutions comprising **IS** in the monomers in  $\text{S} \times \text{mol}^{-1} \times \text{cm}^2$ : **OXT 09** = 0.16, **OXT 03** = 0.2, **HBVE**: = 1.21, **Epilox P 13-21** = 1.76). Thus, there are further parameters regulating reactivity of the systems, which may also relate to the structure of the reactive group of the monomers.

**Table 7** summarizes the final conversions obtained from hybrid photopolymerization using **TMPTA** and **UDMA** for free radical polymerization and **OXT 03**, **HBVE**, **OXT 09**, **Epilox P 13-21** and **Epikote 357** as second monomer for cationic polymerization, respectively. The final conversion of **TMPTA** obviously increased in the presence of **HBVE**, **OXT 03** and **Epilox P 13-21** while the value of **UDMA** decreased in the hybrid systems. The introduction of the less viscous monomers for cationic polymerization significantly improved the mobility of the molecular segments resulting in higher final conversion of the respective reacting group in the monomer. Meanwhile, the final conversion of **OXT 03** increased from around 10% in neat monomer up to 60 % in both hybrid systems while the

final conversion did not visibly change in the case of **OXT 09**. Although this monomer exhibits an interesting structural feature of the covalent connection between different functional parts for free radical and cationic polymerization, it did not bring big impact on the performance in the system investigated. On the other hand, monomers exhibiting low reactivity for cationic polymerization in neat system exhibit higher reactivity as shown in the case of **OXT 03** in the hybrid system with either **TMPTA** or **UDMA**. This beneficial feature in NIR-sensitized photopolymerization systems reported here will hopefully bring interesting impetus in this field.

**Table 7.** Values of final conversions of free radical photopolymerization (FRP) from **TMPTA** and hybrid polymerization from **TMPTA** and cationic polymerization (CP) from cationic monomers applied with initiators comprising **S9** (0.5 wt%) and **IS** (1.5 wt%) upon the exposure of NIR-LED emitting at 860 nm with an intensity of 1.0 W/cm<sup>2</sup> and **UDMA**, respectively. Cited from[91].

$T_g$ (°C) <sup>1</sup>	Tan $\delta$	M1	$x_\infty$ (%) <sup>2</sup>	M2	$x_\infty$ (%) <sup>3</sup>	M3	$x_\infty$ (%) <sup>4</sup>
-10–45 <sup>5</sup>	0.18-0.16	<b>TMPTA</b>	59	-	-	-	-
	X	<b>TMPTA</b>	73	<b>HBVE</b>	94	-	-
-18	0.43	<b>TMPTA</b>	44	<b>Epikote 357</b>	15	-	-
81	0.096	<b>TMPTA</b>	66	<b>Epilox P 13-21</b>	8	-	-
97	0.10	<b>TMPTA</b>	73	<b>OXT03</b>	60	-	-
70	0.24	<b>TMPTA</b>	39	<b>OXT09</b>	CP: 39; FRP: 22	-	-
71	0.17	<b>TMPTA</b>	57	<b>OXT03</b>	60	<b>OXT09</b>	CP: 82; FRP: 31
89	0.39	<b>UDMA</b>	70	-	-	-	-
68	0.49	<b>UDMA</b>	47	<b>HBVE</b>	100	-	-
76	0.36	<b>UDMA</b>	34	<b>Epilox P 13-21</b>	82	-	-
112	0.38	<b>UDMA</b>	38	<b>OXT03</b>	67	-	-
126	0.58	<b>UDMA</b>	63	<b>OXT09</b>	CP: 85; FRP: 73	-	-
88	0.53	<b>UDMA</b>	27	<b>OXT03</b>	63	<b>OXT09</b>	CP: 87; FRP: 53

<sup>1</sup>:  $T_g$  of the polymer films determined from the temperature at the peaks on tan $\delta$  curves obtained from dynamic mechanical analysis (DMA), <sup>2</sup>: final conversions of the first monomer from the hybrid system determined by FTIR, <sup>3</sup>: final conversion of the second monomer, <sup>4</sup>: final conversion of the third monomer, <sup>5</sup>: maximum shows up in a broad range, X: the film from the hybrid polymerization system was too brittle to apply for DMA measurement.

These findings bring big interests to explore the mechanical properties of the materials obtained. **Figure 29** shows the tan $\delta$  curves of DMA profiles of the polymer films from neat **TMPTA**, **UDMA** and their hybrid systems with cationic polymerization, respectively. **Figure**

**29a** depicts that the film of neat **TMPTA** shows a broad shoulder peak between 0°C and 60°C for  $\tan\delta$  curve due to its high hardness and short of elasticity from highly crosslinked polymer network. Surprisingly, this finding differs from previous results where the film occurred to break during the heating process due to its high brittleness when **S7d** served as sensitiser in combination with an iodonium salt comprising another anion of  $[\text{Al}(\text{O}-t\text{-C}_4\text{F}_9)_4]$ -[27, 126]. Thus, the use of **S9** here shows an advantage and the introduction of  $[\text{NTf}_2]$ - can be seen as a benefit since its derivatives are more easily accessible. In addition, the lower molecular weight of the latter facilitates less loading in the coating compared to  $[\text{Al}(\text{O}-t\text{-C}_4\text{F}_9)_4]$ - considering equal amounts.

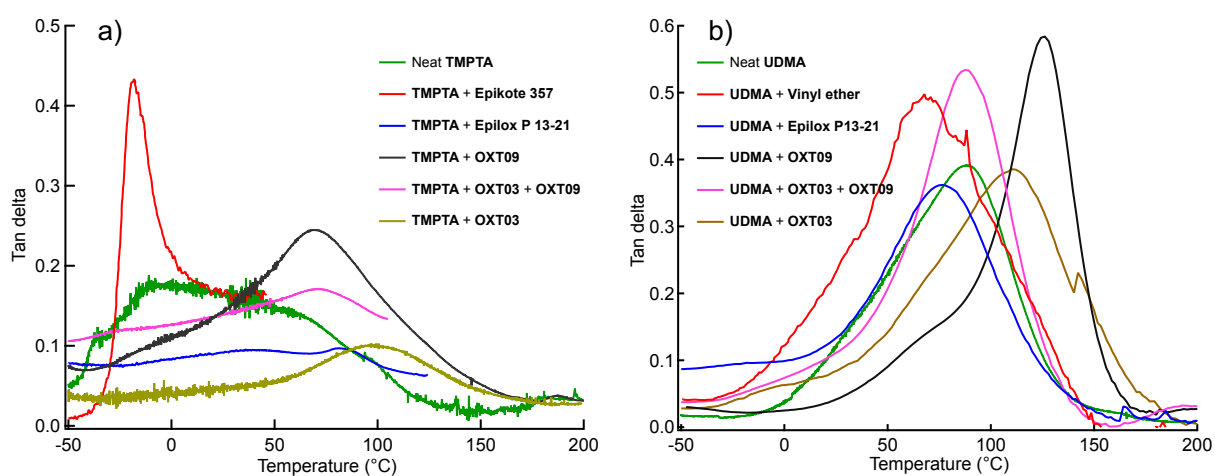


**Figure 29.** Profiles of DMA curves showing  $\tan\delta$  of the polymer films obtained by NIR-sensitized hybrid photopolymerization in the matrix of a) **TMPTA** and b) **UDMA** for free radical polymerization combined with different monomers for cationic polymerization comprising **S9** as sensitiser and **IS** acting as co-initiator. The exposure was applied by 860 nm LED with an intensity of 1.0 W/cm<sup>2</sup>. Cited and modified from[91].

In addition, **Figure 29** exhibits the  $\tan\delta$  curves of the polymer samples from hybrid free radical and cationic photopolymerization applying NIR-excitation. All films show only one fine clear peak indicating that no phase separation occurred during or after exposure, which UV-induced systems failed indicating phase separation[27]. Obviously, the sample comprising **TMPTA** and **Epikote 357** showed the maximum value of  $\tan\delta$  at lower temperature than that in neat **TMPTA**. This could be explained by elastic deformations favoured by insufficient final conversions of both monomers. **Epikote 357** possesses both aromatic and aliphatic structures that may contribute differently to the elasticity and stiffness compared to systems that mainly comprises aliphatic moieties. Sample curve of **HBVE** was not included since the polymer film was too soft and brittle to enable DMA measurement.

Peaks from  $\tan\delta$  of the remaining films obtained from hybrid systems locate in the range between 75°C and 100°C. Among those, the polymer from **TMPTA** and **OXT 09** shows a higher value of  $\tan\delta$  indicating a more overall elastic network due to their excellent compatibility while the presence of **OXT 03** and **Epilox P 13-21** leads to a diminished mechanical behaviour. In addition, the hybrid polymerization based on **UDMA** shown in **Figure 29b** exhibits similar results with the addition of other cationic polymerisable monomers showing the maximum value of  $\tan\delta$  between 0.4-0.6 and a  $T_g$  between 70°C and 120°C. The final conversion of **UDMA** shown in **Table 7** for the hybrid systems slightly dropped but this still appears sufficient while the reactivity of the cationic monomers significantly improved compared to the neat cationic polymerization systems.

Nevertheless, these findings of single peak observed from hybrid polymerization approve the success to prepare homogeneous interpenetrating polymer networks via photopolymerization by NIR-sensitized systems in combination of new high-power LED devices. Mechanical behaviour observed here indicates systems with interesting features that are competitive to those comprising iodonium salt of  $[\text{Al}(\text{O}-t\text{-C}_4\text{F}_9)_4]^+$  *vide supra*.

## 5.3 Heptamethine-Based Cyanine and Iodonium Salt as Initiators for Photocuring of Coatings Based on Sol-Gels Comprising Nanoparticles

### 5.3.1 Efficient Photocuring of the Coatings via NIR Exposure

The reactivity and efficiency of NIR-sensitized photopolymerization of both free radical and cationic systems in combination with cyanine sensitizers and iodonium salts was previously discussed[90, 91]. Herein, the heptamethine cyanine **S7e** coupling with anion  $[\text{PF}_6]^-$  served as NIR sensitizer combined with **IS-PF<sub>6</sub>** was selected to initiate photopolymerization of the sol-gel systems **SG1-SG3** comprising nanoparticles based on the condensation of the silanes following the route of Stöber process[278]. As shown in **Table 2 (Section 3.1.5)**, the samples are prepared by different amounts of silanes comprising distinct functional groups in **Epilox P 13-21** as the main reactive component resulting in sol-gels with higher viscosity compared to neat **Epilox P 13-21**. As a comparison, **ITX** absorbing UV light was selected as sensitizer in combination with **IS-PF<sub>6</sub>** for the initiation combined with a UV-LED device emitting at 395 nm.

**Figure 30** shows the photopolymerization kinetics obtained by real-time FTIR of the sol-gel systems determined based on **Epilox P 13-21** using **IS-PF<sub>6</sub>** as co-initiator in UV system comprising **ITX** and NIR-sensitized system where **S7e** served as sensitiser, respectively. Obviously, the photocuring reactivity of the sol-gels was improved resulting in

a higher final conversion and faster reaction curves compared to that in neat **Epilox P 13-21** especially in the cases of **SG1** and **SG2** in both UV and NIR systems. The final conversions of epoxy groups in **SGs** increased from 50% to 60% in UV-induced system after exposure of 600 s and improved from 50% to almost 70% in NIR-sensitized samples. This indicates the success to initiate the photocuring of nanoparticle-based sol-gels for coating preparation using heptamethine cyanine and iodonium salt in combination with high-power NIR-LED devices resulting in comparable reactivity compared to UV-induced systems. **SG3** showed slightly lower reactivity due to the addition of **vinyl-TEOS** and **MEMO** while absence of tetraethoxysilane (**TEOS**) resulting in insufficient compatibility. Thus, the presence of nanoparticles facilitating the crosslinking process brings benefits regarding the conversion of monomers. Several reasons could be discussed to explain these results. Extended discussion would be therefore avoided. Further research would be needed to bring more light into such complicated systems.

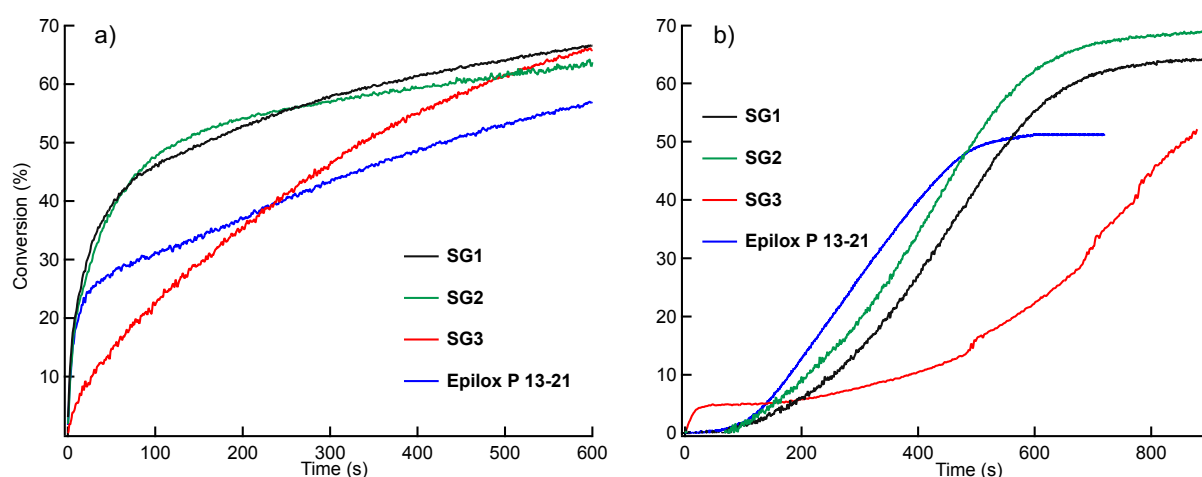


**Figure 30.** Conversion-time profiles of the sol-gels obtained from RT-FTIR evaluated based on the monomer of **Epilox P 13-21** comprising **IS-PF<sub>6</sub>** (2.0 wt%) and a) **ITX** (0.5 wt%) for UV-initiated system exposed by LED device emitting at 395 nm and b) **S7e-PF<sub>6</sub>** (0.5 wt%) for NIR system exposed by LED emitting at 820 nm, respectively. (The intensity of the LED devices were 1.0 W/cm<sup>2</sup>).

**Table 8** depicts the final conversions of the coating films obtained after exposure from UV and NIR irradiation, respectively. Data indicate slight increase of the final conversions compared to that from real-time measurement on the one hand. Comparable values between UV and NIR were observed on the other hand. Nevertheless, these findings bring the probability and impetus of the NIR-sensitized photopolymerization technology to coating field choosing heptamethine cyanine as sensitizer in combination of high-power NIR-LED prototypes.



**Table 8.** Final conversions of the samples after exposure evaluated from FTIR spectra.

$x_{\infty}$ (%) <sup>1</sup>	SG1	SG2	SG3
UV	88	75	53
NIR	62	72	47

<sup>1</sup>: Final conversions were obtained on FTIR spectra collected from the samples after photo irradiation and the evaluation was done based on the evaluation of monomer **Epilox P 13-21**. The data was taken after exposure for 120 s for UV system and 12 mins for NIR system under consideration of the conversion changes after different time of irradiation.

### 5.3.2 Properties of the Coatings Made from Sol-Gels Comprising Nanoparticles by Photopolymerization Technique

These exciting results regarding the photocuring reactivity of the sol-gels motivate to explore the properties of the coating films. The graphs at left in **Figure 31** show the appearance of the coatings applying on glass as substrate obtained from UV and NIR-sensitized systems, respectively. The samples obtained from UV-sensitized exposure appear remarkably cured without showing any sticky surface. Furthermore, it indicates the success of NIR initiation by using the heptamethine cyanine **S7e** carrying a special pattern combined with iodonium salt sharing the same anion  $[\text{PF}_6]^-$  resulting in sufficient compatibility of the initiator system in the sol-gels and efficiency of initiation. It appears that the coatings of **SG1** and **SG3** used in NIR systems were not homogeneously distributed on the substrate. This may be explained by the surface tension of the precursor resulting in insufficient compatibility between the coating precursor and the substrate. **SG2** can be seen as the best candidate considering its homogeneous appearance by eye and the reactivity of photopolymerization.

Meanwhile, the right graph shown in **Figure 31** depicts the performance of the coatings of sol-gels before and after applying adhesion test. It exhibits that the sample made by **SG2** shows excellent adhesion while **SG1** and **SG3** possess similarly sufficient adhesive property with a slight decrease in the case of UV photocuring. Surprisingly, among the coatings exposed by NIR light, **SG1** and **SG3** did not show as good in the adhesion test compared to those from UV systems. Furthermore, **SG2** showed insufficient value with losing around 20% of the coating after removing the tape during the test. Further improvement regarding the precursor preparation should be therefore taken into consideration to obtain such coating systems with better properties. Nevertheless, photocuring of the sol-gels comprising nanoparticles can successfully proceed applying high-power NIR-LED devices.

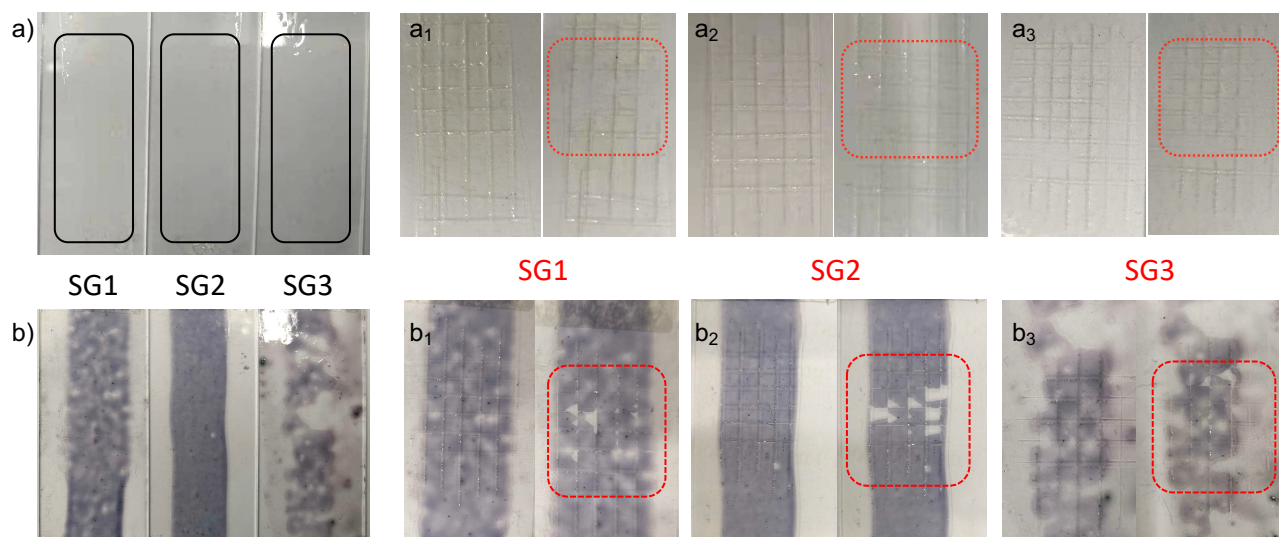


**Figure 31.** Appearance of the coatings obtained (left side) and performance during the adhesion test (right side) from a) UV and b) NIR systems, respectively. The initiator combination of **IS-PF<sub>6</sub>** with either **ITX** for UV system or **S7e-PF<sub>6</sub>** for NIR was applied. The red frame in the graphs focused on the area where adhesion test was applied (The test was carried out following the instruction of ASTM D3359-22 Test Method B).

The DMA profiles in **Figure 32** of the photocured films bring surprisingly exciting results. The original storage modulus of the coating films in neat **Epilox P 13-21** from both UV and NIR systems exhibit around 1800 MPa while the peak of  $\tan\delta$  show up at  $-30^{\circ}\text{C}$  and  $10^{\circ}\text{C}$  with the values of 1.4 and 0.7, respectively. Furthermore, the storage modulus of the **SGs** (**SG1** and **SG2**) films obviously increased in the case of UV initiation while it dropped when initiated by a NIR-sensitized system resulting in a higher  $T_g$  compared to that of neat reactive monomer. Thus, the system comprising nanoparticles retarded the begin of the  $\alpha$ -process starting at the glass transition where larger segments start to move. It can be therefore summarized that the introduction of the silanes comprising distinct functional groups helps to build up highly crosslinked polymer networks exhibiting stronger mechanical properties. The addition of nanoparticles contributes to the hardness of the coating polymer exhibiting decreased value of storage modulus and higher  $T_g$  in the case of NIR-sensitized systems. Moreover, the  $T_g$  evaluated from the  $\tan\delta$  curve exhibits a shift from  $0^{\circ}\text{C}$  in UV to  $20^{\circ}\text{C}$  in NIR in both **SG** samples. The data of **SG3** was not included since its high hardness and brittleness can not enable DMA measurement. In addition, the heat generated and released in NIR systems also facilitates the mobility and transfer of the initiating moieties into the samples. This can be therefore beneficial to promote complete photocuring with high conversion and polymerization of the reactive components. Thus, this technology brings new impetus to the coating industry and opens a new window in this field. Hopefully, many new applications will be established based on this new technology.

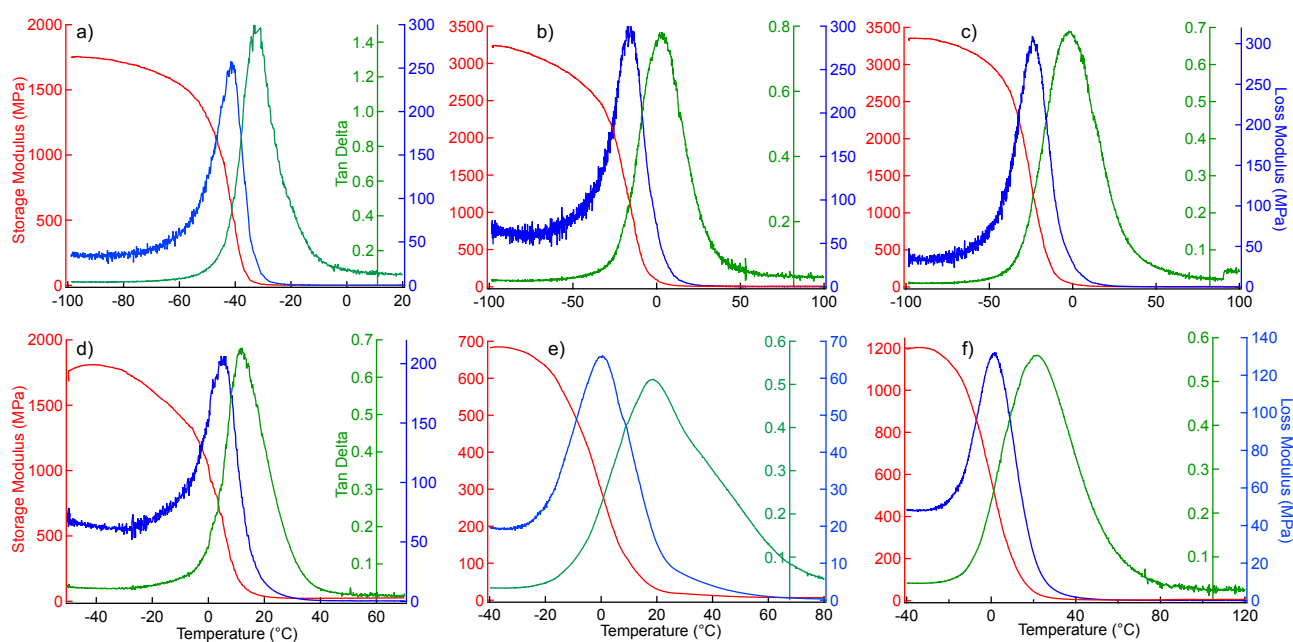


**Figure 32.** DMA profiles from the cured coating films obtained from the monomer of **Epilox P 13-21** (a) and d)) and the sol-gels (b) and e) from **SG1**, c) and f) from **SG2** initiated by UV (a), b) and c)) and NIR (d), e) and f)) systems, respectively. The exposure was finished by either the LED device emitting at 395 nm for UV system or NIR-LED emitting at 820 nm with an intensity of 1.0 W/cm<sup>2</sup>. The data of **SG3** was missing because the coatings from **SG3** were too brittle to be applied for DMA characterization.

## 5.4 Performance of Heptamethine Cyanine Applied to Aqueous Coatings for Physical Drying with NIR-Radiation Followed by Chemical Drying with UV Exposure

### 5.4.1 Physical Drying of Waterborne Polyurethane Dispersions

The NIR sensitizers comprising different structural patterns showed distinct efficiency for the initiation of both free radical and cationic photopolymerization in combination of **ISs** as discussed *vide supra*. The feature to generate heat and release it based on the temperature tracking motivates to explore the performance of the sensitizers carrying special patterns for applications in the coating systems. Here waterborne polyurethane (**PU**) binders comprising a UV-sensitive initiator system for chemical crosslinking fitting well with LED emission at 395 nm was selected as aqueous precursor provided by Rhein Chemotechnik GmbH for photonic physical drying experiment, which is a novel technology applying a NIR-LED device emitting at 860 nm[60]. Water soluble **S7i** was taken as NIR absorber since its absorption spectrum overlaps well with the emission profile of the LED. Unfortunately, the specific structure of the **PU** precursor was not clearly disclosed due to the commercial confidentiality.

**Figure 33** depicts the FTIR spectra of the **PU** dispersion before and after drying in air, indicating the significant decrease of the peak area of OH- vibration after drying at around

3400  $\text{cm}^{-1}$ . The integration area at this peak was therefore used for the evaluation of the drying process. As a result, **Figure 34** shows the profiles with respect to the exposure time of the samples comprising **S7i** with different concentrations upon NIR exposure obtained by real time FTIR evaluated by the water loss. Apparently, the exposure using a high-power light source significantly accelerated the drying of the **PU** precursors to get rid of the water as solvent compared to the evaporation of water in the air. In addition, it also further improved the efficiency to get rid of the solvent with addition of **S7i** applying NIR exposure at 860 nm. Here, a minor loading of the system with 0.02 wt% resulted in a sufficient reactivity and efficiency with final conversion (90%) considering the water loss compared to the sample without sensitizer. An increase of the NIR absorber concentration significantly shorted the time for drying until 0.2 wt%. Higher concentration of sensitizer in the system can generate a big amount of heat upon exposure resulting in rapid evaporation of the solvent, this explains the slight decrease of the percentage of water loss. However, the concentration increase from 0.1% to 0.2% did not appear a big change on both evaporation rate and final conversion.

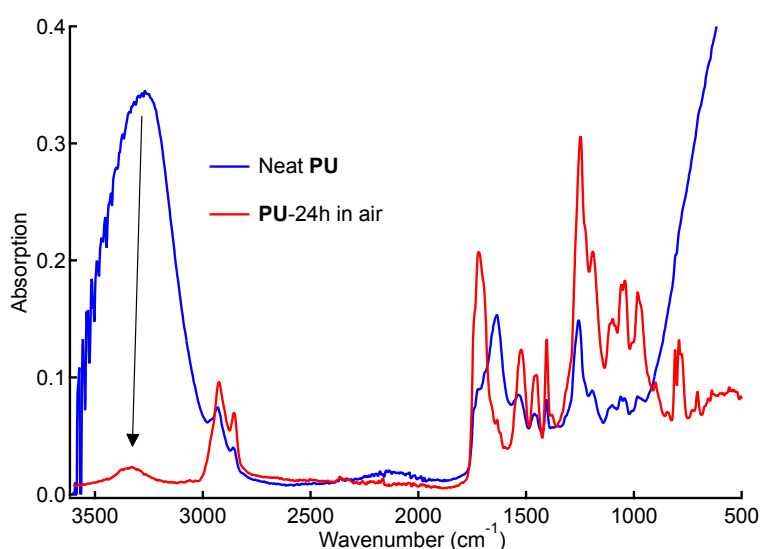


**Figure 33.** FTIR spectra of the PU coating precursor exposed in the ambient for 24h for drying and as a comparison the sample without any treatment.

Nevertheless, one should therefore keep in mind that it is not always necessary to introduce big amount of absorber as heat generator. Since only the absorbed light can contribute to such a process. In case of high concentration, the light would be mainly absorbed in the entrance window while no penetration into deeper areas can proceed. An extinction of about two equals to 1% of light that leaves the sample after penetration of the entire layer while an extinction of about one equals 10% of the light which is not absorbed. This means in the case of the latter that deeper areas receive a better chance to absorb

light where the embedded absorber converts the absorbed light into heat by internal conversion as shown in the **Scheme 20**.

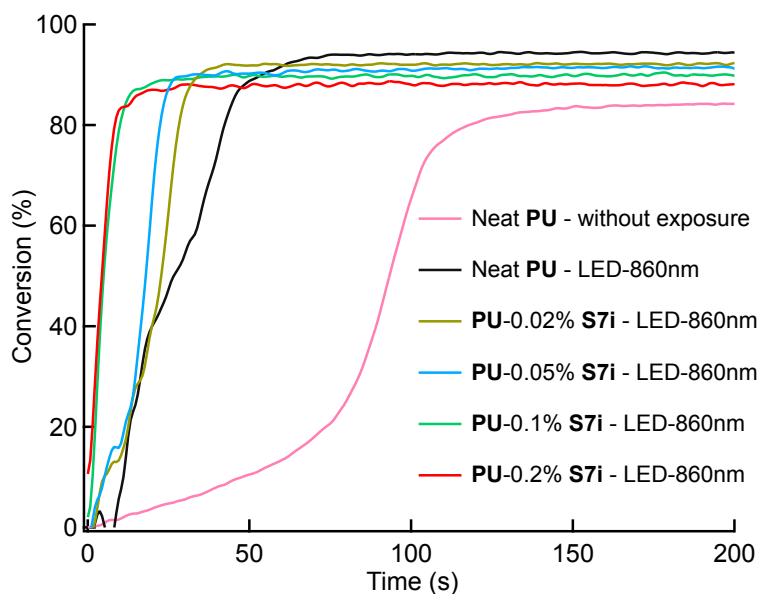


**Figure 34.** Conversion-time profiles collected by real time FTIR spectroscopy of the **PU** coating precursors comprising the absorber **S7i** with different concentration upon exposure by the NIR-LED emitting at 860 nm with an intensity of  $1.0 \text{ W/cm}^2$  for physical drying to get rid of the water. The data of neat **PU** and that without exposure were also included as a comparison, the evaluation of the conversion was based the decrease of the strong O-H bond at  $3200 \text{ cm}^{-1}$  following the results from **Figure 33**. The thickness of the sample applied for the FTIR measurement was  $100 \mu\text{m}$ .

**Figure 35** shows the DMA profiles of the **PU** films obtained from physical drying without crosslinking. It can be seen that the samples of 0.02% and 0.1% as well as the neat **PU** exhibit similar mechanical behaviour with similar original storage and loss modulus of 4000 MPa and 100 MPa, respectively. Thus, the introduction of sensitizer did not diminish the mechanical properties of the physically dried films on the one hand by significantly improving the drying process. The values of storage and loss modulus obviously dropped with high concentration of **S7i** with 0.2 wt% on the other hand. It could be explained that the distribution of highly concentrated absorber moieties in the films more or less interrupts the intersection of the **PU** segments in the coatings.

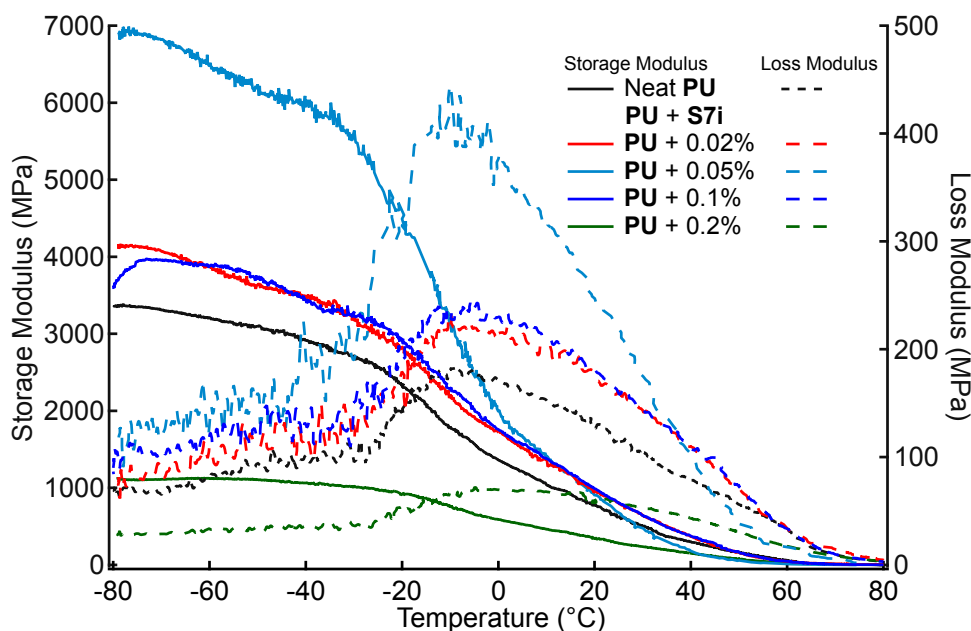


**Figure 35.** Profiles of storage modulus and loss modulus-temperature of the **PU** films obtained from the **PU** precursors comprising different concentration of **S7i** following the previous physical drying collected by DMA characterization following the same method aforementioned.

Surprisingly, there is an increase of original storage modulus value observed of the sample comprising 0.05 wt% **S7i** up to 7000 MPa although loss modulus stays similar to that of neat sample, **Figure 35**. Thus, based on the consideration on both efficiency of this physical drying process, appearance of the coatings obtained (heavy colour due to high concentration) and commercial cost, a lower concentration of the sensitizer **S7i** (0.02%) was chosen for the further experiments and tests.

#### 5.4.2 Chemical Crosslinking by UV Radiation of Physically Dried Films Applying NIR Exposure

**Figure 36a** exhibits the curves of storage and loss modulus of the **PU** coating films comprising additionally UV initiating system for chemically crosslinking. Samples were obtained by physical drying comprising 0.02 wt% **S7i** as heat generator applying NIR-LED emitting at 860 nm upon exposure for 1 min and 2 min, respectively. It shows that the difference of exposure time did not visibly change the mechanical behaviour of the physically dried films. This also agrees with the results in **Figure 34** that irradiation of 60 s is sufficient to get rid of the water in such system. As a result, exposure of 1 min here was chosen as the following experimental conditions. The DMA profiles shown in **Figure 36b** demonstrate that further treatment applying a UV-LED emitting at 395 nm on the physically dried **PU** coatings significantly change their mechanical properties resulting in a crosslinked polymer networks.

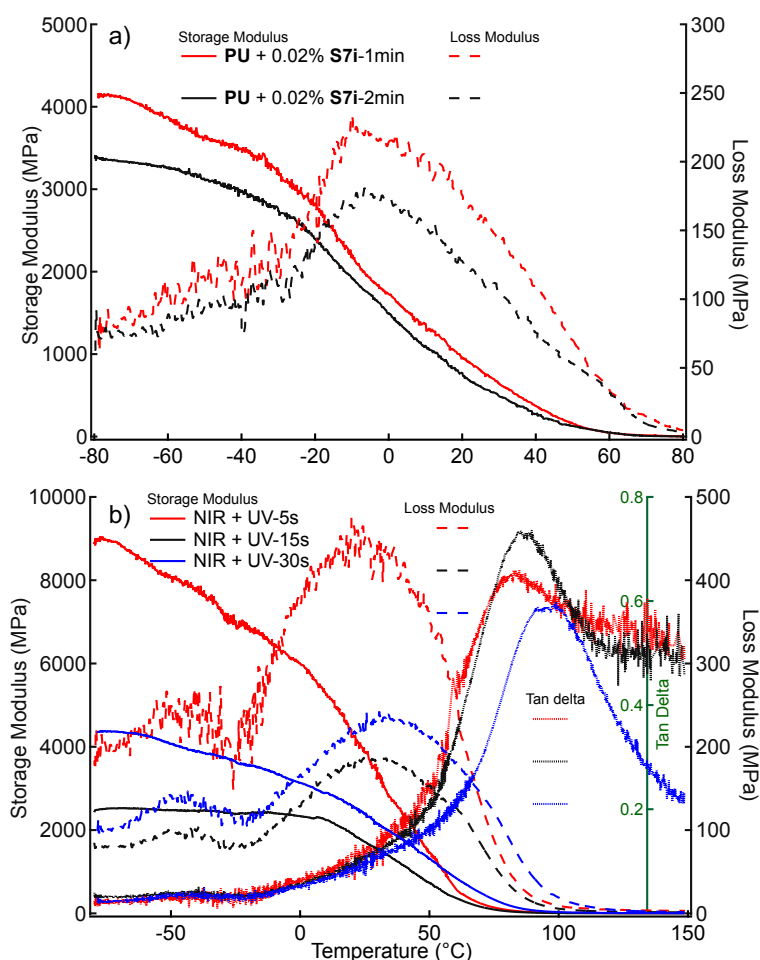


**Figure 36.** DMA profiles of the **PU** films obtained from the **PU** precursor comprising 0.02% **S7i** with a) different time of NIR-LED exposure and b) following with a step of UV exposure for cross-linking, the intensity of the UV-LED emitting at 395 nm is 1.0 W/cm<sup>2</sup>.

It indicates that the value of original storage modulus increased from 4000 MPa to 9000 MPa and loss modulus from 100 MPa to 200 MPa, respectively. This was proceeded in the case of 5 s exposure by UV light resulting in a flexible and elastic polymer film. Longer exposure by UV light leads to polymer films with decreased storage modulus indicating less elasticity caused by higher brittleness of networks formed. Importantly, peaks of  $T_g$  of the samples from different crosslinking time shows up at similar range from point view of both loss modulus and  $\tan\delta$ , that is between around 30°C on loss modulus curve and 80°C on  $\tan\delta$  curves, respectively. Thus, chemical crosslinking resulted in a significant increase of the  $T_g$  caused by the polymer network formed. Such crosslinked materials are called semi-interpenetrating networks. No phase separation occurred as indicated by the appearance of one  $T_g$  on the  $\tan\delta$  curves. These interesting results bring new aspects in coating sciences because it enables to replace oven technologies by photonic physical drying.



## 6. Conclusion & Outlook

The investigations of photochemical systems based on photopolymerization comprising cyanines as sensitizers combined with iodonium salt have brought increasing interests for research due to their high reactivity and efficiency applying NIR excitation. This thesis firstly reported the relation between the structural patterns of cyanines and the performance on photochemical reactions from their excited states in combination with iodonium salts. The electronic structure of the sensitizers exhibit distinct structural aspects including either an open or bridged chain with different numbers of  $\pi$ -electrons, specific substitutions at the *meso*-position as well as distinct indolium groups as terminal patterns. This deeply influenced the efficiency to initiate radical and cationic polymerization.

The sensitizers **S3**, **S5** and **S7b** comprising a terminal benzo[*c,d*]indolium structure exhibited good bathochromic shift of optical absorption on the one hand but relatively low sensitization activity on the other hand. These compounds may bring interesting impetus regarding the generation of heat on demand in technologies by just turning ON and OFF a light source as a replacement of conventional oven technologies, which operate either for initiation of chemical reactions based on a thermal activation or physical process such as the removal of solvent to get rid of volatile components in the system such as coatings. From the point view of energy saving, these features regarding heat contributions of such compounds exhibit big progress and promising aspects in this field. This was confirmed again by the application to initiate physical events such as photonic drying process to remove water in the **PU** precursor dispersion resulting in a high efficiency using **S7i** with low loading in the coatings. This hopefully opens a new foresight to synthesis such compounds in the near future, which will furthermore improve this technology.

Structures of **S7** comprising an indolium terminal group particularly **S7a**, **S7c** and **S9** brought new impetus in this research field. They possess the electronic structure with either an open and non-bridged connecting chain as depicted in **S7a** or bridged chain with substitution at *meso*-position as in **S7c** or even a larger number of  $\pi$ -electron polymethine chain as in the case of **S9**, respectively. Surprisingly, **S7a** exhibited a lower internal deactivation barrier required for photoinitiation of free radical polymerization compared to those comprising the same number of methine groups. They belong to heptamethine derivatives shown in **S7b-j**. **S7a** showed remarkable response in photo-DSC experiment with minor light intensity of the NIR-LED. This can be seen as big benefit for technologies operating with low intensity sources. On the other hand, systems with low internal



activation barrier tolerate a certain amount on day light which becomes beneficial for applications where handling red LED light becomes unacceptable.

Furthermore, **S7a** also shows good fluorescence emission with the highest value of fluorescence lifetime and fluorescence quantum yield among the sensitizers included here. A long lifetime of the excited state increases the probability of the excited state to react with a co-initiator such as an iodonium salt. Particularly, the perfect compatibility between the optical absorption of **S9** and the emission of the new high-intensity NIR-LED emitting at 860 nm brings new impetus into this field. Therefore, the design of these compounds in the future may consider to develop such cyanine-based derivatives comprising a polymethine chain with open non-bridged structure while the issues of high purity and availability at larger scale should also not be ignored. In addition, the results regarding either heat contributions and/or photochemical reactivity of these sensitizers bring valued aspects for the strategical selection/synthesis of cyanines for their function in photopolymer systems such as relating them to initiate photochemical events. Here, structures of **S7** and **S9** present more sufficient reactivity for photochemical reactions than to participate in photophysical process such as photonic drying based on the structure patterns of **S3** and **S5**, respectively.

The combination of these polymethine cyanine sensitizers comprising distinguished terminal patterns and diaryliodonium salt comprising **[NTf<sub>2</sub>]<sup>-</sup>** as counter anion succeeded in the initiation of free radical polymerization using multiple (meth)acrylates. Here, monomers such as **TPGDA**, **UDMA** and **TMPTA** resulting in significant reactivity and efficiency. Although it was previously reported that the **[NTf<sub>2</sub>]<sup>-</sup>** anion might not succeed to initiate cationic photopolymerization, the results obtained here approved the probability in the systems comprising oxetanes and vinyl ethers. Particularly, the introduction of the high-power LED device, whose emission overlaps well with the absorption range of these cyanines provides much more possibilities of applications in this field. The success of cationic photopolymerization with oxetanes reminds us to consider the focus on the monomers tolerating specific nucleophilicity. The significantly high reactivity of vinyl ether requires further attention since the  $\alpha$ -hydrogen of the carbon on the ether moiety possesses a lower C-H bond dissociation energy resulting in formation of a nucleophilic radical which transfers an electron to the iodonium salt leading to additional formation of radicals and conjugate acid. This proceeds also in the dark as chain reaction and enhances the initiation performance of the system.

Moreover, cyanine-based sensitizers comprising a larger number of methine groups in the connecting chain and a benzo[g]indolium pattern as terminal group exhibited significant efficiency for initiation of both free radical and cationic photopolymerization by using NIR-LED devices with strong emitting intensity in the presence of iodonium salt comprising counter anion  $[\text{NTf}_2]^-$ . Thus, this iodonium salt deserves more attention in both scientific research and practical applications following the features of excellent solubility in multitudinous monomers. The fact that this anion exhibits no tendency to release toxic HF makes its use in practice more attractive from an environmentally friendly point of view. In addition, iodonium salt with  $[\text{NTf}_2]^-$  anion can be more easily accessed by synthesis as well as lower cost and availability than the aluminate anion  $[\text{Al}(\text{O}-t-\text{C}_4\text{F}_9)_4]^-$ .

According to the results obtained with **S9**, it would be interesting to investigate more substances with extension of methine moieties based on **S9**. Furthermore, it would be also worthy to study whether these compounds could activate excitation in the wavelength between 1000-1100 nm since the addition of one methine moiety typically leads to a 100 nm bathochromic shift of optical absorption. This would be interesting to couple such chemical systems with respective LEDs emitting around 1000 nm with high intensity. It is still challenging to find alternative cyanines which could activate sufficient PET process in this spectral region due to the fact that the currently available sensitizers mainly contribute with heat generation upon excitation on demand. Thus, those compounds only serve as absorbers and heat generator as molecular oven in the systems. Therefore, the design and synthesis of those substances with respective special structures appear promising with huge potentials in the near future in coating sciences.

Meanwhile, the feature of heat generation in such systems can be also seen as an additional benefit since it would be available in both free radical and/or cationic photopolymerization systems. Particularly, this heat formed promotes the internal conversion between the ground state and excited state of the NIR sensitizers. Here, the excited state of the absorbers can enable processes to overcome a certain internal activation barrier in the systems. This brings great interests to design systems which enable to tolerate certain amount of light with low exposure intensity (e.g. ambient room light) on the one hand while they work with devices equipped with strong radiation source. Such threshold systems have received increasing attention in practical applications because it is easier to establish them in projects applying NIR light for irradiation. Furthermore, the results regarding the distinguished performance of heat release by the absorbers in the systems were in accordance with that obtained in the bleaching

investigation. These are sensitizers exhibiting less reactivity for generation of initiating moieties for photopolymerization. They show a larger amount of heat contribution released into the surrounding matrix compared to those exhibiting higher efficiency and reactivity. Therefore, this feature of heat release can be also beneficial to the systems requesting heat as driving source such as physical drying of an aqueous dispersion and solvent-comprising systems. Photopolymerization represents a green technology since the process immediately starts after turning on the light source. Thus, the so called dead time in production process is extremely short.

The combination of these sensitizers with **IS** where  $[\text{NTf}_2]^-$  as counterion showed remarkable reactivity for the initiation of cationic photopolymerization in the case using a vinyl ether as monomer following by oxetanes while epoxides resulted in insufficient performance. In addition, the introduction of the acrylate **TMPTA** and the methacrylate monomer **UDMA** in hybrid polymerization where cationic polymerization additionally proceeds significantly promoted the polymerization reactivity. It increased the final conversion of the cationic reaction resulting in formation of homogeneous hybrid interpenetration polymer networks (IPNs). This shows huge potentials of such NIR-sensitized systems in the applications to synthesis crosslinked polymer materials in the future. Moreover, the hypsochromic shift observed for some heptamethine compounds such as **S7c** and **S7g** resulted in appearing color change of the polymer films while photobleaching of the sensitizers proceeded at the excitation wavelength after exposure. It provides an interesting and promising view for the preparation of optical materials.

The adapted photocuring of sol-gels comprising nanoparticles using heptamethine-based cyanine sensitizer and iodonium salt as initiator in combination with high-intensity NIR-LED succeeded in preparation of coated films with better mechanical properties compared to the UV-initiated systems. These materials obtained exhibited higher  $T_g$  and provided potential to implement such NIR-initiated polymerization technology in combination with high-power LED devices in practice especially in coating industry. Hopefully, such systems would be introduced to practical application soon because it brings the aforementioned benefits to end users of this new technology.

The connection of multi-wavelength emitting LED devices (here NIR at 860 nm and UV at 395 nm) were applied for physical drying of waterborne **PU** dispersion by NIR exposure and intermediate chemical crosslinking by UV excitation brought interesting new impetus in this field. The remarkable efficiency and satisfying mechanical properties of the coating

materials finally also brought big interests and inspirations into the industry since this technology can be seen as green and highly efficient method in coating industry.

In conclusion, this thesis discussed and disclosed how the structural patterns of methine-based cyanines affect their performance from a broad point of view. This focused on their reactivity in combination with NIR-LED devices emitting between 750-1000 nm. The distinguished performance of these sensitizers relating to their structures/structural patterns hopefully provides some information and instructions for the selection and synthesis for further applications following a specific demand. The aforementioned applications in coating systems by photocuring of sol-gels as well as combination of new physical and chemical drying technologies approved our predication and also provide more potentials based on our investigations for the future.

In addition, there might be also general questions arising regarding the feasibility to access for the design of cyanine-based materials with such structures. From this point of view, the compounds **S7c-S7h** appear more easily available since their connecting bridge chain would be accessible by Vilsmeier reaction. Furthermore, additional focus should be put onto the development of alternative synthetic routes accessing to more structures with open polymethine chain absorbing around 1000 nm in the future. One should also keep in mind the availability to receive materials with acceptable shelf-life in systems comprising iodonium salts and vinyl as well as oxetane monomers.

## 7. References

- [1] H. Staudinger, Über Polymerisation. *Ber. Dtsch. Chem. Ges.* **1920**, 53, 13.
- [2] H. Staudinger, Makromolekulare Chemie und Biologie. *Book* **1947**.
- [3] R. Mülhaupt, Hermann Staudinger and the Origin of Macromolecular Chemistry. *Angew. Chem. Int. Ed. Engl.* **2004**, 43 (9), 1054-1063.
- [4] F.-K. Bruder, R. Hagen, T. Rölle, M.-S. Weiser, T. Fäcke, From the Surface to Volume: Concepts for the Next Generation of Optical–Holographic Data-Storage Materials. *Angew. Chem. Int. Ed.* **2011**, 50 (20), 4552-4573.
- [5] F. A. Rueggeberg, State-of-the-art: Dental photocuring—A review. *Dent. Mater.* **2011**, 27 (1), 39-52.
- [6] B. Strehmel, C. Schmitz, T. Brömme, A. Halbhuber, D. Oprych, J. S. Gutmann, Advances of Near Infrared Sensitized Radical and Cationic Photopolymerization: from Graphic Industry to Traditional Coatings. *J. Photopolym. Sci. Technol.* **2016**, 29 (1), 111-121.
- [7] S. C. Ligon, R. Liska, J. Stampfl, M. Gurr, R. Mülhaupt, Polymers for 3D Printing and Customized Additive Manufacturing. *Chem. Rev.* **2017**, 117 (15), 10212-10290.
- [8] C. Schmitz, B. Strehmel, Photochemical Treatment of Powder Coatings and VOC-Free Coatings with NIR Lasers Exhibiting Line-Shaped Focus: Physical and Chemical Solidification. *ChemPhotoChem* **2017**, 1 (1), 26-34.
- [9] C. Schmitz, D. Oprych, C. Kütahya, B. Strehmel, NIR Light for Initiation of Photopolymerization, J. Lalevée, J.-P. Fouassier, Eds. *Royal Society of Chemistry: 2018*; 431-478.
- [10] C. Schmitz, B. Strehmel, Laser Focus on Curing. *European Coating Journal* **2018**, 124 (4), 40-44.
- [11] B. Strehmel, C. Schmitz, K. Cremanns, J. Gottert, Photochemistry with Cyanines in the Near Infrared: A Step to Chemistry 4.0 Technologies. *Chemistry* **2019**, 25 (56), 12855-12864.
- [12] J. o. T. Cabral, S. D. Hudson, C. Harrison, J. F. Douglas, Frontal photopolymerization for microfluidic applications. *Langmuir* **2004**, 20, 10.
- [13] J. P. Fouassier, J. Lalevée, Photoinitiators for Polymer Synthesis: Scope, Reactivity and Efficiency. Wiley-VCH: Weinheim, **2012**.
- [14] B. Strehmel, T. Brömme, C. Schmitz, K. Reiner, S. Ernst, D. Keil, NIR-Dyes for Photopolymers and Laser Drying in the Graphic Industry, *John Wiley & Sons, Inc.:* **2015**; 213-249.
- [15] J. Jiang, G. Ye, Z. Wang, Y. Lu, J. Chen, K. Matyjaszewski, Heteroatom-Doped Carbon Dots (CDs) as a Class of Metal-Free Photocatalysts for PET-RAFT

- Polymerization under Visible Light and Sunlight. *Angew. Chem. Int. Ed. Engl.* **2018**, 57 (37), 12037-12042.
- [16] Z. Zhang, N. Corrigan, A. Bagheri, J. Jin, C. Boyer, A Versatile 3D and 4D Printing System through Photocontrolled RAFT Polymerization. *Angew. Chem. Int. Ed. Engl.* **2019**, 58 (50), 17954-17963.
- [17] C. A. Spiegel, M. Hippler, A. Muenchinger, M. Bastmeyer, C. Barner-Kowollik, M. Wegener, E. Blasco, 4D Printing at the Microscale. *Adv. Funct. Mater.* **2020**, 30 (26), 1907615.
- [18] J. P. Fouassier, J. Lalevée, Photoinitiators for Polymer Synthesis. Wiley-VCH: Weinheim, **2012**.
- [19] S. Dadashi-Silab, S. Doran, Y. Yagci, Photoinduced Electron Transfer Reactions for Macromolecular Syntheses. *Chem Rev* **2016**, 116 (17), 10212-10275.
- [20] B. Strehmel, C. Schmitz, C. Kütahya, Y. Pang, A. Drewitz, H. Moustroph, Photophysics and photochemistry of NIR absorbers derived from cyanines: key to new technologies based on chemistry 4.0. *Beilstein J Org Chem* **2020**, 16, 415-444.
- [21] Z. Zhang, N. Corrigan, C. Boyer, A Photoinduced Dual-Wavelength Approach for 3D Printing and Self-Healing of Thermosetting Materials. *Angew. Chem. Int. Ed.* **2022**, 61 (11), e202114111.
- [22] M. M. Renfrew, Photopolymerization. US 2448828, *Du Pont de Nemours & Company*, **1948**.
- [23] P. Garra, J. P. Fouassier, S. Lakhdar, Y. Yagci, J. Lalevée, Visible light photoinitiating systems by charge transfer complexes: Photochemistry without dyes. *Prog. Polym. Sci.* **2020**, 107.
- [24] C. Aydogan, G. Yilmaz, A. Shegiwal, D. M. Haddleton, Y. Yagci, Photoinduced Controlled/Living Polymerizations. *Angew. Chem. Int. Ed. Engl.* **2022**, 61 (23), e202117377.
- [25] P. Garra, C. Dietlin, F. Morlet-Savary, F. Dumur, D. Gigmes, J.-P. Fouassier, J. Lalevée, Photopolymerization Processes of Thick Films and in Shadow Areas: a Review for the Access to Composites. *Polymer Chemistry* **2017**, 8 (46), 7088-7101.
- [26] A. Bagheri, J. Jin, Photopolymerization in 3D Printing. *ACS Applied Polymer Materials* **2019**, 1 (4), 593-611.
- [27] Y. Pang, A. Shiraishi, D. Keil, S. Popov, V. Strehmel, H. Jiao, J. S. Gutmann, Y. Zou, B. Strehmel, NIR-Sensitized Cationic and Hybrid Radical/Cationic Polymerization and Crosslinking. *Angew. Chem. Int. Ed. Engl.* **2020**, 2-11.
- [28] N. Corrigan, J. Yeow, P. Judzewitsch, J. Xu, C. Boyer, Seeing the Light: Advancing Materials Chemistry through Photopolymerization. *Angew. Chem. Int. Ed. Engl.* **2019**, 131 (16), 5224-5243.

- [29] C. Schmitz, B. Strehmel, NIR LEDs and NIR lasers as feasible alternatives to replace oven processes for treatment of thermal-responsive coatings. *Journal of Coatings Technology and Research* **2019**, 16 (6), 1527-1541.
- [30] V. A. Bobrin, Y. Yao, X. Shi, Y. Xiu, J. Zhang, N. Corrigan, C. Boyer, Nano- to Macro-scale Control of 3D Printed Materials via Polymerization Induced Microphase Separation. *Nat Commun* **2022**, 13 (1), 3577-3586.
- [31] R. Antonia, J. Dirk, Ö. GmbH, Harmonised VOC Emission Classes for Construction Products: A Tool to Achieve Healthy Buildings, Umweltbundesamt, **2021**.
- [32] A. Javadi, H. S. Mehr, M. Sobani, M. D. Soucek, Cure-on-command technology: A review of the current state of the art. *Prog. Org. Coat.* **2016**, 100, 2-31.
- [33] J. W. Stansbury, C. N. Bowman, S. M. Newman, Shining a light on dental composite restoratives. *Physics Today* **2008**, 61 (4), 82-83.
- [34] M. Mitterbauer, M. Haas, H. Stüger, N. Moszner, R. Liska, Tetrakis(2,4,6-Trimethylbenzoyl)Silane-A Novel Photoinitiator for Visible Light Curing. *Macromol. Mater. Eng.* **2017**.
- [35] J. Radebner, A. Eibel, M. Leypold, C. Gorsche, L. Schuh, R. Fischer, A. Torvisco, D. Neshchadin, R. Geier, N. Moszner, R. Liska, G. Gescheidt, M. Haas, H. Stueger, Tetraacylgermanes: Highly Efficient Photoinitiators for Visible-Light-Induced Free-Radical Polymerization. *Angew. Chem. Int. Ed.* **2017**, 56 (11), 3103-3107.
- [36] J. Radebner, A. Eibel, M. Leypold, N. Jungwirth, T. Pickl, A. Torvisco, R. Fischer, U. K. Fischer, N. Moszner, G. Gescheidt, H. Stueger, M. Haas, Tetraacylstannanes as Long-Wavelength Visible-Light Photoinitiators with Intriguing Low Toxicity. *Chemistry – A European Journal* **2018**, 24 (33), 8281-8285.
- [37] A. Ibrahim, X. Allonas, C. Ley, K. Kawamura, H. Berneth, F.-K. Bruder, T. Faecke, R. Hagen, D. Hoemel, T. Roelle, G. Walze, M. S. Weiser, High Performance Photoinitiating Systems for Holography Recording: Need for a Full Control of Primary Processes. *Chem. - Eur. J.* **2014**, 20 (46), 15102-15107.
- [38] F.-K. Bruder, T. Faecke, T. Roelle, The chemistry and physics of Bayfol HX film holographic photopolymer. *Polymers* **2017**, 9 (472), 1-35.
- [39] B. Strehmel, S. Ernst, K. Reiner, D. Keil, H. Lindauer, H. Baumann, Application of NIR-Photopolymers in the Graphic Industry: From Physical Chemistry to Lithographic Applications. *Z. Phys. Chem.* **2014**, 228 (2-3), 129-153.
- [40] H. Baumann, T. Hoffmann-Walbeck, W. Wenning, H.-J. Lehmann, C. D. Simpson, H. Mustroph, U. Stebani, T. Telser, A. Weichmann, R. Studenroth, Imaging Technology, 3. Imaging in Graphic Arts, *Wiley-VCH Verlag GmbH & Co. KGaA*: **2015**; 1-51.
- [41] J. Zhu, Q. Zhang, T. Yang, Y. Liu, R. Liu, 3D Printing of Multi-Scalable Structures via High Penetration Near-Infrared Photopolymerization. *Nat Commun* **2020**, 11 (1), 1-7.

- [42] V. S. D. Voet, J. Guit, K. Loos, Sustainable Photopolymers in 3D Printing: A Review on Biobased, Biodegradable, and Recyclable Alternatives. *Macromol. Rapid Commun.* **2021**, 42 (3), 2000475.
- [43] Y. Bao, N. Paunović, J. C. Leroux, Challenges and Opportunities in 3D Printing of Biodegradable Medical Devices by Emerging Photopolymerization Techniques. *Adv. Funct. Mater.* **2022**, 32 (15), 2109864-2109873.
- [44] Y. Zhang, L. Josien, J.-P. Salomon, A. Simon-Masseron, J. Lalevee, Photopolymerization of Zeolite/Polymer-Based Composites: toward 3D and 4D Printing Applications. *ACS Appl. Polym. Mater.* **2021**, 3 (1), 400-409.
- [45] C. A. Spiegel, M. Hackner, V. P. Bothe, J. P. Spatz, E. Blasco, 4D Printing of Shape Memory Polymers: From Macro to Micro. *Adv. Funct. Mater.* **2022**, 2110580-2110590.
- [46] Y. Zhang, H. Chen, L. Vidal, G. Schrodj, F. Morlet-Savary, F. Dumur, A. Simon-Masseron, J. Lalevee, Zeolite-Reinforced Interpenetrating Polymer Network Initiated by Chalcone Based Photoinitiating System and Their Application in 3D/4D Printing. *Adv. Mater. Technol. (Weinheim, Ger.)* **2022**, 7 (9), 2200074.
- [47] Y. Zhang, Y. Gao, L. Michelin, L. Josien, L. Vidal, G. Schrodj, A. Simon-Masseron, J. Lalevee, Photopolymerization of ceramic/zeolite reinforced photopolymers: Towards 3D/4D printing and gas adsorption applications. *Eur. Polym. J.* **2022**, 179, 111552.
- [48] G. Wagenblast, H. Reichelt, M. Bueschel, S. Haremza, P. Erk, E. Frank, Photocurable Inks for Offset and/or Jet Printing Containing NIR Absorbers and NIR Absorbers Soluble in Offset and/or High Printing Inks. WO/2005/085372, *BASF Aktiengesellschaft, BASF Drucksysteme GmbH*, **2005**.
- [49] B. Du, S.-s. Zhou, N. Wang, Study on printing techniques of modified aluminum paste printing ink. *Advanced Materials Research (Zuerich, Switzerland)* **2011**, 181-182 (Pt. 2, Advanced Materials Science & Technology), 691-696.
- [50] G. Wagenblast, H. Reichelt, M. Büschel, S. Haremza, P. Erk, E. Frank, Printing Inks for Offset and/or High Printing Containing NIR Absorbers and NIR Absorbers Soluble in Offset and/or High Printing Inks. US 7901494 B2, *BASF SE, Flint Group Germany GmbH*, **2011**.
- [51] M. You, J. Zhong, Y. Hong, Z. Duan, M. Lin, F. Xu, Inkjet printing of upconversion nanoparticles for anti-counterfeit applications. *Nanoscale* **2015**, 7 (10), 4423-4431.
- [52] C. Vazquez-Martel, L. Becker, W. V. Liebig, P. Elsner, E. Blasco, Vegetable Oils as Sustainable Inks for Additive Manufacturing: A Comparative Study. *ACS Sustainable Chem. Eng.* **2021**, 9 (49), 16840-16848.
- [53] Z. Czech, A. Kowalczyk, J. Kabatc, L. Shao, Y. Bai, J. Swiderska, UV-initiated crosslinking of photoreactive acrylic pressure-sensitive adhesives using excimer laser. *Polym. Bull.* **2013**, 70 (479-478).



- [54] N. Wu, Y. Zhang, Y. Wang, Photo-polymerization efficiency of self-etch dental adhesives composed of camphorquinone or trimethylbenzoyl-diphenyl-phosphine oxide. *Int. J. Adhes. Adhes.* **2013**, 45, 53-58.
- [55] E. S. Kim, D. B. Song, K. H. Choi, J. H. Lee, D. H. Suh, W. J. Choi, Robust and recoverable dual crosslinking networks in pressure-sensitive adhesives. *J. Polym. Sci. (Hoboken, NJ, U. S.)* **2020**, 58 (23), 3358-3369.
- [56] M. Bartkowiak, Z. Czech, H. J. Kim, G. S. Shim, M. Nowak, A. K. Antosik, Photoreactive UV-Crosslinkable Acrylic Pressure-Sensitive Adhesives (PSA) Containing Multifunctional Photoinitiators. *Polymers (Basel)* **2021**, 13 (24).
- [57] H. Baumann, Lithographische Druckplatten für Laserbelichtung. *Chem. unserer Zeit* **2015**, 48 (1), 14-29.
- [58] T. Brömme, C. Schmitz, D. Oprych, A. Wenda, V. Strehmel, M. Grabolle, U. Resch-Genger, S. Ernst, K. Reiner, D. Keil, P. Lüs, H. Baumann, B. Strehmel, Digital Imaging of Lithographic Materials by Radical Photopolymerization and Photonic Baking with NIR Diode Lasers. *Chem. Eng. Technol.* **2016**, 39 (1), 13-25.
- [59] F. Dumur, D. Gimes, J. P. Fouassier, J. Lalevee, Organic Electronics: An El Dorado in the Quest of New Photocatalysts for Polymerization Reactions. *Acc. Chem. Res.* **2016**, 49 (9), 1980-1989.
- [60] L. Appelhoff, Q. Wang, B. Strehmel, Farblose Oberflächenbeschichtung. DE2021032211455000, *Niederrehein University of Applied Sciences*, **2021**.
- [61] S. Cirak, B. Strehmel, S. Driesen, Photonic Lacquering of Wires. EP20213339.3, *ASTA Transmission Energy GmbH*, **2021**.
- [62] M. G. Hennessy, A. Vitale, J. T. Cabral, O. K. Matar, Role of heat generation and thermal diffusion during frontal photopolymerization. *Phys Rev E Stat Nonlin Soft Matter Phys* **2015**, 92 (2), 022403.
- [63] A. Shiraishi, H. Kimura, D. Oprych, C. Schmitz, B. Strehmel, Comparison between NIR and UV-Sensitized Radical and Cationic Reactivity of Iodonium Salts Comprising Anions with Different Coordination Behavior. *J. Photopolym. Sci. Technol.* **2017**, 30 (6), 633-638.
- [64] K. D. Jandt, R. W. Mills, A brief history of LED photopolymerization. *Dent. Mater.* **2013**, 29 (6), 605-617.
- [65] Z. Chen, X. Wang, S. Li, S. Liu, H. Miao, S. Wu, Near-Infrared Light Driven Photopolymerization Based On Photon Upconversion. *ChemPhotoChem* **2019**, 3 (11), 1077-1083.
- [66] A. Kocaarslan, C. Kütahya, D. Keil, Y. Yagci, B. Strehmel, Near-IR and UV-LED Sensitized Photopolymerization with Onium Salts Comprising Anions of Different Nucleophilicities. *ChemPhotoChem* **2019**, 3 (11), 1127-1132.

- [67] V. Ferraro, C. R. Adam, A. Vranic, S. Bräse, Recent Advances of Transition Metal Complexes for Photopolymerization and 3D Printing under Visible Light. *Adv. Funct. Mater.* **2023**.
- [68] J. V. Crivello, Cationic polymerization - iodonium and sulfonium salt photoinitiators. *Adv. Polym. Sci.* **1984**, 62 (Initiators, Poly-React., Opt. Act.), 1-48.
- [69] J. V. Crivello, J. Ma, F. Jiang, H. Hua, J. Ahn, R. Acosta Ortiz, Advances in the Design of Photoinitiators, Photo-Sensitizers and Monomers for Photoinitiated Cationic Polymerization. *Macromolecular Symposia* **2004**, 215 (1), 165-178.
- [70] J. V. Crivello, Design of photoacid generating systems. *J. Photopolym. Sci. Technol.* **2009**, 22 (5), 575-582.
- [71] J. V. Crivello, Redox initiated cationic polymerization. *J. Polym. Sci., Part A: Polym. Chem.* **2009**, 47 (7), 1825-1835.
- [72] J. V. Crivello, E. Reichmanis, Photopolymer Materials and Processes for Advanced Technologies. *Chem. Mater.* **2013**, 26 (1), 533-548.
- [73] Y. Kaneko, A. M. Sarker, D. C. Neckers, Mechanistic studies of photobase generation from ammonium tetraorganyl borate salts. *Chem. Mater.* **1999**, 11 (1), 170-176.
- [74] H. Salmi, X. Allonas, C. Ley, Polythiourethane networks catalyzed by photobase generators. *Prog. Org. Coat.* **2016**.
- [75] M. Bouzrati-Zerelli, M. Frigoli, F. Dumur, B. Graff, J. P. Fouassier, J. Lalevee, Design of novel photobase generators upon violet LEDs and use in photopolymerization reactions. *Polymer* **2017**, 124, 151-156.
- [76] C. Ley, A. Siedel, T. Bertaux, C. Croutxe-Barghorn, X. Allonas, Photochemical Processes of Superbase Generation in Xanthone Carboxylic Salts. *Angew. Chem. Int. Ed. Engl.* **2022**, e202214784.
- [77] C. Nason, T. Roper, C. Hoyle, J. A. Pojman, UV-induced frontal polymerization of multifunctional (meth)acrylates. *Macromolecules* **2005**, 38, 7.
- [78] M. S. Malik, S. Schlogl, M. Wolfahrt, M. Sangermano, Review on UV-Induced Cationic Frontal Polymerization of Epoxy Monomers. *Polymers (Basel)* **2020**, 12 (9).
- [79] C. Schmitz, T. Poplata, A. Feilen, B. Strehmel, Radiation crosslinking of pigmented coating material by UV LEDs enabling depth curing and preventing oxygen inhibition. *Prog. Org. Coat.* **2020**, 144.
- [80] N. S. Kenning, B. A. Ficek, C. C. Hoppe, A. B. Scranton, Spatial and temporal evolution of the photoinitiation rate for thick polymer systems illuminated by polychromatic light: selection of efficient photoinitiators for LED or mercury lamps. *Polym. Int.* **2008**, 57 (10), 1134-1140.
- [81] W. A. Green, Industrial Photoinitiators: A Technical Guide. *CRC Press* **2010**.

- [82] H. G. O. Becker, Einführung in die Photochemie. Deutscher Verlag der Wissenschaften: Leipzig, **1983**.
- [83] N. J. Turro, Modern Molecular Photochemistry. University Science Books: Sausalito, **1991**.
- [84] B. Strehmel, H. Hartmann, Photochemie in der DDR. *Chem. unserer Zeit* **2022**, 56 (6), 384-392.
- [85] J. L. Jean-Pierre Fouassier, Cleavable Radical Photoinitiators, **2021**; 55-116.
- [86] J. L. Jean-Pierre Fouassier, Cationic Photoinitiating Systems, **2021**; 199-239.
- [87] J. L. Jean-Pierre Fouassier, Industrial Photoinitiators: A Brief Overview, **2021**; 531-535.
- [88] C. Schmitz, A. Halbhuber, D. Keil, B. Strehmel, NIR-Sensitized Photoinitiated Radical Polymerization and Proton Generation with Cyanines and LED Arrays. *Prog. Org. Coat.* **2016**, 100, 32-46.
- [89] D. Oprych, B. Strehmel, Mediated Generation of Conjugate Acid by UV and Blue Sensitizers with Upconversion Nanoparticles at 980 nm. *Chemistry – A European Journal* **2021**, 27 (13), 4297-4301.
- [90] Q. Wang, S. Popov, A. Feilen, V. Strehmel, B. Strehmel, Rational Selection of Cyanines to Generate Conjugate Acid and Free Radicals for Photopolymerization upon Exposure at 860 nm. *Angew. Chem. Int. Ed. Engl.* **2021**, 60 (51), 26855-26865.
- [91] Q. Wang, S. Popov, V. Strehmel, J. S. Gutmann, B. Strehmel, NIR-sensitized hybrid radical and cationic photopolymerization of several cyanines in combination with diaryliodonium bis(trifluoromethyl)sulfonyl imide. *Polymer Chemistry* **2023**, 14 (2), 116-125.
- [92] European Parliament, Commission Delegated Regulation (EU) 2022/2526 of 23 September 2022 amending Regulation (EU) 2017/852 of the European Parliament and of the Council as regards the temporary storage of mercury waste in liquid form, **2022**.
- [93] A. B. Mukherjee, R. Zevenhoven, J. Brodersen, L. D. Hylander, P. Bhattacharya, Mercury in waste in the European Union: sources, disposal methods and risks. *Resources, Conservation and Recycling* **2004**, 42 (2), 155-182.
- [94] E. Commission [https://environment.ec.europa.eu/news/clean-and-circular-electronics-commission-ends-use-mercury-lamps-mercury-free-alternatives-prevail-2021-12-16\\_en](https://environment.ec.europa.eu/news/clean-and-circular-electronics-commission-ends-use-mercury-lamps-mercury-free-alternatives-prevail-2021-12-16_en). **2021**.
- [95] T. Mukai, S. Nagahama, T. Kozaki, M. Sano, D. Morita, T. Yanamoto, M. Yamamoto, K. Akashi, S. Masui, Current status and future prospects of GaN-based LEDs and LDs. *phys. stat. sol. (a)* **2004**, 201 (12), 2712-2716.

- [96] J. Chen, S. Loeb, J.-H. Kim, LED revolution: fundamentals and prospects for UV disinfection applications. *Environmental Science: Water Research & Technology* **2017**, 3 (2), 188-202.
- [97] M. Uo, E. Kudo, A. Okada, K. Soga, Y. Kogo, preparation and properties of dental composite resin cured under near infrared irradiation. *J. Photopolym. Sci. Technol.* **2009**, 22 (5), 4.
- [98] S. Shanmugam, J. Xu, C. Boyer, Light-Regulated Polymerization under Near-Infrared/Far-Red Irradiation Catalyzed by Bacteriochlorophyll a. *Angew. Chem. Int. Ed. Engl.* **2016**, 55 (3), 1036-1040.
- [99] Z. Wu, K. Jung, C. Boyer, Effective Utilization of NIR Wavelengths for Photo-Controlled Polymerization: Penetration Through Thick Barriers and Parallel Solar Syntheses. *Angew. Chem. Int. Ed. Engl.* **2020**, 59 (5), 2013-2017.
- [100] H. Mustroph, Dyes, General Survey, *Wiley-VCH Verlag GmbH & Co. KGaA*: **2014**; 1-35.
- [101] T. Brömme, J. Moebius, S. Schafer, C. Schmitz, B. Strehmel, Photocuring in a different light: crosslinking can be achieved by near infrared (NIR) radiation. *Eur. Coat. J.* **2012**, (9), 20-21, 24-27.
- [102] C. Kütahya, N. Meckbach, V. Strehmel, J. S. Gutmann, B. Strehmel, NIR Light-Induced ATRP for Synthesis of Block Copolymers comprising UV-absorbing Moieties. *Chemistry – A European Journal* **2020**, 26 (n/a), 10444-10451.
- [103] M.-A. Tehfe, F. Dumur, B. Graff, D. Gigmes, J.-P. Fouassier, J. Lalevée, Blue-to-Red Light Sensitive Push–Pull Structured Photoinitiators: Indanedione Derivatives for Radical and Cationic Photopolymerization Reactions. *Macromolecules* **2013**, 46 (9), 3332-3341.
- [104] N. Corrigan, J. Xu, C. Boyer, A Photoinitiation System for Conventional and Controlled Radical Polymerization at Visible and NIR Wavelengths. *Macromolecules* **2016**, 49 (9), 3274-3285.
- [105] A. H. Bonardi, F. Dumur, T. M. Grant, G. Noirbent, D. Gigmes, B. H. Lessard, J. P. Fouassier, J. Lalevée, High Performance Near-Infrared (NIR) Photoinitiating Systems Operating under Low Light Intensity and in the Presence of Oxygen. *Macromolecules* **2018**, 51 (4), 1314-1324.
- [106] L. Li, M. Wan, Z. Li, Y. Luo, S. Wu, X. Liu, Y. Yagci, Coumarinacyl Anilinium Salt: A Versatile Visible and NIR Photoinitiator for Cationic and Step-Growth Polymerizations. *ACS Macro Lett.* **2023**, 12 (2), 263-268.
- [107] D. E. Hare, S. T. Rhea, D. D. Dlott, R. J. D'Amato, T. E. Lewis, Fundamental Mechanisms of Lithographic Printing Plate Imaging by Near-Infrared Lasers. *J. Imaging Sci. Technol.* **1997**, 41 (3), 291-300.

- [108] G. Hauck, C. Savariar-Hauck, H.-J. Timpe, IR-empfindliche Zusammensetzung und deren Verwendung zur Herstellung von Druckplatten. DE 19906823 (C2), *Kodak Polychrome Graphics GmbH*, **2000**.
- [109] H. Mokbel, F. Dumur, J. Lalevee, On demand NIR activated photopolyaddition reactions. *Polym. Chem.* **2020**, 11 (26), 4250-4259.
- [110] L. Li, M. Wan, Z. Li, Y. Luo, S. Wu, X. Liu, Y. Yagci, Coumarinacyl Anilinium Salt: A Versatile Visible and NIR Photoinitiator for Cationic and Step-Growth Polymerizations. *ACS Macro Letters* **2023**, 263-268.
- [111] A. Bonardi, F. Bonardi, G. Noirbent, F. Dumur, C. Dietlin, D. Gigmes, J. P. Fouassier, J. Lalevee, Different NIR dye scaffolds for polymerization reactions under NIR light. *Polymer Chemistry* **2019**, 10 (47), 6505-6514.
- [112] Y. Xin, S. Xiao, Y. Pang, Y. Zou, NIR-sensitized cationic frontal polymerization of vinyl ether and epoxy monomers. *Prog. Org. Coat.* **2021**, 153, 106149.
- [113] Z. Wu, T. Zhang, X. Shi, N. Corrigan, G. Ng, C. Boyer, Photo-RAFT Polymerization for Hydrogel Synthesis through Barriers and Development of Light-Regulated Healable Hydrogels under NIR Irradiation. *Angew. Chem. Int. Ed. Engl.* **2023**, 62 (25), e202302451.
- [114] G. J. Kavarnos, N. J. Turro, Photosensitization by reversible electron transfer: theories, experimental evidence, and examples. *Chem. Rev.* **1986**, 86 (2), 401-449.
- [115] T. Brömme, C. Schmitz, N. Moszner, P. Burtscher, N. Strehmel, B. Strehmel, Photochemical Oxidation of NIR Photosensitizers in the Presence of Radical Initiators and Their Prospective Use in Dental Applications. *ChemistrySelect* **2016**, 1 (3), 524-532.
- [116] H. Chen, G. Zheng, M. Li, Y. Wang, Y. Song, C. Han, J. Dai, Z. Fu, Photo- and thermo-activated electron transfer system based on a luminescent europium organic framework with spectral response from UV to visible range. *Chem Commun (Camb)* **2014**, 50 (88), 13544-13546.
- [117] A. H. Bonardi, F. Bonardi, F. Morlet-Savary, C. Dietlin, G. Noirbent, T. M. Grant, J. P. Fouassier, F. Dumur, B. H. Lessard, D. Gigmes, J. Lalevee, Photoinduced Thermal Polymerization Reactions. *Macromolecules (Washington, DC, U. S.)* **2018**, 51 (21), 8808-8820.
- [118] C. Schmitz, Y. Pang, A. Gülz, M. Gläser, J. Horst, M. Jäger, New High-Power LEDs Open Photochemistry for Near-Infrared-Sensitized Radical and Cationic Photopolymerization. *Angew. Chem. Int. Ed. Engl.* **2019**, 58, 4400-4404.
- [119] C. Schmitz, B. Strehmel, Laser statt Ofen. *Farbe Lack* **2018**, 124 (2), 40-44.
- [120] R. Wissemborski, R. Klein, Welding and Marking of Plastics with Lasers. *Laser Technik Journal* **2010**, 7 (5), 19-22.

- [121] K.-M. Hong, Y. C. Shin, Prospects of laser welding technology in the automotive industry: A review. *J. Mater. Process. Technol* **2017**, 245, 46-69.
- [122] B. Gachet, M. Lecompère, C. Croutxé-Barghorn, D. Burr, G. L'Hostis, X. Allonas, Highly reactive photothermal initiating system based on sulfonium salts for the photoinduced thermal frontal cationic polymerization of epoxides: a way to create carbon-fiber reinforced polymers. *RSC Advances* **2020**, 10 (68), 41915-41920.
- [123] Y. Cao, D. Wei, L. Yang, Z. Luo, P. Yu, H. Li, C. Zhang, X. Liu, F. Wu, M. Wu, Y. Zeng, Nanoplatfrom Self-Assembly from Small Molecules of Porphyrin Derivatives for NIR-II Fluorescence Imaging Guided Photothermal-Immunotherapy. *Adv Healthc Mater* **2022**, 11 (11), e2102526.
- [124] P. Hu, H. Xu, Y. Pan, X. Sang, R. Liu, Laser Induced Thermal Effect on the Polymerization Behavior in Upconversion Particle Assisted Near-Infrared Photopolymerization. *Chemphyschem* **2022**, 23 (1), e202100670.
- [125] M. Mohseni, S. Bastani, A. Jannesari, Influence of silane structure on curing behavior and surface properties of sol-gel based UV-curable organic-inorganic hybrid coatings. *Prog. Org. Coat.* **2014**, 77 (7), 1191-1199.
- [126] Y. Pang, H. Jiao, Y. Zou, B. Strehmel, The NIR-sensitized cationic photopolymerization of oxetanes in combination with epoxide and acrylate monomers. *Polymer Chemistry* **2021**, 12 (40), 5752-5759.
- [127] Y. Pang, S. Fan, Q. Wang, D. Oprych, A. Feilen, K. Reiner, D. Keil, Y. L. Slominsky, S. Popov, Y. Zou, B. Strehmel, NIR-Sensitized Activated Photoreaction between Cyanines and Oxime Esters: Free-Radical Photopolymerization. *Angew. Chem. Int. Ed. Engl.* **2020**, 59 (28), 11440-11447.
- [128] P. Roschger, S. Michaelis, K. Hassenrueck, H. Berneth, P. Callant, Verfahren zur Herstellung von Cyaninfarbstoffen. DE4331162A1, *Bayer A.-G., Germany* . **1995**.
- [129] J. V. Crivello, Investigation of the photoactivated frontal polymerization of oxetanes using optical pyrometry. *Polymer* **2005**, 46 (26), 12109-12117.
- [130] T. Brömme, D. Oprych, J. Horst, P. S. Pinto, B. Strehmel, New iodonium salts in NIR sensitized radical photopolymerization of multifunctional monomers. *RSC Advances* **2015**, 5 (86), 69915-69924.
- [131] J. G. Huddleston, A. E. Visser, W. M. Reichert, H. D. Willauer, G. A. Broker, R. D. Rogers, Characterization and comparison of hydrophilic and hydrophobic room temperature ionic liquids incorporating the imidazolium cation. *Green Chemistry* **2001**, 3 (4), 156-164.
- [132] C.-W. Cho, T. Phuong Thuy Pham, Y.-C. Jeon, Y.-S. Yun, Influence of Anions on the Toxic Effects of Ionic Liquids to a Phytoplankton *Selenastrum Capricornutum*. *Green Chem.* **2008**, 10 (1), 67-72.

- [133] J. S. Melanie Meixner, Wilfried WSeigt, Monika Zschuppe, Laser statt Trockenöfen. *Farbe und Lack* **2015**, 3, 5.
- [134] H. Baumann, U. Ernst, M. Goetz, A. Griesbeck, M. Oelgemöller, T. Oppenländer, M. Schlörholz, B. Strehmel, Licht als kleinstes Reagenz und Werkzeug. *Nachrichten aus der Chemie* **2014**, 62 (5), 507-512.
- [135] R. A. Marcus, Electron transfer reactions in Chemistry - Theoy and Experiments. *Angew. Chem.* **1993**, 32 (8), 11.
- [136] H. Mokbel, G. Noirbent, D. Gigmes, F. Dumur, J. Lalevee, Towards new NIR dyes for free radical photopolymerization processes. *Beilstein J. Org. Chem.* **2021**, 17, 2067-2076.
- [137] A. H. Bonardi, F. Bonardi, F. Dumur, D. Gigmes, J. P. Fouassier, J. Lalevée, Fillers as Heaters for Photothermal Polymerization upon NIR Light. *Macromol. Rapid Commun.* **2019**, 40 (23), 1900495.
- [138] P. Chinna Ayya Swamy, G. Sivaraman, R. N. Priyanka, S. O. Raja, K. Ponnuvel, J. Shanmugpriya, A. Gulyani, Near Infrared (NIR) absorbing dyes as promising photosensitizer for photo dynamic therapy. *Coord. Chem. Rev.* **2020**, 411.
- [139] B. f. Risikobewertung, Per- and Polyfluoroalkyl Substances (PFASs): Proposal for restriction under the REACH Regulation submitted to the European Chemicals Agency, Bundesinstitut für Risikobewertung, **2023**.
- [140] J. Lalevée, M. El-Roz, X. Allonas, J. Pierre Fouassier, Free-radical-promoted cationic photopolymerization under visible light in aerated media: New and highly efficient silane-containing initiating systems. *J. Polym. Sci., Part A: Polym. Chem.* **2008**, 46 (6), 2008-2014.
- [141] K. Kim, J. Sinha, G. Gao, K. K. Childress, S. M. Sartor, A. M. Salazar, S. Huang, C. B. Musgrave, J. W. Stansbury, High-Efficiency Radical Photopolymerization Enhanced by Autonomous Dark Cure. *Macromolecules* **2020**, 53 (13), 5034-5046.
- [142] Y. Bao, N. Paunović, J. C. Leroux, Challenges and Opportunities in 3D Printing of Biodegradable Medical Devices by Emerging Photopolymerization Techniques. *Adv. Funct. Mater.* **2022**, 32 (15), 10.
- [143] S. Liu, N. Giacoletto, M. Schmitt, M. Nechab, B. Graff, F. Morlet-Savary, P. Xiao, F. Dumur, J. Lalevée, Effect of Decarboxylation on the Photoinitiation Behavior of Nitrocarbazole-Based Oxime Esters. *Macromolecules* **2022**, 55 (7), 2475-2485.
- [144] X. Zou, Y. Zhao, Y. Zhu, R. Liu, Filling Aggregation-Induced Extinction Mechanism in Near-Infrared Photopolymerization for Gradient and Highly Filled Bulk Materials. *Macromolecules* **2022**, 55 (6), 2075-2084.
- [145] K. Mundsinger, B. T. Tuten, L. Wang, K. Neubauer, C. Kropf, M. L. O'Mara, C. Barner-Kowollik, Visible Light Reactive Single-Chain Nanoparticles. *Angew. Chem. Int. Ed. Engl.* **2023**, e202302995.

- [146] M. K. Darani, S. Bastani, M. Ghahari, P. Kardar, E. Mohajerani, NIR induced photopolymerization of acrylate-based composite containing upconversion particles as an internal miniaturized UV sources. *Prog. Org. Coat.* **2017**, 104, 97-103.
- [147] A. Bagheri, Z. Li, C. Boyer, M. Lim, NIR/blue light emission optimization of NaY<sub>1-(x+y)</sub>Yb<sub>x</sub>F<sub>4</sub>:Tm<sub>y</sub> upconversion nanoparticles via Yb(3+)/Tm(3+) dopant balancing. *Dalton Trans* **2018**, 47 (26), 8629-8637.
- [148] D. Oprych, C. Schmitz, C. Ley, X. Allonas, E. Ermilov, R. Erdmann, B. Strehmel, Photophysics of Up-Conversion Nanoparticles: Radical Photopolymerization of Multifunctional Methacrylates Comprising Blue- and UV-Sensitive Photoinitiators. *ChemPhotoChem* **2019**, 3 (11), 1119-1126.
- [149] R. Karplus, M. Neuman, The Scattering of Light by Light. *Physical Review* **1951**, 83 (4), 776-784.
- [150] E. Andrzejewska, Photopolymerization kinetics of multifunctional monomers. *Prog. Polym. Sci.* **2001**, 26, 61.
- [151] Gigahertz-Optik, <https://www.gigahertz-optik.com/en-us/service-and-support/knowledge-base/basics-light-measurement/light-color/opt-rad-wavelength-range/>. **2023**.
- [152] Y. Pang, photopolymerization with new LED system emitting in the near infrared region. *PhD Dissertation* **2021**, University of Duisburg-Essen.
- [153] K. N. Ogle, On the Resolving Power of the Human Eye. *J. Opt. Soc. Am.* **1951**, 41 (8), 517-520.
- [154] B. Strehmel, C. Schmitz, K. Cremanns, J. Göttert, Photochemistry with Cyanines in the Near Infrared: A Step to Chemistry 4.0 Technologies. *Chemistry – A European Journal* **2019**, 25 (56), 12855-12864.
- [155] V. P. Pattani, J. W. Tunnell, Nanoparticle-mediated photothermal therapy: a comparative study of heating for different particle types. *Lasers Surg Med* **2012**, 44 (8), 675-684.
- [156] M. L. Allegranza, Z. M. DeMartini, A. J. Kloster, Z. A. Digby, D. Konkolewicz, Visible and sunlight driven RAFT photopolymerization accelerated by amines: kinetics and mechanism. *Polymer Chemistry* **2016**, 7 (43), 6626-6636.
- [157] L. Zhang, C. Wu, K. Jung, Y. H. Ng, C. Boyer, An Oxygen Paradox: Catalytic Use of Oxygen in Radical Photopolymerization. *Angew. Chem. Int. Ed. Engl.* **2019**, 58 (47), 16811-16814.
- [158] Q. Zou, J. Bao, X. Yan, Functional Nanomaterials Based on Self-Assembly of Endogenic NIR-Absorbing Pigments for Diagnostic and Therapeutic Applications. *Small Methods* **2022**, 6 (4), e2101359.



- [159] A. P. Gorka, R. R. Nani, M. J. Schnermann, Harnessing Cyanine Reactivity for Optical Imaging and Drug Delivery. *Acc. Chem. Res.* **2018**, 51 (12), 3226-3235.
- [160] J. K. G. Karlsson, O. J. Woodford, H. Mustroph, A. Harriman, Cyanine dyes as ratiometric fluorescence standards for the far-red spectral region. *Photochem. Photobiol. Sci.* **2018**, 17 (1), 99-106.
- [161] C. Kütahya, N. Meckbach, V. Strehmel, B. Strehmel, Cyanines Comprising Barbiturate Group Facilitate NIR-Light Assisted ATRP under Anaerobic and Aerobic Conditions at Two Wavelengths Using Fe(III) Catalyst. *Journal of Polymer Science* **2021**, 59 (18), 2023-2035.
- [162] C. E. Hoyle, S. C. Clark, S. Jonsson, M. Shimose, Photopolymerization using maleimides as photoinitiators. *Polymer* **1997**, 38 (22), 3.
- [163] C. Zeiss, <https://zeiss-campus.magnet.fsu.edu/articles/lightsources/mercuryarc.html>.
- [164] M. F. Gendre, Two centuries of electric light source innovations. *Eindhoven Institute for Lighting Technology, Eindhoven Univ. of Technology, Eindhoven, Netherland* **2012**.
- [165] Z. Li, H. Y. Tam, L. Xu, Q. Zhang, Fabrication of long-period gratings in poly(methyl methacrylate-co-methyl vinyl ketone-co- benzyl methacrylate)-core polymer optical fiber by use of a mercury lamp. *Opt. Lett.* **2005**, 30 (10), 3.
- [166] Energy Conservation Program: Energy Conservation Standards for High-Intensity Discharge Lamps, **2015**.
- [167] E. Commission, [https://environment.ec.europa.eu/news/clean-and-circular-electronics-commission-ends-use-mercury-lamps-mercury-free-alternatives-prevail-2021-12-16\\_en](https://environment.ec.europa.eu/news/clean-and-circular-electronics-commission-ends-use-mercury-lamps-mercury-free-alternatives-prevail-2021-12-16_en). **2021**.
- [168] T. M. Okon, J. R. Biard, The First Practical LED. *EdisonTechCenter.org.* **2015**, 14.
- [169] M. Cooke, Going deep for UV sterilization LEDs. *Semiconductor-Today* **2010**, 5 (3), 7.
- [170] M. Matsui, Y. Hashimoto, K. Funabiki, J.-Y. Jin, T. Yoshida, H. Minoura, Application of near-infrared absorbing heptamethine cyanine dyes as sensitizers for zinc oxide solar cell. *Synth. Met.* **2005**, 148 (2), 147-153.
- [171] W. D. Cook, S. Chen, F. Chen, M. U. Kahveci, Y. Yagci, Photopolymerization of vinyl ether networks using an iodonium initiator-The role of photosensitizers. *J. Polym. Sci., Part A: Polym. Chem.* **2009**, 47 (20), 5474-5487.
- [172] P. Brogdon, H. Cheema, J. H. Delcamp, Near-Infrared-Absorbing Metal-Free Organic, Porphyrin, and Phthalocyanine Sensitizers for Panchromatic Dye-Sensitized Solar Cells. *ChemSusChem* **2018**, 11 (1), 86-103.

- [173] M. Bouzrati-Zerelli, M. Maier, C. P. Fik, C. Dietlin, F. Morlet-Savary, J. P. Fouassier, J. E. Klee, J. Lalevee, A low migration phosphine to overcome the oxygen inhibition in new high performance photoinitiating systems for photocurable dental type resins. *Polym. Int.* **2017**, 66 (4), 504-511.
- [174] S. Liu, Z. Ding, H. Zhu, S. Gree, P. Xiao, Y. Xu, J. Lalevée, Near-Infrared Light/Thermal Dual-Responsive Epoxy-Based Polydiacetylene Composite for 3D Printing. *Advanced Materials Interfaces* **2021**, 8 (22).
- [175] D. Jaque, L. Martinez Maestro, B. del Rosal, P. Haro-Gonzalez, A. Benayas, J. L. Plaza, E. Martin Rodriguez, J. Garcia Sole, Nanoparticles for photothermal therapies. *Nanoscale* **2014**, 6 (16), 9494-9530.
- [176] L. Stackova, E. Muchova, M. Russo, P. Slavicek, P. Stacko, P. Klan, Deciphering the Structure-Property Relations in Substituted Heptamethine Cyanines. *J. Org. Chem.* **2020**, 85 (15), 9776-9790.
- [177] R. Ravivarma, E. Sathishvaran, An Advanced Laser Technology in Automobile Architect. *SSRG – IJAP* **2014**, 1 (1), 3.
- [178] J. Hecht, Short history of laser development. *Optical Engineering* **2010**, 49 (9), 091002-091027.
- [179] R. De Loor, L. Penning, R. Slagle, Polygon Laser Scanning. *Laser Technik Journal* **2014**, 11 (3), 32-34.
- [180] W. T. Silfvast, Laser fundamentals. *Cambridge University Press* **1996**.
- [181] R. Liu, H. Chen, Z. Li, F. Shi, X. Liu, Extremely Deep Photopolymerization Using Upconversion Particles as Internal Lamps. *Polym. Chem.* **2016**, 7 (14), 2457-2463.
- [182] B. Schmidt, M. Schaefer, Advanced industrial laser systems and applications, *Proc.SPIE*, **2018**.
- [183] R. Ni, B. Qian, C. Liu, X. Liu, J. Qiu, 3D printing of resin composites doped with upconversion nanoparticles for anti-counterfeiting and temperature detection. *Opt. Express* **2018**, 26 (19), 25481-25491.
- [184] B. Demmig-Adams, W. W. Adams-III, Harvesting Sunlight Safely. *Nature* **2000**, 403, 371-373.
- [185] T. D. Drezner, The importance of microenvironment: Opuntia plant growth, form and the response to sunlight. *Journal of Arid Environments* **2020**, 178.
- [186] D. Wang, Y. Wang, X. Li, Q. Luo, J. An, J. Yue, Sunlight photocatalytic activity of polypyrrole–TiO<sub>2</sub> nanocomposites prepared by ‘in situ’ method. *Catal. Commun.* **2008**, 9 (6), 1162-1166.
- [187] T. Cai, Y. Liu, L. Wang, S. Zhang, Y. Zeng, J. Yuan, J. Ma, W. Dong, C. Liu, S. Luo, Silver phosphate-based Z-Scheme photocatalytic system with superior sunlight

photocatalytic activities and anti-photocorrosion performance. *Applied Catalysis B: Environmental* **2017**, 208, 1-13.

- [188] S. V. Wanasinghe, M. Sun, K. Yehl, J. Cuthbert, K. Matyjaszewski, D. Konkolewicz, PET-RAFT Increases Uniformity in Polymer Networks. *ACS Macro Lett* **2022**, 11 (9), 1156-1161.
- [189] X. Guo, X. Zhao, X. Luo, Y. Pang, B. Tian, S. Liu, S. Li, J. Li, B. Strehmel, Z. Chen, A Sustainable Wood-Based Iron Photocatalyst for Multiple Uses with Sunlight: Water Treatment and Radical Photopolymerization. *Angew. Chem. Int. Ed. Engl.* **2023**, e202301242.
- [190] M. Trujillo, S. M. Newman, J. W. Stansbury, Use of near-IR to monitor the influence of external heating on dental composite photopolymerization. *Dent. Mater.* **2004**, 20 (8), 766-777.
- [191] H. Mokbel, G. Noirbent, D. Gigmes, F. Dumur, J. Lalevee, Towards new NIR dyes for free radical photopolymerization processes. *Beilstein J Org Chem* **2021**, 17, 2067-2076.
- [192] P. Nagtegaele, T. V. Galstian, Holographic Characterization of near infra red photopolymerizable materials. *Synth. Met.* **2002**, 127, 85-87.
- [193] A. Albini, Photochemistry: Past, Present and Future. Springer-Verlag Berlin Heidelberg: **2015**; 1-307.
- [194] J. C. Scaiano, K. G. Stamplecoskie, G. L. Hallett-Tapley, Photochemical Norrish type I reaction as a tool for metal nanoparticle synthesis: importance of proton coupled electron transfer. *Chem Commun (Camb)* **2012**, 48 (40), 4798-4808.
- [195] Education, Photochemistry. [https://uomustansiriyah.edu.iq/media/lectures/6/6\\_2021\\_09\\_18/10\\_01\\_14\\_AM.pdf](https://uomustansiriyah.edu.iq/media/lectures/6/6_2021_09_18/10_01_14_AM.pdf) **2021**, 1047-1048.
- [196] H. F. Gruber, Photoinitiators for Free Radical Polymerization. *Prog. Polym. Sci.* **1992**, 17, 953-1044.
- [197] J. L. Jean-Pierre Fouassier, Anionic, Photoacid, and Photobase Initiating Systems, **2021**; 241-256.
- [198] D. C. Neckers, Development photochemistry: the norrish type II reaction. *J. Org. Chem.* **1971**, 36 (13), 3.
- [199] M. Retailleau, A. Ibrahim, X. Allonas, Dual-Cure Photochemical/Thermal Polymerization of Acrylates: A Photoassisted Process at Low Light Intensity. *Polym. Chem.* **2014**, 5 (22), 6503-6509.
- [200] S. Jockusch, M. S. Landis, B. Freiermuth, N. J. Turro, Photochemistry and photophysics of  $\alpha$ -hydroxy ketones. *Macromolecules* **2001**, 34.
- [201] R. A. Caldwell, H. Sakuragi, T. Majima, Direct observation and chemistry of triplet 1,6-biradicals in the norrish I reaction. *J. Am. Chem. Soc.* **1984**, 106, 3.

- [202] R. D. Jr. Small, J. C. Scaiano, Direct detection of the biradicals generated in the norrish type II reaction. *Chem. Phys. Lett.* **1977**, 50 (3), 4.
- [203] J. C. Scaiano, E. A. Lissi, M. V. Encina, Chemistry of the biradicals produced in the norrish type II reaction. *Review of chemical intermediates* **1978**, 2, 58.
- [204] J. Yeow, R. Chapman, A. J. Gormley, C. Boyer, Up in the air: oxygen tolerance in controlled/living radical polymerisation. *Chem. Soc. Rev.* **2018**, 47 (12), 4357-4387.
- [205] P. Szymaszek, W. Tomal, T. Świergosz, I. Kamińska-Borek, R. Popielarz, J. Ortyl, Review of Quantitative and Qualitative Methods for Monitoring Photopolymerization Reactions. *Polymer Chemistry* **2023**, 1690-1717.
- [206] N. Corrigan, J. Yeow, P. Judzewitsch, J. Xu, C. Boyer, Seeing the Light: Advancing Materials Chemistry through Photopolymerization. *Angew. Chem.* **2019**, 131 (16), 5224-5243.
- [207] R. Tripathy, J. V. Crivello, R. Faust, Photoinitiated polymerization of acrylate, methacrylate, and vinyl ether end-functional polyisobutylene macromonomers. *J. Polym. Sci., Part A: Polym. Chem.* **2013**, 51 (2), 305-317.
- [208] E. Andrzejewska, D. Zych-Tomkowiak, M. Andrzejewski, G. L. Hug, B. Marciniak, Heteroaromatic thiols as co-initiators for type II photoinitiating systems based on camphorquinone and isopropylthioxanthone. *Macromolecules* **2006**, 39, 9.
- [209] Y.-C. Chen, T.-Y. Liu, Y.-H. Li, Photoreactivity study of photoinitiated free radical polymerization using Type II photoinitiator containing thioxanthone initiator as a hydrogen acceptor and various amine-type co-initiators as hydrogen donors. *Journal of Coatings Technology and Research* **2020**, 18 (1), 99-106.
- [210] J. C. Earl, Carbon-carbon bond energies. *Tetrahedron* **1960**, 9, 2.
- [211] I. Alkorta, J. Elguero, The carbon-carbon bond dissociation energy as a function of the chain length. *Chem. Phys. Lett.* **2006**, 425 (4-6), 221-224.
- [212] R. Schwalm, UV Coatings: Basics, Recent Developments and New Applications. *Pigment & Resin Technology* **2008**, 37 (6).
- [213] G. J. Kavarnos, N. J. Turro, Photosensitization by Reversible Electron Transfer: Theories, Experimental Evidence, and Examples. *Chem. Rev.* **1986**, 86, 49.
- [214] R. A. Marcus, On the Theory of Oxidation-Reduction Reactions Involving Electron Transfer. I. *The Journal of Chemical Physics* **1956**, 24 (5), 966-978.
- [215] R. Kaptein, J. L. Oosterhoff, Chemically Induced Dynamic Nuclear Polarization II (Relation with Anomalous ESR Spectra). *Chem. Phys. Lett.* **1969**, 4 (4), 195-197.
- [216] H. G. B. a. D. Pfeifer, CIDNP Effects of Sensitized Photochemical Dediazonation of Arene Diazonium Salts Manipulating CIDNP Intensities by the Experimental Conditions. *Verlag Zeitschrift für Naturforschung in Zusammenarbeit* **1983**, 1592-1597.

- [217] R. Kaptein, Simple Rules for Chemically Induced Dynamic Nuclear Polarization. *Chem. Commun.* **1971**, 732-733.
- [218] G. J. Kavarnos, Fundamental concepts of photoinduced electron transfer, *Photoinduced Electron Transfer I*, Berlin, Heidelberg, 1990//; **1990**, 21-58.
- [219] P. Piotrowiak, Photoinduced electron transfer in molecular systems: recent developments. *Chem. Soc. Rev.* **1999**, 28, 8.
- [220] R. A. Marcus, Chemical and electrochemical electron-transfer theory. *Annu. Rev. Phys. Chem.* **1965**, 15, 42.
- [221] A. H. Zewail, Femtochemistry: Recent Progress in Studies of Dynamics and Control of Reactions and Their Transition States. *J. Phys. Chem.* **1996**, 100, 12701-12724.
- [222] M. Wahl, Time-Correlated Single Photon Counting. *PicoQuant GmbH* **2014**, 1-14.
- [223] C. J. M. a. R. A. Palmer, Design Principles and Instrumentation for Step-Scan FTIR, *7th Intl Conf on Fourier Transform Spectroscopy*, Fairfax, Virginia, **1989**, 577-579.
- [224] C. Kütahya, C. Schmitz, V. Strehmel, Y. Yagci, B. Strehmel, Near-Infrared Sensitized Photoinduced Atom-Transfer Radical Polymerization (ATRP) with a Copper(II) Catalyst Concentration in the ppm Range. *Angew. Chem. Int. Ed. Engl.* **2018**, 57 (26), 7898-7902.
- [225] Y. Wu, J. Hu, C. Zhang, J. Han, Y. Wang, B. Kumar, A facile approach to fabricate a UV/heat dual-responsive triple shape memory polymer. *Journal of Materials Chemistry A* **2015**, 3 (1), 97-100.
- [226] Y. Jiang, J. Huang, C. Xu, K. Pu, Activatable Polymer Nanoagonist for Second Near-Infrared Photothermal Immunotherapy of Cancer. *Nat Commun* **2021**, 12 (1), 1-15.
- [227] Q. Gao, K. Tu, H. Li, L. Zhang, Z. Cheng, A novel reversible-deactivation radical polymerization strategy via near-infrared light-controlled photothermal conversion dividing wall-type heat exchanger. *Science China Chemistry* **2021**, 64 (7), 1242-1250.
- [228] A. Pasciak, R. Marin, L. Abiven, A. Pilch-Wrobel, M. Misiak, W. Xu, K. Prorok, O. Bezkrovnyi, L. Marciniak, C. Chaneac, F. Gazeau, R. Bazzi, S. Roux, B. Viana, V. P. Lehto, D. Jaque, A. Bednarkiewicz, Quantitative Comparison of the Light-to-Heat Conversion Efficiency in Nanomaterials Suitable for Photothermal Therapy. *ACS Appl Mater Interfaces* **2022**, 14 (29), 33555-33566.
- [229] E. Ramirez-Laboreo, C. Sagues, S. Llorente, Dynamic heat and mass transfer model of an electric oven for energy analysis. *Appl. Therm. Eng.* **2016**, 93, 683-691.
- [230] A. Caron, F. Dumur, J. Lalevée, Near-Infrared-Induced photothermal Decomposition of Charge Transfer Complexes: A New Way to Initiate Thermal Polymerization. *Journal of Polymer Science* **2020**, 58 (15), 2134-2139.

- [231] L. Feng, X. Yang, X. Shi, X. Tan, R. Peng, J. Wang, Z. Liu, Polyethylene glycol and polyethylenimine dual-functionalized nano-graphene oxide for photothermally enhanced gene delivery. *Small* **2013**, 9 (11), 1989-1997.
- [232] S. Srinivasan, M. W. Lee, M. C. Grady, M. Soroush, A. M. Rappe, Self-Initiation Mechanism in Spontaneous Thermal Polymerization of Ethyl and n-Butyl Acrylate: A Theoretical Study. *J. Phys. Chem. A* **2010**, 114, 7975-7983.
- [233] T. Wu, Y. Mei, J. o. T. Cabral, C. Xu, K. L. Beers, A new synthetic method for controlled polymerization using a microfluidic system. *J. Am. Chem. Soc.* **2004**, 126, 2.
- [234] L. M. Stevens, C. Tagnon, Z. A. Page, "Invisible" Digital Light Processing 3D Printing with Near Infrared Light. *ACS Appl Mater Interfaces* **2022**.
- [235] C. J. Carling, J. C. Boyer, N. R. Branda, Remote-control photoswitching using NIR light. *J. Am. Chem. Soc.* **2009**, 131 (31), 10838-10839.
- [236] S. Haremza, M. Bueschel, G. Wagenblast, E. Beck, NIR-Hardenable Coating Compositions. WO2008058885, *BASF SE*, **2008**.
- [237] P. Hu, H. Xu, Y. Pan, X. Sang, R. Liu, Upconversion particle-assisted NIR polymerization enables microdomain gradient photopolymerization at inter-particulate length scale. *Nat Commun* **2023**, 14 (1), 3653.
- [238] C. Jiao, N. Zu, K.-W. Huang, P. W. a. J. Wu, Perylene anhydride fused porphyrins as near-infrared sensitizers for dye-sensitized solar cells. *Org. Lett.* **2011**, 13 (14), 4.
- [239] Z. Yuan, S.-L. Lee, L. Chen, C. Li, K. S. Mali, S. De Feyter, K. Müllen, Processable Rylene Diimide Dyes up to 4 nm in Length: Synthesis and STM Visualization. *Chemistry – A European Journal* **2013**, 19 (36), 11842-11846.
- [240] M. Shanmugam, M. Quareshy, A. D. Cameron, T. D. H. Bugg, Y. Chen, Light-Activated Electron Transfer and Catalytic Mechanism of Carnitine Oxidation by Rieske-Type Oxygenase from Human Microbiota. *Angew. Chem. Int. Ed. Engl.* **2021**, 60 (9), 4529-4534.
- [241] Z. Chen, D. Oprych, C. Xie, C. Kütahya, S. Wu, B. Strehmel, Upconversion-Nanoparticle-Assisted Radical Polymerization at  $\lambda = 974$  nm and the Generation of Acidic Cations. *ChemPhotoChem* **2017**, 1 (11), 499-503.
- [242] X. Xue, A. Lindstrom, Y. Li, Porphyrin-Based Nanomedicines for Cancer Treatment. *Bioconjug Chem* **2019**, 30 (6), 1585-1603.
- [243] J. Zhang, M. Yang, C. Li, N. Dorh, F. Xie, F. T. Luo, A. Tiwari, H. Liu, Near-infrared fluorescent probes based on piperazine-functionalized BODIPY dyes for sensitive detection of lysosomal pH. *J Mater Chem B* **2015**, 3 (10), 2173-2184.

- [244] Q. Chen, J. Chen, Z. Yang, L. Zhang, Z. Dong, Z. Liu, NIR-II light activated photodynamic therapy with protein-capped gold nanoclusters. *Nano Research* **2018**, 11 (10), 5657-5669.
- [245] K. Mitra, M. C. T. Hartman, Silicon phthalocyanines: synthesis and resurgent applications. *Org Biomol Chem* **2021**, 19 (6), 1168-1190.
- [246] S. Yang, Y. Yu, X. Gao, Z. Zhang, F. Wang, Recent advances in electrocatalysis with phthalocyanines. *Chem. Soc. Rev.* **2021**, 50 (23), 12985-13011.
- [247] P. Gregory, Industrial Applications of Phthalocyanines. *J. Porphyrins Phthalocyanines* **2000**, 4, 432-437.
- [248] M. Kaiser, C. Würth, M. Kraft, I. Hyppänen, T. Soukka, U. Resch-Genger, Power-dependent upconversion quantum yield of NaYF<sub>4</sub>:Yb<sup>3+</sup>,Er<sup>3+</sup> nano- and micrometer-sized particles – measurements and simulations. *Nanoscale* **2017**, 9 (28), 10051-10058.
- [249] K. Wang, J. Pena, J. Xing, Upconversion Nanoparticle-Assisted Photopolymerization. *Photochem. Photobiol.* **2020**, 96 (4), 741-749.
- [250] Z. Chen, D. Oprych, C. Xie, C. Kütahya, S. Wu, B. Strehmel, Upconversion-Nanoparticle-Assisted Radical Polymerization at  $\lambda=974$  nm and the Generation of Acidic Cations. *ChemPhotoChem* **2017**, 1 (11), 499-503.
- [251] X. Meng, H. Lu, Z. Li, C. Wang, R. Liu, X. Guan, Y. Yagci, Near-infrared light induced cationic polymerization based on upconversion and ferrocenium photochemistry. *Polymer Chemistry* **2019**, 10 (41), 5574-5577.
- [252] X. Zou, J. Zhu, P. Hu, R. Liu, Methods to Evaluate Near-Infrared Photoinitiating Systems for Photopolymerisation Reactions Assisted By Upconversion Materials. *ChemPhotoChem* **2021**, 5 (10), 915-919.
- [253] J. C. Boyer, M. P. Manseau, J. I. Murray, F. C. van Veggel, Surface modification of upconverting NaYF<sub>4</sub> nanoparticles with PEG-phosphate ligands for NIR (800 nm) biolabeling within the biological window. *Langmuir* **2010**, 26 (2), 1157-1164.
- [254] P. Hermes, A. Hermsen, M. Jäger, J. S. Gutmann, V. Strehmel, B. Strehmel, Challenges and limits of upconversion nanoparticles for cationic photopolymerization with UV initiators excited at 980 nm. *Polymer Chemistry* **2022**, 13 (34), 4879-4886.
- [255] H. Mustroph, Cyanine Dyes. *Physical Sciences Reviews* **2020**, 5 (5), 1-24.
- [256] G. T. Dempsey, M. Bates, W. E. Kowtoniuk, D. R. Liu, R. Y. Tsien, X. Zhuang, Photoswitching mechanism of cyanine dyes. *J. Am. Chem. Soc.* **2009**, 131, 2.
- [257] M. Lipowska, G. Patonay, L. Strekowski, New Near-Infrared Cyanine Dyes for Labelling of Proteins. *Synth. Commun.* **1993**, 23 (21), 3087-3094.

- [258] H. A. Shindy, Fundamentals in the chemistry of cyanine dyes: A review. *Dyes and Pigments* **2017**, 145, 505-513.
- [259] L. Stackova, P. Stacko, P. Klan, Approach to a Substituted Heptamethine Cyanine Chain by the Ring Opening of Zincke Salts. *J. Am. Chem. Soc.* **2019**, 141 (17), 7155-7162.
- [260] J. Widengren, P. Schwille, Characterization of Photoinduced Isomerization and Back-Isomerization of the Cyanine Dye Cy5 by Fluorescence Correlation Spectroscopy. *J. Phys. Chem. A* **2000**, 104, 13.
- [261] A. P. Gorka, R. R. Nani, J. Zhu, S. Mackem, M. J. Schnermann, A Near-IR Uncaging Strategy Based on Cyanine Photochemistry. *Journal of the American Chemical Society* **2014**, 136 (40), 14153-14159.
- [262] S. Wan, S. Xia, J. Medford, E. Durocher, T. E. Steenwinkel, L. Rule, Y. Zhang, R. L. Luck, T. Werner, H. Liu, A ratiometric near-infrared fluorescent probe based on a novel reactive cyanine platform for mitochondrial pH detection. *J Mater Chem B* **2021**, 9 (25), 5150-5161.
- [263] H. Muströph, Correspondence on "Cyanine Dyes Containing Quinoline Moieties: History, Synthesis, Optical Properties and Applications". *Chemistry* **2022**, 28 (23), e202103714.
- [264] T. P. Constantin, G. L. Silva, K. L. Robertson, T. P. Hamilton, K. Fague, A. S. Waggoner, B. A. Armitage, Synthesis of New Fluorogenic Cyanines Dyes and Incorporation into RNA Fluoromodules. *Org. Lett.* **2008**, 10 (8), 1561-1564.
- [265] H. Muströph, K. Reiner, J. Mistol, S. Ernst, D. Keil, L. Hennig, Relationship between the Molecular Structure of Cyanine Dyes and the Vibrational Fine Structure of their Electronic Absorption Spectra. *ChemPhysChem* **2009**, 10 (5), 835-840.
- [266] A. V. Kulinich, A. A. Ishchenko, Structural background of fast nonradiative deexcitation of benzo[cd]indole polymethine dyes. *Computational and Theoretical Chemistry* **2020**, 1178.
- [267] A. Pigliucci, E. Vauthey, Vibrational Relaxation Dynamics of Polyatomic Molecules in Solution. *CHIMIA International Journal for Chemistry* **2003**, 57 (4), 200-203.
- [268] G. Calzaferri, H. Gugger, S. Leutwyler, Einfluss intramolekularer Bewegungen auf die Fluoreszenzquantenausbeute. *Helv. Chim. Acta* **1976**, 58, 1969-1987.
- [269] N. D. Ignatyev, A. D. Kucheryna, U. D. Welz-Biermann, H. P. D. Willner, FAP-Farbstoffe. DE10357360 A1, *Merck*, **2005**.
- [270] K. Matyjaszewski, Atom Transfer Radical Polymerization (ATRP): Current Status and Future Perspectives. *Macromolecules* **2012**, 45 (10), 4015-4039.
- [271] T. G. Ribelli, M. Fantin, J. C. Daran, K. F. Augustine, R. Poli, K. Matyjaszewski, Synthesis and Characterization of the Most Active Copper ATRP Catalyst Based on



- Tris[(4-dimethylaminopyridyl)methyl]amine. *J. Am. Chem. Soc.* **2018**, 140 (4), 1525-1534.
- [272] Z. Wu, W. Fang, C. Wu, N. Corrigan, T. Zhang, S. Xu, C. Boyer, An aqueous photo-controlled polymerization under NIR wavelengths: synthesis of polymeric nanoparticles through thick barriers. *Chem Sci* **2022**, 13 (39), 11519-11532.
- [273] Martin Koenemann, Gerhard Wagenblast, S. Ivanovo, Fluorescence Colorants Based on Cyanoaryl-Substituted Naphthoylenebenzimidazole Compounds. WO/2018/134261, *BASF SE*, **2018**.
- [274] H. Mustroph FEW FLUORESCENT DYES. **2017**.
- [275] SpectrumInfo IR-Dyes. **2020**.
- [276] M. Mojzych, M. Henary, Synthesis of Cyanine Dyes, **2008**; 1-9.
- [277] L. Appelhoff. Photonische Trocknung von Lacken mit NIR-Absorbern. *Hochschule Niederrhein*, Krefeld, Germany, **2020**.
- [278] W. Stöber, A. Fink, E. Bohn, Controlled Growth of Monodisperse Silica Spheres in the Micro Size Range. *J. Colloid Interface Sci.* **1968**, 26, 62-69.
- [279] J. Kalisz, Review of methods for time interval measurements with picosecond resolution. *Metrologia* **2004**, 41 (1), 17-32.
- [280] S. Srinivasan, M. W. Lee, M. C. Grady, M. Soroush, A. M. Rappe, Computational evidence for self-initiation in spontaneous high-temperature polymerization of methyl methacrylate. *J. Phys. Chem. A* **2011**, 115 (6), 1125-1132.
- [281] K. P. Menard, N. Menard, Dynamic Mechanical Analysis, **2017**; 1-25.
- [282] M. Stickler, G. Meyerhoff, The spontaneous thermal polymerization of methyl methacrylate: 5\*. Experimental study and computer simulation of the high conversion reaction at 130°C. *POLYMER* **1981**, 22, 6.
- [283] J. L. Bricks, A. D. Kachkovskii, Y. L. Slominskii, A. O. Gerasov, S. V. Popov, Molecular design of near infrared polymethine dyes: A review. *Dyes and Pigments* **2015**, 121, 238-255.
- [284] D. S. Pisoni, L. Todeschini, A. C. Borges, C. L. Petzhold, F. S. Rodembusch, L. F. Campo, Symmetrical and Asymmetrical Cyanine Dyes. Synthesis, Spectral Properties, and BSA Association Study. *J. Org. Chem.* **2014**, 79 (12), 5511-5520.
- [285] D. Frackowiak, The Jablonski Diagram. *J. Photochem. Photobiol., B* **1988**, 2, 399-408.
- [286] G. Herzberg, E. Teller, Schwingungsstruktur der Elektronenübergänge bei mehratomigen Molekülen. *Z. Phys. Chem.* **1933**, 21B (1), 410-446.
- [287] H. Mustroph, Bring Back Order in the Polymethine Dye Medley: Classification, Structure and Spectra. *Dyes and Pigments* **2022**, 208, 1-15.

- [288] N. J. Turro, V. Ramamurthy, J. C. Scaiano, Principles of Molecular Photochemistry. University Science Books: Sausalito, **2009**.
- [289] H. Mauser, Der allgemeine Zusammenhang zwischen Stoffumsatz und Belichtungszeit bei einfachen Photoreaktionen. *Zeitschrift für Naturforschung B* **1967**, 22b, 4.
- [290] K. S. Khuong, W. H. Jones, W. A. Pryor, K. N. Houk, The Mechanism of the Self-Initiated Thermal Polymerization of Styrene. Theoretical Solution of a Classic Problem. *J. Am. Chem. Soc.* **2005**, 127, 13.
- [291] R. Muller, E. Gérard, P. Dugand, P. Rempp, Y. Gnanou, Rheological Characterization of the Gel Point: A New Interpretation. *Macromolecules* **1991**, 24, 1321-1326.
- [292] DMA Q800 specifications. *TA Instruments* **2010**.
- [293] K. P. Menard, N. R. Menard, Dynamic Mechanical Analysis in the Analysis of Polymers and Rubbers, **2015**; 1-33.
- [294] H. Zhang, E. Ruckenstein, Self-Polyaddition of Hydroxyalkyl Vinyl Ethers. *J. Polym. Sci., Part A: Polym. Chem.* **2000**, 38 (20), 3751-3760.
- [295] T. Hashimoto, K. Ishizuka, A. Umehara, T. Kodaira, Synthesis of polyacetals with various main-chain structures by the self-polyaddition of vinyl ethers with a hydroxyl function. *J. Polym. Sci., Part A: Polym. Chem.* **2002**, 40 (22), 4053-4064.

## Acknowledgements

I would like to firstly show my appreciation to Niederrhein University of Applied Sciences for giving me the opportunity to pursue my doctoral study and research in the cooperation program with University of Duisburg-Essen. This was a great opportunity that makes it possible for me to extend my viewpoint and educational background in both fundamental sciences and applied aspects. I would like to thank the vice president for research Prof. Dr. Dr. A. Prange at Niederrhein University of Applied Sciences, who managed the Promotionskolleg program, which receives the funding from the Country of North-Rhine Westphalia and strongly supports PhD students to attend scientific conferences to share and exchange our ideas with other academic peers. We strongly acknowledge the federal ministry for economy and energy (BMWi) within the ZIM program projects (grant numbers ZF4288704WZ9 and KK5297501TA1) for the fundings in cooperation with the companies FEW Chemicals GmbH, Rhein-ChemoTechnik GmbH, in which I was actively involved for research duties and reports. The working experiences from these projects helped me a lot to extend my scientific viewpoints and improve my practical experience in industry.

I would especially like to thank Phoseon Ltd. and EASYTEC GmbH for providing the newly developed high-power NIR-LED light sources of 820 nm and 860 nm, respectively, which played an important role in my research. Furthermore, I would like to give my thanks to Ms. S. Gomoll from FEW Chemicals GmbH who provided the sol-gels for our research and cooperation. On the other hand, I also would give my appreciation to Dr. B. Over from Rhein Chemotechnik, with whom we had a very productive and great cooperation and he also gave us the polyurethane precursor used in this thesis. In addition, I also gratefully acknowledge Dr. S. Popov from Spectrum Info Ltd. in Kiev, from whom we received the NIR absorbers applied with the LED emitting at 860 nm.

At last but not least, I would like to give my special acknowledgements to my supervisors Prof. Dr. B. Strehmel who strongly supports and guides my research in this thesis and study in Germany, and Prof. Dr. J. S. Gutmann who gives me a lot of patience and professional suggestions during the time of this thesis.

## **Curriculum Vitae**

The curriculum vitae is not included in the online version for data protection reasons.